THE
PHYSICAL REVIEW
A Journal of Experimental and Theoretical Physics Established by E. L. Nichols in 1893
VOL. 55, NO. 4 FEBRUARY 15, 1939 SECOND SERIES

Efficiency of Production of Short Range Particles from Lithium and of 4.4-cm Alpha-Particles from Boron Under Proton Bombardment

RALPH B. BOWERSOX*
Ryerson Physical Laboratory, University of Chicago, Chicago, Illinois
(Received November 1, 1938)

The excitation functions for the reactions

$$Li^6+H^1 \rightarrow He^3+He^4$$
$$B^{11}+H^1 \rightarrow Be^8+He^4$$

have been determined up to 400 kv. The cross section of the Li^6 nucleus for this reaction was found to follow an exponential curve throughout this region. It varies from 1.8×10^{-28} at 200 kv to 7.3×10^{-26} at 400 kv. The resonance in the production of 4.4-cm alpha-particles from boron previously reported by other investigators was found to be located at 172 ± 5 kv. The total yield of 4.4-cm alpha-particles from a thick target was found from the observed yield at 90° by integrating the angular distribution function found by Neuert. At 200 kv 13.5 alpha-particles per 10^{11} protons were observed, rising monotonically to 128 per 10^{11} at 400 kv.

INTRODUCTION

TWO groups of doubly charged particles of approximately 0.65- and 1.15-cm range were found by Oliphant, Kinsey and Rutherford[1] when they bombarded lithium with protons. These were ascribed to the reaction $Li^6+H^1 \rightarrow He^3+He^4$ and this reaction was later verified by Oliphant, Shire and Crowther[2] who used separated isotopes of lithium. Neuert[3] by measurements with a cloud chamber, later gave more accurate values of 0.82 and 1.15 cm as the mean ranges of the alpha-particle and the He^3 nucleus, respectively. The curve for the yield of these short range alpha-particles and He^3 nuclei at bombarding potentials ranging from 200 to 400 kv has been obtained in this experiment and the cross section of the Li^6 nucleus calculated for the reaction.

When boron is bombarded by protons, two different groups of alpha-particles seem to be emitted; one with a continuous range distribution from 0 up to about 4 cm, and a homogeneous group of 4.4-cm range. This last group, which probably comes from the reaction $B^{11}+H^1 \rightarrow Be^8+He^4$, is much less intense than the continuous one and has been investigated by Kirchner and Neuert,[4] Oliphant, Kempton and Rutherford[5] and many others. Williams *et al.*,[6] in studying the excitation function of this reaction, observed

* Now at the University of Toledo, Toledo, Ohio.
[1] M. L. E. Oliphant, B. B. Kinsey and Lord Rutherford, Proc. Roy. Soc. **141**, 722 (1933).
[2] M. L. Oliphant, E. S. Shire and B. M. Crowther, Proc. Roy. Soc. **146**, 922 (1934).
[3] H. Neuert, Physik. Zeits. **36**, 629 (1935).
[4] F. Kirchner and H. Neuert, Physik. Zeits. **35**, 292 (1934).
[5] M. L. E. Oliphant, A. E. Kempton and Lord Rutherford, Proc. Roy. Soc. **150**, 241 (1935).
[6] J. H. Williams, W. H. Wells, J. T. Tate and E. L. Hill, Phys. Rev. **51**, 434 (1937).

a resonance level at about 180 kv which was later verified by Bothe and Gentner.[7] There has also been observed a resonance level in the production of gamma-rays at this same potential.[7, 8] The yield of alpha-particles from this reaction was studied in this experiment to verify the resonance level at 180 kv and the yield curve was then extended to 400 kv.

Apparatus

The apparatus used in this research has been previously described in a paper by G. T. Hatch[9] and only a few of the features will be described here. A voltage quadrupling circuit of the Cockcroft-Walton type, controlled by an autotransformer, was used to accelerate the proton beam obtained from a low voltage hydrogen arc source. The voltmeter used to measure the accelerating potential consisted of a column of 750 metallized resistors, ten megohms each, whose resistance was calibrated by applying a known potential of about 40 kv to short sections of the total string of resistors and measuring the resulting current. The 40 kv was obtained from an x-ray source of d.c. potential whose output voltage could be measured by means of a potentiometer designed for that purpose. A further check on the voltage of the proton beam was made by bending it in an electrostatic field and measuring the field strength necessary to produce a known radius of curvature. These measurements agreed with the readings of the voltmeter to within about three percent.

After acceleration through a horizontal tube, the proton beam is analyzed magnetically and at the same time deflected into the target chamber where, before striking the target, it passes through a 28-cm aluminum tube used as a collimator. Diaphragms were mounted in the ends of this tube with circular openings 6 mm in diameter which limited the beam and thus determined the size and position of the focal spot on the target. The geometry of the arrangement was such that every proton which passed through the two diaphragms and thus entered the target chamber, necessarily hit the target. This collimation kept the proton currents low, but gave confidence that the galvanometer readings represented the actual proton current impinging on the target. The aluminum tube was raised to a positive potential of 50 volts to prevent the escape of secondary electrons from it to the target chamber, since this chamber was used as a Faraday cage to measure the proton current; and a diaphragm with a nine-mm hole was placed just beyond the end of the collimating tube to prevent the reverse escape of secondary electrons from the target to the aluminum tube. The beam current was measured by means of a galvanometer and currents of the order of a few tenths of a microampere were used in all of the work. Readings were taken at about three-sec. intervals and recorded and averaged on an adding machine.

The lithium target was formed by pressing lithium metal into a cavity 16 mm in diameter in a steel disk which could be mounted on the target holder at an angle of 45° with the proton beam. During this operation, the pure lithium rapidly oxidized in the air and it was assumed that it changed to the hydroxide. Since in LiOH there are 12 extranuclear electrons for each lithium nucleus as compared to three for pure lithium, the observed yields were multiplied by a factor of four to correct for the increased absorption of the protons by these electrons. As a check on these assumptions, a lithium fluoride target was prepared by melting the compound into a similar cavity in a steel disk and mounting as before. LiF has a high melting point and is a very stable chemical compound, so that it is relatively unlikely to decompose under bombardment by the proton beam. There are likewise 12 extranuclear electrons per lithium nucleus in LiF so the same factor of four should hold in this case. The yields thus calculated were found to fall closely on the curve obtained from the contaminated metal, thus supporting the hypothesis that the surface was actually LiOH.

The boron target was prepared by pressing pure amorphous boron into a shallow cavity in the same type of steel disk, and the boron was found to stick together sufficiently without the use of a binder so that the target could be handled without difficulty. Previous to the

[7] W. Bothe and W. Gentner, Zeits. f. Physik **104**, 685 (1937).
[8] B. Waldman, R. C. Waddel, D. Callihan and W. A. Schneider, Phys. Rev. **54**, 543 (1938).
[9] G. T. Hatch, Phys. Rev. **54**, 165 (1938).

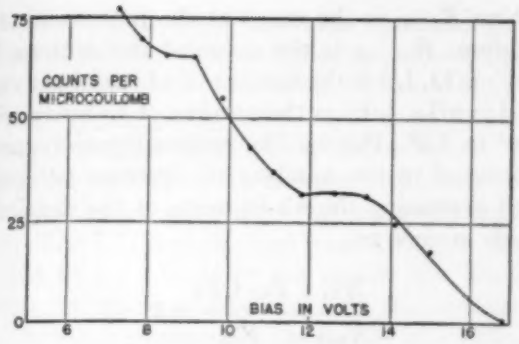

FIG. 1. A sample bias curve. Lithium bombarded by 395-kv protons.

bombardments the targets were heated by a pair of tungsten filaments mounted in a hole in the steel block which comprised the target holder. In this way any film of oil which so often deposits whenever oil diffusion pumps are used was driven off, thus preventing the formation of a carbon deposit on the target as is evidenced by the fact that there is no discoloration of the target even after long use.

The short range particles from lithium were allowed to escape from the target chamber through a window of collodion film whose stopping power was equivalent to two mm of air. This film was mounted on a screen over a hole 0.422 cm in diameter and 3.14 cm from the center of the target. The particles were recorded in an ionization chamber three mm in depth and 1.5 cm in diameter with a positive potential of 500 volts on the front face. This front face of the ionization chamber was placed within a millimeter of the window in the target chamber and the particles were admitted through a one-half inch hole covered with the same type of screen as before. Since the ionization chamber was so close, the window of the target chamber at all times limited the solid angle through which the particles were received.

The screen[10] which covered the windows in the target chamber and the ionization chamber is made of thin copper sheeting with 676 (26^2) regularly spaced holes per square cm. The holes are nearly square and measure 0.216 mm across. The relative area of the holes in the screen is thus seen to be 0.315 of the total area of the screen and this should therefore be the relative number of particles getting through. As a check on this calculation, the transmitting factor of the screen was also measured by means of the natural alpha-particles from polonium. Counts were taken both with and without the screen present between the source of alpha-particles and the ionization chamber and the ratio of these two counts was taken to be the factor desired. This factor came out to be 0.321 and this higher value was the one used in all the calculations. For two screens slightly separated from each other the factor was found to be $(0.321)^2$ since the source used in both cases is an extended one and there is no collimating effect of a single screen. The holes in this screen were found to be small enough so that collodion films of as little as one mm in stopping power would support atmospheric pressure over the area of the hole.

A linear amplifier constructed by J. S. Allen[11] was used to amplify the pulses of the ionization chamber and its output was applied to a scale-of-sixteen counting circuit of the type described by Stevenson and Getting.[12] The output was also applied through an additional stage of amplification to a cathode-ray oscilloscope by means of which a visual check was afforded at all times of the operation of the whole set. Disturbances which would otherwise be recorded as particles can easily be recognized and eliminated by this means.

LITHIUM

The bias on the input to the scaling circuit could be varied so as to control the voltage threshold at which the circuit would begin to record the pulses from the amplifier. In this way bias curves as in Fig. 1 were taken at each value of the accelerating potential and the flat plateaus found were assumed to be a measure of the number of particles entering the chamber at that potential. Since the 8.4-cm range alpha-particles which were always present are not near the end of their range when they are recorded in the ionization chamber, their pulses in the

[10] These screens may be obtained from Evert S. Fink, 230 E. 48 Street, New York City.

[11] J. S. Allen, Phys. Rev. **51**, 182 (1937).

[12] E. C. Stevenson and I. A. Getting, Rev. Sci. Inst. **8**, 414 (1937).

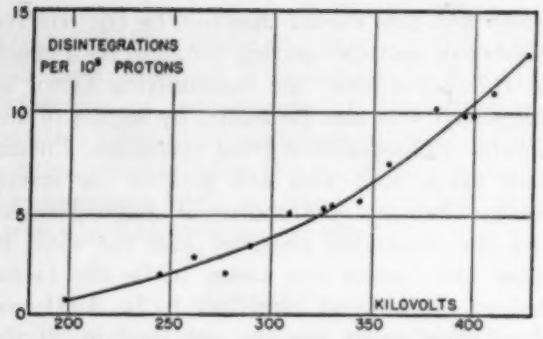

FIG. 2. The thick target yield curve for lithium. The yields as obtained from the experimental data have been multiplied by a factor of 4 to correct for the extra number of electrons per lithium nucleus in the LiOH and LiF targets used.

amplifier are considerably smaller than those of the short range particles. Consequently there were always found two plateaus on the bias curves, the lower one (higher bias voltage) corresponding to the short range particles, and the higher one including both the short range particles and the 8.4-cm range alpha-particles. It was thus found possible to count the short range particles from the reaction in the presence of the long range alpha-particles.

As a check on this, a thin sheet of mica was placed between the target chamber and the front window of the ionization chamber to cut out the short range particles, but thin enough to allow the 8.4-cm alpha-particles to pass through without appreciably cutting down their range. The bias curve taken under these conditions showed only a very slight plateau for the short range particles while the plateau for the 8.4-cm particles remained unchanged; i.e., it was thus shown that the long range alpha-particles produced only the small pulses in the ionization chamber and amplifier.

The observed particle yields from LiOH and LiF, when multiplied by a factor of four, should give the yields from a target of pure lithium bombarded by protons. The factor of four arises from the following considerations. Let N_{Li}/N_{LiF} be the ratio of the yields to be expected from a metallic lithium and a LiF target, respectively, from a given proton beam. Then

$$\frac{N_{Li}}{N_{LiF}}=\frac{R_{p,\,Li}n(\mathrm{Li,\,Li})}{R_{p,\,LiF}n(\mathrm{Li,\,LiF})},$$

where $R_{p,\,Li}$ is the range of the protons in the lithium; $R_{p,\,LiF}$ is the range of the protons in LiF; n(Li, Li) is the number of Li nuclei per cm³ in Li; n(Li, LiF) is the number of Li nuclei per cm³ in LiF. Placing the ranges inversely proportional to the numbers of electrons per cm³, and expressing the n's in terms of the densities leads at once to

$$\frac{N_{Li}}{N_{LiF}}=\frac{Z_{Li}+Z_F}{Z_{Li}}=4.$$

It is clear that the same ratio will hold for the targets lithium: LiOH.

By assuming a spherically symmetrical distribution of ejected particles, the number of disintegrations per proton (half the observed number of particles) could be calculated from the known solid angle subtended by the window. No correction for the momentum of the proton was made, since such a correction amounts to only a little over one percent at 400 kv. Fig. 2 shows the resultant number of disintegrations per proton from a target of metallic lithium.

The cross section σ of the Li^6 nucleus for the proton reaction was computed as follows. Let dy be the yield from a thin target which the

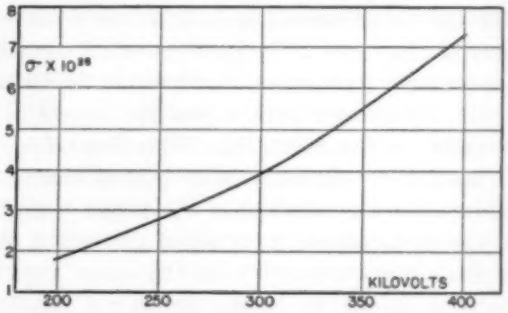

FIG. 3. The excitation cross section of Li^6.

protons traverse without sensible diminution of their velocity. Let dx be the thickness of such a film, and let it contain dn nuclei of Li^6 per cm². Then $\sigma=dy/dn$. The values of dy were found by taking differences along the curve of Fig. 2 at ten-kilovolt intervals. The fraction of the total number of lithium atoms in metallic lithium which are Li^6 is 0.078, and the density of lithium is 0.534. From these values it results that $dn=3.66\times10^{21}dx$.

In order to find the thickness dx of the thin target of lithium whose stopping power is ten kv, use was made of the data of Haworth and King[13] on the stopping power of lithium films for various proton energies. They have listed values of dE/dx for various proton energies and by setting dE equal to ten kv, one can solve for the value of dx. The values of dx range from 2.39×10^{-5} cm at 175 kv to 3.82×10^{-5} cm at 400 kv. These values for dx were substituted in the equation for the cross section and the values of σ calculated for bombarding potentials of 200, 250, 300, 350 and 400 kv. Fig. 3 shows the cross section of the lithium nucleus for this process as a function of the proton bombarding potentials and the curve is seen to be exponential within experimental error over the range investigated.

Boron

For the work on boron the 0.422-cm diameter window in the target chamber was covered with a thin piece of Cellophane whose stopping power was equivalent to 3.2 cm of air. The ionization chamber was then placed one cm away from this window, but the window in the ionization chamber was large enough ($\frac{1}{2}$ inch) so that the solid angle still remained limited by the opening in the target chamber. Since the 4.4-cm alpha-particles are the longest range produced when boron is bombarded by protons, no other particles reached the ionization chamber and the bias on the scaling circuit was set to record all of the particles which entered. As before, a correction was made to the number of alpha-particles recorded to take account of the screen over the window of the ionization chamber, but in this case no such screen was used to cover the window in the target chamber since the Cellophane was strong enough to support the atmospheric pressure.

Table I. *Values of N/N_{90} from Neuert's curve.*

θ	N_θ/N_{90}	$N \sin\theta/N_{90}$
20°	1.90	0.65
30	1.85	0.93
40	1.82	1.17
50	1.70	1.30
60	1.55	1.34
70	1.30	1.22
80	1.05	1.03
90	1.00	1.00
100	1.10	1.08
110	1.35	1.27
120	1.55	1.34
130	1.72	1.32
140	1.70	1.09
150	1.72	0.86

[13] L. J. Haworth and L. D. P. King, Phys. Rev. **54**, 48 (1938).

Neuert[14] has investigated the angular distribution of alpha-particles from this reaction; and he publishes a curve showing the ratio of the number of particles at an angle θ with the incident proton beam to the number at $\theta=90°$. Although Neuert has stated his results as representing the number of particles per unit angular range at an angle θ, it would seem from his experimental arrangement that he has actually measured numbers of particles per unit solid angle. With this assumption in mind, the ordinates on Neuert's curve were multiplied by $\sin\theta$ and the resulting function integrated graphically. This integration gives a factor of 18.6 by which the number of alpha-particles per unit solid angle at $\theta=90°$ must be multiplied to give the total yield. Table I gives the values of N/N_{90} as read from Neuert's curve for various values of θ and the values of $N \sin\theta/N_{90}$ are also listed. The yield of alpha-particles from boron calculated in this way from Neuert's data for various values of the accelerating potential is shown in Fig. 4.

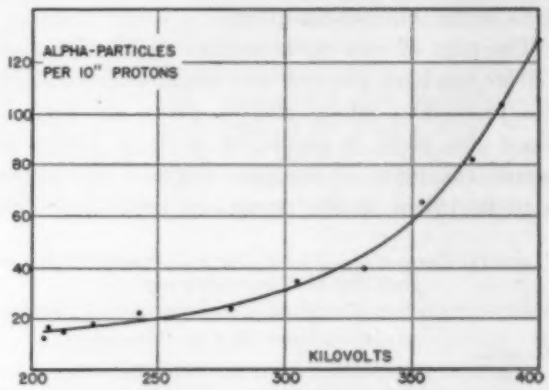

Fig. 4. The yield of 4.4-cm alpha-particles from boron as calculated on the basis of Neuert's data.

Dr. Williams has kindly furnished me with some of the results of the Minnesota group for the angular distribution of alpha-particles from

[14] H. Neuert, Physik. Zeits. **38**, 122 (1937).

this reaction at an accelerating potential of 190 kv. They find the ratio of the number per unit solid angle at angle θ to the number at $\theta=90°$ to be represented by the function $1+0.7\cos^2\theta$. If this distribution function is integrated over the surface of a sphere, one gets the factor 15.5 by which the number of alpha-particles at 90° must be multiplied in order to obtain the total yield. In Table II is given a comparison between the total yield as calculated on the basis of Neuert's data and as calculated from the above data of the Minnesota group.

The part of this curve in the neighborhood of 170 kv has been plotted on a larger scale to show the resonance effect and is given in Fig. 5. Since the yield is given for a thick target of boron, the point of steepest slope of this curve is to be taken as the resonance potential. This point comes at 172±5 kv. Other estimates of this resonance potential are as follows:

Williams *et al.*[6]	180 kv
Allen, Haxby and Williams[15]	160 kv
Bothe and Gentner[7]	180 kv
Waldman *et al.*[8]	165±4 kv

TABLE II. *Comparison of total yield from Neuert's data and from that of Minnesota group.*

Potential (kv)	Total Yield of Alpha-Particles	
	Neuert	Minnesota Group
175	10×10^{-11} per proton	8.65×10^{-11} per proton
200	14.3	12.4
225	16.5	14.3
250	18.7	16.2
275	23.7	20.5
300	31.2	27.2
325	41.2	35.6
350	58.8	50.8
375	88.8	76.7
400	127.5	110.0

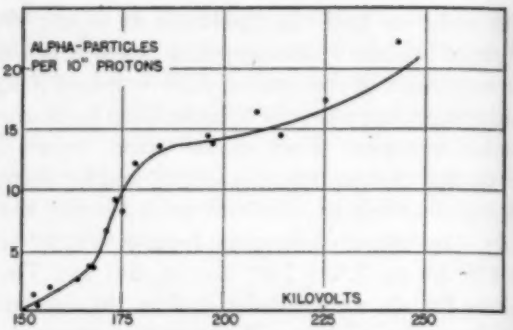

FIG. 5. The yield of alpha-particles from boron in the neighborhood of the resonance potential.

ACKNOWLEDGMENTS

This work was done under the direction of Professor S. K. Allison, and the author wishes to express his gratitude also to Mrs. E. R. Graves, Mr. N. M. Smith, Jr., Mr. L. S. Skaggs and Mr. G. T. Hatch for assistance in the operation of the apparatus and in taking the data.

[15] J. S. Allen, R. O. Haxby and J. H. Williams, Phys. Rev. **53**, 325 (1938).

On Interpreting Related Magnetic Moments of Light Nuclei

D. R. INGLIS
Rowland Physical Laboratory, The Johns Hopkins University, Baltimore, Maryland
(Received January 3, 1939)

Under the assumption that neutrons and protons are simple nuclear building stones, endowed with constant spin magnetic moments and bound together by simple short range interactions of an exchange (primarily space-exchange) nature, it is (a) not found possible to explain the order of magnitude of the observed difference between the magnetic moments of Li^8 and the deuteron, without a very forced theory of spin-orbit coupling; (b) not understandable that the N^{14} and Li^6 moments should differ considerably; (c) not possible to explain the difference between the magnetic moments of Li^7 and the proton in the central-field model (with perturbations) within 25 percent, and not possible to reduce the smaller discrepancy in the alpha-particle model to less than four percent, unless the electric polarizability of the triton is much greater than estimated by the central-field model; (d) understandable in the central-field model that the F^{19} nucleus is in a ^2S state with magnetic moment about five percent less than that of the proton, due to slight admixture of neutron spin; (e) possible to understand the observed angular momentum (sign of spin-orbit coupling) of N^{15} in either of the models. The discrepancies (a) and (c) are quite small and suggest especially that the intrinsic spin magnetic moments of protons and neutrons are constant to within a few percent, as does (d). The discrepancy (b) is larger but involves more particles. The discrepancies may plausibly be attributed either to influence of the binding forces on the spin magnetic moments, or perhaps to a term in the interaction containing the angles between the spin directions and the displacement vectors between the particles.

THE new magnetic resonance method[1a] yields direct precision values[1] of nuclear magnetic moments which previously could be measured only indirectly by means of their elusive coupling to atomic moments. The few magnetic moments of the simpler nuclei which are now reliably known[1] fall into two groups: those with an "extra proton" (H^1, Li^7, F^{19}), which have large magnetic moments ($\sim 3\mu_N$); and the "odd-odd" nuclei (H^2, Li^6, N^{14}), with comparatively small magnetic moments ($<\mu_N$). In the present unsatisfactory state of nuclear theory, it is gratifying to have at least this rough confirmation of the simple concept of neutrons and protons as nuclear building-stones, endowed with intrinsic spin magnetic moments, and bound by forces whose saturation is linked to the exclusion principle and to spin compensation. To seek further interpretation may be meaningless, but quantitatively understandable nuclear data are so sparse as to encourage the attempt to find some meaning even in the small differences of the related magnetic moments. We shall ask whether these differences are of a sign and order of magnitude which might plausibly be the result of the simplest assumptions that one may make about the forces and intrinsic moments, or whether they are more reasonably attributed to deviations from the simple assumptions, such as might be expected from a field theory of the forces and intrinsic moments.[2] Although there are other indications of the inadequacy of the simple interactions (perhaps the earliest in reference 3b, the most direct in the recently reported $1d$ quadripole moment of the deuteron), it may be expected that knowledge of their various successes and failures will aid in the selection of the necessary modifications.

Of the representations available to facilitate approximations to a theory, the central-field ("Hartree") model[3] is advantageous for the simplicity with which it deals directly with the assumed interactions between the protons and

[1] (a) I. I. Rabi, J. R. Zacharias, S. Millman and P. Kusch, Phys. Rev. **53**, 318 (1938); (b) **53**, 495 (1938); (c) S. Millman, P. Kusch and I. I. Rabi, Phys. Rev. **54**, 968 (1938); (d) J. M. B. Kellogg, I. I. Rabi, N. F. Ramsey and J. R. Zacharias, Abstract 24 as reported at the Washington meeting of the American Physical Society, December 27, 1938; (e) S. Millman and P. Kusch, Abstracts 27 and 28 as reported at the Washington meeting of the American Physical Society, December 27, 1938.

[2] W. E. Lamb and L. I. Schiff, Phys. Rev. **53**, 651 (1938); and others there cited.

[3] (a) M. E. Rose and H. A. Bethe, Phys. Rev. **51**, 205 (1937); Erratum: The authors agree that their Eq. (35) should contain $V/(E-E_0)$ quadratically, thereby decreasing their estimated theoretical difference between the Li^6 and N^{14} moments; (b) D. R. Inglis, Phys. Rev. **51**, 531 (1937); (c) Phys. Rev. **53**, 882 (1938). The details of the model there used are relatively unimportant for the magnetic moment of Li^6, which depends on the fact that the ground state is an ^3S, as must follow from almost any model, and on the order of magnitude of the spin-orbit coupling and of the spin dependence of the forces.

neutrons themselves, and because of the possibility of carrying out the second order of a perturbation theory to account in part for the interdependence of the motions of the various particles. The alpha-particle model has the advantage that one may introduce the large binding of the alpha-particle, and other parameters concerning alpha-particles, to begin with, thus avoiding the necessity of accounting for them in the same step which calculates further nuclear properties. The alpha-particle model agrees with experiment better than does the central-field model in two cases in Li^7 where comparison is possible. First, it interprets the 440 kv$=0.8mc^2$ separation of the two observed low states as caused by a difference in "orbital" angular momentum, so as to be compatible with the dependence of the reactions on the velocity of the incident particle.[4] In the central-field model this was interpreted as spin-orbit coupling (doublet separation) of a low p state, which happened to agree with the intensity ratio at the incident velocity used in the earliest experiments.[4] It is noteworthy that the argument originally advanced for the applicability of the central-field model, with perturbations, to Li^6 was based primarily on this now doubtful interpretation—otherwise the minimum that one obtains in the energy, while varying a parameter related to the average distance between particles, may be merely a local minimum (the only one within the range of short distances where the method apparently converges), an absolute minimum at larger distances then corresponding vaguely to the alpha-particle picture.[5] Second, the alpha-particle model gives a value of the magnetic moment of Li^7 more nearly in agreement with experiment than does the central model, as will be discussed further below. In applying the convenient central-field model to $\mu(Li^6)$ nevertheless, we may at least repeat that the truth is likely to lie between the two models, and that the central approximation should have more meaning for Li^6 than for Li^7, judging by the ratio of the internal binding of the deuteron or triton to its binding to the alpha-particle.[5]

[4] L. H. Rumbaugh and L. R. Hafstad, Phys. Rev. **50**, 681 (1936); L. H. Rumbaugh, R. B. Roberts and L. R. Hafstad, Phys. Rev. **54**, 657 (1938).

[5] See "discussion of the central approximation" in reference 3b, p. 542.

The Magnetic Moment of Li^6

The accuracy recently attained[1] in the measurement of the magnetic moments of the deuteron and of Li^6 shows that they differ slightly $[\mu(H^2)-\mu(Li^6)\approx 0.03\mu_N]$, although within the previous limits of error they had been equal.[6] The approximate equality of the two moments is surely to be attributed in some way to the stability and nonmagnetic nature of the alpha-particle that must be added to one to produce the other. Insofar as protons and neutrons have constant intrinsic (spin) magnetic moments and insofar as spin-orbit coupling and Coulomb energy are negligible, one would, in fact, expect theoretically that $\mu(H^2)=\mu(Li^6)$ exactly. We propose here to show that the observed difference is too large to be attributed either to the Coulomb energy (judging by the central-field model) or to the usual (implicit) spin-orbit coupling. It is therefore not explained by the usual simple scheme. Whether the difference is chiefly due to an influence of the binding forces on the "intrinsic" magnetic moments of the heavy particles (which would not be surprising[2]) or to an explicit spin-orbit coupling term in the binding interaction, such as a term with a factor $(\boldsymbol{\sigma}_1\cdot\mathbf{r}_{12})(\boldsymbol{\sigma}_2\cdot\mathbf{r}_{12})$ suggested by the Yukawa ("mesontron") theory of the forces, is here left undecided.

The ground state of Li^6 in the central-field model[3] is ssp; ssp, $^3S(^2p;\ ^2p)$ (symbols before a semicolon refer to neutrons, after it to protons), and the lowest (i.e., "doubly excited") states which contribute to the magnetic moment in second order are the $^3S(^4P;\ ^2P)$ and $^3S(^2P;\ ^4P)$ arising[3bc] each from each of the excitations $s\rightarrow s'$ and $s\rightarrow d$. The reason that these contributions do not exactly cancel out in pairs is that the state arising from neutron excitation ($ss'p$; ssp, for example) is slightly higher than the corresponding state arising from proton excitation (ssp; $ss'p$), because of their different Coulomb terms.[7] Excited states having different parity from, or the same magnetic moment as, that of the ground state do not contribute.

In an equivalent and even simpler representation, the corresponding states arising from the

[6] J. H. Manley and S. Millman, Phys. Rev. **51**, 19 (1937).

[7] R. F. Bacher, quoted in reference 3a, p. 212.

excitation $s \to s'$ are $s^+s'^+p^+$; $s^+s^-p^-$ and $s^+s^-p^-$; $s^+s'^+p^+$ (interacting with the ground state $s^+s^-p^+$; $s^+s^-p^+$). The first of these has the spin magnetic moment $\mu_1=\mu_0+2(\mu_p-\mu_n)$ (where μ_0 is that of the ground state, $\mu_p+\mu_n$), and the second, $\mu_2=\mu_0-2(\mu_p-\mu_n)$. The second-order contribution of these two states to the magnetic moment is then*

$$\delta\mu=2(\mu_p-\mu_n)\{[H_{01}'/(E_1-E_0)]^2 - [H_{01}'/(E_2-E_0)]^2\}.$$

Here the matrix element is $H_{01}'\approx g_0(s'p/J/sp)$, where g_0 (supposedly $\approx 2/9$) is a measure of the spin dependence of the unlike-particle forces. Using $\psi_{s'}=3^{-\frac{1}{2}}(H_{200}+H_{020}+H_{002})e^{-\rho^2/2}$ and (14) of reference 3b, we have

$$H_{01}'=-g_0(f_{2101}+2f_{2000}f_{1010})Bu = 2^{-\frac{1}{2}}g_0(3-5/\tau)Bu/\tau,$$

in the notation and with the assumptions of reference 3bc. Since $E_1-E_0=2\alpha\sigma\approx 53mc^2$, we have

$$\delta\mu=2(\mu_p-\mu_n)(3-5/\tau)^2(g_0Bu/\tau)^2(E_2-E_1)/(2\alpha\sigma)^3\approx -3\times 10^{-4}((E_2-E_1)/mc^2)\mu_N.$$

Since (E_2-E_1), the change of the Coulomb energy by proton excitation, is of the order of $-mc^2/10$, this with a few smaller contributions from other pairs of excited states is very much too small to account for the discrepancy—so much too small that the result is probably valid even if the model used is not. The sign of the change arises qualitatively thus: spreading out the protons reduces the Coulomb energy, so excited-proton states lie below the corresponding excited-neutron states in Li^6, proton spins thus contributing more than neutron spins, which would make $\mu(Li^6)>\mu(H^2)$ (since μ_p is positive, μ_n negative). It is observed,[1] on the contrary, that $\mu(Li^6)<\mu(H^2)$.

It has been assumed that, excepting the Coulomb force, the interactions between neutrons are the same as those between protons. This assumed symmetry is based, aside from its aesthetic appeal, both on estimates of the expected neutron excess of heavy elements and on relative binding energies of pairs of light isobars. It seems very unlikely that the interactions could contain a dissymmetry capable of having a much greater effect than has the Coulomb force, *and of opposite sign*, in the present calculation, and yet an effect of the same order of magnitude as has the Coulomb force, and not reversing the sign, in the estimate of the neutron excess of heavy elements and of energy differences of isobaric pairs.

If spin-orbit coupling is neglected, the p neutron and p proton of the central-field model of Li^6 give rise to the states $^1,{}^3S$, P, D, of which the ^3S is the ground state. The spin-orbit coupling in its simplest form[8a] $H'=\Sigma a(\mathbf{l}\cdot\mathbf{s})$ has matrix elements between states differing by $\Delta l=\pm 1$, since $\mathbf{l}$ is a vector operator (as is the corresponding operator appearing in its place in Breit's more general theory of spin-orbit coupling[8b]). It therefore mixes the ^1P and ^3P with the ground state. These have the magnetic moments $\frac{1}{2}\mu_N$ and $[\frac{1}{4}\mu_N+\frac{1}{2}\mu(H^2)]$, respectively, or roughly $\mu-\mu_0\approx-\frac{1}{4}\mu_N$. Their elevation in energy above the ground state by a simple space-exchange ("Majorana") interaction is given by Feenberg and Phillips[9] as $E-E_0=2L-K\approx 13K \approx 21mc^2$. (Other values of the constants,[3e] which agree better with the newest scattering data,[10] give $28mc^2$.) This separation can be understood in order of magnitude as follows: In the alpha-particle the forces are saturated and the size of the alpha-particle is essentially the range of the forces. The average value of one interaction in the alpha-particle is thus roughly half of its maximum depth, or about $40mc^2$. The binding energy of each particle in the alpha is about

* The ground state is an S state, and we consider only that magnetic level with maximum projection $M_S(=1)$. If an excited state a (having $M_{Sa}\neq M_{S0}$ but $M_{La}+M_{Sa}=M_{S0}$) is admixed to the ground state 0 so as to make the wave function $\psi_0+c_a\psi_a$, with $c_a=H_{a0}'/(E_a-E_0)\ll 1$, then the contribution to the magnetic moment is

$$\delta\mu=\int(\psi_0+c_a\psi_a)^*(g_L\mathbf{L}_z+g_S\mathbf{S}_z)(\psi_0+c_a\psi_a)\,d\tau \Big/ \int(\psi_0+c_a\psi_a)^*(\psi_0+c_a\psi_a)\,d\tau-\mu_0=(\mu_0+c_a^2\mu_a)/(1+c_a^2)-\mu_0\approx c_a^2(\mu_a-\mu_0).$$

The property of the excited state is thus substituted for that of the ground state to the extent c_a^2. There is no term linear in c_a (nor bilinear in c_a and c_b) because L_z and S_z are diagonal in this representation.

[8] (a) D. R. Inglis, Phys. Rev. **50**, 783 (1936); (b) G. Breit, Phys. Rev. **51**, 248 (1937); (c) G. Breit and J. R. Stehn, Phys. Rev. **53**, 459 (1938).

[9] (a) E. Feenberg and E. Wigner, Phys. Rev. **51**, 95 (1937); (b) E. Feenberg and M. Phillips, Phys. Rev. **51**, 597 (1937).

[10] G. Breit, H. M. Thaxton and L. Eisenbud, Abstract 66, as reported at the Washington meeting of the American Physical Society, December 27, 1938, based on data of Tuve, Heydenburg, Hafstad; Herb, Kerst, Parkinson and Plain.

$14mc^2$. The last two particles in Li^6 are more loosely bound—their average binding is about $4mc^2$. The average value of the interaction between them may be expected to be correspondingly smaller, say $-(4/14)40mc^2=-12mc^2$ in order of magnitude. The space-exchange operation on a P wave function introduces a negative sign because of its antisymmetry, so the P state is elevated and the S state depressed by this amount, separating them by about $24mc^2$.

The strength of the spin-orbit coupling, a, depends on the range of the forces in a very sensitive manner, and therefore also on the validity of the model used, and its theoretical evaluation is quite uncertain. It is thus desirable to determine it empirically. The p particles being less tightly bound in Li^6 than in Li^7, a is surely smaller in Li^6 on the central-field model. If this model applies to Li^7 (which seems very doubtful) it does to Li^6, and the $0.8mc^2$ separation in Li^7 is to be interpreted as equal to $(3/2)a$. This gives an upper limit to a in Li^6 as $0.6mc^2$. We take this to be a measure of the nondiagonal matrix element (since orders of magnitude will suffice). We thus have

$$\delta\mu=(\mu-\mu_0)[H'_{0a}/(E-E_0)]^2\approx-2\times10^{-4}\mu_N,$$

which is much too small. The coupling parameter a in H'_{0a} decreases so rapidly with increasing radius that we may assume that the corresponding effect in the deuteron is even smaller.

In Breit's more general treatment, the spin-orbit coupling caused by a space-exchange interaction is a sum, over the various pairs of particles, of terms of the form

$$H'(1,2)=(a^M-\tfrac{1}{2})(\mathbf{A}_{12}+\mathbf{A}_{21})\cdot(\boldsymbol{\sigma}_1+\boldsymbol{\sigma}_2)+\tfrac{1}{2}(\mathbf{A}_{21}-\mathbf{A}_{12})\cdot(\boldsymbol{\sigma}_1-\boldsymbol{\sigma}_2).$$

Here $\langle\mathbf{A}_{12}\rangle$ is comparable in its vectorial nature and in order of magnitude (when summed over all other particles) with a1 above, and this treatment reduces in effect to the simpler one when $a^M=1$, except that $\mathbf{A}_{12}$ contains a space-exchange operator. In the interaction of a p particle with the s shell, this space-exchange reduces the average interaction, corresponding to the saturation involved in the effective force which determines the constant a in the simpler treatment. Of the $p-p$ interaction $H'(1,2)$ only the space-antisymmetric term (not containing a^M) enters the $^3S-^1,^3P$ nondiagonal elements. Both a and $\langle\mathbf{A}_{12}\rangle$ depend on the radius so sensitively that there is some arbitrariness in their evaluation. It seems that one must always use questionably small radii in order to get the $0.8mc^2$ splitting in Li^7. Using reasonable radii, one has the alternative of supposing that a^M is rather large. The separation is about $(0.05+0.2a^M)mc^2$, with a typical evaluation of the parameters,[3e] so one[3c] would assume $a^M\approx4$. The term in a^M being the larger, we are effectively determining empirically the product $\langle\mathbf{A}_{12}\rangle a^M$ instead of the constant a in the simpler treatment. Since a^M enters linearly (multiplied by $\mathbf{A}_{12}$) in the nondiagonal elements, the possibility of its being large with $\langle\mathbf{A}_{12}\rangle$ correspondingly small does not introduce a danger of increasing the nondiagonal element exorbitantly. Thus the more general form of the spin-orbit coupling will apparently not explain the difference, in the central-field model.

If, on the other hand, the alpha-particle model applies both to Li^6 and to Li^7, the spin-orbit coupling does not cause the $0.8mc^2$ separation in Li^7, but merely a fine structure of these lines. It is smaller than in the previous interpretation by at least a factor five, judging by the sharpness of the lines[4] (and probably very much smaller—see below). This could be expected to keep the calculated difference small in this case. But there is the further possibility that the alpha-model applies to Li^7 and the central model better to Li^6. In this case the value of Breit's parameter a^M could be very large, since $\langle\mathbf{A}_{12}\rangle$ is extremely small for the alpha-model of Li^7. Values of $a^M\approx30$ would suffice to explain the difference $\mu(H^2)-\mu(Li^6)$, if the central model for Li^6 is used. The theory of spin-orbit coupling does, however, seem very forced with such a value of the arbitrary parameter, so we prefer the opinion that the difference arises either from a slight breakdown of the constancy of the intrinsic heavy-particle moments, or perhaps from a $(\boldsymbol{\sigma}_1\cdot\mathbf{r})(\boldsymbol{\sigma}_2\cdot\mathbf{r})$ term in the Hamiltonian.

The Magnetic Moment of N^{14}

In comparing the magnetic moment of N^{14} with that of Li^6, one meets, intensified, the same difficulty as in comparing Li^6 with H^2. The simple theory would have the two moments

equal, but their experimental values[1b,e] are $\mu(N^{14})=0.4\mu_N$, $\mu(Li^6)=0.82\mu_N$. The calculation of the difference to be expected as a consequence of the Coulomb dissymmetry proceeds exactly as for Li^6 above. The elevation of the excited states considered is again $13K$, with K about the same as before,[9b] (perhaps slightly smaller, because of the larger size of N^{14}, but of the same order of magnitude). The decrease in the Coulomb energy, when one excites a proton, is about three times as great in N^{14} as in Li^6, since one proton interacts with six others in nitrogen and with two in lithium. The estimated $\delta\mu$ is thus roughly three times as great as above, or $\sim 10^{-5}\mu_N$, less than 10^{-4} of the experimental difference (compare erratum to a previous estimate, in footnote 3). Use of the central model for N^{14} is, however, more questionable than for Li^6.

The Magnetic Moment of Li^7

Now that the new value of the proton magnetic moment $\mu=(2.78\pm0.02)\mu_N$ has been announced,[1d] one may draw the conclusion from a previous paper[3c] that the theoretical value of $\mu(Li^7)$, calculated by the central field model in second order, with any reasonable parameters in the usual four-term symmetrical Hamiltonian, is not greater than $(2.80+0.33)\mu_N=3.13\mu_N$. The experimental difference $\mu(Li^7)-\mu_\tau \gtrsim 0.45\mu_N$ is to be compared with a value $<0.33\mu_N$ calculated by the central model. The value from the alpha-model[11] depends slightly on the way the model is handled, but is in any case almost as great[11b] as the value[3c] $(3/7)\mu_N=0.43\mu_N$ given by a "raindrop" model in which all the particles have the same radius (three out of seven being charged). In the calculation by the central model, the second order gave a very small positive contribution, due to excitations of the s shell, indicating a slight tendency toward the alpha-model. Likewise in the alpha-model, one could introduce a correction due to the fact that a "proton hole" is jumping between the alphas. The wave function of the hole has a node between the two alphas, which means that it is relatively unlikely to be near the center of gravity. This increases the probability that a proton is at the center and tends to reduce the average radius of the protons. Even in the extreme in which one proton is put at the center, the magnetic moment would not be reduced below $(1/3)\mu_N$. The fact that the binding due to the hole $(\alpha+H^3-Li'\approx 5mc^2)$ is only about $\frac{1}{8}$ of the magnitude of the binding of the hole to an alpha $(\alpha-H^3-\pi\approx -40mc^2)$ suggests that this extreme should be weighted rather lightly in estimating the influence of this effect on the magnetic moment. The value of μ_3 in the alpha-model might thus be reduced by perhaps $0.01\mu_N$, indicating again that we have a problem of approximation of which the true answer lies between the two models.

There is one further modification of the alpha-model which increases the calculated μ_L slightly. The Coulomb repulsion of the protons tends to distort the triton and alpha-particle in such a way as to make the average radius of the protons larger than that of the neutrons. It is obvious that neither the radial expansion nor the polarization of the compact alpha-particle is as important as the polarization of the triton, so only the latter will be considered in estimating the order of magnitude of the effect. ("Polarization" here means the displacement of the center of charge from the center of mass, multiplied by the charge.) Treating the field of the alpha at the triton as homogeneous, and estimating the polarizability of the triton by the central-field model, as used in reference 3bc, we will show that the effect is negligible. The perturbation caused by the external electric field F is

$$H'=eFx=eF(\alpha\sigma)^{-\frac{1}{2}}H_1[(\alpha\sigma)^{\frac{1}{2}}x],$$

neglecting a factor $\pi^{\frac{1}{4}}/2^{\frac{1}{2}}$, where $H_1[(\alpha\sigma)^{\frac{1}{2}}x]$ multiplied by the wave function of the ground state 0, 0; 0 is the wave function of the "singly excited" state 0, 0; 1.[3b] The matrix element of H' between these states is thus $H_{0a}'=eF/(\alpha\sigma)^{\frac{1}{2}}$. Here we may put

$$\alpha\approx 22mMc^2/\hbar^2=22[1840/(137)^2](mc^2/e^2)^2 \approx 220(mc^2/e^2)^2,$$

and σ may be determined by minimization of the first-order energy $(3/2)\alpha\sigma-(3-4g_0)B\times[\sigma/(\sigma+2)]^{\frac{1}{2}}$, with $B=92mc^2$ which has a minimum of $-5.3mc^2$ at $\sigma=1.3$. The elevation of the excited state is $E_a-E_0=\alpha\sigma$ so the "Stark-

[11] (a) L. R. Hafstad and E. Teller, Phys. Rev. **54**, 681 (1938); (b) H. A. Bethe, Phys. Rev. **53**, 842 (1938).

effect" energy of the triton is $\epsilon=(H_{0a}')^2/(E_a-E_0)=(eF/\alpha\sigma)^2M/\hbar^2$. The electric polarization of the triton is $\partial\epsilon/\partial F$, and, for the sake of orders of magnitude, we may describe it as caused by the displacement δr of a charge e away from the alpha-particle. We thus have

$$e\delta r=\partial\epsilon/\partial F=2(e/\alpha\sigma)^2FM/\hbar^2.$$

F is not larger than $2e/r^2$ with $r=e^2/mc^2$, so we have, as an upper limit,

$$e\delta r=2Me^3(\hbar\alpha\sigma r)^{-2}.$$

The magnetic moment of the displaced charge is increased from $er^2\omega/2c$ to $e(r+\delta r)^2\omega/2c$ by the distortion (taking the center of gravity about at the edge of the triton) so the increase in magnetic moment is

$$\begin{aligned}\delta\mu&\approx 2r\delta re\omega/2c\approx 8Me^3(\hbar\alpha\sigma)^{-2}\omega/2cr\\&\approx(e^2/220\sigma\hbar c)^2(8M\omega r^2)e/2mc\\&\approx\{1840/(137\times220\sigma)^2\}\mu_N\approx 10^{-6}\mu_N,\end{aligned}$$

which is quite negligible. The small polarizability of the triton in this model is associated with the penetration of the fictitious potential barrier by the excited wave function and the consequent high excitation energy. This model does not give a discrete excited state of the triton, although there is some experimental evidence for its existence. That the negligibility of the estimated Coulomb repulsion might be partly a consequence of artificialities of the model is suggested by the following almost plausible estimate in which the excitation energy is due to kinetic energy only. Let the triton be limited by a deep well of radius $r=e^2/mc^2$. The excited state has momentum $p\sim\hbar/r$ and kinetic energy $E_a-E_0\sim\hbar^2/(2Mr^2)$. Its electric matrix element with the ground state is of the order of magnitude $H_{0a}'\sim Fer\sim e^2/r$ and the energy $\epsilon=(H_{0a}')^2/(E_a-E_0)\approx 2Me^2r^4F^2/\hbar^2$. Thus

$$e\delta r=\partial\epsilon/\partial F=4Me^2r^4F/\hbar^2=4(1840/137^2)er=0.4er$$

and the increase in magnetic moment is $\delta\mu\sim er^2\omega/2c=\mu_N$, estimated by this method which ignores the necessity of explaining the small binding of the deuteron. Although this correction due to the repulsion is negligible according to the better estimate, the discrepancy is small in the alpha-model. It is, in fact, of the same order of magnitude as the Li^6-H^2 discrepancy discussed above, so the two may be associated with the same break-down of the simple assumptions (such as the assumption of constant intrinsic moments).

There is no difficulty in interpreting the observed 30-cm group of protons[4,11] in the reaction $Li^6(d,p)Li^7$ as being caused by an unresolved ^2P of Li^7: the spin-orbit coupling calculated on the alpha-model, using for definiteness the Thomas precession, is much smaller than the observed width of the 30-cm group, as was remarked above. The splitting factor is $\hbar\omega_T$ with $\boldsymbol{\omega}_T=\ddot{\mathbf{r}}\times\dot{\mathbf{r}}/2c^2$. For a circular orbit, or for a proton riding around the center of gravity of Li^7 on a triton, $\ddot{\mathbf{r}}\perp\dot{\mathbf{r}}$, $\dot{r}=\omega r$, $\ddot{r}=\omega^2 r$, so $\omega_T=\omega^3r^2/2c^2$. In the Hartree model one may put roughly $r\approx e^2/mc^2$, and, for a p state, $M\omega r^2=\hbar$, so

$$\begin{aligned}\hbar\omega_T=\hbar^4/(2c^2M^3r^4)&\approx(\hbar c/e^2)^4(m/M)^3mc^2/2\\&=\tfrac{1}{2}(137^4/1840^3)mc^2=0.03mc^2.\end{aligned}$$

This is only about one-twentieth of the value $(2/3)0.8mc^2$ required by the first interpretation of the separation, so one needs a radius smaller by a factor $20^{-\frac{1}{3}}=\frac{1}{2}$ for this interpretation (or even a factor $60^{-\frac{1}{3}}=0.36$ if one includes the symmetry of the wave function). In the alpha-model the angular momentum is due to all the particles so the angular velocity is much smaller. If in order of magnitude we keep $r=e^2/mc^2$, ω is reduced by a factor 1/7, for Li^7, making $\hbar\omega_T$ only $10^{-4}mc^2$, about 7^{-3} of the value calculated by the single-particle model. (This estimate might easily be in error by a factor 10, as it is rather sensitive to assumptions about r.) This splitting is, of course, still enormously larger than magnetic energies of nuclear particles in external fields, so excludes any nuclear Paschen-Back effect. The smaller magnetic term in the splitting is correspondingly reduced, and is of the same sign as the term in ω_T for a proton, so the sign of the coupling is unaltered and the ground state has $I=\frac{3}{2}$.

The Magnetic Moment of F^{19}

The experimental value[1b] of the magnetic moment F^{19} is $2.64\mu_N$, differing from that of the proton by $\delta\mu=-0.14\mu_N$. This small difference practically demands that the ground state of F^{19} be a ^2S. The sign of the difference can be understood as due to the fact that the sum of the

proton spins is not a perfect constant of the motion, so that the total spin contains a small contribution from the neutron spins (with their negative magnetic moments). This may be described by a perturbation calculation, in which the ground state is a neutron singlet and a proton doublet, the admixed excited state is a neutron triplet and a proton doublet, the total spin being $\frac{1}{2}$ for each state. The magnetic moment is $\mu_0=\mu_\tau$ for the ground state and $\mu_a=(4/3)\mu_\tau-(1/6)\mu_\tau$ for the excited state. The elevation of the excited state is probably caused principally by the fact that the space wave function must be changed from being symmetric to antisymmetric in the two neutrons when one puts the neutron spins parallel. This changes the sign of the leading (space-exchange) term of the interaction between the two neutrons. The nondiagonal matrix element H_{0a}' between the excited state and the ground state arises from the spin-dependent term of this interaction, which is supposedly smaller than the leading term by about a factor $g_0\approx 2/9$. The ratio $H_{0a}'/(E_a-E_0)$ may thus be expected to have the order of magnitude g_0. We may thus estimate

$$\delta\mu=(\mu_a-\mu_0)[H_{0a}'/(E_a-E_0)]^2 \approx[(4/3)\mu_\tau-(7/6)\mu_\tau]g_0^2\approx-0.3\mu_N,$$

agreeing in order of magnitude with experiment.

The fact that the ground state is a ^2S is also understandable in an approximate way. One has less reason to trust the alpha-model here than in the lighter nuclei,[11a] and perhaps more reason to trust the central model beyond the completion of a closed shell. The central model with oscillator potential gives us degenerate s and d states for the last two neutrons and one proton of F^{19}. The configurations giving rise to a singlet-doublet ^2S are then ss, s and dd, d and sd, d, while only the latter would form a triplet-doublet ^2S. The combined singlet-doublet ^2S would be expected to be the ground state for the same reasons of symmetry that must be responsible for the vanishing of the magnetic moments of even-even nuclei. It is of interest to note, however, that a potential which puts s below d, as postulated to simplify the discussion[12] of K^{39} and K^{41}, also leads very simply to a ground state ^2S, and to a smaller estimated $\delta\mu$.

[12] D. R. Inglis, Phys. Rev. **53**, 174 (1938).

The Angular Momentum of N^{15}

The magnetic moment of N^{15} has not yet been announced, but the angular momentum has recently been found[13] to be $I=\frac{1}{2}$. This is satisfactory from the point of view either of the central-field model or of the alpha-model. In the central model, which has a p shell closed at O^{16}, the result is due to the simple inversion for an almost-closed shell familiar in atomic spectra: the "hole" in N^{15} has $^2P_{\frac{1}{2}}$ lowest if the proton in Li^7 has $^2P_{\frac{3}{2}}$ lowest. The alpha-model of N^{15} is four alphas with a proton hole jumping between them, in such a way that the nucleus is in a p state. In the extreme case in which the average "orbital" angular momentum is caused almost entirely by nuclear rotation, the hole staying on one alpha, we have simply a triton with spin $\frac{1}{2}$ rotating and accelerated (in a positive electric field) and the sign of the spin-orbit coupling is positive, as in Li^7 and disagreeing with the experimental result. If, on the other hand, the angular momentum is due primarily to the motion of protons between the alphas, the "hole" concept is essential to a description in terms of a one-body problem, and the coupling is negative, agreeing with experiment. In the former extreme case, the angular velocity is smaller than in the latter by about a factor 15 (because the angular momentum is shared by so many particles), so the positive coupling in the former extreme is only about 15^{-3} times as large as the negative coupling in the latter. This suggests that the actual case would have to be extremely close to the former extreme for the actual coupling to be negative, and thus that the calculated coupling would be positive, as observed, unless the alpha-particles retain their identity to a surprising degree in nuclei. Although correlation of binding energies by means of the exchange of the hole is not very exact, it does suggest that the exchange of the hole is associated with only about 1/20 as much energy as the binding of the hole to an alpha ($Q\ll B$ in Fig. 4 of reference 11a, much of the binding being due to the static term R because there is no repulsion between alphas like that between ions in the molecular analog). This may be taken to indicate that the actual case is rather close to the former extreme (which

[13] G. H. Dieke and R. W. Wood, J. Chem. Phys. **6**, 908 (1938).

would correspond to no exchange), and casts some doubt on the surmise that the coupling should be positive, in the alpha-model. Since both models agree that the ground state of N_{15} is a ^2P, which is, experimentally, a $^2P_{\frac{1}{2}}$, its magnetic moment is $(2\mu_L-\mu_S)/3$. This is $-0.3\mu_N$ in the central model[3a] with $g_L=1$, and about $-0.6\mu_N$ in the alpha-model (near the "former extreme") with $g_L\approx 1/2$, and $\mu_S=\mu_\pi$. Since, furthermore, the data on the odd-proton nuclei indicate a tendency[13] for μ_S to be rather near μ_π, especially for the lighter nuclei, and for g_L to be almost unity, one should expect at least to find the N^{15} magnetic moment rather small and negative.

The theory of spin-orbit coupling and the consequent nuclear magnetic moments in the alpha-model will be the subject of a future paper by Sachs, Goeppert-Mayer and Teller.

Thanks are due especially to Professor Rabi, Drs. Zacharias and Kellogg, Professors Wood and Dieke for advance experimental information and to Professors Breit and Teller for discussions.

FEBRUARY 15, 1939 PHYSICAL REVIEW VOLUME 55

The Emission of Secondary Electrons from Metals Bombarded with Protons

JAMES S. ALLEN
Department of Physics, University of Minnesota, Minneapolis, Minnesota
(Received December 10, 1938)

A study has been made of the yield of secondary electrons from various metals bombarded with protons. For metals that have not been outgassed the secondary electron-proton ratio was about three for protons having energies between 48 and 212 kev. The ratio from outgassed targets of C, Cu, Ni and Pt was about two for protons of the same energies as above. Be gave a yield of about 7.5 electrons per proton. The secondary electron yield was found to be proportional to the cosecant of the angle between the proton beam and the target.

INTRODUCTION

IN RECENT years little work has been done on the emission of secondary electrons from metals bombarded with protons. Healea and Chaffee[1] have investigated the secondary emission from thick Ni targets bombarded by protons having energies up to 1600 electron volts. For a hot target the secondary electron-proton ratio increased with the energy of the protons and reached a value of about 22 percent at 1600 volts. Moreover, the ratio increased to 90 percent for targets that had not been outgassed by heating. Schneider[2] has investigated the energy distribution of the secondary electrons ejected by the passage of protons through very thin films of Au and Al. The secondaries produced by 23 and 53 kev protons had a continuous energy distribution with a broad peak at about 20 to 40 electron volts. The total number of electrons ejected from thick targets of Au, Cu and Al placed at an angle of 90 degrees to the proton beam was also determined. The secondary electron-proton ratio for the three metals had a value of approximately four. This ratio did not change as the energy of the protons was varied from 23 to 53 kev. These targets were not outgassed by external heating, but merely by the local heat produced by the proton beam hitting the metal surface.

Because of the lack of information concerning the electron yields from outgassed metals bombarded by protons of greater energies a study was made of the emission from various metals that could be outgassed by heating.

APPARATUS

A transformer-kenotron set supplied voltages up to 250 kev to a five-section accelerating tube described by Williams, Wells, Tate and Hill.[3] A resistance-type voltmeter was used to measure the accelerating voltages. After magnetic analysis the proton beam passed through a number of slits into the long Faraday cage shown in Fig. 1. The end of this cage was covered with a glass

[1] Monica Healea and E. L. Chaffee, Phys. Rev. **49**, 925 (1936).
[2] G. Schneider, Ann. d. Physik **11**, 357 (1931).
[3] J. H. Williams, W. H. Wells, J. T. Tate and E. L. Hill, Phys. Rev. **51**, 434 (1937).

plate so that the position of the proton beam could be seen by the pale blue fluorescence caused by the protons striking the glass. In order to prevent the collection of surface charges the glass was covered by a coarse mesh, copper screen.

The target was a Ni cylinder, one inch in length, and having a square cross section with the sides $\frac{5}{8}$ inch wide. By means of a tungsten coil inside this cylinder the target could be heated to a bright red color. Targets other than Ni were hung on the forward surface of the cylinder. Both the secondary and primary currents were measured by the same galvanometer, *G*. When the double-throw switch was thrown to the right, the target and the Faraday cage were connected together and the proton current alone was measured. With the switch to the left the net electron current from the target to the collecting cage was measured.

The accelerating tube was operated at a pressure of approximately 5×10^{-5} mm of Hg. The fact that the observed ratios did not change when this pressure was tripled indicated that the pressure was sufficiently low. The position of the proton beam on the target could be adjusted by moving the Faraday cage and target with respect to the main accelerating tube until the beam did not show on the glass end of the tube. It was possible to focus the beam sharply enough to make a spot $\frac{1}{8}$ inch in diameter on the glass plate at the end of the tube. For most of the measurements proton currents of from two to three microamperes were used.

Results

Before attempting to measure the yield of secondary electrons from various metals it was necessary to determine whether or not the voltage between the collector and the target was sufficient to remove all the secondaries from the target. This was done by keeping the proton current constant and recording the current to the collector as this voltage was varied. Fig. 2 shows the relation between the collector potential and the ratio of the collector current to the proton current for a target of sheet Al. The target was not outgassed, but was bombarded until consistent readings were obtained. It is evident that when the collector was 45 volts positive with respect to the target, a saturation current was produced. The measured collector current was the difference between the number of electrons leaving the target and the number of protons either scattered from the target or missing the target and consequently reaching the collector. By making the collector sufficiently negative to return all electrons to the target, the positive current from the target to the collector was measured. According to Fig. 2 this was about 20 percent of the proton current. However, this current was the sum of the number of protons from the target and the number of electrons going from the collector to the target. Later results showed that about three electrons were ejected by every proton hitting the collector. Thus, the measured positive current to the collector was at least four times the actual current of protons. Thus the number of protons scattered from the target or missing the target was about five percent of the proton current bombarding the target. When the switch was in the position necessary for recording the proton current to the target, both this current and also that to the collector was actually measured. Consequently, it was necessary to correct the observed values by subtracting about five percent.

As a preliminary investigation, the yields of secondaries from targets of Be, C, Al, Cu, Ni and

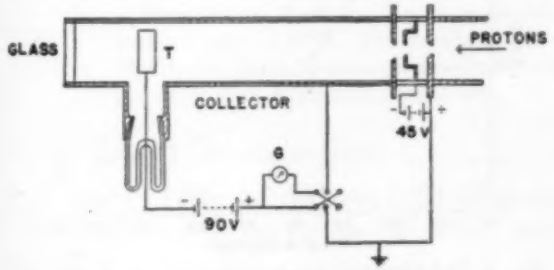

FIG. 1. Diagram of the target assembly.

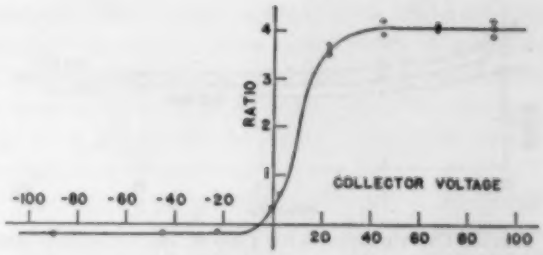

FIG. 2. The secondary electron-proton ratio from Al as a function of the collector potential. The energy of the protons was 120 kev.

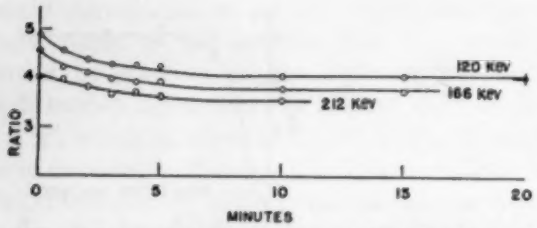

FIG. 3. The variation with time of the secondary electron-proton ratio from a Ni target that had not been outgassed. The proton currents were held constant at three microamperes.

Pt that had not been outgassed were determined. In each case the target was a circular disk placed at an angle of 45 degrees to the proton beam. By means of a ground joint the target could be rotated so as to present a fresh surface to the beam. Fig. 3 shows the variation of the yield with the time that the target had been bombarded. The decrease in the yield during the first ten minutes is typical of all the metals studied. This was caused by the local outgassing of the target by the proton beam. All the metals studied showed a similar decrease with time. The yield showed a slight increase with decreasing energy of the protons. Within the experimental error, all the metals studied had a secondary electron-proton ratio of about four for protons of 120-kev energy.

Since the yield appeared to depend strongly upon the amount of outgassing undergone by the metal, it was considered important to investigate targets that were well outgassed. The target arrangement shown in Fig. 1 was used. The targets were heated to a bright red color and readings taken after the pressure in the system had returned to its normal value. For all metals studied other than Be the yield dropped during the first ten minutes of heating and did not change appreciably after continued heating. The secondary yield from Be rose to about 7.5 after it had been brought to a red color for ten minutes. Prolonged heating did not alter this value. The Be targets were formed by evaporation of the metal in a vacuum onto sheets of copper or nickel. The same yield was obtained from a plate of solid Be ground flat and merely polished with fine emery cloth before it was introduced into the vacuum system. The carbon targets were formed by coating a piece of sheet copper with Aquadag. Table I gives the secondary electron-proton ratio for targets perpendicular to the beam. The ratio appeared to be independent of the energy of the protons in the range between 48 and 212 kev. Some rough measurements for protons having energies as low as 20 kev indicated that the ratio had not changed appreciably at this voltage.

TABLE I. *The secondary electron-proton ratio from outgassed targets placed at an angle of 90 degrees with the proton beam.*

Proton Energy kev	Be	C	Cu	Ni	Pt
48				1.7	
72	7.3	2.3		1.8	
120	7.6	2.3	1.8	1.7	2.4
166	7.5	2.1	1.8	1.7	2.2
212	7.8	2.0	2.1	1.9	2.1

In order to study the yield of secondary electrons as a function of the angle between the proton beam and the surface of the target, the target shown in Fig. 1 was replaced by one of sheet nickel one inch long and $\frac{1}{8}$ inch wide. This target could be rotated through a ground glass joint. Since it was impractical to heat the metal, the target was bombarded at each angular position until the secondary yield reached a constant value before readings were taken. It was found that for angles less than 20 degrees the effective width of the target was so small that an appreciable amount of the beam showed upon the glass at the end of the tube. Consequently no readings were made at angles smaller than this value.

Figure 4 shows the secondary yield as a function of the angle between the proton beam and the surface of the target. The solid circles represent the experimental values while the open

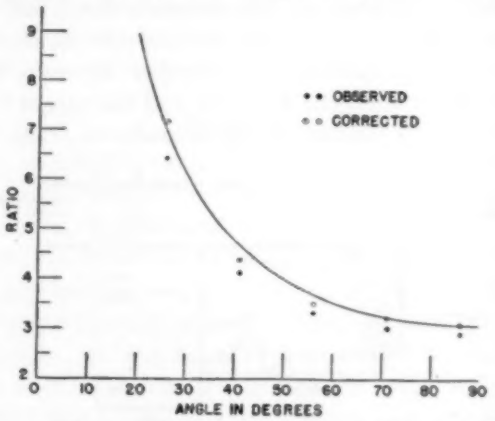

FIG. 4. The secondary electron-proton ratio as a function of the angle between the proton beam and the surface of the target. The energy of the protons was 120 kev.

circles represent the values corrected for the fraction of the beam of protons that either missed the target or were scattered from it. The curve is a plot of the function $R=3\csc\theta$, where θ is the angle between the proton beam and the surface of the target.

Conclusion

The disagreement between the value of three obtained in the present experiment and that of four obtained by Schneider as the value of the secondary electron-proton ratio from thick targets perpendicular to the proton beam probably may be explained by a difference in the outgassing of the targets. If a very small proton current were used, the ratio would decrease very slowly with time and thus would remain near the value obtained when the metal was first exposed to the beam.

The high yield obtained from Be after a short heating is similar to the results obtained recently by Kollath[4] for Be bombarded by electrons. He investigated very carefully the effects of heating and oxidizing upon the secondary electron-primary electron ratio. The value of 0.5 or 0.6 obtained for this ratio from a freshly evaporated target was raised to about 5.5 when the target had been heated at a temperature of about 700 degrees centigrade for a few minutes in a good vacuum. The same results were obtained by heating the metal in an atmosphere of oxygen. Kollath attributed the increased yield not to the formation of a layer of oxide upon the surface, but to a change in the crystal structure of the surface.

The variation of the yield with the angle between the target and the proton beam may be explained at least qualitatively by assuming that the secondaries that are able to reach the surface are produced along a part of the proton path near the surface in the metal. Then the efficiency of the production of the secondaries will be constant for this very short distance. As the angle is decreased, more and more of the total path of the protons becomes effective in producing secondaries according to a $\csc\theta$ law. This is true only if the penetration of the incident particles is much greater than that of the secondaries which is clearly true in the present case. Müller[5] gives a similar explanation for the angular dependence of the yield of the secondaries created by electrons having energies of a few thousand volts.

In conclusion, the author wishes to express his gratitude to Professor J. H. Williams for placing the facilities of the nuclear research laboratory at his disposal and for many helpful discussions during the course of this investigation.

[4] R. Kollath, Ann. d. Physik **33**, 285 (1938).

[5] H. Müller, Zeits. f. Physik **104**, 475 (1937).

FEBRUARY 15, 1939 PHYSICAL REVIEW VOLUME 55

The Scattering of Slow Neutrons by Gaseous Ortho- and Parahydrogen: Spin Dependence of the Neutron-Proton Force

W. F. Libby and Earl A. Long*
Department of Chemistry, University of California, Berkeley, California
(Received October 6, 1938)

Room temperature and liquid-air neutrons have been scattered by gaseous ortho- and parahydrogen at 90°K. The results check with those of Brickwedde, Dunning, Hoge and Manley for liquid hydrogen if reasonable allowances are made for the Doppler effect of the motion of the scattering H_2 molecules.

I. Introduction

As Teller[1,2] has pointed out, the different orientations of the protons in ortho- and parahydrogen must affect the scattering of slow neutrons by these molecules if the neutron proton scattering is dependent on the relative orientations of the spins of the neutron and the proton. A second point is that the absolute magnitude of the elastic scattering cross sections must also

* Fellow of the Lalor Foundation, 1937–38.

[1] E. Teller, Phys. Rev. **49**, 420 (1936).

[2] J. Schwinger and E. Teller, Phys. Rev. **52**, 286 (1934).

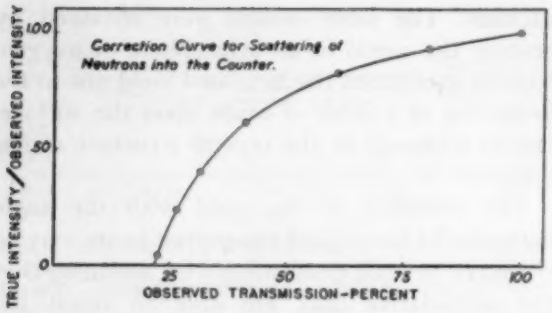

FIG. 1. Correction curve for scattering of neutrons into the counter.

depend very seriously on whether the singlet state (first excited state, and presumably mainly responsible for slow neutron scattering by protons) of the deuteron is real or virtual, i.e., has a positive or negative binding energy. Schwinger and Teller[2] have calculated the predicted cross sections in detail for the case of the virtual level and have clearly indicated how those for the real level are to be obtained.

Though the results of Halpern, Estermann, Simpson and Stern[3] and of Brickwedde, Dunning, Hoge and Manley[4] on the scattering by liquid hydrogen showed that the scattering was spin dependent and indicated that the singlet state was virtual, it seemed desirable to perform the experiment in the gaseous state, where intermolecular liquid forces could hardly enter. The theoretical calculations[2] had been made for gaseous hydrogen molecules with negligible velocity along the neutron beams. It was necessary, therefore, to keep the gas as cool as possible in order that the motion of the scattering molecules would not smooth out the predicted results of changing neutron temperature to unobservably small values. There was the additional consideration that the parahydrogen had been supposed to be entirely in the ground rotational state ($J=0$). This required that the temperature be no higher than 90°K.

II. Apparatus and Method

The scattering gas was contained in a cylindrical copper bomb ten cm in diameter and twenty-five cm long. The wall was one millimeter thick. On the surface of the bomb were soldered two flat coils of copper tubing, so placed as not to obstruct the neutron beam. Liquid air was circulated through this tubing to keep the gas at 90°K. A pressure line connected the bomb to the storage hydrogen tank and a calibrated pressure gauge. The temperature of the gas in the bomb was measured by observing the pressure increase on warming to room temperature. It averaged within two or three degrees of 90°K.

The neutron detector was a BF_3 counter[5] (in one case five of them working in parallel) of conventional design. The source of neutrons was two hundred milligrams of radium as bromide mixed with about ten grams of powdered beryllium metal and placed in a sealed steel tube. For the work with room temperature neutrons a paraffin "howitzer" was used. The "liquid-air" neutrons were obtained through the walls of a metal Dewar vessel containing a cylinder of paraffin immersed in liquid air and surrounding the radium source. The boron absorption coefficient of the neutrons was carefully measured and found to have the value of 1.55 ± 0.05 times the value for neutrons from room temperature paraffin. This corresponds to a neutron temperature[5] of $125°\pm10°$K. This value for the ratio of the boron absorption coefficients of liquid-air and room temperature neutrons has been reported frequently in the literature with good agreement among the values. The neutron temperature given by the method certainly is most reasonable.

The parahydrogen gas was made by placing a few hundred cc of carefully pumped charcoal in about eight liters of liquid normal hydrogen in a Pyrex Dewar surrounded by a metal can and a bath of liquid air. Conversion was then allowed to occur for a period of about twenty-four hours until the composition was pure *para* within one or two percent (as shown by analysis of samples of the gas over the liquid). This left about two and one-half liters of liquid, which was then evaporated into a large oil-filled gas holder by means of a heater coil. The hydrogen compressor was then used to transfer the parahydrogen to a twenty-cubic-foot steel cylinder at a pressure of about one hundred atmospheres. The gas was immediately transferred to the

[3] J. Halpern, I. Estermann, O. C. Simpson and O. Stern, Phys. Rev. **52**, 142 (1937).
[4] F. G. Brickwedde, J. R. Dunning, H. J. Hoge and J. H. Manley, Phys. Rev. **54**, 266 (1938).
[5] W. F. Libby and E. A. Long, Phys. Rev. **52**, 592 (1937).

copper bomb and the experiment started. Samples of the gas were taken at the beginning and at the end of all runs, but in no case was the conversion in the copper bomb measurable during the three or four hours required for each run. It was found that the compressor did not convert the gas appreciably. It was necessary to flush the pressure lines free of normal hydrogen, of course, before transferring parahydrogen. The runs with parahydrogen were made with gas at least 98 percent *para* in most cases. The gas analyses were made by the heat conductivity method of Bonhoeffer.[6] Two entirely independent gauges were used and the analyses were checked by different observers. A further check was made by measuring the difference in vapor pressure of normal hydrogen and a particular sample of para-rich liquid at the boiling point of the latter. The result checked the heat conductivity analysis of the gas. The authors believe the compositions were good to one or two percent.

The apparatus was arranged so the distances from the scatterer to the source and to the counter were each about twenty-five cm. The cross-sectional area of the neutron beam at the source was about one hundred square cm. The counter was 2.3 cm in diameter and 13 cm long. The whole neutron beam was protected and defined in all directions by cadmium sheets. A cadmium sheet (1 mm thick) served as shutter between the source and scatterer. It was necessary to surround the copper bomb with a tinned iron box to prevent the collection of snow and ice on the bomb. (The hydrogen in the ice would have scattered neutrons.) This box was lined with cadmium except for two windows defining the beam. These windows were kept free of ice by means of warm air blasts and periodic heating.

Because of the finite size of the scatterer and the necessarily relatively short distances between it, the source, and the counter, it was necessary to make a correction for the scattering into the counter of neutrons which would have missed it if the scatterer had not been present. This correction, shown in Fig. 1, was calculated graphically from the dimensions of the apparatus on the assumption of isotropic scattering, and was checked experimentally by measuring the scattering cross sections of the gases ethane, ethylene, and methane in the apparatus. Presumably the scattering cross section of the protons in ethane should be nearly the same as the value for the protons in paraffin, paper, etc. It was found that the use of the data of state for ethane[7] and the above correction curve gave a logarithmic transmission curve (within the limits of error) corresponding to a cross section of $46\pm3\times10^{-24}$ cm^2 per proton for room temperature neutrons after the known value for carbon had been subtracted. This is in approximate agreement with the values for paraffin, etc. Ethylene gave the same value and methane gave $36\pm4\times10^{-24}$ cm^2. The corrections to the transmissions are serious for transmissions of fifty percent or less, but the authors believe it to be unlikely that the corrections should introduce

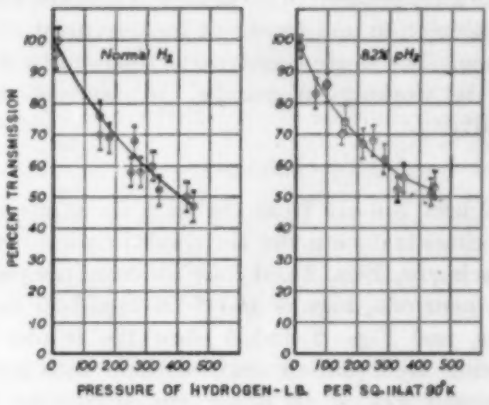

FIG. 2. FIG. 3.

FIGS. 2 and 3. Data for room temperature neutrons and normal H_2 (Fig. 2); 82 percent *para* H_2 (Fig. 3).

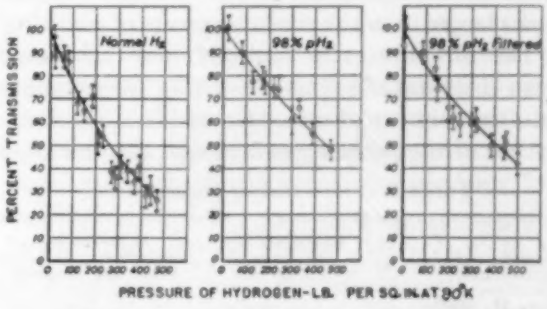

FIG. 4. FIG. 5. FIG. 6.

FIGS. 4, 5, and 6. Data for liquid-air neutrons and normal H_2 (Fig. 4); 98 percent *para* H_2 (Fig. 5); 98 percent *para* H_2 (Fig. 6) after filtering out 50 percent of beam with 98 percent *para* H_2.

[6] A. Farkas, *Orthohydrogen, Parahydrogen and Heavy Hydrogen* (Cambridge University Press, 1935), p. 23.

[7] B. H. Sage, D. C. Webster and W. N. Lacey, Ind. Eng. Chem. **29**, 658 (1937).

more than about five percent error in the absolute value of the cross sections providing the scattering by the hydrogen molecules is approximately isotropic, as it is expected to be.

From the theoretical work[3] it is clear that if the singlet state of the deuteron is virtual, filtering out fifty percent of a beam of liquid-air neutrons with parahydrogen gas at 90°K should result in a reduction in the scattering cross section of parahydrogen for the residual fifty percent. In order to test this point two bombs identical with the one described above were arranged in series in the neutron beam. The first was filled with parahydrogen gas till the beam intensity had fallen to about half-value and the scattering curve was then run with the second bomb. The distances were such that the scattering correction was the same as with the single bomb arrangement. (This point was checked both by calculation and by direct measurement with ethane.) The single counter was replaced by five like it working in parallel to increase the sensitivity.

Results

Figures 2–6 are from the data for scattering experiments done under the conditions indicated in each case. Figs. 2 and 3 are for room temperature neutrons, Figs. 4 and 5 for liquid-air neutrons, and Figs. 5 and 6 show the results of filtering the liquid-air neutron beam with parahydrogen gas at 90°K on the scattering by parahydrogen. Fig. 5 is for the unfiltered beam and Fig. 6 for the filtered beam. The errors indicated in the figures are about one and one-half times larger than the probable errors of counting.

The absolute cross sections were calculated from these data by first converting the pressures into the number of molecules of H_2 in the beam by use of the perfect gas laws and the thickness of the bomb. Correction was then made for scattering of neutrons into the counter which would have missed the counter had the scattering gas been absent. This was done according to Fig. 1. Each point was then plotted on a plot of logarithm of intensity against number of molecules in the beam and the best straight line drawn. The errors for the cross sections were obtained by consideration of the scattering of the points on this plot and are standard deviations.

Table I. *Cross section of protons in* H_2.

Experimental Conditions	Cross Section per Proton ($\times 10^{24}$ cm)	Results of Brickwedde, Dunning, Hoge and Manley[4]
Para H_2 300° neutrons	22±4	15
Ortho H_2 300° neutrons	22±4	28
Para H_2 130° neutrons	19±4	9
Ortho H_2 130° neutrons	39±5	39

Table I shows the four different cross sections obtained from the data together with those of Brickwedde, Dunning, Hoge and Manley[4] obtained with liquid hydrogen.

Comparison of the results with those of Brickwedde, Dunning, Hoge and Manley[4] for liquid hydrogen shows that instead of a fourfold ratio of *ortho* to *para* cross sections for liquid-air neutrons the gas gives a twofold ratio. The authors believe that this can be understood on the basis of the Doppler effect of the motion of the H_2 molecules along the neutron beam direction. (Calculation of this effect with a 130°K Maxwellian neutron velocity distribution and the theoretical curves given by Schwinger and Teller[3] for the variation of the various cross sections with relative velocity of the neutron and the H_2 molecule bears this out more or less quantitatively.)

Of course there is the additional point that the neutrons used in this work may have been somewhat warmer than those used in the work with the liquid. This would cause the *ortho* and *para* cross sections to differ less than they would have with colder neutrons. However, it seems unlikely that this effect could have been large enough to account for the main part of the difference between the two experiments. The whole problem is seriously complicated, in both cases, by the presence of the high energy neutrons which are absorbed by the cadmium shutter but are still much above the energies for which the theoretical calculations apply. It seems to be necessary to eliminate these neutrons before the best results can be obtained from the experiment.

The failure to observe a decrease in parahydrogen cross section on filtering is not contradictory to the results obtained for the liquid because the errors in the gas work are large enough to have masked an effect of the size

found in the liquid. However, the data do show that the filtration effect for gaseous hydrogen is not much larger than that found for the liquid.

In general, the results check the liquid work and show no evidence of serious interference of liquid forces in the scattering phenomena. The difference between the scattering cross sections for ortho- and parahydrogen appear to be large enough to establish definitely a spin dependence of the neutron proton force.

The authors are grateful to Professor Gilbert N. Lewis for the suggestion that a gaseous scatterer be used and for helpful criticism in general. They also are indebted to Professor J. R. Oppenheimer, Dr. Willis E. Lamb, and Dr. L. I. Schiff of the Physics Department and to both Professor Felix Bloch of Stanford University and Professor Enrico Fermi of the University of Rome for advice concerning theoretical aspects of the problem.

FEBRUARY 15, 1939 PHYSICAL REVIEW VOLUME 55

Atomic Electron Velocities in Nitrogen and Methane

A. L. Hughes and Merle A. Starr
Wayman Crow Hall of Physics, Washington University, St. Louis, Missouri
(Received December 30, 1938)

When sufficiently fast electrons are scattered by gas atoms it can be shown that the *distribution of energies* among the inelastically scattered electrons has exactly the same shape as the *distribution of component velocities* among the atomic electrons. An experimental determination of the distribution of energies among the electrons scattered inelastically by nitrogen and methane has been made. From these results the distributions of component velocities among the atomic electrons in nitrogen and methane have been computed. Half of the electrons have component velocities less than 1.80×10^7 cm/sec. in nitrogen, and less than 1.55×10^7 cm/sec. in methane. The experimental results refer to the L electrons only, as the apparatus would not permit the use of electrons of high enough energy to give the same information about the K electrons. The experimentally determined distributions of component velocities among the atomic electrons for nitrogen and methane are decidedly flatter than the theoretical calculated distributions for atomic nitrogen and atomic carbon. No theoretical calculations are available for molecular nitrogen and methane, hence comparisons were made with the calculations for the atoms.

Introduction

MANY investigations, both theoretical and experimental, have been carried out during the last twenty years on the "atomic structure factor." The significance of the factor is that it gives us the probability of finding an electron at each point in the atom. A knowledge of the distribution of momenta among the electrons is complementary to this and is essential to a complete description of the state of the electrons in an atom. Whereas an immense amount of work has been done on the first distribution, that relating to the positions of the electrons, comparatively little has been accomplished in describing the momenta of the electrons. Since the mass of an electron does not depend appreciably on its velocity in the range with which we are concerned, we can use the term "atomic electron velocity" as equivalent to momentum insofar as we are interested in variations of these quantities. Information as to the distribution of atomic electron velocities has been obtained from a study of the profile of the modified band in the Compton effect.[1] A different method was devised later in which a study of the distribution of energies among the electrons scattered by a gas was used to give information about the velocities of atomic electrons.[2] When electrons of sufficient energy are scattered through an appreciable angle by a gas at low pressure it is possible to regard the process as resulting from

[1] P. A. Ross, Proc. Nat. Acad. Sci. **9**, 246 (1923); G. E. M. Jauncey, Phys. Rev. **25**, 314, 723 (1925); J. W. M. DuMond, Phys. Rev. **33**, 643 (1929); J. W. M. DuMond and H. A. Kirkpatrick, Phys. Rev. **37**, 136 (1931); **38**, 1094 (1931); J. W. M. DuMond and A. Hoyt, Phys. Rev. **37**, 1443 (1931); J. W. M. DuMond, Rev. Mod. Phys. **5**, 1 (1933); G. E. M. Jauncey, Phys. Rev. **46**, 667 (1934); J. W. M. DuMond and H. A. Kirkpatrick, Phys. Rev. **52**, 419 (1937); H. A. Kirkpatrick and J. W. M. DuMond, Phys. Rev. **54**, 802 (1938).

[2] A. L. Hughes and M. M. Mann, Jr., Phys. Rev. **53**, 50 (1938). A. L. Hughes and M. A. Starr, Phys. Rev. **54**, 189 (1938).

the interaction of the impinging electron with either the nucleus or an atomic electron. If the "collision parameter" corresponding to the deflection under consideration is much smaller than the average distance between a nucleus and any atomic electron, then we can safely assume that the observed scattering is due to one, and only one, center, i.e., either to a nucleus or to an atomic electron. When this condition obtains we expect to find two distinct groups of scattered electrons, those scattered by the nuclei without loss of energy, and those scattered by the atomic electrons with loss of energy. If the atomic electrons are assumed to be at rest before collision, simple considerations based on the conservation of energy and momentum show that the electrons scattered by them through an angle θ would retain an amount of energy $V_0 \cos^2 \theta$, where V_0 is the energy of the impinging electron. If, however, the atomic electrons are in random motion, the electrons scattered through θ have a distribution of energies symmetrically arranged about $V_0 \cos^2 \theta$, the most probable value. The observed distribution of energies among the scattered electrons can therefore be used to give information as to the way in which the atomic electrons are moving. A particularly simple relationship exists between $f(u)$ the distribution of *component velocities* among the atomic electrons and $F(V'')$ the distribution of *energies* among the scattered electrons. The functions $f(u)$ and $F(V'')$ have precisely the same shape.[3] V'' is the excess energy (positive or negative) which the scattered electron acquires as a result of a collision with an atomic electron which has a component velocity u in a specific direction. (The particular component of velocity which determines V'' is the one which the atomic electron had, before collision, in a direction at right angles to that of the scattered electron after collision. As we may consider the distribution of atomic electron velocities to be isotropic, the determination of any particular component velocity automatically determines the other two, and also the resultant.) Thus a measurement of the distribution of *energies* among the scattered electrons gives at once the distribution of *component velocities*, which can then be compared with theoretical distributions. It can be shown that $f(u)$ is also identical in shape with $f(\lambda'')$ the distribution of intensity across the modified band in the Compton effect. Detailed discussion of the relationships will be found in an earlier paper.[4] These ideas have been applied to the determination of atomic electron velocities in helium and hydrogen.[2] In the present paper we shall discuss an exactly similar investigation to determine the atomic electron velocities in nitrogen and methane. It is un-

[3] G. E. M. Jauncey, Phys. Rev. **50**, 326 (1936).
[4] A. L. Hughes and M. M. Mann, Jr., Phys. Rev. **53**, 50 (1938).

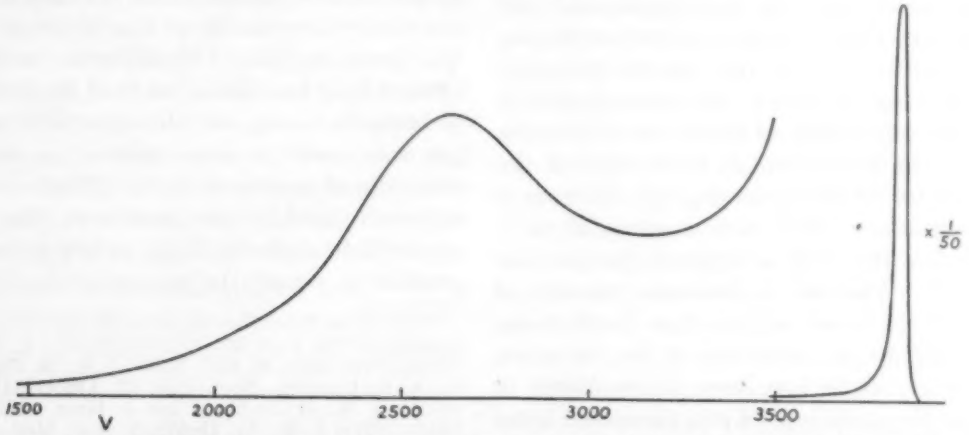

FIG. 1. Distribution in energy of 3825-volt electrons scattered through 34.2° by nitrogen. The narrow peak at 3825 volts (on a 1/50 scale) represents the electrons scattered elastically by the nucleus. The "foot" is due to the modifying effect of the K electrons. Collisions with the L electrons involve a loss of energy $V_0 \sin^2 34.2°$, plus or minus an amount depending on the component velocity of the L electron perpendicular to the direction of observation. The distribution of such component velocities is reflected in the distribution of energies centered at 2640 volts. The asymmetry of this distribution is due to the effect of the "foot" extending from the elastic peak.

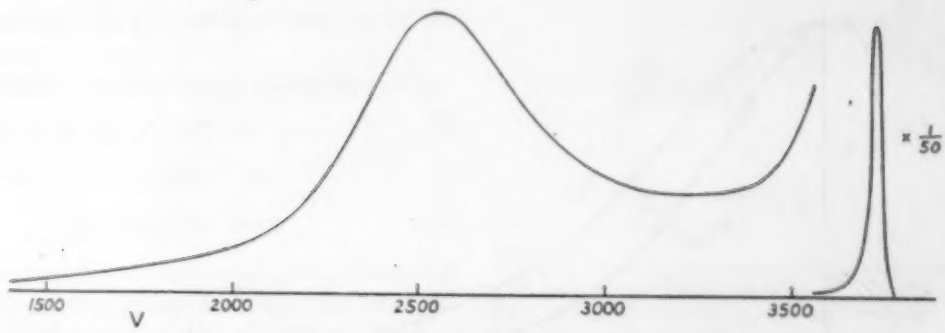

FIG. 2. Distribution in energy of 3725-volt electrons scattered through 34.2° by methane. Conditions for "single center scattering" are better fulfilled than in the case of nitrogen, because of the smaller perturbing effect of the "foot" of the elastic peak on the inelastic band.

necessary to describe the apparatus and method of using it as they are precisely the same as in our experiments on hydrogen and helium. The reader is referred to the published accounts of these experiments.[2]

Nitrogen was obtained from a commercial tank. It was said to be 99.5 percent pure, the chief impurity probably being oxygen. It was passed over hot copper and through charcoal cooled by "dry-ice" into the gas reservoir in our apparatus. Methane was obtained from a tank of the gas at high pressure. The manufacturers stated that the gas contained 86 percent methane, 12 percent ethane and 1 percent each of oxygen and nitrogen. We purified the gas by fractional distillation after condensation by liquid air and rejecting the last tenth of the liquid. This was repeated three times. Unlike the nitrogen, it was not passed through cooled charcoal.

RESULTS

In view of the fact that, in our earlier work on hydrogen and helium,[2] we had obtained the same values for $f(u)$ with incident electrons of various energies, it was not considered necessary in the work on nitrogen and methane to use any electron energy other than the highest we could conveniently use in the apparatus. This was 3800 volts. The angle of scattering was 34.2°, as before. The results are shown in the form of curves (Figs. 1 and 2) similar to those published in the papers on helium and hydrogen. Each curve in Figs. 1 and 2 is a mean curve constructed from nine separate curves representing individual runs. The total number of observations from which each of the curves shown here was drawn, exceeded 250. While the elastic peak is shown in each case in order to follow the scheme adopted in the previous papers, our efforts were concentrated on determining the shape of that part of the curve giving the distribution of inelastically scattered electrons. It will be noticed that the band representing the inelastically scattered electrons is not symmetrical about the maximum. The discussion given later in this paper will show that this lack of symmetry is to be attributed to the fact that we have not completely satisfied the requirements for perfect "single center scattering." To satisfy this requirement for nitrogen and methane calls for much higher electron energies than we can use in our present apparatus.

The ultimate purpose of this research is to determine the value of $f(u)$ for the atomic electrons in nitrogen and methane. Whereas it was possible to use both halves of the inelastic band for hydrogen and helium, since it was symmetrical, to compute $f(u)$, here we choose to use only the left half, or the low energy half. The reason we reject the high energy half is that we believe it to be distorted somewhat by the lack of perfect "single center scattering." A discussion of the underlying reasons for this action will be given later in the paper.

From the low energy half of each of the inelastic bands in Figs. 1 and 2, we obtain a pair of curves giving, by definition, $F(V'')$. As shown in a previous paper,[2] to get $f(u)$ we merely change the abscissas in V'' into abscissas in u (or β) by the substitution

$$\beta(=u/c)\times 10^3=\lambda''=V''\div(0.5782V_0^{\frac{1}{2}}), \quad (1)$$

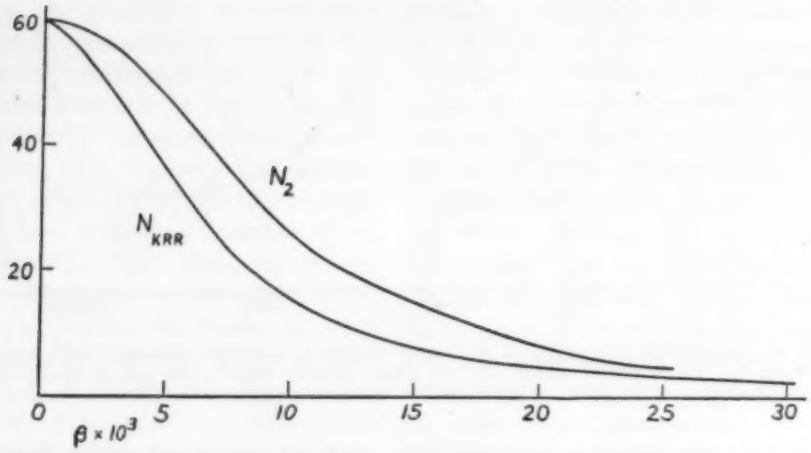

FIG. 3. Distribution of component velocities among the electrons in molecular nitrogen as obtained from the experimental curve shown in Fig. 1, and in atomic nitrogen as computed by Kirkpatrick, Ross and Ritland. (The latter curve includes the K electrons as well as the L electrons.)

where V'' is measured from the center of the inelastic band, V_0 is the energy of the impinging electrons, and c the velocity of light. Should we want to know the shape of the Compton modified band for nitrogen and methane for a primary wave-length of $\lambda = 695$ x.u. and $\theta = 90°$ we take the $F(V'')$ curve and relabel the abscissas in terms of λ'' as computed by the above formula. The experimentally computed $f(u)$ curves for nitrogen and methane are shown in Figs. 3 and 4. As we believe that the results are considerably more accurate than can be indicated in a small sized graph, we give the values of the ordinates of $f(u)$ for different values of u in Table I.

DISCUSSION

The accuracy of the calculated values for the atomic electron velocities depends on the accuracy to which the basic assumptions of the method are satisfied in the experimental measurement. As was shown in the first paper[4] of this series, it is necessary that the collision parameter, p, for a finite deflection of an electron by a scattering center, which may be a nucleus or an atomic electron, be small compared with the average distance between any two scattering centers in order to meet the requirement that the observed scattering must be due to one, and only one, center. If the observed scattering is due to the cooperation of two or more scattering centers, we cannot use our method to compute the atomic electron velocities from the experimental results. In Fig. 5 we have shown the relation between the collision parameters for electrons of 4000 volts energy scattered through 34° by a helium atom, and the mean distance between the nucleus and an atomic electron. This mean distance is taken to be 0.31A which is obtained by combining the mean distance between the nucleus and the electron in a hydrogen atom, *viz.* 0.53A, and $Z' = 1\frac{11}{16}$ as the effective

TABLE I. *Theoretical velocity distributions for atomic electrons in* N *and* C *and experimental velocity distributions for atomic electrons in* N_2 *and* CH_4, *and the profile of the associated Compton modified band for* $\lambda = 695$ *x.u. and* $\theta = 90°$.*

$\beta \times 10^3$ AND λ'' (x.u.)	u (CM/SEC.)	$f(u)$ N (K.R.R.)	$f(u)$ N_2 EXPERIMENTAL	$f(u)$ C (K.R.R.)	$f(u)$ CH_4 EXPERIMENTAL
0	0×10^7	60.0	60.0	60.0	60.0
1	3	57.0	59.3	56.4	59.5
2	6	52.5	57.7	49.8	57.6
3	9	46.9	55.1	42.0	53.5
4	12	41.6	51.7	34.4	48.4
5	15	36.0	47.5	27.4	42.9
6	18	30.6	43.0	22.2	37.5
8	24	21.4	33.9	14.9	27.2
10	30	15.3	25.8	10.8	19.5
12	36	11.4	20.2	8.3	14.5
14	42	8.65	16.6	6.5	11.0
16	48	6.84	13.5	5.2	8.8
18	54	5.5	10.5	4.3	7.5
20	60	4.55	8.0	3.68	6.5
25	75	3.2	4.7	—	4.0
30	90	—	—	1.7	—

* The last four columns could be labeled $f(\lambda'')$ thus giving the profile of the Compton modified band, (1) as calculated by Kirkpatrick, Ross and Ritland, and (2) as predicted from electron scattering experiments.

atomic number for calculating distances in the helium atom.

The collision parameters are given by

$$p_n = (Ze^2/mv^2) \cot \tfrac{1}{2}\theta \qquad (2)$$

for a deflection by a nucleus, and

$$p_e = (2e^2/mv^2) \cot \theta \qquad (3)$$

for a deflection by an atomic electron. Here Z is the atomic number, e the electronic charge, m the mass of the electron, v the velocity of the electron, and θ the angle of deflection. These equations give $p_n = 0.0117$A and $p_e = 0.00525$A for 4000-volt electrons scattered through 34° by helium atoms. One may conclude that when a helium atom scatters 4000-volt electrons through 34°, the scattering is due either to the nucleus or to an atomic electron but not to both.[5] The electrons scattered by a nucleus are distinguished from those scattered by an atomic electron by the fact that the former have the same energy as they had before collision, V_0, and the latter retain only a part, *viz.*, $V_0 \cos^2 \theta$.

We shall now apply these considerations to the nitrogen atom. Using Eqs. (2) and (3), we find

[5] To be sure, there is a possibility that on rare occasions the nucleus and an atomic electron are so orientated that they both contribute deflections of the same order to the observed deflection. If, in Fig. 5, we allow the atomic electron to take all possible positions on a sphere of radius 0.31A whose center is at the nucleus, it is easily seen that the chance of a deflection arising from a considerable contribution by both scattering centers, with the parameters appropriate to 4000-volt electrons, is small enough to be neglected.

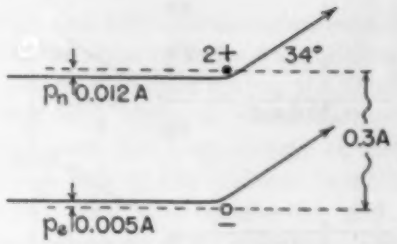

FIG. 5. Relation between collision parameters for 4000-volt electrons scattered through 34° by helium and the most probable nucleus to atomic electron distance in helium.

$p_n = 0.041$A and $p_e = 0.00525$A for 4000-volt electrons deflected through 34°. The mean distance between the nucleus and a K electron is approximately 0.08A, while the mean distance between the nucleus and an L electron is approximately 0.7A. These are shown in Fig. 6. It is evident that we may regard the scattering of 4000-volt electrons through 34° by the L electrons to be as unaffected by the nucleus as in the case of the helium atom. (Indeed by stretching the diagram for helium until it fits over the diagram for nitrogen, and allowing for the partial shielding of the nucleus by the K electrons, it can be seen that the conditions are at least as satisfactory in the case of nitrogen as in the case of helium for the application of our method to the L electrons.) On the other hand, since the distance between a K electron and the nucleus is of the same order as the nuclear collision parameter, p_n, it is impossible to use

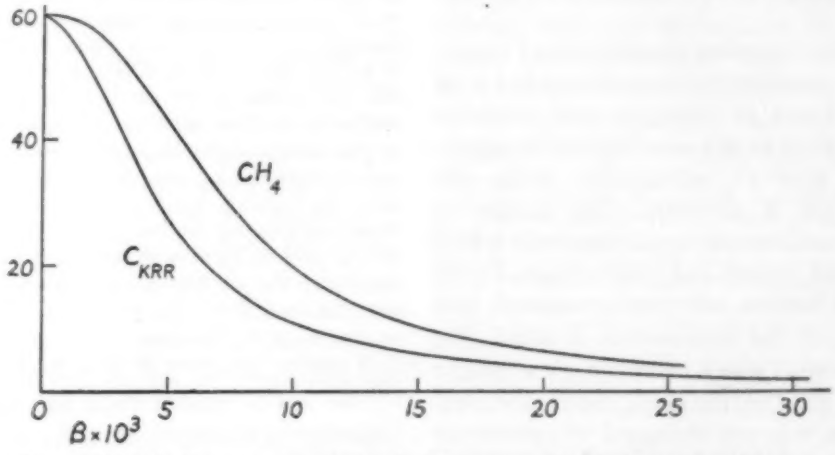

FIG. 4. Distribution of component velocities among the electrons in methane as obtained from the experimental curve shown in Fig. 2, and in atomic carbon as computed by Kirkpatrick, Ross and Ritland. (The latter curve includes the K electrons as well as the L electrons.)

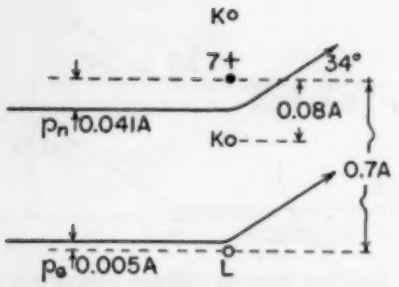

FIG. 6. Relation between the collision parameters for 4000-volt electrons scattered through 34° by nitrogen and the most probable nucleus to atomic electron distances in nitrogen.

our method to determine the velocities of the K electrons by means of 4000-volt electrons. To get the same degree of separation between the effect of a K electron and the effect of the nucleus in the nitrogen atom as we get in the helium atom, we must increase the electron energy by 7/2 to compensate for the change in nuclear charge (see Eq. (2)), and increase it again by a factor of 0.31/0.08 to compensate for the smaller distance between the scattering centers with which we are concerned in nitrogen as compared with the corresponding distance in helium. The final result is a factor of 14. Thus 56,000-volt electrons in nitrogen would be necessary to allow us to calculate the velocities of *all* its atomic electrons with the same degree of accuracy as we obtain in helium at 4000 volts. However, if we are content with information about the velocities of the L electrons, then it is quite unnecessary to use electrons of energy 56,000 volts.

In view of the foregoing considerations it may be asked why experiments were attempted with 4000-volt electrons in nitrogen and methane when it was known in advance that the measurements would give no information about the velocities of the K electrons. The answer is that we had available the apparatus with which very dependable results had been obtained with hydrogen and helium and that it seemed well worth getting all the information it could give us about some other gases, even though we might have to forego information about the K electrons. The apparatus was not designed to operate at more than about 4000 volts. However within its operating range it gave excellent results with helium and hydrogen as judged by the remarkable agreement between our results and those obtained by a totally different method using the scattering of x-rays,[6] and as judged by the agreement in the case of helium with Hicks' theoretical computations.[7] These considerations lead us to infer that the apparatus when used for helium and hydrogen yielded unusually dependable values for $f(u)$ and that unrecognized sources of error in the apparatus and method do not exist to any considerable extent. It seemed highly desirable therefore to use the same apparatus, without modification, for the study of other gases. The results so obtained could then be regarded just as dependable as those obtained for hydrogen and helium, even though they are limited to electrons outside the K shell. The results would also have value for comparison with the results obtained with a future apparatus of very different design in which we hope to make use of electrons of much higher energies to secure information about the K electrons.

The investigation on nitrogen and methane cannot be regarded as fully completed until we have as much information about the velocities of the K electrons as we have about the L electrons. All that is necessary—in principle at any rate—is to use electrons with energies of the order of 50,000 volts. However the change from our present apparatus to one suitable for use with 50,000-volt electrons introduces a number of difficult technical problems. In the first place a different kind of electron gun will have to be developed. Difficulties due to high voltage will be much accentuated, and in particular it is doubtful whether our present type of electrostatic analyzer will stand the necessary 16,000 volts. However, a magnetic analyzer would remove this particular difficulty but it has the disadvantage that it does not give directly a distribution in energy. The greatest difficulty of all is in connection with the measurement of the scattered electrons. The number of scattered electrons varies inversely as the square of the energy of the impinging electrons. Moreover we cannot offset this by making the defining slits wider, for, since the inelastic band will be relatively narrower at higher energies, we need at least as good resolution as we have at present. In view of the fact that, with our present apparatus, the number of scattered electrons is so small as to tax our FP-54 tube severely, it seems that we shall be compelled to measure the scattered electrons by a G-M counter tube when we go to much higher energies.

The bands representing the distributions of inelastically scattered electrons, shown in Figs. 1

[6] H. A. Kirkpatrick and J. W. M. DuMond, Phys. Rev. **54**, 802 (1938); J. W. M. DuMond and H. A. Kirkpatrick, Phys. Rev. **52**, 419 (1937).
[7] B. Hicks, Phys. Rev. **52**, 436 (1937).

and 2, are unsymmetrical about the (inelastic) maximum. This is to be attributed to the disturbing effect of the "foot" which makes the elastic peak unsymmetrical and extends from it towards smaller energies. Because of the rapid way it falls off, it has a negligible distorting effect on the *low* energy side of the inelastic band, even though the effect on the *high* energy side is appreciable. The "foot" is probably due to the combined effect of the nucleus and the K electrons on the impinging electrons which pass close to them. Had only the nucleus been involved, the electrons passing close to it would have lost no energy and the elastic peak would have been as narrow as the resolution would allow. The presence of the K electrons in the vicinity of the nucleus modifies the situation. The scattering center is now made up of a nucleus together with two K electrons. Inasmuch as these electrons are of small mass, it is possible for them to be set in motion by the impinging electron thereby taking energy away from it. Thus we may see qualitatively how the complex center may result in an appreciable number of electrons being scattered with some loss of energy, in addition to those which are scattered elastically. The situation is, in fact, very similar to the scattering of low energy electrons (say below 300 volts) by helium atoms since the nucleus and the two K electrons constitute a system exactly like a helium atom. We may summarize the broader features of the experimental results with low energy electrons in helium by saying that most electrons are scattered without any loss of energy (giving the elastic peak) and that the number of electrons losing energy decreases very rapidly as the amount of that energy loss increases. Returning again to our present experiments, this is just what we observe to happen near the elastic peak and which is to be explained by similarity of the inner part of the nitrogen atom to the helium atom. Thus when the two sides of the inelastic band are unsymmetrical, it is clear that the *low* energy side is the one to use in computing the atomic electron velocities.

This use of the low energy side of the inelastic band may also be justified by the following argument. In the earlier work on helium and hydrogen[2] both sides of the inelastic bands obtained with 3000- and 4000-volt electrons were identical and led to the same value for $f(u)$ the distribution of component velocities among the atomic electrons. But with 1000-volt electrons the foot of the elastic peak was large enough to distort the high energy side of the inelastic band, yet the low energy side was unaffected and led to the same values for $f(u)$ as before. This result then gives us an empirical justification for using only the low energy side of an inelastic band when it is unsymmetrical.

In the experiments on hydrogen and helium it was possible to compare the experimental values of $f(u)$ with the values calculated by wave mechanics. Unfortunately no such calculations are available for comparison with our results on nitrogen and methane. We are forced therefore to attempt a comparison with what calculations are available. Kirkpatrick, Ross and Ritland have calculated $f(u)$ values for atomic carbon and atomic nitrogen.[8] We shall compare these with our experimental results for molecular nitrogen and methane. One might perhaps expect a considerable divergence between the experimental $f(u)$ curve for methane and the theoretical $f(u)$ curve for atomic carbon, because of the modifying effect of the four hydrogen atoms. However it is interesting and perhaps significant to find that the experimental $f(u)$ curves for nitrogen and methane obtained in this paper and for hydrogen obtained in an earlier paper are all wider, and by approximately the same amount, than the theoretical curves computed by Kirkpatrick, Ross and Ritland for atomic nitrogen, carbon and hydrogen.[9] The comparisons are shown graphically in Figs. 3 and 4 and in Table I. No further comparison between theory and experiment can be made in this field until

[8] P. Kirkpatrick, P. A. Ross, and H. O. Ritland, Phys. Rev. **50**, 928 (1936). These authors actually express their results in terms of $f(\lambda'')$ which gives the profile of the modified band in the Compton effect, for x-rays of wave-length 695 x.u. scattered through 90°. To convert their computed $f(\lambda'')$ curves into $f(u)$ curves, all that is necessary is to relabel the abscissas in terms of u in place of λ'' by means of Eq. (1).

[9] Some question might be raised as to why we do not make the comparison with the theoretical work of Hicks in the case of hydrogen. While admitting that Hicks' work is probably the more accurate as judged by the better agreement with our previous results on hydrogen, it seemed somewhat more consistent to make the comparison for all three cases with the theoretical curves of Kirkpatrick, Ross and Ritland since all their computations were made according to the same procedure.

theoretical physicists provide us with $f(u)$ values computed for molecules. It is unfortunate that the gases which are relatively easy to study experimentally are very difficult to investigate theoretically.

We take this opportunity of thanking Professor Kirkpatrick for sending us the numerical values of the $f(\lambda'')$ curves for atomic carbon and nitrogen. The senior author takes pleasure in acknowledging the assistance afforded by a grant from the Penrose Fund of the American Philosophical Society.

FEBRUARY 15, 1939 PHYSICAL REVIEW VOLUME 55

Scattering of Fast Electrons in Gases

A. L. HUGHES
Wayman Crow Hall of Physics, Washington University, St. Louis, Missouri
(Received December 30, 1938)

When sufficiently fast electrons are scattered elastically by atoms, it is possible to regard the effect as being due to the nuclei alone, the atomic electrons playing only a negligible part. The criterion which will allow such a simplification to be made is that the collision parameter for a deflection of an incoming electron by the nucleus must be small compared with the distance between the nucleus and the nearest atomic electron. When this is the case, the observed scattering should be that predicted by the Rutherford scattering formula. Kuper has recently made an experimental investigation of the scattering of electrons of energy above 49,000 volts by helium, neon and argon. His results for helium can be accounted for on the viewpoint proposed, *viz.*, that the nucleus is almost entirely responsible for the observed scattering and that, to a first approximation, the scattering is simple Rutherford scattering. The wave-mechanical formula, which takes into account the effect of the atom as a whole does not give as good agreement with Kuper's results for helium as the Rutherford scattering formula.

THE purpose of this note is to call attention to a simple way of interpreting certain experimental results in the scattering of fast electrons by gases, and in particular to apply it to an important experimental investigation recently published by Kuper.[1] Since an atom is made up of various centers (the nucleus and the atomic electrons), each individually acting on an electron passing through it with a force varying inversely as the square of the distance between the center and the electron, it is natural to regard the scattering of electrons by a single center of force as a first step in discussing the scattering of electrons by an atom. An electron of mass m, charge e and velocity v, on approaching a nucleus whose charge is Ze will be deflected by it. If p_n is the collision parameter, the angle of deflection θ will be given by

$$p_n=(Ze^2/mv^2)\cot(\theta/2). \quad (1)$$

If the scattering center is an electron at rest, the angle of deflection θ is related to the collision parameter by

$$p_e=(2e^2/mv^2)\cot\theta. \quad (2)$$

[1] J. B. Horner Kuper, Phys. Rev. **53**, 993 (1938).

The scattering of an electron passing through the atom is ordinarily the result of the interaction of that electron with several, possibly all, of the scattering centers in the atom. We could visualize the scattering of electrons by an atom as the result of each scattering center in the atom acting on the incoming electrons with an inverse square force. The mathematical difficulties encountered in attempting to solve such a problem are so formidable that no attempt has been made along these lines. The problem has been attacked successfully along very different lines. The electron stream impinging on the atom is replaced by an electron wave of the proper wave-length, and the atom is replaced by a region of suitably varying refractive index. Methods carried over from physical optics lead to scattering formulas. In many cases the results are in excellent quantitative accord with experiment and it may be concluded that, in principle, this wave-mechanical approach is quite satisfactory. In those cases in which quantitative agreement is wanting, it is generally due to technical mathematical difficulties in securing exact solutions of the equations.

A simpler viewpoint can be adopted with quantitative accuracy provided a certain condition is satisfied. The condition is as follows. If the collision parameter is much smaller than the distance between any two scattering centers in the atom, then any scattering that takes place can safely be attributed to one, and only one, scattering center. When this condition holds, we can apply the scattering formulas for the interaction of an electron with either a nucleus or another electron. This simplified viewpoint has been used successfully by the author and his collaborators.[2] It is of interest to show that it can be applied with fair success to Kuper's results on the scattering of fast electrons by helium atoms.

Kuper measured the elastic scattering of electrons with energies from 49,500 to 87,700 electron volts, through angles between about 0.5° and 2.5°, by helium, neon and argon. He compared his experimental results with the wave-mechanical calculations of Mott and Massey. While satisfactory agreement was obtained in the case of argon and neon, no agreement at all was found in the case of helium. We shall show, first of all, that the relation of the collision parameters to the distance between the nucleus and an atomic electron in the helium atom, for the scattering of 50,000-volt electrons through 1°, is such as to allow us to regard the scattering as a good approximation to a single center scattering problem. The relation is shown to scale in Fig. 1. It is evident that the electrons, passing close

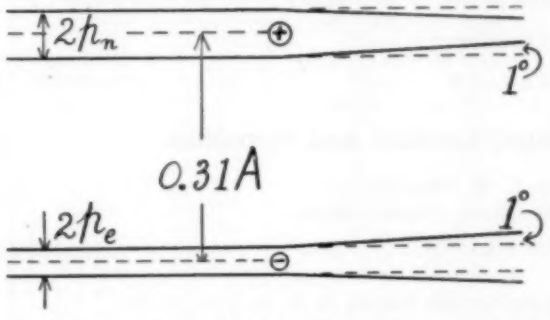

FIG. 1. Comparison of the collision parameters for the scattering of 50,000-volt electrons through 1° by a helium atom with the most probable distance between the nucleus and an atomic electron. The incoming electrons move from left to right.

[2] A. L. Hughes and S. S. West, Phys. Rev. **50**, 320 (1936); **52**, 43 (1937). A. L. Hughes and Marvin M. Mann, Jr., Phys. Rev. **53**, 50 (1938). A. L. Hughes and Merle A. Starr, Phys. Rev. **54**, 189 (1938). A. L. Hughes and Merle A. Starr (preceding paper).

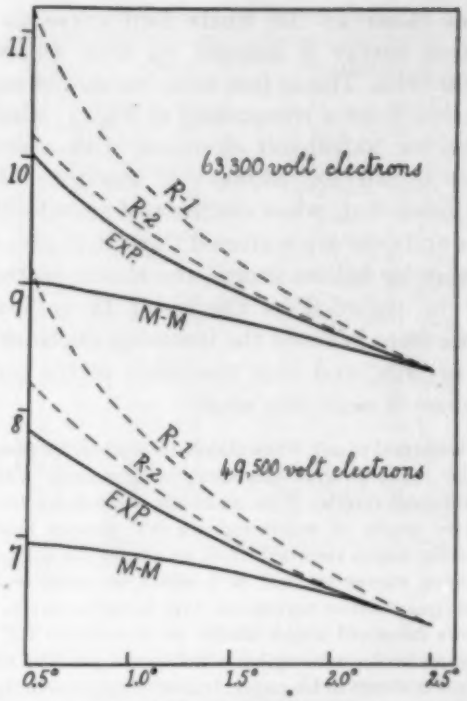

FIG. 2. Scattering of fast electrons through small angles by helium. EXP.—experimental values due to Kuper. M–M.—theoretical curve due to Mott and Massey. R–1.—Rutherford scattering. R–2.—Rutherford scattering on the assumption that the effective angle differs from the measured angle by 0.5°. The ordinates are the logarithms of the scattered current.

enough to the nucleus to be scattered through 1°, are practically unaffected by the presence of the atomic electrons. This justifies us in supposing that the elastic scattering is due practically entirely to the nucleus and that the well-known formula for scattering by a nucleus applies. According to this, the number of electrons scattered through unit solid angle at θ should be proportional to $\mathrm{cosec}^4(\theta/2)$, the well-known Rutherford scattering law. In Fig. 2 we have reproduced Kuper's experimental curves for 49,500- and 63,300-volt electrons, together with those calculated from Mott and Massey's theory. It will be seen that not only is there no numerical agreement but that the curvature of the experimental and theoretical curves are in opposite directions. The curves marked R–1 are calculated by means of the Rutherford scattering law. While the R–1 curves are steeper than the experimental curves, it is interesting to note that their curvatures are in the same direction. It is of some significance that the experimental curve

comes closer to the Rutherford curve as the electron energy is stepped up from 49,500 to 63,300 volts. This is just what we should expect to follow from a comparison of Fig. 1, which is drawn for 50,000-volt electrons, with a similar figure drawn for 63,000-volt electrons. It is concluded that, when electrons of energy 50,000 volts and over are scattered through angles of 1° or more by helium atoms, the elastic scattering may be regarded as the result of an inverse square force between the incoming electrons and the nucleus, and that the effect of the atomic electrons is negligibly small.

It is natural to ask if the simple interpretation proposed can be made to give quantitative agreement with the experimental results. If we make the assumption that the effective angles of scattering are 0.5° greater than the scattering angles recorded, then we obtain the Rutherford scattering curves marked R–2 which are seen to be in almost quantitative agreement with Kuper's curves. That Kuper's measured angles should be in error by 0.5° is of course an *ad hoc* assumption which is not justified by any internal evidence in his paper. Indeed Kuper states that his angles were correct of 0.05°. It could be argued, however, that while the measured angles are correct to 0.05°, the effective angles may differ appreciably from the measured angles. In experiments of this kind the stream of electrons shot into the gas is not a strictly parallel beam. The electrons accepted by the analyzer are also to be found in a narrow cone. We have therefore the difficult problem of determining just what the effective angle is when we have a stream of electrons limited within a narrow cone from which electrons are scattered into another cone, which makes an angle of only 1° or so with the first, and when in addition, the scattering varies inversely as the fourth power of the angle. As in all problems of scattering of electrons in gas, it is necessary to correct for the change in scattering volume as the angle θ alters by introducing a factor of $\sin\theta$. This factor is very sensitive to errors in θ when it is small. In addition the factor $\sin\theta$ is strictly true only for intersecting cylinders and when the primary and scattered electrons are quite parallel to the axes of their respective cylinders. The replacement of intersecting cylinders by intersecting cones, especially at very small angles, may make $\sin\theta$ only a rough approximation as a scattering volume correction factor. These considerations indicate that the accurate determination of the effective angle in a small angle scattering experiment is a very difficult matter. The uncertainty in the effective angle may possibly account for some, or perhaps all, of the differences between the experimental curves and the curves computed by the Rutherford scattering formula.

It is not the purpose of the preceding paragraph to insist that we must add 0.5° to each of Kuper's angles, but merely to point out that one should be aware of the real difficulty in determining the effective scattering angle when it is very small. The main purpose of this paper is to point out that the elastic scattering of fast electrons by helium may be regarded as a simple Rutherford scattering by the nucleus and that it gives a better description of what happens than the more complicated Mott and Massey formula. In the case of argon and neon the Rutherford scattering is unapplicable because there are many more scattering centers in the atom. In particular the K electrons are so close to the nucleus that the distance between either of them and the nucleus is no longer much larger than the collision parameter p_n. Hence the considerations raised in this paper do not apply to neon and argon.

FEBRUARY 15, 1939 PHYSICAL REVIEW VOLUME 55

Sodium-Like Spectra of Potassium, Calcium and Scandium

P. GERALD KRUGER AND L. W. PHILLIPS
Physics Department, University of Illinois, Urbana, Illinois
(Received December 30, 1938)

Further identifications have been made in the sodium-like spectra of K, Ca and Sc. The constant second difference law has been used for some time in the analysis of spectra of isoelectronic ions. It is shown that this second difference can be calculated readily, and that to a first approximation it depends only on the total quantum numbers of the initial and final states. Correspondence between calculated and observed second differences is shown for several transitions. Application of the law to ionization potentials is indicated.

REFERENCES to previous work on the first six ions of the sodium sequence are listed in a paper on the Cl VII spectrum recently reported from this laboratory.[1] Edlén[2] has re-

[1] L. W. Phillips, Phys. Rev. **53**, 248 (1938).
[2] B. Edlén, Zeits. f. Physik **100**, 621 (1936).

ported the identification of several multiplets in the spectra of each of the ions from K IX to Cu XIX. The potassium and calcium lines which he has identified were taken from the wavelength table published by Ekefors.[3]

From plates taken in this laboratory on the twenty-one-foot grazing incidence vacuum spectrograph, it has been possible to identify a number of additional lines as radiations belonging to the sodium-like ions, K IX and Ca X. Three more multiplets in Sc XI, which were either outside the range of Edlén's instrument or too weak to be observed, have also been identified.

Potassium spectrograms were obtained by using electrodes made by packing KCl in an aluminum shell, and the K lines sorted out by comparison with an adjacent LiCl-Al spectrum. Aluminum lines, or lines from an overlapping copper spectrum, served as standards. A calculation based on the series $3p-nd$ was used to fix absolute term values.

Calcium and scandium lines belonging to the sequence were identified on plates taken for previous investigations.[4, 5] In the case of calcium, absolute term values were obtained from the series $3d-nf$.

Edlén, in the paper mentioned above, has given absolute term values for all ions, his complete term tables are based on an extrapolation of the Moseley law for the $4f\,^2F$ term. On this basis, he obtains 174.90 volts and 210.21 volts for the ionization potentials of K IX and Ca X, respectively. From the present series calculations, the values 175.10 volts and 210.29 volts are obtained. Since the series calculations are based on only three series members, it is entirely possible that the extrapolation method gives results which are as nearly correct as those based on the calculation of the series limit, especially since the first six ions of the sequence have been quite completely analyzed, and are known to be regular in every respect.

Absolute term values for K IX and Ca X listed in Tables IV and V are based on the series limit calculations. Classified lines are listed in Tables I and II.

A list of the newly identified lines in Sc XI is given in Table III. Since no series of more than

TABLE I. *Classified lines of* K IX.

INT	λ(VAC.)	ν(CM^{-1})	CLASSIFICATION
5	636.300*	157,159	$3s\ ^2S_{1/2} - 3p\ ^2P_{1/2}$
9	621.422*	160,921	$\ ^2S_{1/2}\quad\ ^2P_{3/2}$
4	466.943	214,159	$3p\ ^2P_{3/2} - 3d\ ^2D_{5/2}$
2	459.498	217,629	$\ ^2P_{1/2}\quad\ ^2D_{3/2}$
3	260.834	383,386	$3d\ ^2D_{5/2} - 4p\ ^2P_{1/2}$
5	260.052	384,538	$\ ^2D_{3/2}\quad\ ^2P_{3/2}$
15	205.862*	485,762	$3d\ ^2D_{5/2} - 4f\ ^2F_{7/2}$
12	205.772*	485,975	$\ ^2D_{3/2}\quad\ ^2F_{5/2}$
10	185.883*	537,973	$3p\ ^2P_{3/2} - 4s\ ^2S_{1/2}$
7	184.586*	541,750	$\ ^2P_{1/2}\quad\ ^2S_{1/2}$
1	147.973	675,799	$3p\ ^2P_{3/2} - 4d\ ^2D_{5/2}$
8	147.943	675,936	$\ ^2P_{3/2}\quad\ ^2D_{5/2}$
6	147.157	679,546	$\ ^2P_{1/2}\quad\ ^2D_{3/2}$
5	145.753	686,092	$3d\ ^2D_{5/2} - 5f\ ^2F_{7/2}$
5	145.702	686,332	$\ ^2D_{3/2}\quad\ ^2F_{5/2}$
4	131.896	758,173	$3s\ ^2S_{1/2} - 4p\ ^2P_{1/2}$
6	131.646	759,613	$\ ^2S_{1/2}\quad\ ^2P_{3/2}$
4	112.581	888,249	$3p\ ^2P_{3/2} - 5d\ ^2D_{5/2}$
2	112.113	891,957	$\ ^2P_{1/2}\quad\ ^2D_{3/2}$

* Reported by Edlén.

TABLE II. *Classified lines of* Ca X.

INT	λ(VAC.)	ν(CM^{-1})	CLASSIFICATION
2	574.007*	174,214	$3s\ ^2S_{1/2} - 3p\ ^2P_{1/2}$
4	557.740	179,295	$3s\ ^2S_{1/2} - 3p\ ^2P_{3/2}$
1	420.493	237,816	$3p\ ^2P_{3/2} - 3d\ ^2D_{3/2}$
8	419.757*	238,233	$3p\ ^2P_{3/2} - 3d\ ^2D_{5/2}$
3	411.690	242,901	$3p\ ^2P_{1/2} - 3d\ ^2D_{3/2}$
	(207.386)†	(482,192)	$3d\ ^2D_{3/2} - 4p\ ^2P_{1/2}$
2	206.746	483,685	$3d\ ^2D_{3/2} - 4p\ ^2P_{3/2}$
10	167.034*	598,681	$3d\ ^2D_{3/2} - 4f\ ^2F_{7/2}$
8	166.945*	599,000	$3d\ ^2D_{3/2} - 4f\ ^2F_{5/2}$
6	153.012*	653,544	$3p\ ^2P_{3/2} - 4s\ ^2S_{1/2}$
3	151.832*	658,623	$3p\ ^2P_{1/2} - 4s\ ^2S_{1/2}$
5	123.733	808,189	$3p\ ^2P_{3/2} - 4d\ ^2D_{5/2}$
2	122.995	813,044	$3p\ ^2P_{1/2} - 4d\ ^2D_{3/2}$
4	118.223	845.856	$3d\ ^2D_{5/2} - 5f\ ^2F_{7/2}$
2	118.174	846,210	$3d\ ^2D_{3/2} - 5f\ ^2F_{5/2}$
2	111.197	899,305	$3s\ ^2S_{1/2} - 4p\ ^2P_{1/2}$
3	110.962	901,209	$3s\ ^2S_{1/2} - 4p\ ^2P_{3/2}$
2	101.977	980,613	$3d\ ^2D_{3/2} - 6f\ ^2F_{7/2}$
2	93.502	1,069,500	$3p\ ^2P_{3/2} - 5d\ ^2D_{5/2}$
1	93.069	1,074,470	$3p\ ^2P_{1/2} - 5d\ ^2D_{3/2}$

* Identified by Edlén.
† Obscured by close Cu triplet.

TABLE III. *Newly classified lines in* Sc XI.

INT	λ(VAC.)	ν(CM^{-1})	CLASSIFICATION
2	522.810	191,274	$3s\ ^2S_{1/2} - 3p\ ^2P_{1/2}$
4	505.117	197,974	$3s\ ^2S_{1/2} - 3p\ ^2P_{3/2}$
7	381.151	262,363	$3p\ ^2P_{3/2} - 3d\ ^2D_{3/2}$
3	372.507	268,451	$3p\ ^2P_{1/2} - 3d\ ^2D_{3/2}$
5	105.145	951,070	$3p\ ^2P_{3/2} - 4d\ ^2D_{3/2}$
3	104.441	957,480	$3p\ ^2P_{1/2} - 4d\ ^2D_{3/2}$
4	97.841	1,022,070	$3d\ ^2D_{3/2} - 5f\ ^2F_{7/2}$
2	97.788	1,022,620	$3d\ ^2D_{3/2} - 5f\ ^2F_{5/2}$

[3] E. Ekefors, Zeits. f. Physik **71**, 53 (1931).
[4] P. G. Kruger and L. W. Phillips, Phys. Rev. **51**, 1087 (1937).
[5] P. G. Kruger and H. S. Pattin, Phys. Rev. **52**, 621 (1937).

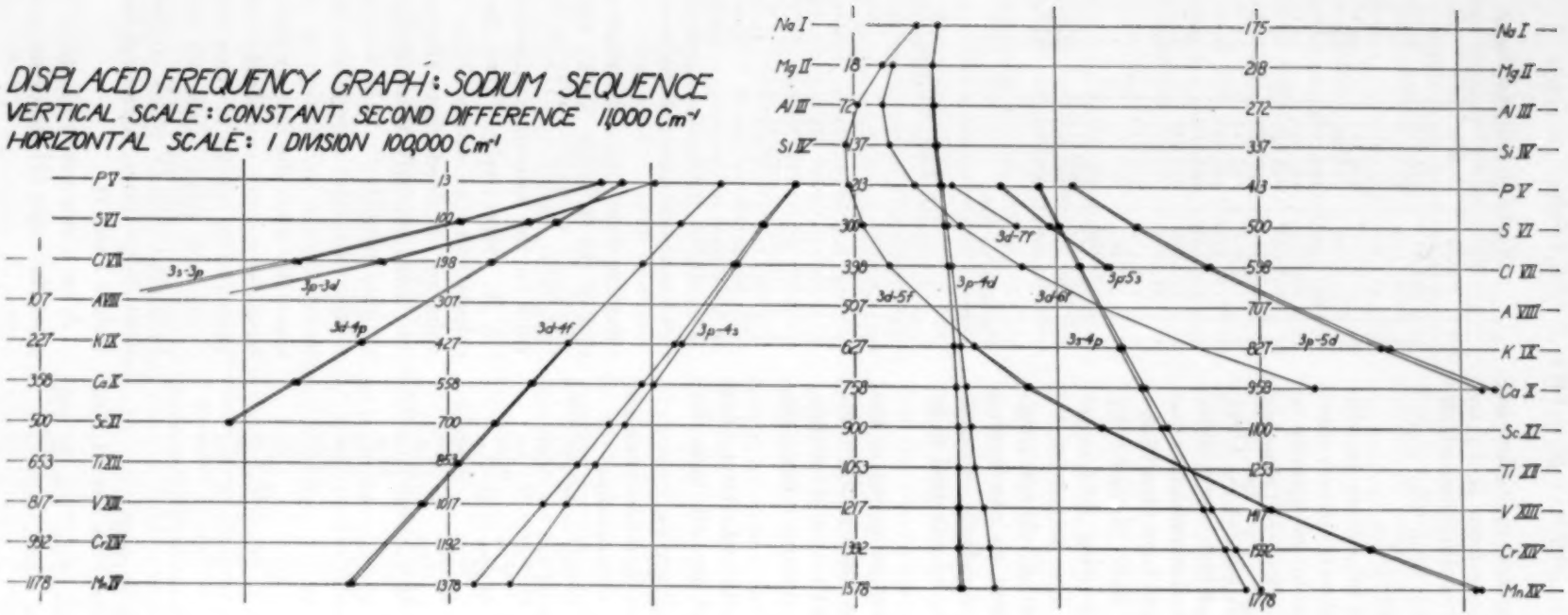

FIG. 1. Displaced frequency diagram for the ions Na I-Mn XV. Constant second difference is 11,000 cm^{-1}. Horizontal scale, 1 division = 100,000 cm^{-1}. (We wish to take this opportunity to point out an error in Fig. 1 of the Cl VII report, reference 1. Both in the diagram and in the caption the transition labeled $3p-3d$ should have been $3p-4d$.)

TABLE IV. K IX *term values and effective quantum numbers.*

CONFIGURATION	TERM VALUE	n^*
$3s\ ^2S_{1/2}$	1,419,425	2.5024
$3p\ ^2P_{1/2}$	1,262,266	
$^2P_{3/2}$	1,258,500	2.6576
$3d\ ^2D_{3/2}$	1,044,637	
$^2D_{5/2}$	1,044,345	2.9174
$4s\ ^2S_{1/2}$	720,523	3.5123
$4p\ ^2P_{1/2}$	661,251	
$^2P_{3/2}$	659,810	3.6704
$4d\ ^2D_{3/2}$	582,722	
$^2D_{5/2}$	582,564	3.9061
$4f\ ^2F_{5/2}$	558,662	
$^2F_{7/2}$	558,583	3.9891
$5d\ ^2D_{3/2}$	370,311	
$^2D_{5/2}$	370,251	4.8997
$5f\ ^2F_{5/2}$	358,305	
$^2F_{7/2}$	358,253	4.9811

TABLE V. Ca X *term values and effective quantum numbers.*

CONFIGURATION	TERM VALUE	n^*
$3s\ ^2S_{1/2}$	1,704,660	2.5372
$3p\ ^2P_{1/2}$	1,530,446	
$^2P_{3/2}$	1,525,365	2.6822
$3d\ ^2D_{3/2}$	1,287,547	
$^2D_{5/2}$	1,287,133	2.9199
$4s\ ^2S_{1/2}$	871,822	3.5478
$4p\ ^2P_{1/2}$	805,355	
$^2P_{3/2}$	803,450	3.6957
$4d\ ^2D_{3/2}$	717,401	
$^2D_{5/2}$	717,176	3.9117
$4f\ ^2F_{5/2}$	688,547	
$^2F_{7/2}$	688,452	3.9925
$5d\ ^2D_{3/2}$	455,974	
$^2D_{5/2}$	455,869	4.9063
$5f\ ^2F_{5/2}$	441,337	
$^2F_{7/2}$	441,277	4.9868
$6f\ ^2F_{7/2}$	306,520	5.9834

TABLE VI. Sc XI *term values and effective quantum numbers.*

CONFIGURATION	TERM VALUE	n^*
$3s\ ^2S_{1/2}$	2,015,340	2.5668
$3p\ ^2P_{1/2}$	1,824,070	
$^2P_{3/2}$	1,817,370	2.7030
$3d\ ^2D_{3/2}$	1,555,620	
$^2D_{5/2}$	1,555,010	2.9222
$4s\ ^2S_{1/2}$	1,037,620	3.5773
$4p\ ^2P_{1/2}$	963,700	
$^2P_{3/2}$	961,170	3.7168
$4d\ ^2D_{3/2}$	866,590	
$^2D_{5/2}$	866,300	3.9150
$4f\ ^2F_{5/2}$	832,460	
$^2F_{7/2}$	832,350	3.9941
$5f\ ^2F_{5/2}$	533,000	
$^2F_{7/2}$	532,940	4.9915

two members has been classified, a reasonably accurate series calculation is impossible. Term values for the newly identified levels have been obtained by merely fitting them into the term table published by Edlén. The complete term scheme is given in Table VI.

The relationship of these spectra to the spectra of other ions in the sequence is shown in Figs. 1 and 2. In Fig. 1, the irregular doublets $3s\ ^2S-3p\ ^2P$ and $3p\ ^2P-3d\ ^2D$ are plotted on a constant first difference graph. Fig. 2 is a displaced frequency graph plotted with a constant second difference of 11,000 cm^{-1}. It is interesting to note that of all the transitions plotted, only those for which the total quantum number changes from 3 to 4 give straight lines.

It was pointed out by Kruger and Pattin[5] that one would expect the constant second difference law to apply in those cases where there is a change in quantum number, and that one would expect the second differences to vary slightly as a result of small variations in the screening constants. If one neglects the variation in screening constants, it is possible to calculate the second differences.

If the term values are expressed by

$$T_1=R(Z-\sigma_1)^2/n_1^2 \quad \text{and} \quad T_2=R(Z-\sigma_2)^2/n_2^2,$$

then the radiated frequency of a transition between the two states is given by

$$\nu=R(Z-\sigma_2)^2/n_2^2-R(Z-\sigma_1)^2/n_1^2.$$

If now one writes down the frequencies ν' and ν'' for the corresponding transitions in the next two ions of the sequence, $(Z+1)$ and $(Z+2)$, respectively, one obtains for the first difference

$$\Delta_1=\nu'-\nu=(n_1n_2)^{-2}[(2Z+1)R(n_1^2-n_2^2) -2R\{n_1^2(\sigma_2'-\sigma_2)-n_2^2(\sigma_1'-\sigma_1)\} +R\{n_1^2(\sigma_2''-\sigma_2^2)-n_2^2(\sigma_1''-\sigma_1^2)\}],$$

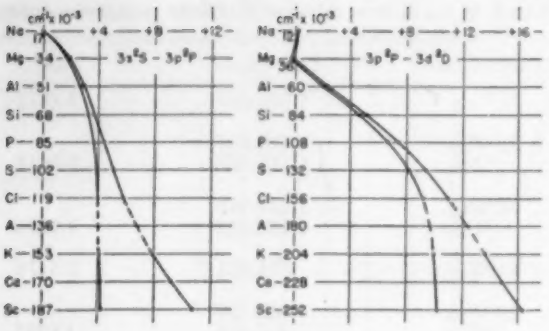

FIG. 2. Displaced frequency diagram for the irregular doublets $3s-3p$ and $3p-3d$.

where the primes refer to the ion of atomic number $(Z+1)$. Experimentally it is observed that for a particular state the σ's vary quite slowly from ion to ion, i.e., $(\sigma_n'-\sigma_n)\to 0$. Assuming $\sigma_n'=\sigma_n$, we can write that approximately

$$\Delta_1=\nu'-\nu=(2Z+1)R(n_1^2-n_2^2)/(n_1n_2)^2.$$

Similarly,

$$\Delta_1'=\nu''-\nu'=[(2Z+3)R(n_1^2-n_2^2)/n_1n_2]^2,$$

and the second difference becomes

$$\Delta_1'-\Delta_1=\Delta_2=2R(n_1^2-n_2^2)/(n_1n_2)^2.$$

That is, the second difference, to a first approximation, depends only on the quantum numbers, and is independent of Z. Deviations of the experimental second differences from the calculated differences will be a measure of the variation in screening constants.

Second differences have been calculated for several different quantum number changes, by using for R the value of the Rydberg constant for infinite mass. The calculated differences are listed in Table VII, together with observed second differences for a number of transitions for comparison. In almost all cases it is found that the observed differences, for the first few ions of a sequence, show comparatively large deviations from the calculated values, but for the higher stages of ionization, approach more or less asymptotically a limiting value which agrees quite well with the calculated second difference. The observed Δ_2's listed in Table VII were

TABLE VII. *Calculated and observed second differences.*

n FOR INITIAL STATE	n FOR FINAL STATE	CALC. Δ_2 (cm^{-1})	OBS. Δ_2 (cm^{-1})	SEQUENCE	TRANSITION
2	3	30,510	30,600	Li I-O VI[1]	$2s\ ^2S-3p\ ^2P$
			30,000	Ne I-Al IV[1]	$2p\ ^2P-3s\ ^2S$
2	4	41,260			
2	5	46,090			
3	4	10,750	10,600	S I-Fe IX[1, 2]	$3s^23p^4\ ^3P-3s^23p^34s\ ^3S$
			10,500	S I-Fe IX[1, 2]	$3s^23p^4\ ^1D-3s^23p^34s\ ^1D$
			10,800	Ni I-Br VIII[1, 3]	$3d^{10}\ ^1S-3d^94p\ ^1P$
			10,600	Na I-Cr XIV	$3d\ ^2D-4f\ ^2F$
3	5	15,580	15,750	Na I-Mn XV	$3d\ ^2D-5f\ ^2F$
3	6	18,220			
4	5	5,050	5,000	Pd I-I VIII[1, 3]	$4d^{10}\ ^1S-4d^95p\ ^1P$
4	6	7,680			
		CALC. Δ_2 (VOLTS)	OBS. Δ_2 (VOLTS)		GROUND STATE CONFIGURATION
1	∞	27.1	27.1	H I-O VIII[4]	$1s$
			27.1	He I-N VII	$1s^2$
2	∞	6.85	7.	Li I-O VI[1]	$1s^22s$
			7.	B I-F V[1]	$1s^22s^22p$
3	∞	3.01	3.1	Na I-Sc XI	$1s^22s^22p^63s$

[1] R. F. Bacher and S. Goudsmit, *Atomic Energy States* (McGraw-Hill Book Co., 1932).
[2] P. G. Kruger and S. G. Weisberg, Phys. Rev. **52**, 314 (1937).
[3] P. G. Kruger and W. E. Shoupp, Phys. Rev. **46**, 124 (1934).
[4] B. Edlén, Nova Acta Reg. Soc. Sci. Upsaliensis, Ser. IV, **9**, No. 6 (1934).

obtained by plotting the second differences and estimating roughly the limiting values.

Experimental second differences for two transitions of the sodium sequence are shown in Table VIII. The second differences for the $3d-4f$ transition are seen to be approaching a value which is slightly below 11,000 cm^{-1}, and for the $3d-5f$ transition, the differences are approaching a value somewhat less than 16,000 cm^{-1}. From

TABLE VIII. *Observed radiated frequencies with first and second differences.*

Ion	$3d\,^2D_{3/2}-4f\,^2F_{7/2}$	Δ_1	Δ_2
Na I	5,406		
		16,903	
Mg II	22,309		12,433
		29,336	
Al III	51,645		12,802
		42,138	
Si IV	93,783		12,472
		54,610	
P V	148,393		12,221
		66,821	
S VI	215,214		11,825
		78,646	
Cl VII	293,860		(11,624)
		(90,270)	
A VIII	(384,130)		(11,362)
		(101,632)	
K IX	485,762		(11,287)
		112,919	
Ca X	598,681		11,043
		123,962	
Sc XI	722,643		11,058
		135,020	
Ti XII	857,660		11,080
		146,100	
V XIII	1003,760		10,720
		156,820	
Cr XIV	1160,580		

Ion	$3d\,^2D_{3/2}-5f\,^2F_{7/2}$	Δ_1	Δ_2
Na I	6,876		
		25,323	
Mg II	32,199		16,397
		41,720	
Al III	73,919		17,700
		59,420	
Si IV	133,339		17,502
		76,922	
P V	210,261		17,213
		94,135	
S VI	304,396		16,639
		110,774	
Cl VII	415,170		(16,496)
		(127,270)	
A VIII	(542,440)		(16,382)
		(143,652)	
K IX	686,092		(16,112)
		159,764	
Ca X	845,856		16,446
		176,210	
Sc XI	1022,070		15,870
		192,080	
Ti XII	1214,150		15,780
		207,860	
V XIII	1422,010		16,060
		223,920	
Cr XIV	1645,930		15,800
		239,720	
Mn XV	1885,650		

TABLE IX. *Ionization potentials, with first and second differences.*

Ion	I.P	Δ_1	Δ_2
Na I	5.113		
		9.847	
Mg II	14.960		3.497
		13.344	
Al III	28.304		3.267
		16.611	
Si IV	44.915		3.172
		19.783	
P V	64.698		3.128
		22.911	
S VI	87.609		3.21
		26.12	
Cl VII	113.73		
A VIII			
K IX	175.10		
		35.19	3.13
Ca X	210.29		
		38.32	
Sc XI	248.61		

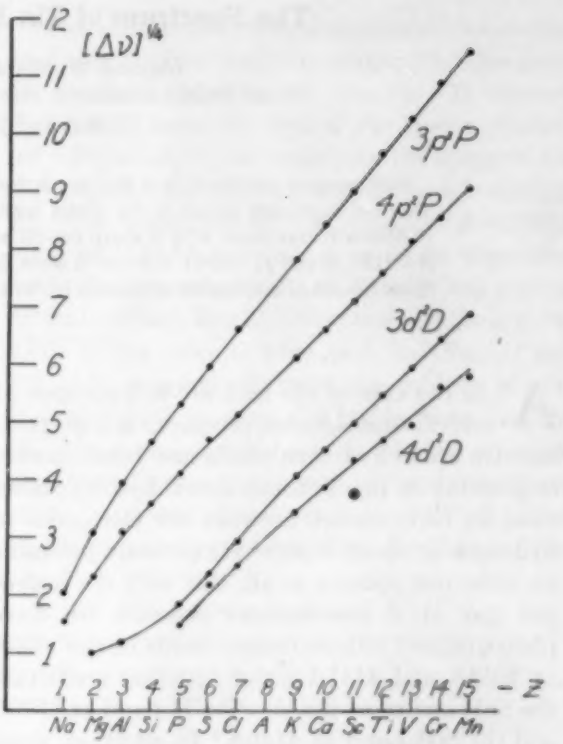

FIG. 3. Term separation diagram for the ions Na I–Mn XV. (Term separation)$^{\frac{1}{4}}$ *vs.* stage of ionization.

Table VII, one finds that the calculated second differences for these two cases are 10,750 cm^{-1} and 15,580 cm^{-1}, respectively.

In Fig. 3 the fourth roots of the term separations are plotted against atomic number for several of the terms. Good agreement with the regular doublet law is indicated, especially for the higher stages of ionization. The double circle represents the point obtained from Edlén's values for the $4d\,^2D$ terms for Sc XI. These terms are based on two lines, 105.144A and 104.430A, resulting from the $3p-4d$ transition. Remeasurement of the lines on our plates gives wave-lengths of 105.145A and 104.441A. These wave-lengths give a higher ^2D separation, with the result that the point now falls more nearly in line with the rest of the sequence.

Ionization potentials, with first and second differences, are listed in Table IX. The second differences agree quite well with the calculated value, 3.01 volts, which, it should be remembered, is only an approximation if there is a change, from ion to ion, in the screening constant.

The Spectrum of Tin Hydride at High Pressure

WILLIAM W. WATSON AND RALPH SIMON
Sloane Physics Laboratory, Yale University, New Haven, Connecticut
(Received January 3, 1939)

SnH spectra produced in a d.c. arc in hydrogen at 5 atmospheres pressure are described. Two red-degrading bands in the violet with first heads at 4054A and 4447A together are a $(0,0)^2\Delta\rightarrow{}^2\Pi$ transition with a sharp cut-off at $K'=17$. For the $^2\Pi$ state $B_0=5.31$, $r_0=1.822$A, $A=2182.70$ and $p_0=0.991$. For the $^2\Delta$ state $B_0=4.91$, $r_0=1.848$A, $A=-1.75$ and $\gamma_0=+0.694$. Some details of another band system in the red with principal head at 6095A are given.

AS in the case of the lead arc in hydrogen at several atmospheres pressure,[1] a high pressure tin arc in hydrogen yields new band spectra originating in the diatomic metal hydride molecule. In fact, an arc between tin electrodes in hydrogen at about 5 cm of Hg pressure produces no molecular spectra at all. But with the hydrogen gas at 5 atmospheres pressure we have photographed red-degrading bands in the violet at 4054A and 4447A which together constitute the SnH analog of the $^2\Delta\rightarrow{}^2\Pi$ CH band at 4300A and the SiH band at 4140A.[2] In addition, some bands which are undoubtedly SnH occur in the visible red with principal head at 6095A.

The experimental procedure was much the same as that of the previous investigation.[1] Because of the higher boiling point of tin, both the gas pressure and current were increased (5 atmospheres and 1 ampere, respectively) in order to vaporize a sufficient amount of the metal. Good spectrograms of the violet bands were obtained in the second order of the 21-foot grating, average dispersion 2.47A per mm, in four hours, but double this exposure time failed to yield a complete registration of the band system in the red. Still longer times of exposure and current strength are not possible owing to the intensity of the ever-present continuum arising from the high ion density in the source. If this continuous spectrum is too intense the weaker band lines are obliterated.

The effectiveness of the high gas pressure in producing these SnH spectra probably lies in the more nearly thermodynamic equilibrium then existing among all the possible states of the molecule. Thus the population of the excited states, ordinarily depleted by predissociation into neighboring repulsion states, is maintained at a sufficiently high level. Frequently, however, the probability of the radiationless transitions to repulsion states may be very large, the predissociation may be of the "induced" type, or there may be a complete lack of stable levels. In any of these cases the high pressure would not produce discrete spectra. For example, we find that the $^2\Delta\rightarrow{}^2\Pi$ SnH band produced at 5 atmospheres pressure is sharply cut off at $K'=17$, while the levels of the upper $^2\Sigma$ state of the red PbH spectrum are similarly cut off at a point about $\frac{1}{3}$ volt above $J=0$, $v=0$. Work in this laboratory with an Sb arc at this same high pressure, as well as at reduced pressure of hydrogen, has failed to produce any SbH spectrum.

THE $^2\Delta\rightarrow{}^2\Pi$ SnH BANDS

The violet spectrum of SnH consists of just the two isolated bands with first heads at 4054A and 4447A. Subsidiary stronger heads lie at 4071A and 4466A, respectively, and both bands are only some 90A long. Preliminary analysis showed the shorter wave-length band to have twelve branches while the longer wave-length band has but six. This fact, together with the magnitude of the interval between the bands and the knowledge of expected transition types for SnH indicated that the two constitute the 0,0 band of a $^2\Delta\rightarrow{}^2\Pi$ system. Since the $^2\Pi$ is practically pure case *a*, the levels of the $^2\Pi_{1/2}$ component should have negligible Λ-doubling while those of the $^2\Pi_{3/2}$ component should have large Λ-doubling. And since the Λ-doubling of Δ-states is always negligible, the $^2\Delta\rightarrow{}^2\Pi_{1/2}$ sub-band would be expected to

[1] W. W. Watson, Phys. Rev. **54**, 1068 (1938).
[2] C. V. Jackson, Proc. Roy. Soc. **126**, 373 (1930); R. S. Mulliken, Phys. Rev. **37**, 733 (1931).

display but six branches for moderately low J values. The $^2\Delta \rightarrow {}^2\Pi_{\frac{1}{2}}$ sub-band, on the other hand, should have the full complement of twelve branches, with satellite branches about as intense as the main branches. This reasoning indicates at once that the $^2\Pi$ state is regular.

Assignments of all the measured lines based on the usual combination relations are given in Table I. A rather large number of multiple assignments in the head-forming ${}^RQ_{21}$, R_1, Q_2 and ${}^QR_{12}$ branches is necessitated in part by the pressure broadening of all lines. Because of this line breadth we list the wave numbers to just one decimal place. The satellite branches are practically as intense as the main branches, and in all branches there is a sharp drop in intensity as the last $K'=17$ is approached.

The various molecular constants are assembled in Table II. It is highly probable that this band is the 0,0 transition of the $^2\Delta \rightarrow {}^2\Pi$ system. For the $^2\Pi$ state, in view of the case a relation $B^*=B(1\pm 2B/A)$, we may take the mean of the B_1^* and B_2^* values, 5.31, as the correct value of B_0. The magnitude of the constant $A=2182.7$ cm^{-1} of the $A\Sigma$ interaction is to be compared with the intervals 1692 and 1736 in the ground ^3P state of SnI. In a $^2\Delta \rightarrow {}^2\Pi$ transition the separations of the pairs of lines such as ${}^SR_{21e}(J)$ and ${}^SR_{21d}(J)$ measure directly the widths of the Λ-doubling. The case a relation that for the $^2\Pi_{\frac{1}{2}}$ terms $\Delta\nu_{de}=\pm p(J+\frac{1}{2})$ is obeyed since no departure from a linear increase in the doubling with J is noted. The large size of the observed $p_0=0.99$ is not surprising since the A is so large

TABLE I. *Quantum assignments in the* $^2\Delta \rightarrow {}^2\Pi$ SnH *band. d denotes fused lines.*

$J''+\frac{1}{2}$	P_{1de}	P_{1ed}	Q_{1e}	Q_{1d}	R_{1de}	R_{1ed}	${}^QP_{21e}$	${}^QP_{21d}$	${}^RQ_{21de}$
1									
2									24544.8*d*
3							24516.5*d*	24520.5*d*	47.0*d*
4							10.3*d*		49.1*d*
5			24502.1		24552.0*d*	24556.4*d*	01.4	06.9*d*	49.3*d*
6			493.1		52.0*d*	58.3*d*	490.4*d*	496.8	49.1*d*
7	24424.3	24431.3	83.0	24490.4*d*	52.0*d*	58.3*d*	79.9*d*	86.8	47.0*d*
8	03.6	10.7*d*	72.1	79.9*d*	50.0*d*	58.3*d*	67.9	75.8	44.8*d*
9	382.0	391.0	60.3	69.2	47.0*d*	56.4*d*	55.0	64.0	41.8*d*
10	59.8*d*	69.9	47.2	57.2	44.3*d*	54.6*d*	41.2	51.1	36.8*d*
11	36.5*d*	47.2	33.1	43.9	38.8	49.1*d*	26.5	37.3	31.6
12	12.2	23.9	18.0	29.7	32.7	44.3	10.7	22.4	24.7*d*
13	286.6	299.5	01.6	14.2	24.7*d*	36.8*d*	393.5	06.1	16.5
14	60.0	73.6	383.7	397.3	16.5*d*	29.2*d*	75.2	388.7	06.9
15	32.1	46.8	63.5	78.8	05.0	20.5*d*	55.4	69.9	495.8
16	02.9	18.3	43.3	58.6			34.1	49.5	83.0*d*
17	171.7	188.3	20.5	36.5*d*	477.2*d*		12.2*d*	27.2	69.2*d*
18	39.1	56.4	295.4	12.2			286.6*d*	03.5	
19	03.9		68.8					277.5	

$J''+\frac{1}{2}$	${}^RQ_{12ed}$	${}^SR_{12e}$	${}^SR_{12d}$	${}^OP_{12}$	P_2	${}^PQ_{12}$	Q_2	${}^QR_{12}$	R_2
1		24563.7	24564.8						
2	24547.0*d*	75.4	77.5				22376.2*d*	22376.2*d*	22407.1
3	50.0*d*	86.8	89.8			22350.7	80.4*d*	80.4*d*	19.7
4	52.7*d*	97.5	601.7	22312.8	22343.6*d*	43.6*d*	82.6*d*	83.2*d*	30.6
5	54.6*d*	607.4	12.3	295.5	34.3*d*	35.4	82.6*d*	85.1*d*	40.6
6	54.6*d*	16.3	22.3	77.1	24.2	26.3	82.6*d*	85.1*d*	49.9
7	54.6*d*	24.4	31.5*d*	57.3	12.8	16.2	80.4*d*	85.1*d*	57.5
8	52.7*d*	31.5*d*	39.3*d*	36.6	00.7	05.0*d*	77.4	83.2*d*	64.5
9	50.0*d*	37.3	46.0*d*	15.0	287.8	292.9	74.2	80.4*d*	70.3
10	47.0*d*	42.0	52.1	192.3	73.6	79.7	69.5	76.2	74.5
11	41.8*d*	46.0*d*	56.4	68.2	58.6	65.2	63.8*d*	70.8*d*	77.5*d*
12	36.8*d*	47.8*d*	59.6	43.5	42.1	49.5	55.9*d*	63.8*d*	79.1*d*
13	29.2	47.8*d*	60.9	17.8	24.4	32.4	47.2	55.9*d*	79.1*d*
14	20.5	47.8*d*	60.9		05.3	13.9	37.0	45.9	77.5*d*
15	10.3	44.1	58.7		184.9	193.8	25.1	34.3	73.7
16	498.5*d*	39.3*d*	54.7		62.8	71.8	11.3	20.5	68.2
17	84.2*d*				38.9	48.0	295.5*d*	05.0	
18					13.2	22.5			

and the existence of something like "pure precession" interaction with other states coming from the same electron configuration is probable.

There is some difficulty in the calculation of the constants of the terms of the $^2\Delta$-state. The combination differences show that the state is inverted with the spin doubling small in magnitude, and increasing roughly linearly with K at the lower K values but at a rapidly decreasing rate as the final $K'=17$ is approached. We therefore first apply the case b doublet separation relation[3] $\Delta f(K)=[A\Lambda^2/K(K+1)+\gamma](K+\frac{1}{2})$ to the spin doublet intervals for $K<12$. This yields mean values $A=-1.75$ for the LS coupling and $\gamma=+0.694$ for the SK coupling. Corrections $-2A(1/(K+2)-1/K)-\gamma$ and $+2A(1/(K+1)-1/(K-1))+\gamma$ are then applied to the $\Delta_2F_1'(J)$ and $\Delta_2F_2'(J)$ combination differences, respectively, after which the simple, strictly case b relations are used. This yields $B_0'=4.911$ and $D'=-5.0\times10^{-4}$. The rather sudden change in the rate of increase of the spin-doublet widths near the sharp cut-off points in the band branches could arise from the interaction with the neighboring electronic state.

TABLE II. *Constants of the energy terms for* SnH (*cm^{-1} units*).

CONSTANT	$^2\Pi$	$^2\Delta$
B_1^*	5.293	
B_2^*	5.331	
B_0	5.31	4.911
r_0	1.822A	1.848A
D_0	-1.94×10^{-4}	-5.0×10^{-4}
A	2182.70	-1.75
γ_0		$+0.694$
p_0	0.991	

THE RED SnH SYSTEM

Study of the incomplete data on these bands leads to a few definite conclusions. They are not similar to the PbH bands[1] in this same spectral region. Whereas the latter possess four branches with very large second differences between successive lines in a branch, indicative of a large change in the moment of inertia of the molecule in the transition, these SnH bands have more than four branches and with small second differences. Associated with the strongest (Q) head at 6095A are subsidiary heads at 6022A and 6063A which seem to belong to $^sR_{21}$ and R branches, respectively. Since the R branch is considerably less intense than the P branch, the transition may be either $\Sigma\rightarrow\Pi$ or $\Pi\rightarrow\Delta$. A second weaker band is present with principal head at 6214A.

No combination differences common with those of the violet SnH bands can be found. Probable combinations that have been tabulated indicate $B''\sim5.5$, a reasonable value for SnH. But since there is apparently no electronic state common to these two band systems, we believe that the analysis should not be presented until it is more complete and checked by the comparison of internal combination differences. The difficulties in the obtaining of better experimental data have been already mentioned.

[3] R. S. Mulliken, Rev. Mod. Phys. **2**, 60 (1930).

A General Solution for the Equations of Natural Line Breadth

LYMAN SPITZER, JR.*
Harvard College Observatory, Cambridge, Massachusetts
(Received December 27, 1938)

A rigorous solution is given to the Dirac radiation equations for a single radiative transition between two atomic states. The resultant formulas are valid for any appropriate variation with frequency both of the density of light quanta and of the matrix component for the transition. The usual infinity at high frequencies is eliminated naturally. Applications of the formulas are made for the case of an absorption or an emission line.

THE solution of the Dirac radiation equations given by Weisskopf and Wigner[1] and by Weisskopf[2] for the absorption or emission of a light quantum assumes either that N_ρ, the number of quanta in a state ρ with a frequency ν_ρ, is independent of ρ, or that N_ρ differs from zero for only one ρ. The equations may also be solved in the general case where N_ρ and $j_{AB}{}^\rho$ are both arbitrary functions of ρ, provided that $N_\rho{}^{\frac{1}{2}}\nu_\rho j_{AB}{}^\rho$ is bounded at infinity; $j_{AB}{}^\rho$ is proportional to the matrix element for the transition. For convenience a two-state atom is taken here, with ground state A and excited state B. Only single transitions will be considered. In Section 1 the general formulas are derived. In Section 2 these are applied to the particular case of an absorption or emission line.

1.

In accordance with the usual notation, let $a(t)$ denote the probability amplitude of the state in which the electron is in A and there are N_ρ quanta in state ρ; similarly let $b_\rho(t)$ denote the amplitude of the state in which the electron is in B, with a higher energy than in A, and the number of quanta in the ρth state is now $N_\rho-1$. The differential equations for $a(t)$ and $b_\rho(t)$ are[3]

$$ih\frac{da}{dt}=\sum_\rho b_\rho\left(\frac{hN_\rho}{G\nu_\rho}\right)^{\frac{1}{2}}j_{AB}{}^\rho, \tag{1}$$

$$ih\frac{db_\rho}{dt}=(E_A-E_B+h\nu_\rho)b_\rho+a\left(\frac{hN_\rho}{G\nu_\rho}\right)^{\frac{1}{2}}j_{AB}{}^{*\rho}, \tag{2}$$

where

$$j_{AB}{}^\rho=ih\int\sum_k dq\psi_A{}^*\exp\left[i\mathbf{K}_\rho\cdot\mathbf{q}_k\right]\frac{e_k}{m_k}(\boldsymbol{\epsilon}_\rho\cdot\nabla)\psi_B. \tag{3}$$

The sum is taken over different electrons, $\boldsymbol{\epsilon}_\rho$ and $\mathbf{K}_\rho$ are the polarization and momentum vectors of the photon, and other symbols have their usual meanings.

With the substitutions

$$g_\rho(t)=\frac{1}{h}\left(\frac{hN_\rho}{G\nu_\rho}\right)^{\frac{1}{2}}j_{AB}{}^\rho b_\rho(t)\exp\left[\frac{i(E_A-E_B+h\nu_\rho)t}{h}\right],$$
$$\phi_\rho=(N_\rho/hG\nu_\rho)\,|j_{AB}{}^\rho|^2, \tag{4}$$

Eqs. (1) and (2) become

$$da/dt=-i\sum_\rho g_\rho\exp\left[-(it/h)(E_A-E_B+h\nu_\rho)\right], \tag{5}$$

$$dg_\rho/dt=-i\phi_\rho a\exp\left[(it/h)(E_A-E_B+h\nu_\rho)\right]. \tag{6}$$

As usual it is assumed that G, the volume of the *hohlraum*, approaches infinity; the sum in (5) may thus be replaced by an integral. Let $S_\rho d\nu_\rho$ be the number of states for the radiation quanta in a frequency interval $d\nu_\rho$. If we make the substitutions

$$z=\nu_\rho+(E_A-E_B)/h,$$
$$g(z,t)=S_{\rho(z)}g_{\rho(z)}(t), \tag{7}$$
$$F(z)=S_{\rho(z)}\phi_{\rho(z)}=(8\pi/hc^3)N_{\rho(z)}\nu_{\rho(z)}|j_{AB}{}^{\rho(z)}|^2,$$

using (4) and the usual formula $8\pi\nu^2G/c^3$ for S_ρ,

* National Research Fellow.
[1] V. Weisskopf and E. Wigner, Zeits. f. Physik **63**, 54 (1930).
[2] V. Weisskopf, Ann. d. Physik **9**, 23 (1931); Zeits. f. Physik **85**, 451 (1933).
[3] For a review of the subject: G. Wentzel, *Handbuch der Physik*, Vol. 24/1, p. 740. The probability amplitudes above are complex conjugates of those more usually used.

then we find that (5) and (6) reduce to

$$\frac{da}{dt}=-i\int_{-\infty}^{+\infty}g(z,t)e^{-2\pi izt}dz, \tag{8}$$

$$\partial g/\partial t=-iF(z)a(t)e^{2\pi izt}. \tag{9}$$

The lower limit of integration in (8) has been extended from $-(E_B-E_A)/h$ to $-\infty$. This is legitimate provided $F(z)$ is taken to be identically zero in this extended range.

From (9) we obtain

$$g(z,t)=-iF(z)\int_0^t e^{2\pi iz\tau}a(\tau)d\tau, \tag{10}$$

satisfying $g(z,0)=0$. The substitution of (10) into (8) yields the integral equation for da/dt:

$$\frac{da}{dt}=-\int_{-\infty}^{+\infty}e^{-2\pi izt}F(z)dz\int_0^t e^{2\pi iz\tau}a(\tau)d\tau. \tag{11}$$

This equation may be solved provided $F(z)$ is sufficiently well behaved. We shall assume that $F(z)$ may be expressed as the sum of H and $G(z)$, where H is constant, and $G(z)$ is of Lebesgue class $L^2(-\infty,+\infty)$; i.e., $|F(z)|^2$ may be integrated over the entire range $(-\infty,+\infty)$. In practice H must equal zero since $F(z)$ vanishes for z infinitely negative; it is included here so that its effect may be compared with that of $G(z)$. Under these conditions a solution of (11) for da/dt may be found which belongs to $L^2(0,\infty)$, if the additional restriction is made that $a(t)$ is of class $L(0,\infty)$, and regular for $0<t<\infty$.

By standard theorems on Fourier integrals, (11) reduces at once[4] to

$$\frac{da}{dt}=-\tfrac{1}{2}Ha(t)-\int_0^\infty L(t-\tau)a(\tau)d\tau, \tag{12}$$

where

$$L(x)=\begin{cases}\displaystyle\int_{-\infty}^{+\infty}G(z)e^{-2\pi izx}dz, & x>0,\\ 0, & x<0.\end{cases} \tag{13}$$

The factor $\frac{1}{2}$ in the first term of (12) arises from the discontinuity of the integral at $t=\tau$. To change (11) to an infinite integral over τ as well as z, so that the usual theory of Fourier integrals applies, the integrand must be set equal to zero for $\tau>t$. The double integral will therefore equal one-half the value of $a(t)$ at the point of discontinuity $\tau=t$. The second term on the right-hand side of (12) arises from an inversion of the order of integration in (11). This inversion is justified provided $L(x)$ is of $L^2(0,\infty)$ and $a(t)$ is of $L(0,\infty)$.[5] That $L(x)$ is of $L^2(0,\infty)$ follows from the fact that $G(z)$ is of $L^2(-\infty,\infty)$.[6]

If we define

$$\Gamma^+(\xi)=\int_0^\infty\frac{da}{dt}(t)e^{2\pi i\xi t}d\tau,$$

$$L^+(\xi)=\int_0^\infty L(x)e^{2\pi i\xi x}dx, \tag{14}$$

and use the formula

$$\int_0^\infty a(t)e^{2\pi i\xi t}d\tau=\frac{-1}{2\pi i\xi}\left\{1+\int_0^\infty\frac{da}{dt}(t)e^{2\pi i\xi t}dt\right\}, \tag{15}$$

which is valid provided $a(t)$ is unity for t equal to zero and vanishes for t infinite, we find that the Fourier transform of (12) becomes

$$\Gamma^+(\xi)=\frac{H}{4\pi i\xi}(\Gamma^+(\xi)+1)+\frac{L^+(\xi)}{2\pi i\xi}(\Gamma^+(\xi)+1),$$

$$\Gamma^+(\xi)=-\frac{\frac{1}{2}H+L^+(\xi)}{\frac{1}{2}H+L^+(\xi)-2\pi i\xi}. \tag{16}$$

The validity of (16) follows from the same considerations as that of (12). $\Gamma^+(\xi)$ is of $L^2(-\infty,\infty)$, and its Fourier transform gives for da/dt the following expression, valid for $0<t<\infty$:

$$\frac{da}{dt}(t)=-\int_{-\infty}^{+\infty}\frac{\frac{1}{2}H+L^+(\xi)}{\frac{1}{2}H+L^+(\xi)-2\pi i\xi}e^{-2\pi i\xi t}d\xi, \tag{17}$$

provided only that the denominator does not vanish for real ξ. (If this condition is violated, $a(t)$ will not belong to $L(0,\infty)$ as stipulated

[4] E. C. Titchmarsh, *Introduction to the Theory of Fourier Integrals* (Oxford University Press, 1937), Theorem 12, p. 25.

[5] E. C. Titchmarsh, reference 4, Theorem 65, p. 90. The theorem may clearly be adapted to include the present case, for which the classes of f and g are reversed, and the lower limits of integration are zero rather than negative infinity.

[6] E. C. Titchmarsh, reference 4, Theorem 48, p. 69.

above.) For $g(z, \infty)$, giving the frequency distribution of the absorbed radiation, one obtains from (10), (15) and (16) the simple formula

$$g(z, \infty)=\frac{F(z)}{2\pi}\frac{1}{z+(iH/4\pi)+(iL^+(z)/2\pi)}. \quad (18)$$

This analysis is immediately applicable to the case of spontaneous transitions if N_ρ is set equal to unity throughout. As z approaches infinity, $F(z)$ will behave as $\nu_{\rho(s)}\cdot|j_{AB}{}^{\rho(s)}|^2$ from (7). Using (3) and the Riemann-Lebesgue theorem we find that $j_{AB}{}^{\rho(s)}$ varies asymptotically as $1/\nu_{\rho(s)}$. Hence $F(z)$ is asymptotically proportional to $1/z$ for $\nu_{\rho(s)}$ positive. Since $F(z)$ is nowhere infinite, its square may be integrated from $-\infty$ to $+\infty$; i.e., $F(z)$ is of L^2, and the above analysis applies.[7] It has thus been proved that the equations of natural line breadth admit a rigorous solution for the case of a single transition. The infinity at the high frequency end of the spectrum, which in approximate treatments must be eliminated by the use of separate considerations,[8] here disappears quite naturally.

2.

It is of some interest to note the form taken by (17) and (18) when $G(z)$ is given by

$$G(z)=G/(z^2+\gamma^2), \quad (19)$$

and from (13) and (14)

$$L^+(\xi)=\frac{G}{2\gamma}\frac{1}{\gamma-i\xi}. \quad (20)$$

Straightforward analysis, with the use of contour integration, leads to the formulas

$$\frac{da}{dt}=\frac{-1}{2(1+\alpha)R}\{[C-\tfrac{1}{2}H(1+\alpha)(1-R)]\times\exp[-\pi\gamma t(1+\alpha)(1-R)]-[C-\tfrac{1}{2}H(1+\alpha)(1+R)]\times\exp[-\pi\gamma t(1+\alpha)(1+R)]\}, \quad (21)$$

where

$$\alpha=H/4\pi\gamma, \quad C=H+G/\gamma^2=F(0), \quad R=\left(1-\frac{C}{\pi\gamma(1+\alpha)^2}\right)^{\frac{1}{2}}. \quad (22)$$

Also

$$a(t)=\frac{1}{2R}\left\{\left[\frac{1-\alpha}{1+\alpha}+R\right]\exp[-\pi\gamma t(1+\alpha)(1-R)]-\left[\frac{1-\alpha}{1+\alpha}-R\right]\exp[-\pi\gamma t(1+\alpha)(1+R)]\right\} \quad (23)$$

and

$$g(z, \infty)=\frac{F(z)}{4\pi R}\left\{\frac{(1-\alpha)/(1+\alpha)+R}{z+\frac{1}{2}i\gamma(1+\alpha)(1-R)}-\frac{(1-\alpha)/(1+\alpha)-R}{z+\frac{1}{2}i\gamma(1+\alpha)(1+R)}\right\},$$

$$=\frac{F(z)}{2\pi}\frac{z+i\gamma}{z^2+i\gamma(1+\alpha)z-\gamma C/4\pi}. \quad (24)$$

When G equals zero, formulas (21), (23) and (24) reduce to the usual expressions with the natural line half-width equal to $H/4\pi$. By analogy, $F(0)/4\pi$ or $C/4\pi$ may be termed the "normal" half-width, or the half-width which would result if the energy density multiplied by the matrix element were constant with frequency, and equal to its value at the line center $z=0$. When γ is greater than this normal half-width, the square root in the above formulas is nearly unity, and may be expanded. This is the usual case, since under all practicable conditions the natural width $C/4\pi$ due to induced transitions alone is a negligible quantity, much less than the corresponding natural width for spontaneous transitions. With this approximation, (21), (23) and (24) become, respectively,

$$da/dt=-\tfrac{1}{2}[Ce^{-Ct/2}-(G/\gamma^2)e^{-2\pi\gamma t}], \quad (25)$$

$$x(t)=e^{-Ct/2}-(G/4\pi\gamma^2)e^{-2\pi\gamma t}, \quad (26)$$

$$g(z, \infty)=\frac{F(z)}{2\pi}\left(\frac{1}{z+iC/4\pi}-\frac{G}{4\pi\gamma^2}\frac{1}{z+i\gamma}\right). \quad (27)$$

Thus C, or $F(0)$, is the damping constant for the transition.

[7] For spontaneous transitions, moreover, the denominator of (16) never vanishes when ξ is real. For H may be set equal to zero, and the real part of $L^+(\xi)$ equals $G(\xi)/2$, which vanishes only for $-\xi>(E_B-E_A)/\hbar$. With such ξ the imaginary part of $L^+(\xi)$, known as a Hilbert transform of $G(z)$, is positive, and hence cannot equal $2\pi\xi$. For induced transitions a similar result holds if $N_\rho>0$ for all $\nu_\rho>0$.

[8] V. Weisskopf and E. Wigner, reference 1, p. 64.

It will be noted that in addition to the ordinary absorbed radiation of half-width $C/4\pi$, there is an additional absorption of radiation over the entire half-width γ. The intensity of this additional absorption is much less than that of the normal absorption, to which it bears the ratio of the square of $G/4\pi\gamma^2$. When H equals zero, this is the ratio of the normal half-width $C/4\pi$ to the half-width γ of the incident radiation. In general this ratio is small and therefore the usual analysis, which assumes $F(z)$ equal to a constant C, may be legitimately applied. This verifies Weisskopf's[9] conclusion.

The above formulas give the order of magnitude of the effects involved. When γ becomes much less than Γ, defined as the corresponding half-width for transitions from B to A, the consideration of the transitions A to B alone becomes a poor approximation to the actual state of affairs. The double transition A to B to A may be treated by a direct application of the foregoing analysis, provided the ordinary approximations are made for the spontaneous jumps B to A. In addition to the usual substitution of $C/4\pi+\Gamma$ for $C/4\pi$ in (27), the most important result is that $\gamma+\Gamma$ replaces γ in the square root in (22). Since Γ will include a term G/γ^2 because of the induced transitions B to A, the square root will apparently be real whenever $G(z)$ is given by (19). Thus there will be no shift of the absorbed line; this is again in agreement with Weisskopf's result[9] when the frequency of his strictly monochromatic radiation coincides with the line center, $(E_B-E_A)/h$.

[9] V. Weisskopf, Ann. d. Physik **9**, 23 (1931).

FEBRUARY 15, 1939 PHYSICAL REVIEW VOLUME 55

Static Solutions of Einstein's Field Equations for Spheres of Fluid

RICHARD C. TOLMAN
Norman Bridge Laboratory of Physics, California Institute of Technology, Pasadena, California
(Received January 3, 1939)

A method is developed for treating Einstein's field equations, applied to static spheres of fluid, in such a manner as to provide explicit solutions in terms of known analytic functions. A number of new solutions are thus obtained, and the properties of three of the new solutions are examined in detail. It is hoped that the investigation may be of some help in connection with studies of stellar structure. (See the accompanying article by Professor Oppenheimer and Mr. Volkoff.)

§1. INTRODUCTION

IT IS difficult to obtain explicit solutions of Einstein's gravitational field equations, in terms of known analytic functions, on account of their complicated and nonlinear character. Even in the physically simple case of static gravitational equilibrium for a spherical distribution of perfect fluid, there are only two explicit solutions which are at present well known. These are Einstein's original cosmological solution for a uniform distribution of fluid with constant density ρ and constant pressure p throughout the whole of space, and Schwarzschild's so-called interior solution for a sphere of incompressible fluid of constant density ρ and a pressure p which drops from its central value to zero at the boundary.[1] To these, by regarding empty space as the limiting case of a fluid having zero density and pressure, we can also add de Sitter's cosmological solution for a completely empty universe, and Schwarzschild's so-called exterior solution for the field in the empty space surrounding a spherically symmetrical body, thus giving four solutions in all.

The present paper has a twofold purpose. In the first place, a method will be given for treating

[1] In addition to these explicit solutions for a spherical distribution of fluid, we also have Lemaitre's interesting explicit solution for a spherical distribution of solid, each concentric layer of which supports its own weight by purely transverse stresses. See Eq. (5.11), Ann. de la Soc. Scient. de Bruxelles **A53**, 51 (1933).

the nonlinear differential equations, applying to the gravitational equilibrium of perfect fluids, in such a manner as to make it somewhat easy to obtain a variety of explicit solutions. In the second place, it will then be shown that this method of treatment leads directly not only to the four well-known solutions mentioned above, but also to a number of others which may have a measure of physical interest. In particular, it is hoped that some of these new solutions may be of use in trying to understand the internal constitution of stars.[2]

§2. The General Form of Solution for an Equilibrium Distribution of Fluid

If for simplicity units are chosen which make the velocity of light and the constant of gravitation both equal to unity, Einstein's field equations (connecting the distribution of matter and energy as described by the components of the energy-momentum tensor $T_{\mu\nu}$ with the resulting gravitational field as described by the potentials $g_{\mu\nu}$) can be written in the form

$$-8\pi T_{\mu\nu}=R_{\mu\nu}-\tfrac{1}{2}Rg_{\mu\nu}+\Lambda g_{\mu\nu}, \qquad (2.1)$$

where the cosmological constant is denoted by Λ, and where the contracted Riemann-Christoffel tensor $R_{\mu\nu}$ and its trace R are known functions of the potentials $g_{\mu\nu}$ and their first and second derivatives with respect to the space-like and time-like coordinates $x^1\cdots x^4$. Owing to the complicated and nonlinear dependence of $R_{\mu\nu}$ and R on the $g_{\mu\nu}$ and their derivatives, no general precise, explicit solution for these equations is known, and special solutions are difficult to obtain in explicit analytic form as has already been mentioned. The problem of solution is made particularly difficult by the nonlinear character of the equations which prevents the construction of further solutions by the superposition of those already obtained.

In searching for solutions of the field equations (2.1) that would correspond to an equilibrium distribution of perfect fluid, considerable simplification can be introduced at the start.

In the first place, since the condition of gravitational equilibrium for a fluid will on physical grounds be a static and spherically symmetrical distribution of matter, we can begin by choosing space-like coordinates r, θ and ϕ, and a time-like coordinate t such that the solution will be described by the simple form of line element

$$ds^2=-e^{\lambda}dr^2-r^2d\theta^2-r^2\sin^2\theta d\phi^2+e^{\nu}dt^2, \qquad (2.2)$$

with λ and ν functions of r alone, as is known to be possible in the case of any static and spherically symmetrical distribution of matter. With the simple expressions for the gravitational potentials appearing in (2.2), the application of the field equations (2.1) then leads to the following expressions for the only surviving components of the energy-momentum tensor

$$8\pi T_1^1=-e^{-\lambda}\left(\frac{\nu'}{r}+\frac{1}{r^2}\right)+\frac{1}{r^2}-\Lambda,$$

$$8\pi T_2^2=8\pi T_3^3$$

$$=-e^{-\lambda}\left(\frac{\nu''}{2}-\frac{\lambda'\nu'}{4}+\frac{\nu'^2}{4}+\frac{\nu'-\lambda'}{2r}\right)-\Lambda, \qquad (2.3)$$

$$8\pi T_4^4=e^{-\lambda}\left(\frac{\lambda'}{r}-\frac{1}{r^2}\right)+\frac{1}{r^2}-\Lambda,$$

where differentiations with respect to r are indicated by accents.[3]

[2] My own present interest in solutions of Einstein's field equations for static spheres of fluid is specially due to conversations with Professor Zwicky of this Institute, and with Professor Oppenheimer and Mr. Volkoff of the University of California, who have been more directly concerned with the possibility of applying such solutions to problems of stellar structure. Professor Zwicky in a recent note (Astrophys. J. **88**, 522 (1938); see also Phys. Rev. **54**, 242 (1938)) has suggested the use of Schwarzschild's interior solution for a sphere of fluid of constant density as providing a model for a "collapsed neutron star." He is making further calculations on the properties of such a model, and it is hoped that the considerations given in this article may be of assistance in throwing light on the questions that concern him. Professor Oppenheimer and Mr. Volkoff have undertaken the specific problem of obtaining numerical quadratures for Einstein's field equations applied to spheres of fluid obeying the equation of state for a degenerate Fermi gas, with special reference to the particular case of neutron gas. Their results appear elsewhere in this same issue. My own solutions of the field equations, as given in the immediately following, can make only an indirect contribution to the physically important case of a Fermi gas, since it will be seen that they correspond to equations of state which cannot be chosen arbitrarily. My thinking on these matters has, however, been largely influenced by discussions with Professor Oppenheimer and Mr. Volkoff, and it is hoped that the explicit solutions obtained will at least assist in the general problem of developing a sound intuition for the kind of results that are to be expected from the application of Einstein's field equations to static spheres of fluid.

[3] See for example, R. C. Tolman, *Relativity, Thermodynamics and Cosmology* (Oxford, 1934), Eq. (95.3).

In the second place, since the matter involved in the distribution is by hypothesis a perfect fluid, we can obtain a direct connection with the properties of the fluid by making use of the general expression

$$T^{\mu\nu}=(\rho+p)\frac{dx^\mu}{ds}\frac{dx^\nu}{ds}-g^{\mu\nu}p, \tag{2.4}$$

which by definition gives the components of the energy-momentum tensor $T^{\mu\nu}$ of a perfect fluid at any point and time of interest in terms of the proper (macroscopic) density ρ, the proper pressure p, and the components of "velocity" dx^μ/ds and dx^ν/ds of the fluid at that point and time. With the simple form of line element (2.2), this then leads to

$$T^1_1=T^2_2=T^3_3=-p, \quad T^4_4=\rho, \tag{2.5}$$

as expressions for the only surviving components of the energy-momentum tensor in terms of the pressure and density of the fluid.

Substituting (2.5) in (2.3), we now have

$$\begin{aligned} 8\pi p&=e^{-\lambda}\left(\frac{\nu'}{r}+\frac{1}{r^2}\right)-\frac{1}{r^2}+\Lambda,\\ 8\pi p&=e^{-\lambda}\left(\frac{\nu''}{2}-\frac{\lambda'\nu'}{4}+\frac{\nu'^2}{4}+\frac{\nu'-\lambda'}{2r}\right)+\Lambda, \qquad (2.6)\\ 8\pi\rho&=e^{-\lambda}\left(\frac{\lambda'}{r}-\frac{1}{r^2}\right)+\frac{1}{r^2}-\Lambda \end{aligned}$$

as the desired expressions which make direct connection with the properties of the fluid in terms of its pressure and density. In the case of gravitational equilibrium for a distribution of perfect fluid, we are thus provided with the general form of solution for the gravitational potentials $g_{\mu\nu}$ which is described by the line element (2.2), and with three differential equations (2.6) which relate the unknown functions λ and ν appearing in that form of solution, along with the pressure p and density of the fluid ρ, to coordinate position r within the distribution of fluid.

§3. Method of Obtaining Explicit Analytic Solutions

In accordance with the foregoing we now have three differential equations for the four unknown quantities λ, ν, p and ρ as functions of r. The problem will hence become determinate as soon as we introduce one further independent equation corresponding to some additional hypothesis as to the nature of the fluid or of the distribution.

From a physical point of view, it might seem most natural to introduce this additional hypothesis in the form of an "equation of state" describing the relation between pressure p and density ρ which could be expected to hold for the fluid under consideration. Or since the properties of the fluid could also depend on position, as would be the case in treating a fluid of varying composition or in making an approximate application to a fluid of varying temperature, it might seem natural to test the consequences of adding some equation connecting p and ρ with r.

From a mathematical point of view, however, the derivatives of λ and ν occur in our Eqs. (2.6) in such a complicated and nonlinear manner that we cannot in general expect to obtain explicit analytic solutions when we complete the set by adding a further equation connecting p with ρ or p and ρ with r, and should usually have to resort to a method of approximate quadrature to obtain solutions in that way. In order to obtain explicit analytic solutions, it proves more advantageous to introduce the additional equation necessary to give a determinate problem in the form of some relation, connecting λ or ν or both with r, so chosen with reference to the occurrence of the derivatives of λ and ν in expressions (2.6) as to make the resulting set of equations readily soluble. By adopting such a mathematically rather than physically motivated procedure, we of course run the risk of obtaining solutions which may not be physically interesting or even physically possible. Nevertheless, having once obtained an explicit solution, it then becomes relatively easy to examine the implied physics and see if this has a character which affords insight into the equilibrium conditions that could be expected for actual fluids.

To carry out the suggested method of attack, it is desirable to re-express Eqs. (2.6) in a somewhat different form which will make it easier to ascertain what conditions on λ and ν can be introduced to secure solubility. In the first place, it is helpful to equate the two different expressions for the pressure p given by (2.6) and thus obtain a single equation for the dependence of λ

and ν on r. In the second place, it is then helpful to rewrite this result in a form which is already nearly integrable so that the desired kind of condition on λ and ν can be more easily seen. Introducing such a re-expression, Eqs. (2.6) are then found to be equivalent to the set

$$\frac{d}{dr}\left(\frac{e^{-\lambda}-1}{r^2}\right)+\frac{d}{dr}\left(\frac{e^{-\lambda}\nu'}{2r}\right)+e^{-\lambda-\nu}\frac{d}{dr}\left(\frac{e^{\nu}\nu'}{2r}\right)=0, \tag{3.1}$$

$$8\pi p=e^{-\lambda}\left(\frac{\nu'}{r}+\frac{1}{r^2}\right)-\frac{1}{r^2}+\Lambda, \tag{3.2}$$

$$8\pi\rho=e^{-\lambda}\left(\frac{\lambda'}{r}-\frac{1}{r^2}\right)+\frac{1}{r^2}-\Lambda, \tag{3.3}$$

where the first of these equations (3.1) has been obtained in the manner just described. The one term in (3.1) which is not immediately integrable contains λ and ν in a sufficiently simple manner so that conditions on those quantities can be readily found which will make it easy to obtain a first integral of that equation.

§4. Specific Solutions

This method of attack can now be used to obtain a number of specific solutions. We shall summarize the results thus provided by first stating the additional *assumed equation* expressing the condition on λ or ν that was taken to secure the integrability of (3.1), and then giving the *resulting solution* for e^{λ}, e^{ν}, ρ and p as functions of r which can be obtained by combining the new equation with (3.1), (3.2) and (3.3). New symbols such as A, B, R, c, m, n, etc. will be used in these expressions to denote constants of integration; they are to be regarded as adjustable parameters having real, not necessarily integral, values.

Solution I. (Einstein universe)

Assumed equation

$$e^{\nu}=\text{const.}$$

Resulting solution

$$e^{\lambda}=\frac{1}{1-r^2/R^2}, \qquad e^{\nu}=c^2, \tag{4.1}$$

$$8\pi\rho=3/R^2-\Lambda, \quad 8\pi p=-1/R^2+\Lambda.$$

In this case the assumed equation makes (3.1) immediately integrable since the second two terms drop out. The resulting solution is the well-known one for a static Einstein universe with uniform density and pressure throughout. The solution could correspond to a distribution of actual fluid, with ρ and p non-negative, only with the cosmological constant satisfying the condition $3/R^2>\Lambda>1/R^2$.

Solution II. (Schwarzschild-de Sitter solution)

Assumed equation

$$e^{-\lambda-\nu}=\text{const.}$$

Resulting solution

$$e^{\lambda}=\left(1-\frac{2m}{r}-\frac{r^2}{R^2}\right)^{-1}, \tag{4.2}$$

$$e^{\nu}=c^2\left(1-\frac{2m}{r}-\frac{r^2}{R^2}\right),$$

$$8\pi\rho=3/R^2-\Lambda, \quad 8\pi p=-3/R^2+\Lambda.$$

In this case the assumed equation makes it immediately possible to obtain a first integral of (3.1), since it makes the third term at once integrable. The necessary second integration then also proves to be possible and leads to the well-known combined Schwarzschild-de Sitter solution for a de Sitter universe with a spherically symmetrical body at the origin of coordinates. With ρ and p both non-negative the space around this body has to be empty with $3/R^2=\Lambda$ and $\rho=p=0$. With $R=\infty$ the solution goes over into the usual form for the Schwarzschild solution surrounding an attracting particle of mass m, and with $m=0$ it goes over into the usual form for the de Sitter universe.

Solution III. (Schwarzschild interior solution)

Assumed equation

$$e^{-\lambda}=1-r^2/R^2.$$

Resulting solution

$$e^{\lambda}=\frac{1}{1-r^2/R^2}, \quad e^{\nu}=[A-B(1-r^2/R^2)^{\frac{1}{2}}]^2, \tag{4.3}$$

$$8\pi\rho=3/R^2-\Lambda,$$

$$8\pi p=\frac{1}{R^2}\left(\frac{3B(1-r^2/R^2)^{\frac{1}{2}}-A}{A-B(1-r^2/R^2)^{\frac{1}{2}}}\right)+\Lambda.$$

In this case the assumed equation immediately simplifies (3.1) by making the first term drop out, and a first integral can at once be obtained, after multiplying through by $e^{\nu}\nu'/2r$. The second integration then also proves to be easily possible and leads at once to the well-known Schwarzschild interior solution for a sphere of fluid of constant density ρ and a pressure p which decreases with r. With the constant $B=0$ the solution degenerates into the Einstein universe and with $A=0$ into the de Sitter universe.

It should be noted that Schwarzschild's interior solution as given by (4.3) is not the most general solution for a sphere of constant density, since a more general assumed equation, $e^{-\lambda}=1-r^2/R^2+C/r$ with C an arbitrary constant, would also correspond to $\rho=$ const.[4] The consequences of not setting $C=0$ in this expression have been studied by Mr. Volkoff and will be communicated elsewhere.

Solution IV

Assumed equation

$$e^{\nu}\nu'/2r=\text{const.}$$

Resulting solution

$$e^{\lambda}=\frac{1+2r^2/A^2}{(1-r^2/R^2)(1+r^2/A^2)},$$

$$e^{\nu}=B^2(1+r^2/A^2), \tag{4.4}$$

$$8\pi\rho=\frac{1}{A^2}\,\frac{1+3A^2/R^2+3r^2/R^2}{1+2r^2/A^2}+\frac{2}{A^2}\,\frac{1-r^2/R^2}{(1+2r^2/A^2)^2}-\Lambda,$$

$$8\pi p=\frac{1}{A^2}\,\frac{1-A^2/R^2-3r^2/R^2}{1+2r^2/A^2}+\Lambda.$$

In this case, we obtain the first of the new solutions to be considered. The assumed equation makes (3.1) immediately integrable by eliminating the third term. The solution for λ and ν then becomes easy. With suitable values for A and R the solution represents a sphere of compressible fluid with the pressure dropping to zero at the boundary as will be discussed more fully later.

Solution V

Assumed equation

$$e^{\nu}=\text{const.}\ r^{2n}.$$

Resulting solution

$$e^{\lambda}=\frac{1+2n-n^2}{1-(1+2n-n^2)(r/R)^N},\qquad e^{\nu}=B^2r^{2n}, \tag{4.5}$$

where $N=\dfrac{2(1+2n-n^2)}{1+n}$,

$$8\pi\rho=\frac{2n-n^2}{1+2n-n^2}\,\frac{1}{r^2}+\frac{3+5n-2n^2}{(1+n)R^2}\left(\frac{r}{R}\right)^M-\Lambda,$$

$$8\pi p=\frac{n^2}{1+2n-n^2}\,\frac{1}{r^2}-\frac{1+2n}{R^2}\left(\frac{r}{R}\right)^M+\Lambda.$$

where $M=\dfrac{2n(1-n)}{1+n}$.

In this case the substitution of the values of e^{ν} and ν' which are given by the assumed equation makes (3.1) immediately integrable if we multiply through by $r^{-M}/(n+1)$. The solution is a natural one to use in investigating spheres of fluid with infinite density and pressure at the center, as will be discussed in more detail later.

Solution VI

Assumed equation

$$e^{-\lambda}=\text{const.}$$

Resulting solution

$$e^{\lambda}=2-n^2,\quad e^{\nu}=(Ar^{1-n}-Br^{1+n})^2, \tag{4.6}$$

$$8\pi\rho=\frac{1-n^2}{2-n^2}\,\frac{1}{r^2}-\Lambda,$$

$$8\pi p=\frac{1}{2-n^2}\,\frac{1}{r^2}\,\frac{(1-n)^2A-(1+n)^2Br^{2n}}{A-Br^{2n}}+\Lambda.$$

In this case, it is convenient to substitute the assumed equation in the form $e^{-\lambda}=(2-n^2)^{-1}$, and

[4] See R. C. Tolman, *Relativity, Thermodynamics and Cosmology* (Oxford, 1934), § 96. In connection with the treatment of Schwarzschild's interior solution given in that place, it should be mentioned that the precise upper limits for r_1^2 and $2m$ should really be taken only eight-ninths as large as given in (96.14), since the solution ceases to have physical significance when the pressure p becomes infinite at $r=0$, i.e., when A becomes equal to B rather than when A becomes imaginary.

perform the indicated differentiations in (3.1). A first integral of the equation can then be obtained after multiplying through by $r^{a+1}e^{\nu/2}$, and the second integral after multiplying the result by r^{-1-2a}. The solution gives a very simple expression for the dependence of ρ on r, and is again a natural one to use in investigating spheres of fluid with infinite density and pressure at center, as will be discussed in more detail later.

Solution VII

Assumed equation

$$e^{-\lambda}=1-\frac{r^2}{R^2}+\frac{4r^4}{A^4}.$$

Resulting solution

$$e^{\lambda}=\frac{1}{1-r^2/R^2+4r^4/A^2}, \tag{4.7}$$

$$e^{\nu}=B^2\left[\sin\log\left(\frac{e^{-\lambda/2}+2r^2/A^2-A^2/4R^2}{C}\right)^{\frac{1}{2}}\right]^2,$$

$$8\pi\rho=\frac{3}{R^2}-\frac{20r^2}{A^4}-\Lambda,$$

$$8\pi p=-\frac{1}{R^2}+\frac{4r^2}{A^4}+\frac{4e^{-\lambda/2}}{A^2}(B^2e^{-\nu}-1)^{\frac{1}{2}}+\Lambda.$$

In this case, the substitution of the assumed equation into the first term of Eq. (3.1) makes it reduce to a constant times r, and the equation then becomes integrable after multiplication by $e^{\nu}\nu'/2r$. The dependence of p on r, with $e^{-\lambda/2}$ and $e^{-\nu}$ explicitly expressed in terms of r, is so complicated that the solution is not a convenient one for physical considerations.

Solution VIII

Assumed equation

$$e^{-\lambda}=\text{const.}\ r^{-2b}e^{\nu}.$$

Resulting solution

$$e^{-\lambda}=\frac{2}{(a-b)(a+2b-1)}-\left(\frac{2m}{r}\right)^{a+2b-1}-\left(\frac{r}{R}\right)^{a-b},$$

$$e^{\nu}=B^2r^{2b}e^{-\lambda},$$

$$8\pi\rho=\left\{1-\frac{2}{(a-b)(a+2b-1)}-(a+2b-2)\left(\frac{2m}{r}\right)^{a+2b-1}+(a-b+1)\left(\frac{r}{R}\right)^{a-b}\right\}\frac{1}{r^2}-\Lambda, \tag{4.8}$$

$$8\pi p=2be^{-\lambda}/r-8\pi\rho,$$

with $(a+b)(a-1)-2b-2=0$.

In this case, it is convenient to substitute the assumed expression for $e^{-\lambda}$ in (3.1) and perform the indicated differentiations. A first integral of Eq. (3.1) can then be obtained after multiplying through by r^a where a is connected with b by the last of Eqs. (4.8); and the second integral can then be obtained after multiplying through by r^{-2a-b}. With $a=2$, $b=0$, the solution degenerates into the Schwarzschild-de Sitter solution as already treated under (4.2).

This is the last of the new solutions which we shall present.

§5. Connection of Interior and Exterior Solutions

With an appropriate choice of parameters, some of the foregoing solutions would correspond to a distribution of fluid in which the pressure p drops from its central value at $r=0$ to the value zero at some particular radius $r=r_b$ where the density ρ still remains finite. Such a solution could then be taken as describing the condition inside a limited sphere of fluid with a definite boundary at $r=r_b$, and in the empty space outside this boundary would be taken as replaced by the Schwarzschild-de Sitter solution, in accordance with Birkhoff's theorem as to the most general spherically symmetrical solution in empty space. It will now be of interest to consider the interconnection of the two forms of solution at the surface of discontinuity at $r=r_b$.

Inside the sphere of fluid, we may take the solution as described by a line element of the general form (2.2)—on which we have based our considerations

$$ds^2=-e^{\lambda}dr^2-r^2d\theta^2-r^2\sin^2\theta d\phi^2+e^{\nu}dt^2, \tag{5.1}$$

where λ and ν are functions of r. Outside the sphere, we may take the solution as described by a line element of the simple Schwarzschild form

$$ds^2 = -\frac{dr^2}{1-2m/r} - r^2 d\theta^2 - r^2 \sin^2\theta d\phi^2 + \left(1-\frac{2m}{r}\right)dt^2, \quad (5.2)$$

which arises from the full expression for the Schwarzschild-de Sitter solution (4.2), when we set $\Lambda = 3/R^2 = 0$ in agreement with the known fact that the cosmological constant is too small to produce appreciable effects within a moderate spatial range, and where for convenience we set $c^2 = 1$ in order that m shall be the mass of the sphere—as measured by its external gravitational field—expressed in the usual units which make the velocity of light and the gravitational constant equal to unity. At the boundary of the sphere at $r = r_b$ both forms of the solution must then give the same results for physical measurements made at that radius.

Since the pressure p of the fluid falls to zero at the boundary, we may calculate the radius of the boundary r_b by setting the general expression for p given by (3.2) equal to zero. With $\Lambda = 0$, this then gives us

$$e^{-\lambda(r=r_b)}\left[\frac{\nu'(r=r_b)}{r_b} + \frac{1}{r_b^2}\right] - \frac{1}{r_b^2} = 0 \quad (5.3)$$

as the equation which determines the radius of the boundary r_b. At this radius (employing for simplicity a unified system of coordinates r, θ, ϕ, t applicable both inside and outside the sphere) we must then demand the equalities

$$e^{\nu(r=r_b)} = e^{-\lambda(r=r_b)} \quad (5.4)$$

and

$$e^{-\lambda(r=r_b)} = 1 - 2m/r_b \quad (5.5)$$

in order that the two forms of line element shall lead to the same results for measurements made at the boundary with stationary meter sticks and clocks.

We shall make use of the three equations (5.3), (5.4) and (5.5) in the following three sections where we consider specific examples of fluid spheres surrounded by empty space. In using these equations, it is convenient to regard Eq. (5.3) as determining the radius r_b of the sphere of fluid in terms of the parameters appearing in the expressions for e^{λ} and e^{ν} in the line element (5.1). Eq. (5.4) may then be regarded as imposing a condition which connects the parameters appearing in e^{ν} with those in e^{λ} and with r_b, a condition which can always be readily satisfied since it will be noted that e^{ν} is originally always arbitrary as to a multiplicative factor. Finally, Eq. (5.5) may then be used to calculate a value of the gravitational mass of the sphere m in terms of r_b and the parameters mentioned. It will be noted from the form of (5.5) that the gravitational mass of the sphere m can in any case not be larger than $r_b/2$, and hence can go to infinity only as the size of the sphere goes to infinity. This, however, does not necessarily imply that the mass M of the fluid before it has been condensed into the sphere could not go to infinity with r_b finite.

§6. Detailed Consideration of Solution IV

We shall take Solution IV as providing the first of the examples of a sphere of fluid surrounded by empty space, which we wish to consider in more detail.

The *line element* describing this solution has the form

$$ds^2 = -\frac{1+2r^2/A^2}{(1-r^2/R^2)(1+r^2/A^2)}dr^2 - r^2 d\theta^2 - r^2\sin^2\theta d\phi^2 + B^2(1+r^2/A^2)dt^2. \quad (6.1)$$

Inside the sphere of fluid, the *density* ρ and *pressure* p (with $\Lambda = 0$) are given by expressions of the form

$$8\pi\rho = \frac{1}{A^2}\,\frac{1+3A^2/R^2+3r^2/R^2}{1+2r^2/A^2} + \frac{2}{A^2}\,\frac{1-r^2/R^2}{(1+2r^2/A^2)^2}, \quad (6.2)$$

and

$$8\pi p = \frac{1}{A^2}\,\frac{1-A^2/R^2-3r^2/R^2}{1+2r^2/A^2}. \quad (6.3)$$

The *central density* ρ_c and *central pressure* p_c

have the values

$$8\pi\rho_c=\frac{3}{A^2}+\frac{3}{R^2}, \quad \text{and} \quad 8\pi p_c=\frac{1}{A^2}-\frac{1}{R^2}. \tag{6.4}$$

In terms of these central values, the *equation of state*, connecting the density and pressure of the fluid inside the sphere, can then be written in the convenient simple form

$$\rho=\rho_c-5(p_c-p)+8\frac{(p_c-p)^2}{\rho_c+p_c}. \tag{6.5}$$

The *boundary of the sphere* occurs at

$$r_b=\frac{R}{3^{\frac{1}{2}}}(1-A^2/R^2)^{\frac{1}{2}}, \tag{6.6}$$

where the pressure has dropped to the value zero, and the *boundary density* has the value

$$\rho_b=\rho_c-5p_c+8p_c^2/(\rho_c+p_c). \tag{6.7}$$

From the connection with *Schwarzschild's exterior solution* (5.2), holding outside the boundary, we have

$$B^2=(1-r_b^2/R^2)/(1+2r_b^2/A^2), \tag{6.8}$$

as a *condition* on the *parameter* B^2 appearing in e^ν. And we have

$$m=\frac{r_b}{2}\left\{1-\frac{(1-r_b^2/R^2)(1+r_b^2/A^2)}{1+2r_b^2/A^2}\right\}, \tag{6.9}$$

as an expression for the *mass of the sphere* as measured by its external gravitational field.

It will be seen from the foregoing that all the properties of the sphere and its surrounding field can be regarded as determined by the choice of the two independent parameters A and R, although it is not necessarily most convenient to express those properties solely in terms of these parameters. With $R^2>A^2$, it will be found that the pressure and density of the fluid would both fall continuously from their central to their boundary values where the density would still be positive. And with $R^2<11.5A^2$, it will be found that the ratio of pressure to density would nowhere exceed one-third. As R^2 and A^2 go to infinity the central density and pressure approach zero, and the sphere becomes larger without limit.

The solution may be a useful one in studying the properties of spheres of compressible fluid since the equation of state (6.5) which connects the density of the fluid with its pressure is relatively simple. This equation of state, however, is of course a very special one, since the coefficients in the terms which give the linear and quadratic dependence of density on pressure are not arbitrary but are of the form which has arisen from the particular assumption that was introduced to secure integrability. Nevertheless, it has been shown by Professor Oppenheimer and Mr. Volkoff, in the article mentioned, that this equation of state leads to results in some respects similar to those which would be obtained from the equation of state for a Fermi gas in cases of intermediate central densities.

§7. Detailed Consideration of a Special Case of Solution V

We shall take Solution V as providing the second of the examples of a sphere of fluid surrounded by empty space which we wish to consider in more detail. In carrying this out we shall make the specific choice $n=\frac{1}{2}$ for the parameter n which appears in the description of the solution (4.5), since this will give a ratio of central density to pressure of special physical interest.

The *line element* describing the solution (with $n=\frac{1}{2}$) has the form

$$ds^2=-\frac{7}{4-7(r/R)^{7/2}}dr^2-r^2d\theta^2 -r^2\sin^2\theta d\phi^2+B^2rdt^2. \tag{7.1}$$

Inside the sphere of fluid the *density* ρ and *pressure* p (with $\Lambda=0$) are given by expressions of the form

$$8\pi\rho=\frac{3}{7r^2}+\frac{10}{3R^2}\left(\frac{r}{R}\right)^{\frac{1}{2}}, \tag{7.2}$$

and

$$8\pi p=\frac{1}{7r^2}-\frac{2}{R^2}\left(\frac{r}{R}\right)^{\frac{1}{2}}. \tag{7.3}$$

The *central density* ρ_c and *central pressure* p_c then become infinite with the ratio

$$p_c/\rho_c=\tfrac{1}{3}. \tag{7.4}$$

The *equation of state* connecting the density and pressure of the fluid inside the sphere can be written in the form

$$\rho=3p+\frac{7}{6\pi R^{7/3}}\left\{\frac{1}{4\pi(3\rho+5p)}\right\}^{1/6} \tag{7.5}$$

The *boundary of the sphere* occurs at

$$r_b=R/14^{3/7}, \tag{7.6}$$

where the pressure has dropped to zero and the *boundary density* has the value

$$8\pi\rho_b=28/(3\times 14^{1/7}R^2). \tag{7.7}$$

From the connection with *Schwarzschild's exterior solution* (5.2), holding outside the boundary, we have

$$B^2=14^{3/7}/2R, \tag{7.8}$$

as a *condition* on the *parameter* B^2 appearing in e^ν. And we have

$$m=r_b/4=R/(4\times 14^{3/7}) \tag{7.9}$$

as an expression for the *mass of the sphere*, as measured by its external gravitational field.

It will be noted in this case that the solution corresponds to a sphere of fluid of infinite density and pressure at the center, having at that point the ratio which would hold for radiation, or for particles of such high kinetic energy that their rest mass may be neglected in comparison with their total mass. Other ratios could, of course, be obtained with a different choice for the parameter n in (4.5).

With the adjustable parameter R lying anywhere in the range $0<R<\infty$, it will be seen that the solution satisfies the necessary physical conditions for a sphere of fluid, with a pressure which drops continuously from an infinite value at the center to zero at the boundary, with a density which drops continuously from an infinite value at the center to a value which is still positive at the boundary, and with a ratio of pressure to density which never exceeds one-third. As R approaches infinity, the ratio of pressure to density approaches one-third throughout and the sphere becomes larger without limit.

The solution may in some cases be a useful one in studying the properties of *finite* spheres of fluid which have *infinite* central pressures and densities. In accordance with the equation of state (7.5), however, the ratio of pressure to density drops too fast with decreasing density to correspond very closely with what would be expected in the case of a Fermi gas having infinite central pressure and density.

§8. Detailed Consideration of a Special Case of Solution VI

We shall now take Solution VI as providing the last of the examples of a sphere of fluid surrounded by empty space which we wish to consider in more detail. In carrying this out we shall make the specific choice $n=\frac{1}{2}$ for the parameter n which appears in the description of the solution (4.6), which will again give us the value one-third for the ratio of central pressure to density.

The *line element* describing the solution (with $n=\frac{1}{2}$) has the form

$$ds^2=-(7/4)dr^2-r^2d\theta^2-r^2\sin^2\theta d\phi^2 +(Ar^{\frac{1}{2}}-Br^{\frac{1}{2}})^2dt^2. \tag{8.1}$$

Inside the sphere of fluid the *density* ρ and *pressure* p (with $\Lambda=0$) are given by expressions of the form

$$8\pi\rho=3/7r^2, \tag{8.2}$$

and

$$8\pi p=\frac{1}{7r^2}\,\frac{1-9(B/A)r}{1-(B/A)r}. \tag{8.3}$$

The *central density* ρ_c and *central pressure* p_c then become infinite with the ratio

$$p_c/\rho_c=\tfrac{1}{3}. \tag{8.4}$$

The *equation of state* connecting the density and pressure of the fluid inside the sphere can be written in the form

$$p=\frac{\rho}{3}\,\frac{1-9(3/56\pi)^{\frac{1}{3}}(B/A)\rho^{-\frac{1}{3}}}{1-(3/56\pi)^{\frac{1}{3}}(B/A)\rho^{-\frac{1}{3}}}. \tag{8.5}$$

The *boundary of the sphere* occurs at

$$r_b=A/9B, \tag{8.6}$$

where the pressure has dropped to zero and the *boundary density* has the value

$$8\pi\rho_b=3^5B^2/7A^2. \tag{8.7}$$

From the connection with *Schwarzschild's exterior solution* (5.2), holding outside the boundary, we have

$$A^2=(3^6/2^4\times 7)(B/A) \tag{8.8}$$

as a *condition* on the parameter A^2 appearing in e^ν, where B/A may still be taken as arbitrary. And we have

$$m=3r_b/14=A/42B, \tag{8.9}$$

as an expression for the *mass of the sphere* as measured by its external gravitational field.

Again it will be noted as in the previous case discussed in §7, that the solution corresponds to a sphere of fluid of infinite density and pressure at the center, having at that point the ratio which would hold for radiation or for particles of such high kinetic energy that their rest mass may be neglected in comparison with their total mass. Other ratios could be obtained with a different choice for n in (4.6).

With the adjustable parameter B/A lying anywhere in the range $0<B/A<\infty$, it will be seen that the solution satisfies the necessary physical conditions for a sphere of fluid, with a pressure which drops continuously from an infinite value at the center to zero at the boundary, with a density which drops continuously from an infinite value at the center to a value which is still positive at the boundary, and with a ratio of pressure to density which never exceeds one-third. As B/A approaches zero, the ratio of pressure to density approaches one-third throughout, the sphere becomes larger without limit, and the solution as given by (8.1) approaches the same form as is approached by the solution given by (7.1) as R goes to infinity. This limiting form, which agrees with that given in the article of Professor Oppenheimer and Mr. Volkoff by Eq. (22), might be called the blackbody radiation solution.

The solution in its more general form proves to be a somewhat helpful one for use in connection with the results of Professor Oppenheimer and Mr. Volkoff, since with ρ large the equation of state (8.5) goes over into the approximate form $\rho-3p=\text{const.}\,\rho^{\frac{1}{3}}$ which is that for a highly compressed Fermi gas.

§9. Concluding Remarks

In conclusion we must call attention to two points which are more completely considered in the article of Professor Oppenheimer and Mr. Volkoff. It is necessary to mention these points also here in order to guard against misconceptions as to the nature of the static solutions of Einstein's field equations for spheres of fluid which have been presented in this paper.

In the first place, it should be remarked that the static character of any such solution is in itself only sufficient to assure us that the solution describes a possible state of equilibrium for a fluid, but is not sufficient to tell us whether or not that state of equilibrium would be stable towards disturbances. Further investigation is necessary to settle the question of stability under any given set of circumstances. The question is an important one, since we cannot regard a static solution as representing a physically permanent state of a fluid if the equilibrium turns out to be unstable towards small disturbances, as for example in the well-known case of the Einstein static universe.

In the second place, it should be emphasized that the imposition of static character on the solutions to be considered is from a physical point of view a severe restriction. It is, of course, immediately evident that solutions having a strictly static character could in any case be applicable only in first approximation to spheres of fluid where slow changes are actually taking place. In addition it is to be noted that there might be a possibility for an important class of quasi-static solutions with $e^\nu=g_{44}$ going to zero at the center of the sphere, as in certain of static solutions considered above. Such solutions could be said to have quasi-static character, since changes taking place at the center would exhibit a very slow rate when measured by an external observer. Further discussion of the possible existence and importance of such solutions will be found in the article by Professor Oppenheimer and Mr. Volkoff.

On Massive Neutron Cores

J. R. OPPENHEIMER AND G. M. VOLKOFF
Department of Physics, University of California, Berkeley, California

(Received January 3, 1939)

It has been suggested that, when the pressure within stellar matter becomes high enough, a new phase consisting of neutrons will be formed. In this paper we study the gravitational equilibrium of masses of neutrons, using the equation of state for a cold Fermi gas, and general relativity. For masses under $\frac{1}{2}\odot$ only one equilibrium solution exists, which is approximately described by the nonrelativistic Fermi equation of state and Newtonian gravitational theory. For masses $\frac{1}{2}\odot < m < \frac{3}{4}\odot$ two solutions exist, one stable and quasi-Newtonian, one more condensed, and unstable. For masses greater than $\frac{3}{4}\odot$ there are no static equilibrium solutions. These results are qualitatively confirmed by comparison with suitably chosen special cases of the analytic solutions recently discovered by Tolman. A discussion of the probable effect of deviations from the Fermi equation of state suggests that actual stellar matter after the exhaustion of thermonuclear sources of energy will, if massive enough, contract indefinitely, although more and more slowly, never reaching true equilibrium.

I. INTRODUCTION

FOR the application of the methods commonly used in attacking the problem of stellar structure[1] the distribution of energy sources and their dependence on the physical conditions within the star must be known. Since at the time of Eddington's original studies not much was known about the physical processes responsible for the generation of energy within a star, various mathematically convenient assumptions were made in regard to the energy sources, and these led to different star models (e.g. the Eddington model, the point source model, etc.). It was found that with a given equation of state for the stellar material many important properties of the solutions (such as the mass-luminosity law) were quite insensitive to the choice of assumptions about the distribution of energy sources, but were common to a wide range of models.

In 1932 Landau[2] proposed that instead of making arbitrary assumptions about energy sources chosen merely for mathematical convenience, one should attack the problem by first investigating the physical nature of the equilibrium of a given mass of material in which no energy is generated, and from which there is no radiation, presumably in the hope that such an investigation would afford some insight into the more general situation where the generation of energy is taken into account. Although such a model gives a good description of a white dwarf star in which most of the material is supposed to be in a degenerate state with a zero point energy high compared to thermal energies of even 10^7 degrees, and such that the pressure is determined essentially by the density only and not by the temperature, still it would fail completely to describe a normal main sequence star, in which on the basis of the Eddington model the stellar material is nondegenerate, and the existence of energy sources and of the consequent temperature and pressure gradients plays an important part in determining the equilibrium conditions. The stability of a model in which the energy sources have to be taken into account is known to depend also on the temperature sensitivity of the energy sources and on the presence or absence of a time-lag in their response to temperature changes. However, if the view which seems plausible at present is adopted that the principal sources of stellar energy, at least in main sequence stars, are thermonuclear reactions, then the limiting case considered by Landau again becomes of interest in the discussion of what will eventually happen to a normal main sequence star after all the elements available for thermonuclear reactions are used up. Landau showed that for a model consisting of a cold degenerate Fermi gas there exist no stable equilibrium configurations for

[1] A. Eddington, *The Internal Constitution of the Stars* (Cambridge University Press, 1926); B. Strömgren, Ergebn. Exakt. Naturwiss. **16**, 465 (1937); Short summary in G. Gamow, Phys. Rev. **53**, 595 (1938).

[2] L. Landau, Physik. Zeits. Sowjetunion **1**, 285 (1932).

masses greater than a certain critical mass, all larger masses tending to collapse. For a mixture of electrons and nuclei in which on the average there are two protonic masses per electron Landau found the critical mass to be roughly $1.5\odot$, and in general the critical mass is inversely proportional to the square of the mass per particle obtained by spreading out the total mass over only those particles which essentially determine the pressure of the Fermi gas.

The possibility has been suggested[3] that in sufficiently massive stars after all the thermonuclear sources of energy, at least for the central material of the star, have been exhausted a condensed neutron core would be formed. The minimum mass for which such a core would be stable has been estimated by Oppenheimer and Serber,[4] who on taking into account some effects of nuclear forces give approximately $0.1\odot$ as a reasonable minimum mass. The gradual growth of such a core with the accompanying liberation of gravitational energy is suggested by Landau as a possible source of stellar energy.

In this connection it seems of interest to ask whether this model of the final state of a star can be right for arbitrarily heavy stars, i.e., to investigate whether there is an upper limit to the possible size of such a neutron core. Landau's original result for a cold relativistically degenerate Fermi gas quoted above gives in the case of a neutron gas an upper limit of about $6\odot$ beyond which the core would not be stable but would tend to collapse. Two objections might be raised against this result. One is that it was obtained on the basis of Newtonian gravitational theory while for such high masses and densities general relativistic effects must be considered. The other one is that the Fermi gas was assumed to be relativistically degenerate throughout the whole core, while it might be expected that on the one hand, because of the large mass of the neutron, the nonrelativistically degenerate equation of state might be more appropriate over the greater part of the core, and on the other hand the gravitational effect of the kinetic energy of the neutrons could not be neglected. The present investigation seeks to establish what differences are introduced into the result if general relativistic gravitational theory is used instead of Newtonian, and if a more exact equation of state is used. A discussion of the general relativistic treatment of the equilibrium of spherically symmetric distributions of matter is first given, and then the special ideal case of a cold neutron gas is treated. A discussion of the results, and comparison with some results of Professor R. C. Tolman reported in an accompanying paper are given in the concluding sections.

II. Relativistic Treatment of Equilibrium

It is known[5] that the most general static line element exhibiting spherical symmetry may be expressed in the form

$$ds^2=-e^{\lambda}dr^2-r^2d\theta^2-r^2\sin^2\theta d\phi^2+e^{\nu}dt^2, \qquad \lambda=\lambda(r), \quad \nu=\nu(r). \tag{1}$$

If the matter supports no transverse stresses and has no mass motion, then its energy momentum tensor is given by[6]

$$T_1^1=T_2^2=T_3^3=-p, \quad T_4^4=\rho \tag{2}$$

where p and ρ are respectively the pressure and the macroscopic energy density measured in proper coordinates. With these expressions for the line element and for the energy momentum tensor, and with the cosmological constant Λ taken equal to zero, Einstein's field equations reduce to:[7]

$$8\pi p=e^{-\lambda}\left(\frac{\nu'}{r}+\frac{1}{r^2}\right)-\frac{1}{r^2}, \tag{3}$$

$$8\pi\rho=e^{-\lambda}\left(\frac{\lambda'}{r}-\frac{1}{r^2}\right)+\frac{1}{r^2}, \tag{4}$$

$$\frac{dp}{dr}=-\frac{(p+\rho)}{2}\nu', \tag{5}$$

where primes denote differentiation with respect to r. These three equations together with the equation of state of the material $\rho=\rho(p)$ de-

[3] G. Gamow, *Atomic Nuclei and Nuclear Transformations* (Oxford, 1936), second edition, p. 234. L. Landau, Nature **141**, 333 (1938) and others.

[4] J. R. Oppenheimer and R. Serber, Phys. Rev. **54**, 540 (1938).

[5] R. C. Tolman, *Relativity, Thermodynamics and Cosmology* (Oxford, 1934), pp. 239–241.

[6] R. C. Tolman, reference 5, p. 243.

[7] R. C. Tolman, reference 5, p. 244.

termine the mechanical equilibrium of the matter distribution as well as the dependence of the $g_{\mu\nu}$'s on r.

The boundary of the matter distribution is the value of $r=r_b$ for which $p=0$, and such that for $r<r_b$, $p>0$. For $r<r_b$ the solution depends on the equation of state of the material connecting p and ρ. For many equations of state a sharp boundary exists with a finite value of r_b.

In empty space surrounding the spherically symmetric distribution of matter $p=\rho=0$, and Schwarzschild's exterior solution is obtained:[8]

$$e^{-\lambda(r)}=1+A/r, \quad e^{\nu(r)}=B(1+A/r). \tag{6}$$

The constants A and B are fixed by the requirement that at great distances away from the matter distribution the $g_{\mu\nu}$'s must go over into their weak-field form, i.e., $B=1, A=-2m$ where m is the total Newtonian mass of the matter as calculated by a distant observer.[9]

Inside the boundary Eqs. (3), (4) and (5) may be rewritten as follows. Using the equation of state $\rho=\rho(p)$ Eq. (5) may be immediately integrated.

$$\nu(r)=\nu(r_b)-\int_0^{p(r)}\frac{2dp}{p+\rho(p)},$$

$$e^{\nu(r)}=e^{\nu(r_b)}\exp\left[-\int_0^{p(r)}\frac{2dp}{p+\rho(p)}\right].$$

The constant $e^{\nu(r_b)}$ is determined by making e^{ν} continuous across the boundary.

$$e^{\nu(r)}=\left(1-\frac{2m}{r_b}\right)\exp\left[-\int_0^{p(r)}\frac{2dp}{p+\rho(p)}\right]. \tag{7}$$

Thus e^{ν} is known as a function of r if p is known as a function of r. Further in Eq. (4) introduce a new variable

$$u(r)=\tfrac{1}{2}r(1-e^{-\lambda}) \quad \text{or} \quad e^{-\lambda}=1-2u/r. \tag{8}$$

Then Eq. (4) becomes:

$$du/dr=4\pi\rho(p)r^2. \tag{9}$$

In Eq. (3) replace $e^{-\lambda}$ by its value from (8) and ν' by its value from (5). It becomes:

$$\frac{dp}{dr}=-\frac{p+\rho(p)}{r(r-2u)}[4\pi pr^3+u]. \tag{10}$$

[8] R. C. Tolman, reference 5, p. 203.
[9] R. C. Tolman, reference 5, pp. 203 and 207.

Equations (9) and (10) form a system of two first-order equations in u and p. Starting with some initial values $u=u_0$ $p=p_0$ at $r=0$, the two equations are integrated simultaneously to the value $r=r_b$ where $p=0$, i.e., until the boundary of the matter distribution is reached. The value of $u=u_b$ at $r=r_b$ determines the value of $e^{\lambda(r_b)}$ at the boundary, and this is joined continuously across the boundary to the exterior solution, making.

$$u_b=\frac{r_b}{2}[1-e^{-\lambda(r_b)}]=\frac{r_b}{2}\left[1-\left(1-\frac{2m}{r_b}\right)\right]=m.$$

Thus the mass of this spherical distribution of matter as measured by a distant observer is given by the value u_b of u at $r=r_b$.

The following restrictions must be made on the choice of p_0 and u_0, the initial values of p and u at $r=0$:

(a) In accordance with its physical meaning as pressure, $p_0\geqq 0$.

(b) From Eq. (8) it is seen that for all finite values of $e^{-\lambda}$, $u_0=0$. Since $g_{11}=-e^{\lambda}$ must never be positive, $u_0\leqq 0$ for infinite values of $e^{-\lambda}$ at the origin. However, it may be shown that of all the finite values of p_0 at the origin $p_0=0$ is the only one compatible with a negative value of u_0, and that for equations of state of the type occurring in this problem even this possibility is excluded, so that u_0 must vanish.[10]

(c) A special investigation for any particular equation of state must be made to see whether solutions exist in which $0\geqq u_0\geqq -\infty$ and $p\to\infty$ as $r\to 0$.

III. Particular Equations of State

The above arguments show that Eqs. (9) and (10) together with a given equation of state completely determine the distribution of matter.

[10] This can be seen from the following argument. Having chosen some particular value of p_0 one may usually represent the equation of state in that pressure range by $\rho=Kp^s$ with some appropriate value of s. Using this equation of state and taking the approximate form of Eq. (10) near the origin for the case $u_0<0$, and finite p_0, one obtains:

$$\frac{dp}{dr}=\frac{p+\rho(p)}{2r}=\frac{p+Kp^s}{2r}.$$

Integration of this equation shows that for $s<1$ $p_0\geqq 0$ can not be satisfied, and for $s\geqq 1$ only the value $p_0=0$ is possible. For the equations of state used in this problem always $s<1$ holds. It may also be noted that the above equation together with Eq. (7) show that $e^{\nu(r)}\to\infty$ as $r\to 0$.

The assumption $\rho=$const., $u_0=0$ makes it possible to integrate Eqs. (9) and (10) explicitly and leads to Schwarzschild's interior solution.[11] Other matter distributions corresponding to other equations of state are given by Professor Tolman in an accompanying paper.

If the matter is taken to consist of particles of rest mass μ_0 obeying Fermi statistics, and their thermal energy[12] and all forces between them are neglected, then it may be shown that a parametric form for the equation of state is:[13]

$$\rho=K(\sinh t-t), \tag{11}$$

$$p=\tfrac{1}{3}K(\sinh t-8\sinh \tfrac{1}{2}t+3t), \tag{12}$$

where $$K=\pi\mu_0^4c^5/4h^3 \tag{13}$$

and $$t=4\log\left(\frac{\hat{p}}{\mu_0c}+\left[1+\left(\frac{\hat{p}}{\mu_0c}\right)^2\right]^{\frac{1}{2}}\right), \tag{14}$$

where $\hat{p}$ is the maximum momentum in the Fermi distribution and is related to the proper particle density N/V by

$$\frac{N}{V}=\frac{8\pi}{3h^3}\hat{p}^3. \tag{15}$$

Substituting the above expressions for p and ρ into Eqs. (9) and (10) one gets:

$$\frac{du}{dr}=4\pi r^2K(\sinh t-t), \tag{16}$$

$$\frac{dt}{dr}=-\frac{4}{r(r-2u)}\frac{\sinh t-2\sinh \frac{1}{2}t}{\cosh t-4\cosh \frac{1}{2}t+3}$$
$$\times[(4/3)\pi Kr^3(\sinh t-8\sinh \tfrac{1}{2}t+3t)+u]. \tag{17}$$

These equations are to be integrated from the values $u=0$, $t=t_0$ at $r=0$ to $r=r_b$ where $t_b=0$ (which makes $p=0$), and $u=u_b$.

A note must be made of the units employed in these equations. Eqs. (3), (4) and (5) from which (16) and (17) are derived are stated in relativistic units,[14] i.e., such that $c=1$, $G=1$ (c is the velocity of light, G is the gravitational constant). This determines the unit of time and the unit of mass in terms of a still arbitrary unit of length. The unit of length is now fixed by the requirement that $K=1/4\pi$. Eqs. (16) and (17) now become:

$$\frac{du}{dr}=r^2(\sinh t-t), \tag{18}$$

$$\frac{dt}{dr}=-\frac{4}{r(r-2u)}\frac{\sinh t-2\sinh \frac{1}{2}t}{\cosh t-4\cosh \frac{1}{2}t+3}$$
$$\times[\tfrac{1}{3}r^3(\sinh t+8\sinh \tfrac{1}{2}t+3t)+u]. \tag{19}$$

The unit of length has been fixed to be

$$a=\frac{1}{\pi}\left(\frac{h}{\mu_0c}\right)^{\frac{1}{3}}\frac{c}{(\mu_0G)^{\frac{1}{2}}},$$

while the unit of mass is

$$b=\frac{c^2}{G}a=\frac{1}{\pi}\left(\frac{h}{\mu_0c}\right)^{\frac{1}{3}}\frac{c^3}{(\mu_0G^3)^{\frac{1}{2}}}.$$

For a neutron gas $a=1.36\times10^6$ cm, $b=1.83\times10^{34}$ g. The general character of the solution is seen to be independent of the mass of the neutron which determines only the scale of the result.

No way was found to carry out the integration analytically, so Eqs. (18) and (19) were integrated numerically for several finite values of t_0. For all these cases u_0 was taken to be equal to zero, since the equation of state near the origin for finite t_0 behaves like $\rho(p)=Kp^s$, $s<1$. The first four entries in Table I were thus obtained.

For $t_0\to\infty$ Eqs. (18) and (19) may be replaced by their asymptotic expressions:

$$du/dr=\tfrac{1}{2}r^2e^t, \tag{20}$$

$$\frac{dt}{dr}=-\frac{4}{r(r-2u)}\left[\frac{r^3}{6}e^t+u\right]. \tag{21}$$

[11] R. C. Tolman, reference 5, pp. 246–247.

[12] The condition for thermal equilibrium in a static gravitational field is given by Tolman (reference 5, p. 318) as $T_0(g_{44})^{\frac{1}{2}}=$const. where T_0 is the proper temperature. The equilibrium state of a matter distribution which no longer radiates appreciably corresponds to a low surface temperature T_0. If g_{44} is everywhere finite, then T_0 will be small throughout the matter distribution. For those singular solutions in which g_{44} vanishes at the origin it is conceivable that the central temperature may be high. However, on the one hand from Eq. (7) it is seen that the vanishing of g_{44} at the origin corresponds to infinite central pressure, and in this limit the equation of state given below reduces to $\rho=3p$ so that temperature introduces no radically new effects, and on the other hand zero values of g_{44} indicate the slowing down of all physical processes near the origin and thus may correspond to nonstatic solutions describing states which have not yet attained equilibrium, and which are not discussed in this paper.

[13] Cf. S. Chandrasekhar, Monthly Notices of R.A.S. **95**, 222 (1935), but introduce *energy* density in place of his *mass* density.

[14] R. C. Tolman, reference 5, pp. 201–202.

An exact solution[15] of these equations is:

$$e^t = 3/7r^2, \qquad u = 3r/14, \tag{22}$$

which corresponds to $t_0 = \infty$, $u_0 = 0$. A careful examination of Eqs. (20) and (21) shows that there are no other solutions corresponding to $t_0 = \infty$, $0 \geqq u_0 \geqq -\infty$. The exact solution (22) of the approximate equations (20) and (21) was taken out to that value of r where $t = 6$ (the approximation in the form of Eq. (20) and (21) it quite good for $t \geqq 6$), and then the integration of the exact equations (18) and (19) was carried out numerically to $r = r_b$ where $t = 0$. This gave the last entry in Table I.

It is of interest to ask whether perhaps a finite gravitational mass might correspond to an infinite number of particles, and an infinite gravitational binding energy. It may be seen that this is not the case by the following argument. Although the proper particle density becomes infinite when the central pressure becomes infinite, still it remains integrable, so that the total number of particles always remains finite. The element of proper volume of a spherical shell is $4\pi e^{\lambda/2} r^2 dr$. As the solution of the approximate equations shows in the neighborhood of the origin:

$$e^{\lambda/2} = \left(1 - \frac{2u}{r}\right)^{-\frac{1}{2}} = \left(1 - \frac{3}{7}\right)^{-\frac{1}{2}} = \left(\frac{7}{4}\right)^{\frac{1}{2}},$$

$$N/V \propto \hat{p}^{\frac{3}{4}} \propto e^{3t/4} \propto 1/r^{\frac{3}{2}} \text{ for large } t \text{ and } \hat{p};$$

$$\therefore \quad N \propto \int_0^r \frac{r^2}{r^{\frac{3}{2}}} dr \propto r^{\frac{1}{2}} \text{ near the origin.}$$

A fortiori the number of particles is finite for nonsingular solutions.

[15] This solution is a limiting form of the solutions V, VI given by Tolman in the accompanying paper.

For very small values of t the equation of state (11), (12) reduces to $p = K\rho^{5/3}$ and $\hat{p} \propto t$. Using this equation of state and Newtonian gravitational theory (which is expected to give a good result for small masses and densities), one finds that $\hat{p} \propto m^{\frac{1}{3}}$, or that $m \propto t^{\frac{3}{2}}$. Fig. 1 gives a schematic plot of the dependence of m on t_0 for the case that the elementary particles are neutrons. The mass m is plotted in units of sun's mass (2×10^{33} g) against $\tan^{-1} t_0$. The curve near the origin is dotted since, as has been already pointed out, a neutron core with a mass less than about $0.1\odot$ will disintegrate into nuclei and electrons.

The striking feature of the curve is that the mass increases with increasing t_0 until a maximum is reached at about $t_0 = 3$, after which the curve drops until a value roughly $\frac{1}{3}\odot$ is reached for $t_0 = \infty$. In other words no static solutions at all exist for $m > \frac{3}{4}\odot$, two solutions exist for all m in $\frac{3}{4}\odot > m > \frac{1}{3}\odot$, and one solution exists for all $m < \frac{1}{3}\odot$.

Some insight into this situation may be gained from the following considerations. In the nonrelativistic polytrope solutions of Emden[16] the equation of state was assumed to be $p = K\rho^\gamma = K\rho^{1+1/n}$. Solutions which at first sight seem to be quite satisfactory (i.e., giving a finite mass within a finite radius) were found for values of $n < 5$ or $\gamma > 6/5$. But Landau[2] pointed out that although these solutions in every case give an equilibrium configuration, they do not in every case give *stable* equilibrium. Thus, unless $\gamma \geqq 4/3$ the equilibrium configuration is unstable. This may be seen from the following rough calculation. The gravitational part of the free energy of the system is negative and proportional to $\rho^{\frac{1}{3}}$ where

[16] Emden, *Gaskugeln* (1907), or cf. *Handbuch der Astrophys.* Vol. 3, p. 186.

TABLE I. *Mass, radius and neutron density for various values of* t_0.

t_0	Mass: In Units of Eqs. (18), (19)	Mass: In Units of $\odot$ for Neutrons	Radius: In Units of Eqs. (18), (19)	Radius: In Kilometers, for Neutrons	$\left(\frac{\hat{p}}{\mu c}\right)_{r=0}$	$\left(\frac{N}{V}\right)_{r=0}$ Neutrons CM^3
1	0.033	0.30	1.55	21.1	0.25	0.062×10^{39}
2	0.066	0.60	0.98	13.3	0.52	0.56×10^{39}
3	0.078	0.71	0.70	9.5	0.82	2.2×10^{39}
4	0.070	0.64	0.50	6.8	1.17	6.4×10^{39}
∞	0.037	0.34	0.23	3.1	∞	∞

ρ is an appropriate average density (Newtonian gravitational theory is used). The part of the free energy caused by compression is proportional to $\int pdv$, and hence to $\rho^{\gamma-1}$ ($\gamma \neq 1$). Thus

$$F = -a\rho^{\frac{1}{3}} + b\rho^{\gamma-1}.$$

Polytrope solutions exist for both $\gamma = 5/3 (> 4/3)$, i.e., for $n = 3/2$ and for $\gamma = 5/4 (< 4/3$, but $> 6/5)$, i.e., for $n = 4$, but as may be seen from the schematic plot of the free energy curves in Fig. 2, the former corresponds to stable equilibrium and the latter to unstable equilibrium.

In the present relativistic calculations the results for small masses and small central densities and pressures (small values of t_0), as was already mentioned above, may be expected to agree quite closely with nonrelativistic calculations with the equation of state $p = K\rho^{\frac{5}{3}}$. Since ρ is a monotonic function of t, the curves of free energy against t_0 for fixed total number of particles, and thus for a fixed M_0 (gravitational mass at zero density; the gravitational mass will vary somewhat along a curve of constant particle number, as the density increases), will for small masses have the same general character as the curves of free energy against some average density in the nonrelativistic case (cf. the curve for $\gamma = 5/3$ in Fig. 2). Then as the number of particles is increased the character of the free energy curves must change in order to admit the possibility of a second equilibrium position. Since the free energy must be a continuous function of t_0, and since we know from nonrelativistic calculations that for small masses (and low densities) we have a position of stable equilibrium (a minimum in the free energy curve) we can conclude that the second equilibrium position corresponds either to a maximum or to an inflection point in the free energy curve (and certainly not to a minimum). Fig. 3 gives a schematic plot of free energy against t_0 for different values of M_0 which would explain the existence of one equilibrium position for small masses, two for intermediate masses, and none for large masses. The masses marked on the curves are the actual gravitational masses corresponding to the equilibrium points of the critical free energy curves separating the solutions into the three types mentioned above.

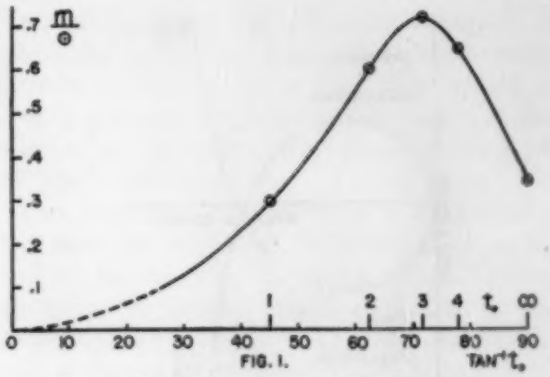

FIG. 1.

FIG. 1. Dependence of m on t_0 for neutrons.

IV. Discussion—Relation to Tolman's Solutions

Before we study the physical implications of these results, we may try to show how their qualitative features may be obtained from the analytic solutions recently discovered by Professor Tolman.[17] This will also help us to understand the probable effect of alterations in the equation of state of the neutron gas at high densities.

On the one hand Tolman's solution IV, discussed in §6 of his paper, enables us to understand the existence of a limiting mass for static solutions and to give an estimate of its magnitude; on the other hand Tolman's solution VI, discussed in §8 (and less directly solution V), has for $n = \frac{1}{2}$, very much the character of our singular solution for $t_0 \to \infty$, and, with appropriately chosen constants, gives a mass of the same order of magnitude as we have found.

Tolman's solution IV is nonsingular, and corresponds to the quadratic equation of state (6.5) of his paper:

$$8\frac{(p_c - p)^2}{p_c + \rho_c} - 5(p_c - p) + \rho_c - \rho = 0 \quad \text{(Tolman, 6.5)},$$

where ρ_c and p_c are the central density and pressure. From Eqs. (6.4), (6.6) and (6.9) of Tolman's paper the mass corresponding to this solution is given in terms of p_c and ρ_c by

$$m = 4\left(\frac{p_c}{\rho_c + 3p_c}\right)^{\frac{1}{2}}\left[\frac{8\pi}{3}(\rho_c - 3p_c)\right]^{-\frac{1}{2}}. \quad (23)$$

[17] We are very much indebted to Professor Tolman for letting us see these results before publication, and for helpful discussions of them.

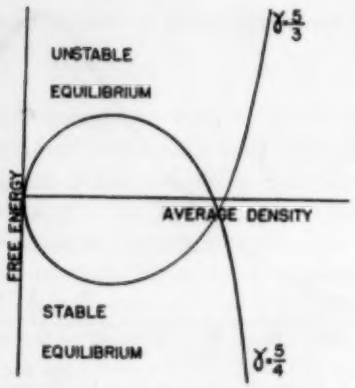

FIG. 2. Free energy as a function of average density.

If ρ_c and p_c are now themselves connected by the Fermi equation of state (11), (12), then $p_c \propto \rho_c^{5/3}$ as $\rho_c \to 0$, and $\rho_c - 3p_c \sim 0(\rho_c^{1/2})$ as $\rho_c \to \infty$, and m is seen to have a maximum value. For values of ρ_c corresponding to this maximum the equation of state (Tolman 6.5) does not differ qualitatively from the Fermi equation of state (11), (12), as may be seen by comparing for the two solutions the values of $d \ln p / d \ln \rho$; and the maximum mass in fact turns out from (23) to be $\sim 0.4\odot$, agreeing in order of magnitude with our value of $\sim 0.7\odot$.

Tolman's solution V, with $n=\frac{1}{2}$, $R \to \infty$, and his solution VI, with $n=\frac{1}{2}$, $B/A \to 0$, are just our solution (22) corresponding to the equation of state $p=\frac{1}{3}\rho$, a unique unstable singular solution. For solution V, with $n=\frac{1}{2}$ and finite R, the pressure differs from $\frac{1}{3}\rho$ by terms of the order of $\rho^{-1/6}$; however, for VI with $n=\frac{1}{2}$ and finite B/A, for large ρ, $\rho - 3p = \text{const.}\ \rho^{1/2}$, which is just the behavior of a highly compressed Fermi gas. Using for the mass of this solution

$$m = A/42B \qquad \text{(Tolman, 8.9)}$$

and adjusting the ratio B/A to make the equation of state of VI, i.e.,

$$p = \tfrac{1}{3}\rho \frac{1 - 9(B/A)(3/56\pi)^{1/3}\rho^{-1/3}}{1 - (B/A)(3/56\pi)^{1/3}\rho^{-1/3}} \qquad \text{(Tolman, 8.5)}$$

agree to terms of order $\rho^{1/3}$ with (11), (12), we get $B/A = (7/3)^{1/3}$, and $m \sim (1/7)\odot$, to compare with the value of $\frac{1}{3}\odot$ which the Fermi equation gives.

These necessarily somewhat rough comparisons may thus serve to give an idea of the analytic character of the solutions corresponding to maximum mass and to maximum (infinite) central density which we obtained above.

V. Discussion—Application to Stellar Matter

We have seen that for a cold neutron core there are no static solutions, and thus no equilibrium, for core masses greater than $m \sim 0.7\odot$. The corresponding maximum mass M_0 before collapse is some ten percent greater than this. Since neutron cores can hardly be stable (with respect to formation of electrons and nuclei) for masses less than $\sim 0.1\odot$, and since, even after thermonuclear sources of energy are exhausted, they will not tend to form by collapse of ordinary matter for masses under $1.5\odot$ (Landau's limit), it seems unlikely that static neutron cores can play any great part in stellar evolution;[18] and the question of what happens, after energy sources are exhausted, to stars of mass greater than $1.5\odot$ still remains unanswered. It should be observed that for the critical solution with $m \sim 0.7\odot$ the potentials $g_{\mu\nu}$ are nowhere singular, and that in particular such a core does not tend to "protect itself" from the addition of further matter by the vanishing of g_{44} at the boundary. There would then seem to be only two answers possible to the question of the "final" behavior of very massive stars: either the equation of

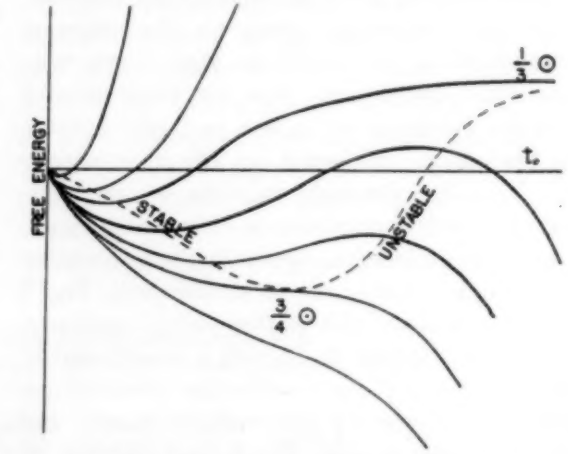

FIG. 3. Schematic plot of free energy as a function of t_0.

[18] The mass of the shell of ordinary (but dense) matter surrounding the core must be small for cores much more massive than the lightest core stable with respect to disintegration into electrons and nuclei.

state we have used so far fails to describe the behavior of highly condensed matter that the conclusions reached above are qualitatively misleading, or the star will continue to contract indefinitely, never reaching equilibrium. Both alternatives require serious consideration.

The central density in the "critical" core is even higher than nuclear density, so that our extrapolation of the Fermi equation of state can hardly rest on a very sure basis. Under these conditions the disintegration of neutrons, either into protons and electrons, or into mesotrons, will be energetically unfavorable and will not occur. And the relatively weak attractive forces which are known to act between neutrons will facilitate, and not prevent, the collapse of the core. If, however, under extreme compression, phenomena occurred which have the effect of repulsive forces, i.e., of raising the pressure for a given density above the value given by the Fermi equation of state, this could tend to prevent the collapse.

Such repulsive forces, even if they exist, will hardly make possible static solutions for arbitrarily large amounts of matter. For at low densities they cannot appreciably affect the equation of state, so that the dimensions of the core will necessarily be finite, and so will be the gravitational mass m of the core

$$m=\tfrac{1}{2}r_b(1-e^{-\lambda_b}) \quad \text{(Tolman, 5.5)}.$$

Nor can the mass M_0 before collapse be infinite. For this to be true we should have to have a singular solution. But the effect of repulsive forces can for high density at most be to make $3p$ even more nearly equal to ρ than for the Fermi equation of state; and for $\rho=3p$, as has been remarked above, and as is also suggested by Tolman's solutions V and VI, the *only* singular static solution is (22), for which the total particle number is finite.

We may obtain an extreme limit on the increase in the limiting mass which strong repulsive forces at high densities could give, by the following simple argument. For $\rho<10^{15}$ g/cm^3 these forces can hardly be important. Let us assume that for $\rho\geqslant 10^{15}$, they have the extreme effect of making $p=\frac{1}{3}\rho$. Then the mass of a sphere for which this equation of state holds down to $\rho=10^{15}$, and for which p falls rapidly as $\rho\to 0$, is given by our solution (22), and is of the order of $\odot$. It seems likely that our limit of $\sim 0.7\odot$ is near the truth.

This argument is based on the requirement that even for arbitrarily high densities, $\rho-3p$ shall not be negative; and this is in turn closely related to the positive definite character of the (proper) energy density of neutrons and of the fields of force (apart from gravitation) associated with them. It seems probable that if p could be very much greater than $\frac{1}{3}\rho$, static solutions of arbitrarily large mass could be found.[19]

From this discussion it appears probable that for an understanding of the long time behavior of actual heavy stars a consideration of nonstatic solutions must be essential. Among all (spherical) nonstatic solutions one would hope to find some for which the rate of contraction, and in general the time variation, become slower and slower, so that these solutions might be regarded, not as equilibrium solutions, but as quasi-static. Some reason for this we may see in the following argument: for large enough mass the core will collapse; near the center the density and pressure will grow, and $g_{44}=e^{\nu}$ will be small (cf. Eq. (7)); and as e^{ν} grows smaller, all processes will, as seen by an outside observer, slow down in the central region. Formally one sees this, in the occurrence, in Einstein's equations, of products of the form

$$e^{-\nu}\frac{d^2\lambda}{dt^2},\quad e^{-\nu}\left(\frac{d\lambda}{dt}\right)^2,\quad e^{-\nu}\frac{d\lambda}{dt}\frac{d\nu}{dt}.$$

For high enough central densities it is no longer justified to neglect even a very slow time variation; and the singular solutions which presumably represent very massive neutron cores cannot be obtained unless this is taken into account. These solutions are now being investigated.

[19] Thus for $\rho=$const. there is a class of singular static solutions, for which $p\sim k/r^2$, and which would seem to lead, for $K\to\infty$, to infinite masses, and which one of us (G.M.V.) hopes to discuss in detail elsewhere.

The Mechanism of the Positive Point-to-Plane Corona in Air at Atmospheric Pressure

G. W. TRICHEL
Department of Physics, University of California, Berkeley, California
(Received November 5, 1938)

Attention is called to the fluctuating character of the current in the positive point-to-plane corona in air at atmospheric pressure. It is shown that in the self-sustaining corona the current is due to a large number of individual current-pulses or bursts which are distributed over the surface of the point in regions of adequate field strength. The bursts of current are quite random in time, space, and intensity, and in general are composed of many successive avalanches of electron ionization which flow into regions of high field strength caused by space charges left by preceding avalanches. These bursts propagate outward across the gaps until extinguished by space charge accumulations, diffusion, self-repulsion, and ion migration in the field as well as by infelicitous coincidences of avalanche and the space charge distribution in the gap. The succeeding electron avalanches are initiated in air by photoelectrons produced in the gas ahead of the point. Evidence of an electrical, visual, and photographic character is presented confirming the existence of bursts and giving orders of magnitude of various features under operating conditions. The ionization produced is most intense at the point in the early stages and the number and intensity of the bursts increase with field strength. The development of a burst at one spot is exceedingly rapid (about 10^{-8} sec.) and is followed by a longer period (of about 10^{-4} sec.) as regards that spot, in which the field clears the space charge. In air it appears that the *self-sustaining* corona requires a high enough potential to overcome the space charge, an adequate current to furnish photoelectrons, and in addition the formation of negative ions to insure that fluctuations shall not break off the discharge. As both the field at the point and clearing field increase, the bursts propagate further into the gap and ultimately form streamers from 6 to 11 mm long. When these catch up with previous extinct space charge streamers further out in the gap, they project themselves further and further towards the cathode much in the manner of the leader-strokes in lightning discharge. If such a streamer striking the cathode creates an active cathode spot the return discharge produces a spark or an arc.

THE late W. A. Hillebrand called attention to the presence in positive point-to-plane corona of luminous streamers in regions where field strengths adequate to support ionization by collision would not be expected to exist. A visual study of such streamers produced in experiments by Leigh convinced Loeb[1] that the fine blue lines observed against the lavender glow in these regions were due to discrete discharges like minute lightning strokes. In the present investigation the discontinuous nature of the current in the positive point-to-plane corona is demonstrated electrically and the orders of magnitude of the essential characteristic are determined.

The circuit arrangement for the electrical study of the characteristics of the positive point-to-plane corona is shown in Fig. 1. Signals from the shock-excited antenna circuit containing the point are picked up by a tuned radio receiver consisting of a simple biased detector circuit with resistance-coupled amplifier. The output of this receiver could be fed into a DuMont oscillograph, an output meter, a counter, or earphones. The signals were strongest when the radio set was tuned to a specific frequency which varied from 2 to 4×10^6 cycles/sec. The source of potential was a conventional 25-kv, Kenotron rectifier. The discharge gap was completely enclosed in a metal box about one meter on the side, inside of which was placed the radio set used to pick up the corona signals. The box was grounded and all leads to and from the radio set were through shielded cables, the shields being grounded to the box. Potentials were measured by a 25-kilovolt electrostatic voltmeter which was calibrated against one of the standard Taylor resistance towers of the Physics Department. Since this voltmeter was not sensitive to small changes in voltage, a 200-megohm resistance tower, R_1, was used in conjunction with one section of a White potentiometer as a secondary method; the potentiometer resistor was set so that it checked with the full scale reading of the electrostatic voltmeter. The potentiometer was capable of reading differences of potential of ten volts. Current was measured by a Weston microammeter, P_0, having

[1] W. Leigh and L. B. Loeb, Phys. Rev. **51**, 149 (1937).

three and thirty microampere scales and also by measuring the voltage drop across a 1000-ohm resistor, R_2, with the remaining section of the White potentiometer. This last instrument was sensitive to changes of current of the order of 10^{-11} ampere. The discharge gap used in open air consisted of a six-inch brass plate, P_s, having rounded edges as the grounded electrode and points of several different materials and shapes as the high potential electrode. Most experiments were conducted with platinum points having a cylindrical body and a hemispherical end. A few experiments were made with sharp points (commercial sewing needles) having a conical point with an included angle of about 30 degrees, and one experiment was performed with a set of confocal paraboloids as a discharge gap. Several types of pick-up were used. Either a radio antenna T could be tuned to pick up signals at a frequency determined by the small coil C inserted in series with the point, or else it could be connected through a capacity C_1 across the resistor R_3 in series with the plate. At times a tuned circuit was placed across R_3, giving large signals of calculable frequency which could be picked up by the circuit. In general the signals picked up by the radio antenna and by the untuned resistor R_3 were quite similar, and in discussion we will present only those oscillograms picked up by R_3. The tuned circuit connected with R_3 complicated the oscillograms by superposing oscillations on already complicated signals. They served, however, clearly to show the high rate of current change in the states of corona current and their random character.

Typical oscillograms obtained are shown in Figs. 2 and 3. Fig. 2*A* shows an oscillogram obtained of the *intermittent* corona near onset with low amplification. The fluctuations giving rise to the *noise* are the *small* irregularities. The larger vertical lines apparently indicate *points of temporary extinction of corona*. These observations apply to the very upper limit of the Geiger counter regime discussed by Kip.[3] The amplitude of the current change between corona and no corona relative to the resolved *fluctuations* of the corona itself are of the order of forty-fold.

[3] A. F. Kip, Phys. Rev. **54**, 139 (1938).

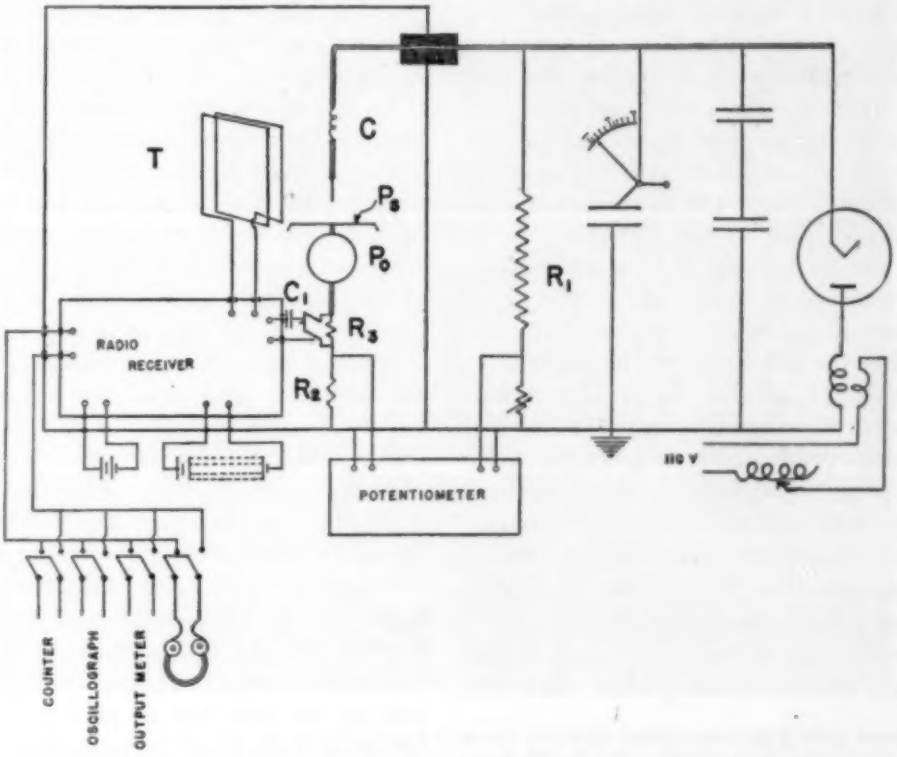

FIG. 1. Diagram of connections used in the study of positive point-to-plane corona.

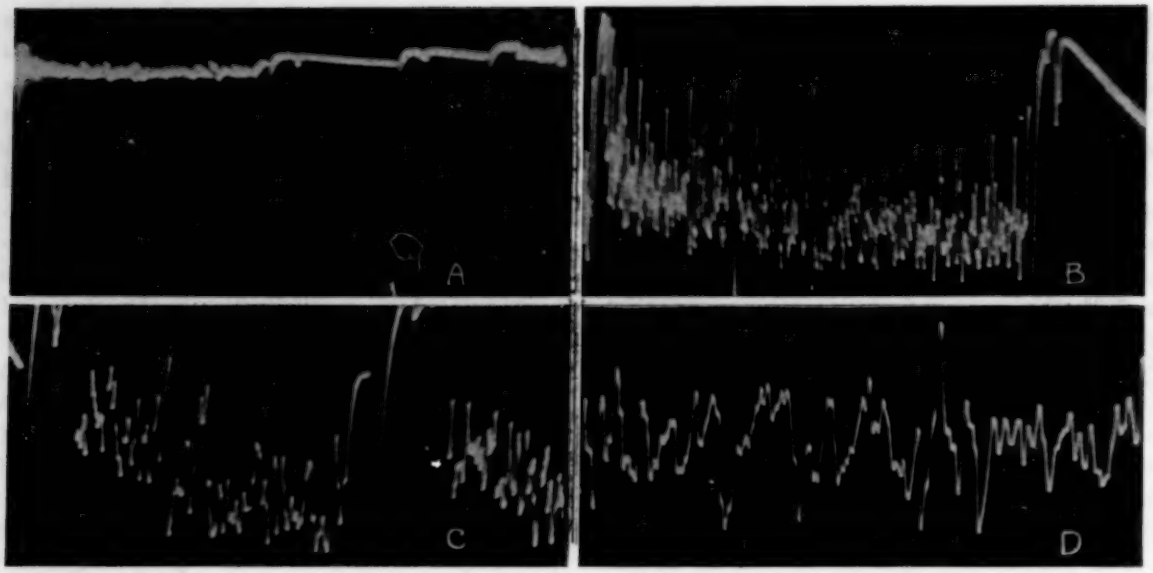

FIG. 2. *A*. Oscillogram of an intermittent positive corona for a current near onset with low magnification. Steady current is 20 to 40 times the amplitude of the oscillations. *B*. Same as 2*A* with large amplification and slower sweep. *C*. Same as 2*A* with larger amplification and the same sweeping rate. *D*. Oscillogram of a section of stable positive corona at 62,500 resolved fluctuations per second, at 1μA current.

Further below onset the fluctuations are relatively much greater. Fig. 2*B* shows the same sort of occurrence at large amplification and with a slower sweep, while Fig. 2*C* shows the greater amplification with the higher sweeping rate. Fig. 2*D* shows the results obtained with 62,500 fluctuations per second and 1μA current. Fig. 3 shows:—*A*, an 8000-cycle timing wave, *B*, the parasitic background of oscillations (no corona and full gain on the amplifier); *C*, *D*, and *E*, the corona in a gap of 3 cm with a point 0.5 mm in diameter with, respectively, 0.5, 1 and 2 microamperes of corona current. It is to be noted that the amplitude of the fluctuations is the greater the smaller the corona current. The self-sustaining corona began at 4.84 kv with current about 0.1μA. It was preceded above 4.75 kv by a region of intermittent corona with vanishingly small currents. Individual bursts of intermittent corona could be seen visually on the oscillograph. We were, however, never fortunate enough to photograph one.[3]

The above observations make it clear that the positive point-to-plane corona current is made up of imperfectly resolved current impulses of extremely high frequency. The fluctuations observed make up only a small fraction of the nearly steady background once the stable corona is established.

To determine the frequency of the current impulses, assumed random, from the frequency of the observed fluctuations the following method was adopted. The oscillograph and amplifier were capable of resolving evenly spaced pulses having frequencies up to 2×10^5 per sec. From the theory of fluctuations if N_0 is the limit of resolution for evenly spaced pulses and if N is the number of individual fluctuations assumed to be random the number z of fluctuations recorded is given by $z=Ne^{-N/N_0}$. In this case z is about 6×10^4 and N_0 about 2×10^5. It follows from the above that N may have either of two values, 10^5 and 3.5×10^5. The fact that the resolution of the fluctuations relative to the whole current is so far from complete favors the assumption of the higher value of the frequency. It also seems to be true that the higher the current, i.e., N, the lower the value of z. This conclusion is also borne out by the fact that no matter how the point circuit was modified the radio pick-up could not be detected at frequencies below 1.8×10^6 cycles.

[3] Very recently individual intermittent bursts of corona in the Geiger region have been photographed by Kip below regular onset by using radioactive ion sources (see Fig. 8).

With low onset current at frequencies N much above 10^6 per sec. the fluctuations in the current despite high rates of change would not have had energy enough to broadcast with the observed intensities.

If we assume, therefore, for convenience that for a corona current of 1μA from a point 0.5 mm in diameter N is 5×10^5 we can draw the following conclusions. First, the average current per impulse or burst consists of roughly 1.25×10^7 ions. Visual observation with a telemicroscope shows that with this current the point is covered with a thin sheath of glow of maximum intensity *at* the surface of electrode. The glow just covers the hemispherical end over an area of 0.39 mm^2. It is most intense at the point and fades towards the edges where the field is weak. Persistence of vision causes the eye to see as a continuous film of luminosity all the 5×10^4 pulses in about 0.1 second. This gives an area per burst of 7.8×10^{-6}

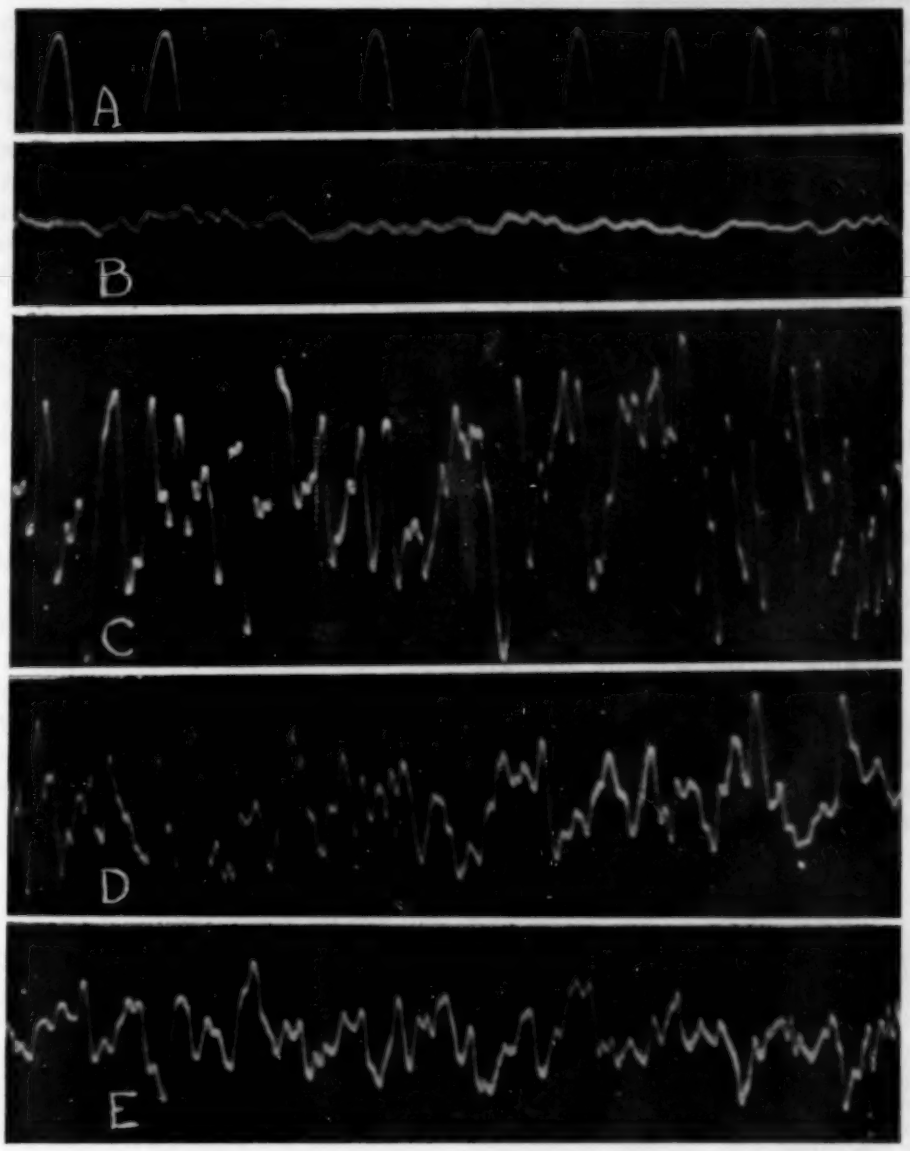

FIG. 3. *A*. An 8000 cycle per second timing wave. *B*. Parasitic background oscillations with full gain on the amplifier and no corona. *C*. Corona with 0.5-mm diameter point, current 0.5μA. *D*. Same as *C* current 1μA. *E*. Same as *C* current 2μA.

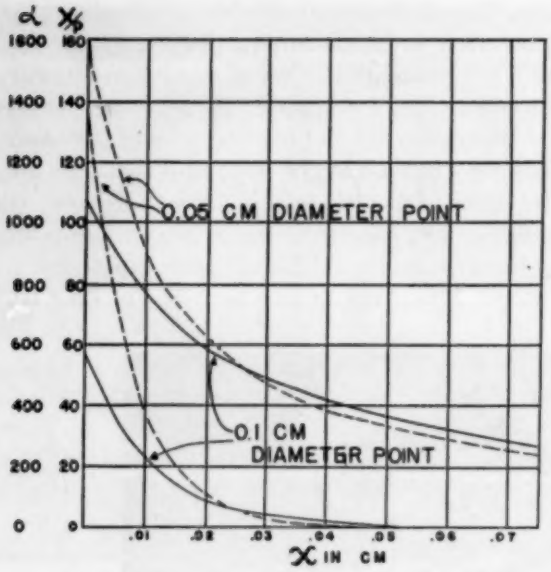

FIG. 4. Field strength divided by pressure, X/p, after Kip and Townsend's coefficient α for ionization by electron impact in air after Sanders as a function of distance from point for 0.05 (dashed) and 0.1 (full) cm diameter points at starting potentials for positive corona. The curves above give the values of X/p. Those asymptotic at about 0.04 cm give the values of α.

mm[2] or individual bursts spaced at about 2.8×10^{-3} mm. These could not be resolved as separate in the telemicroscope and the glow appears continuous. It has the color of the spark spectrum of nitrogen and this is confirmed by recent spectrographs taken by Kip. At higher field strengths when the discharge penetrates into the gap some of the separate steamers, especially with sharp points, can be visually resolved as stated in the introduction.[4] It is seen, therefore, that the estimated frequency of pulses is consistent with visual data.

The character of the current bursts or pulses giving rise to the fluctuations can be inferred from field strength data taken by Kip[5] using confocal paraboloids as electrodes. These estimates may be applied without serious error to the case of the point-to-plane discharge with a point of 0.5-mm diameter and 3-cm gap length. The data are accurate to about ten percent when the fields are undistorted by space charge. The field strength, or better, the ratio of field strength to pressure X/p, can be computed for the onset of the steady-state corona as a function of distance from the point in cm, as shown by the curves of Fig. 4 for points 0.5 and 0.1 mm in diameter. From Sanders' data on the first Townsend coefficient α as a function of X/p for air it is possible to plot the curve of the coefficient α as a function of the distance x from the points. From Townsend's equation for ionization by collision, which says that $n=n_0e^{\alpha x}$, it is possible to determine the greatest distance x at which in these fields an electron from the outside can produce a second electron by setting $n/n_0=2$ and solving for x from the values of α. This gives x as approximately 0.04 cm and a value of $X/p=40$. The values are not materially changed for a point 0.1 mm in diameter. For negative ions the work of Loeb[6] has shown that a value of $X/p=90$ is required before the electron is detached so that it can ionize. Hence if negative ions are to start a burst they must start only from 0.005 cm for the 0.5-mm point and from 0.01 cm for the 0.1-mm point. Since an electron produces αdx ions in a distance dx if one starts with n electrons the number of ions produced in dx will be $dn=\alpha n dx$. Now α as we have seen is a function $f(x)$ of x. Hence $dn/n=f(x)dx$. The number of ions produced by one electron starting at $x=0.04$ cm from the point in its path to the point is given by $n=n_0\int_{0.04}^{0}f(x)dx$. This graphically integrated for the cases above gives $\int_{0.04}^{0}f(x)dx=6.2$ and 11.2 so that $n=450$ for the 1.0-mm point and 73,000 for the 0.5-mm[7] point. Of course occasional electrons will by chance

[4] The appearance of the long separate visible streamers with increasing potential seems to be relatively sudden. This makes the exact process of the development of visible streamers from bursts somewhat difficult to picture. The streamers are most prominent with needle points and can be produced according to recent results of Kip at lower fields by sources of energetic α-rays or properly timed ions. Thus one must not at present speculate too freely on the mechanism of streamer production, except to state that streamers appear to be bursts propagating under certain favorable field conditions.

[5] There is a transposition in Kip's article (reference 2) on page 145, column 1, line 6, after subtitle, *Field Intensities at Onset*. Referring to the 80 and 120 kv/cm in the line above the words *small and large* should be transposed; that is, field strength X is *greater near the small point* than the large point, but changes further out and becomes smaller.

[6] L. B. Loeb, Phys. Rev. **48**, 685 (1935).

[7] It is to be noted that owing to the rapid increase in α with X/p and the short distances involved, the electron multiplication near the smaller point gives larger avalanches at onset than the larger point. This must continue until the point reaches such a size that the distance x, despite large values of α is insufficient for effective ionization. The fields at large points eventually become effective as the effective field becomes large enough at large values of x so that small values of α will suffice.

start out further in the gap and be fortunate enough to ionize producing more ions, and others will give less. Such ion production by a single incoming electron or ion we will call an *electron avalanche*. In the case of a negative *ion* the avalanche because of the short distance will consist of some 10 to 1100 electrons. At higher fields with larger currents or with larger radii the values of x for appreciable field strengths are greater and the avalanches will be larger. It is also clear that the ionization produced will be cumulative towards the point and that the highest ion density, and hence greatest luminosity, will lie at the surface of the point as is observed. This is in marked contrast to the negative point discharge. The high fields will also insure the excitation of spark lines.

The avalanche size which is here computed in contrast to the magnitude of 10^7 ions in the current pulses or bursts in the initial stages of corona discharge, clearly indicates that these two are not the same. There must therefore be some mechanism active in the normal self-sustaining positive point corona which produces pulses, bursts or stabs in place of the usual avalanches. It may, at this juncture, be stated that if by radioactive ionization *enough electrons are furnished* so that the current can be taken care of by the *electron multiplication in avalanches alone*, the pulses or stabs disappear. The clue to the process active comes from the appearance of streamers at higher fields and leads to the following picture. A single electron or ion wandering into the point produces an avalanche of some 10 to 10^5 electrons, perhaps more, depending on point radius and applied potential. These are rapidly drawn into the point and leave a positive space charge ahead of the point, which slowly moves outwards. Such a space charge distorts the field and constitutes a virtual prolongation of the point with an intense local field at its tip, as shown in Fig. 5. In the process of ionization in the first avalanche, especially near the point, the high fields excite the emission of spark lines. These ionize molecules ahead of the space charge photoelectrically.[8] If a new electron finds itself at the proper point ahead of the space charge, it will give a *new avalanche*, still further extending the space charge into the gap. This process of avalanches can repeat itself until the tip of the burst or incipient streamer advances to gradients too weak to allow it to continue, or until the coincidence of electrons from widely different directions of the gas about the space-charge-point so adds to the space charge as to decrease the field intensity about it to such a value that photoelectrons are no longer capable of propagating the point further by successive avalanches. Diffusion and self-repulsion of positive space charge, as well as its motion from the point, will aid in this attenuating action. From the values of the distances and

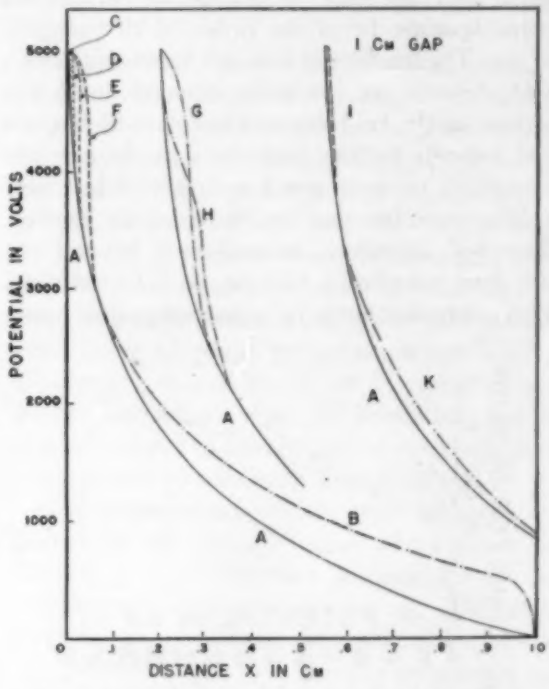

FIG. 5. Potential distribution and burst formation with a 0.5-mm diameter point 1μA current and 1-cm gap. Curve *A* is the undistorted potential in each case. Curve *B* shows the space charge distortion near the *cathode* due to extinct bursts. Curves *C*, *D*, *E*, and *F* show successively the approximate potentials after the first, second, fifth, and tenth avalanches in burst formation. Curves *G* and *H* show later stages of a burst where diffusion and movement in the field occur. Curves *I* and *K* show a new burst starting as the old one recedes. At higher fields this may overtake the old burst forming a streamer.

[8] In the absence of ionization by positive (reference 9) ions, and of a cathode to furnish electrons photoelectrically or by positive ion impact, the photoelectric ionization in the gas is the only possible mechanism. Such ionization has been directly observed by both Cravath and Dechene (reference 10).

[9] See L. B. Loeb, Rev. Mod. Phys. **8**, 267 (1936).

[10] A. M. Cravath, Phys. Rev. **47**, 254 (1935); C. Dechene, J. de. phys. et rad. **7**, 533 (1936).

fields involved in the process of successive avalanches, the time consumed between producing the burst and its extinction must be exceedingly short; not more than 10^{-9} sec. is required per avalanche and thus perhaps 10^{-8} second for the whole burst. Depending on field distortion and other purely chance factors, the ion production in a *series of such avalanches* will fluctuate widely and may vary from 10^4 to 10^8 or more ions. Such a succession of electron avalanches occurring very closely in time at one point constitute the burst or current stab and are the cause of the fluctuations studied. The average currents in each burst which are of the order of 10^{-12} ampere are at onset apparently large enough to shock-excite the circuit to give a signal, and the rate of change of current responsible must be of the order of 10^{-4} ampere per sec. The number of ions per burst, it is clear, must depend on the field strength, and will increase as the field strength becomes higher and as it extends further into the gap. At first the bursts will be very small and extend but very slightly into the gap as the analysis showed. They will, however, extend well beyond the 0.04 mm calculated for the undistorted field. With adequate fields in a gap devoid of space

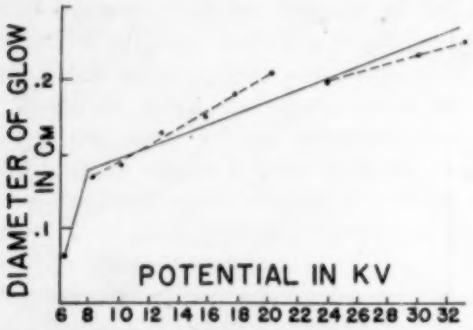

FIG. 6. Plot of the diameter of the glow of the positive point corona as the potential increases.

charge, the burst becomes a streamer extending one or two cm from the point even below onset. If the gap is fouled by space charge the streamers cannot form, and only relatively short bursts are observed. With increasing potentials above onset and in the region of the linear current-potential ratio of Kip[2] the bursts again extend into the gap.

After the bursts have terminated, the immediate region occupied by them is no longer active until the space charge can be dissipated by the movement of the positive ions in the field away from the point. There is thus a period of inactivity which will be longer the lower the field. The length of this period must lie in the vicinity of the time for positive ions to move 10^{-3} to 10^{-2} cm in fields of 50,000 volts/cm or from 10^{-8} to 10^{-7} second. The photoionization may, however, have started a burst at another neighboring spot on the surface of the point so that wherever the field is adequate there will be a succession of bursts or stabs of current which are completely random in phase and size.

Because of the high electron mobility, electrons are swept out long before the positive space charge can clear itself. Hence there must be a sufficient number of stabs or a sufficient intensity of photoionization so that in the microseconds required for the clearing of the space charge from extinct bursts, new electrons or ions are at hand to again initiate the discharge. In air this action is facilitated by the formation of negative ions by electron attachment in the gas. If ions can be formed from 0.5 cm to 1 cm from the point in sufficient numbers, calculation shows that there will always be a mechanism for the self-sustaining corona. Obviously the *ions* need not always initiate the new burst since timely photoionization by a more distant burst may also be active. However, evidence strongly indicates *that the negative ions are necessary in some gases.* Very pure N_2 gas where photoionization occurs, where electrons are free and where the ionizing radiations are absorbed about as much as in air, *does not give any evidence of bursts, current fluctuations or noise* unless soiled with minute traces of O_2. Pure H_2, which also has free electrons and in which *photoionization of the gas is not likely*, on the other hand does give fluctuations much like air. The presumption is that in the case of H_2, the transparency of H_2 to radiations allows electron emission from distant electrodes and the glass walls, these electrons then arrive in time to perpetuate the discharge. This is confirmed by recent observations in air.

In any case, it is clear that for the self-sustaining corona in air, a value of $X/p=90$ requisite for the detachment of an electron from a negative ion is required at some distance from the electrode, together with sufficient current to

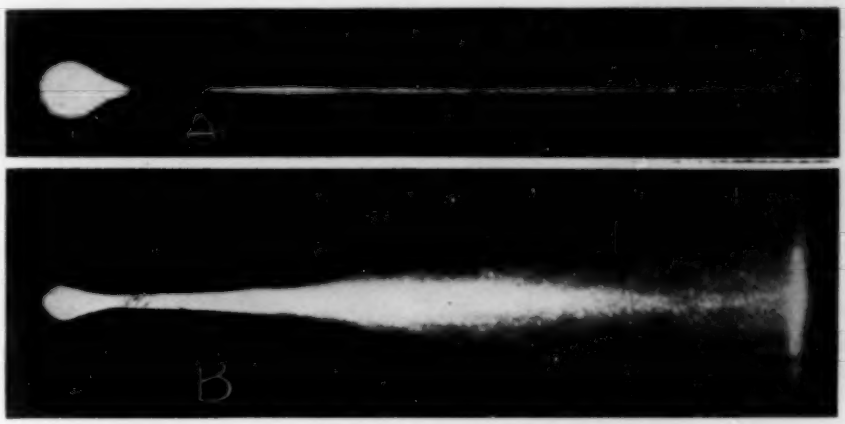

FIG. 7. *A*. Photograph of the positive point corona just before the appearance of streamers. A few incipient streamers may be seen beyond the edge of the glow. Potential 20.0 kv. *B*. Photograph of streamers propagating across the gap shortly after streamer onset. The cathode is distinguished by the glow over its surface. Potential 21.5 kv.

insure a continuous supply of ions or electrons. If the current is too small for this and the field strength becomes so low that adequate avalanches cannot be produced, we reach the Geiger-counter regime studied by Kip[2] in which bursts initiated by a single electron continue for longer or shorter intervals until the space charge of positive ions in transit in the gap so lowers the field that bursts cannot form, or until some inauspicious chance distribution of ions causes the discharge to break off. This is nicely seen in the Figs. 2*A*, 2*B* and 2*C*, and even more strikingly in recent observations of Kip well below the threshold for self-sustaining corona (see Fig. 8). While these discontinuities can be observed by the oscillograph, the light from a single short burst cannot readily be seen at the point, though it might be photographed.

As one raises the potential of a given point, burst production can occur over larger areas of the point as the field in such regions becomes large enough. Hence the glow, unlike the case of the negative corona, spreads evenly and progressively over the surface. At the same time the number of ions per avalanche and per burst increase and extend further into the gap. This extension shortly after onset of self-sustaining corona is not perceptible to the eye but is shown by the camera. From his photographs Kip has plotted the apparent size of the glow for the point and gap discussed in this paper as a function of potential. This is shown in Fig. 6, and it is seen that, except for the first point, the increase is approximately linear. As seen in Fig. 7*A* for the needle point at a potential of 20 kilovolts near breakdown, the high field so clears the space charge that the bursts again begin to propagate as individual streamers of 10^9 to 10^{10} ions, which are longer than the average. Fig. 7*B* shows the same needle point at 21.5 kilovolts. Here the appearance of many streamers can be seen, some of which propagate across the gap. By putting a high resistance in series with the point, breakdown can be inhibited and the gradual spread of the individual streamers across the gap can be seen with the naked eye.

The phenomenon is best seen with the finer points as the voltage range of streamer production is then extended. Eventually the field becomes so high that an extinct positive ion streamer moving away from the point towards the cathode in the field has not progressed very far when some later adjacent streamer propagates out sufficiently rapidly and far to overtake and utilize the ionized path of the extinct streamer. It is thus able to propagate further than its predecessor or than it could have done otherwise. One has then streamer propagation of the leader-stroke character observed by Schonland and Collens.[11] The use of old channels in this fashion can nicely be shown by blowing air

[11] B. F. J. Schonland, Proc. Roy. Soc. **A164**, 132 (1938); also B. F. J. Schonland and H. Collens, Proc. Roy. Soc. **A145**, 654 (1934); **A152**, 595 (1935).

across the lower ends of the streamers. The deflection of the ionized channels by the air blast in the weak field near the cathode causes them to be deflected and the luminosity follows the old channels. When finally the streamers or bursts propagate all the way to the cathode, and create fields at it sufficient to start efficient secondary electron emission at some spot, the leader stroke channel is utilized by the return stroke and results in a spark or an arc. This mechanism thus not only describes the character of the onset and the mechanism of the positive point-to-plane corona in air, but its eventual development to a spark as well. In this regard the later phases show remarkable similarity to lightning stroke propagation in air and to the long sparks photographed by Allibone and Meek.[12]

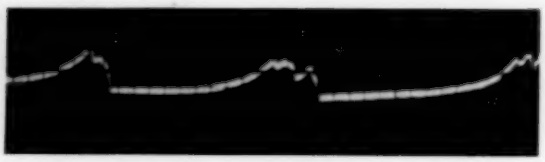

FIG. 8. Oscillograph by Kip showing the intermittent corona just below onset. Three intermittent discharges are seen. The fluctuations cannot be clearly resolved. The sweep is from right to left and the time covered in the oscillogram is 0.015 sec. The asymptotic decline to the left is instrumental.

The writer wishes to acknowledge his indebtedness to Professor Leonard B. Loeb, at whose suggestion the problem was undertaken and under whose guidance it was carried out, for his considerable assistance in interpreting the complicated phenomena observed. He further wishes to express his sincere thanks to Professor L. F. Fuller, Chairman of the Department of Electrical Engineering, for his timely advice and the many courtesies accorded him, and to Professor L. C. Marshall and Dr. T. A. Rogers of the Department of Electrical Engineering, for their kindly advice and the use of the facilities of their oscillographic laboratory. Thanks are also due to A. F. Kip for his assistance in taking oscillographs and for the photographs of corona discharge here shown. To Mr. Walter Noller and to Mr. Ben Davis, senior students in Electrical Engineering, he expresses his thanks for their assistance with the mechanical oscillograph. Finally the writer must acknowledge his sincere thanks for the help afforded by the W.P.A. workers, Mr. Edward Nunes and Mr. R. L. Melton, in building the amplifiers and counters used, and to Mr. F. T. Bogard for his aid in preparing the drawings for this and a previous paper.

[12] T. E. Allibone and J. M. Meek, Proc. Roy. Soc. **A166**, 97 (1938).

Use of Interference to Extinguish Reflection of Light from Glass

KATHARINE B. BLODGETT
Research Laboratory, General Electric Company, Schenectady, New York
(Received December 24, 1938)

The phenomena of interference of light rays reflected from the two boundaries of a thin film cause the intensity I_R of the resultant light to be greater or less than the intensity of the individual rays. The value of I_R is determined by (a) the refractive index of the film, n_1, and the substance on which the film is deposited, n_0, (b) the thickness of the film, (c) the angle of incidence at which light strikes the film, (d) the wave-length of the light. The conditions necessary to obtain extinction of reflected light are described. In the case of monochromatic perpendicular light $I_R=0$ when $n_1=n_0^{\frac{1}{2}}$ and the thickness t is given by $t=0.25\lambda(2a+1)/2$ where a is zero or an integer. The technique of building films which have the required values of n_1 and t is described. The films are made by building up monomolecular layers, each layer consisting of 50 percent cadmium arachidate and 50 percent arachidic acid. The film is then soaked in alcohol which dissolves the arachidic acid and leaves a skeleton of cadmium arachidate. The refractive index of the skeleton is determined by the amount of arachidic acid which has been removed from the film. Since the interstices are of molecular size there is no appreciable scattering of the reflected light.

THE reflection of light from glass surfaces has created many difficult problems. It is well known that the design of optical instruments, and the methods of illuminating objects by means of light shining through a glass window, are much hampered by this characteristic feature of glass.

When light of intensity E falls on a transparent plate, the light T transmitted by the plate is given by $T=E(1-I_R)^2(1-\alpha t)$ where I_R is the fraction of the light which is reflected by a single face of the plate, t is the distance which the light travels in the plate which is assumed to be large compared with a wave-length of light, and α is the absorption per unit distance. Therefore a plate which is treated in such a way as to diminish I_R shows a corresponding increase in light transmission T.

In 1892 Harold Dennis Taylor,[1] the English lens expert, discovered that a badly tarnished photographic lens transmitted more light than a new lens. He found that he could develop this tarnish chemically by immersing the lens in an aqueous solution of ammonia and sulphureted hydrogen.

In 1916 F. Kollmorgen[2] found means of treating most of the glasses used in optical work with different chemicals so as to diminish the light reflected from their surfaces. He prepared disks of a barium crown glass of refractive index 1.6 and showed that an untreated disk transmitted 89 percent of light, whereas the transmission of a similar disk was increased by suitable treatment to a maximum value of 96 percent. Kollmorgen calculated that the light transmitted by a gunsight containing seven untreated lenses and two prisms was reduced by reflection at the several surfaces to 36.2 percent of the incident light. He showed that in a periscope the loss by reflection reduced the light received by the observer to 25 percent of the light received by the periscope. He also pointed out that multiple reflections in a lens system gave rise to a veil of stray light which caused a loss of brilliancy and contrast in the image.

Kollmorgen believed that the chemical treatment "formed at the surface a vitreous compound having a refractive index considerably lighter than that of the glass itself." Wright[3] also experimented with various chemical treatments to produce a surface layer of this type. Neither experimenter was aware that the effects which he observed were due to interference between the light rays reflected from the upper and lower surfaces of the layer.

In 1935 Strong[4] coated plate glass ($n_0=1.52$) with evaporated films of fluorite for the purpose of using interference to decrease reflection. One of these films caused a decrease of 54 percent in

[1] Harold Dennis Taylor, *The Adjustment and Testing of Telescope Objectives* (T. Cook, York, England, 1896).
[2] F. Kollmorgen, Trans. Soc. Ill. Eng. **11**, 220 (1916).
[3] F. E. Wright, Ordnance Department Document No. 2037, p. 76.
[4] J. Strong, J. Opt. Soc. Am. **26**, 73 (1936).

the light reflected at normal incidence, and another a decrease of 85 percent.

Recent developments in experimental work with built-up films[5, 6] have provided a means of coating glass with a type of film which extinguishes the reflection of monochromatic light. When a plate of glass, coated on both sides with a film which is built so as to extinguish sodium light at perpendicular reflection, is held a few inches from a 6000-lumen sodium vapor lamp and the glass is seen against a black background, the image of the lamp is almost completely imperceptible and the glass has the appearance of black velvet. When a stripe of the same type of film is built on soda-lime glass and one looks through the glass at a sheet of white paper or at the sky, the effect of the increased transmission is very striking. The stripe has the appearance of clean glass and the clean glass on either side of the stripe appears to be slightly smoked. The contrast is plainly visible since the transmission of the stripe is 99.2 percent for white light, and of clean glass is 92 percent.

In order that a film shall extinguish monochromatic light the properties of the film must be suited to the refractive index of the glass, the wave-length of the light, and the angle at which the light is to be extinguished. This paper will describe the methods by which skeleton films of cadmium arachidate are built so as to meet these requirements.

Cadmium arachidate is a soft substance which is completely removed from glass if the glass is wiped with a cloth. The film is permanent, however, if it is not touched and is not exposed to bright sunlight for long periods of time. The writer has a film which has been kept for four months in an unstoppered tube in a desk drawer, and has shown no perceptible change during that time. These films therefore supply an exceedingly useful tool for the exact study of interference.

Cartwright and Turner[7] have shown that evaporated films of LiF, MgF_2, CaF_2, NaF and chiolite will reduce the reflection of visible light from two glass surfaces to about 0.4 percent. This results in a transmission of about 99.6 percent, as recorded by the Hardy color analyzer.

[5] K. B. Blodgett, J. Am. Chem. Soc. **57**, 1007 (1935).
[6] K. B. Blodgett and I. Langmuir, Phys. Rev. **51**, 964 (1937).
[7] C. H. Cartwright, and A. F. Turner, Bull. Am. Phys. Soc. **13**, 10 (1938).

Conditions for Extinguishing Reflection of Monochromatic Light

When a glass surface is covered with a thin transparent film the light reflected by the glass is governed by the laws of interference. The ray reflected from the air-film boundary interacts with the ray reflected from the film-glass boundary to form a resultant ray of intensity I_R. The value of I_R is given by

$$I_R = B^2 + C^2 + 2BC\cos(2\pi D/\lambda), \qquad (1)$$

where B and C are the amplitudes of the rays reflected from the air-film and film-glass boundaries, respectively. These rays will be called the B ray and the C ray. The symbol D denotes the difference in optical path between the path traveled by the B ray and that traveled by the C ray. The value of D is given by

$$D = 2n_1 t\cos r_1, \qquad (2)$$

where t is the thickness and n_1 is the refractive index of the film, and r_1 is the angle of refraction of light in the film when light is incident at an angle i. In the case where the film is an isotropic substance, or where it is a uniaxial crystal and the measurements deal with the ordinary ray, the value of $\cos r$ can be calculated from i and n_1 since $n_1 = \sin i/\sin r_1$.

The Fresnel formulae for the amplitudes B and C reflected at perpendicular incidence are

$$B = (n_0 - n_1)/(n_0 + n_1), \qquad (3)$$

$$C = (n_1 - n_g)/(n_1 + n_g), \qquad (4)$$

where n_g, n_1 and n_0 denote the refractive indices of the glass, the film, and the medium in which the glass is viewed which is commonly air. When n_0 refers to air we have $n_1 > n_0$ and the value of B is negative, the negative value indicating that the ray undergoes a phase reversal at the boundary. In Eqs. (3) and (4) the amplitude of the ray incident on a boundary is taken as unity.

The formula of Eq. (1) neglects multiple reflections in the film. The effect of multiple reflections is slight in the case of transparent films built on glass, since the number of these reflections is very small, the intensity of a single

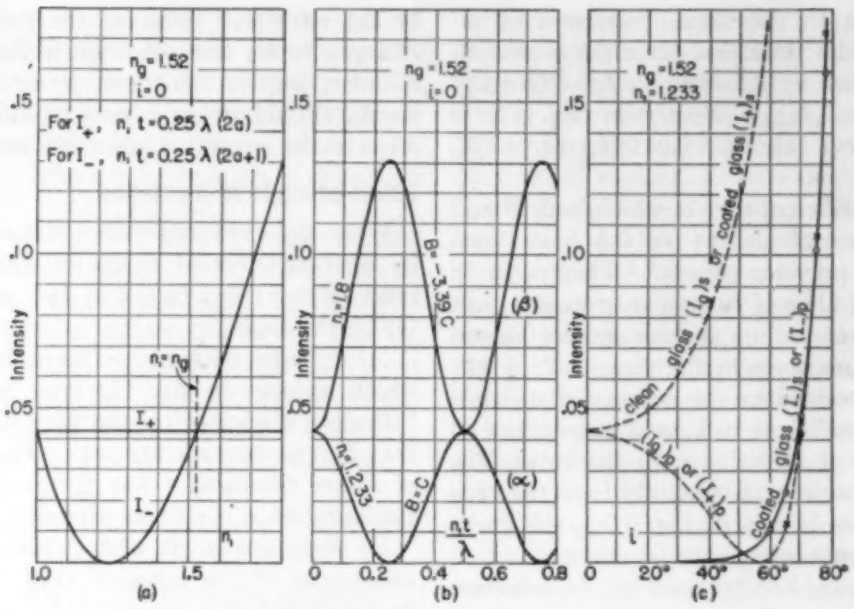

FIG. 1. Reflection of light from films built on glass $n_g=1.52$. Intensity as a function of: (a) refractive index n_1 of films; (b) optical thickness of film, measured in terms of wave-length λ; (c) angle of incidence i. Incident intensity was 1.0.

reflection being usually about 1 percent. The correction which can be applied to Eq. (1) for multiple reflections has been derived[6] for the cases $D=a\lambda$ and $D=\lambda(2a+1)/2$ where a is zero or an integer.

For $D=a\lambda$, $\quad I_+=[(B+C)/(1+BC)]^2$, (5)

For $D=\lambda(2a+1)/2$, $\quad I_-=[(B-C)/(1-BC)]^2$, (6)

where I_+ and I_- are corrected values of I_R. The calculation of the correction for other values of D is complicated. The theory of the problem is similar to that of the reflection of light by a Fabry and Perot interferometer, but in the present case the reflection at the boundaries is so small that the correction becomes negligible.

Effect of refractive index

The curves in Fig. 1 represent the reflection of light from films built on glass $n_g=1.52$. Fig. 1(a) shows the maximum and minimum values of the intensity, plotted as a function of n_1, for the case of perpendicular light ($i=0$). These intensities I_+ and I_- were calculated by means of Eqs. (3), (4), (5) and (6). The curves show that I_- is the minimum value when $n_1<n_g$, but becomes the maximum value when $n_1>n_g$.

Strong[4] pointed out in his paper that the intensity was zero when n_1 was given by

$$n_1^2=n_g n_0. \tag{7}$$

In the present case the value of n_1 given by Eq. (7) was $n_1=1.233$.

Effect of film thickness

Equation (1) shows that the intensity of reflected monochromatic light varies as a function of $\cos(2\pi D/\lambda)$ where D is proportional to $n_1 t$ in accordance with Eq. (2). The curves in Fig. 1(b) represent the variation of intensity of perpendicular light, plotted as a function of $n_1 t/\lambda$.

The values of B and C which were used to calculate the curves of Fig. 1(b) were obtained by means of Eq. (3) and Eq. (4), for the cases $n_1=1.233$ and $n_1=1.80$. For curve (α), $n_1=1.233$, $B=C=-0.1043$; for curve (β), $B=-0.2857$, $C=0.0843$. The maximum and minimum values of the intensity were calculated from Eq. (5) and Eq. (6) and correspond to points on the curves in Fig. 1(a) for the given values of n_1. The curves of Fig. 1(b) are cosine curves drawn through these values of I_+ and I_-. Curves drawn in this way represent a close

approximation to the actual variation of intensity with film thickness, since the correction which is applied by substituting $I_{\pm}=[(B\pm C)/(1\pm BC)]^2$ for $(I_R)_{\pm}=(B\pm C)^2$ in Eq. (1) is small. For curve (α), $BC=0.011$; for curve (β), $BC=-0.024$.

Cases of a different sort in which both B and C have values about 0.4 to 0.6 have been considered in previous papers.[6,8] They occur in practice when films of barium stearate are built on a polished chromium surface and are viewed at angles of incidence in the range 68° to 84°. Under these conditions the number of multiple reflections is sufficient to have a large effect on the variation of intensity with thickness. The intensity curve departs markedly from the type of cosine curve shown in Fig. 1(b), the curve assuming sharp minima and flat maxima.

In the curves of Fig. 1(a) and (b) the reflection I_g from a single surface of clean glass is $I_g=0.0426$, the intensity of the incident light being unity. This value was obtained from $I_g=(B_g)^2$ where B_g is the value of B from Eq. (3) when $n_1=n_g$.

In the case of film-coated glass, substituting the values of B and C from Eq. (3) and Eq. (4) in Eq. (5), we have the result

$$I_+=[(n_0-n_g)/(n_0+n_g)]^2. \qquad (8)$$

Therefore, *for the case of perpendicular light* I_+ is independent of n_1, and the value of I_+ is identical with the value of B_g^2. That is, when $n_1t=0.5a\lambda$ the intensity of light reflected by a film of any transparent substance is the same as the intensity I_g reflected by clean glass. In order to diminish the reflected intensity below this value the surface film must have a refractive index which is less than that of the glass. The minimum intensity is obtained when

$$n_1t=0.25\lambda(2a+1).$$

In interference phenomena the optical thickness n_1t is more useful as a unit of measurement than the actual thickness t. If a film is built in a series of steps which have increasing values of t and the same value of n_1, and the film is illuminated by monochromatic light of wavelength λ, the intensity minimum is seen at the step which has the thickness $t=0.25\lambda(2a+1)/n_1$. If the refractive index of the entire series is changed to n_2, the minimum is then seen at a different step of thickness $t_2=n_1t/n_2$. In other words, the minimum is seen to shift to thicker steps as the refractive index is lowered.

[8] K. B. Blodgett, J. Phys. Chem. **41**, 975 (1937).

Effect of angle of incidence

When glass covered with a film is illuminated by light at different angles of incidence i, the reflected light is affected in two ways (a) and (b) by the angle.

(a) *Effective thickness.*—The path difference D which appears in Eq. (1) may be called the "effective thickness" of the film. Eq. (2) shows that D is proportional to $\cos r_1$. Therefore a film of given thickness t has its greatest *effective* thickness when it reflects perpendicular light.

(b) *Reflection at B and C boundaries.*—The amplitudes of the reflected rays B and C can be calculated as a function of i, n_1, and plane of polarization by means of the following Fresnel formulae:

$$R_s=-\sin(i-r)/\sin(i+r), \qquad (9)$$

$$R_p=-\tan(i-r)/\tan(i+r). \qquad (10)$$

Here i and r are the angles of incidence and reflection at a given boundary, and R_s and R_p are the amplitudes of the reflected rays having the plane of polarization perpendicular and parallel, respectively, to the incident plane.

The dashed lines in Fig. 1(c) give the calculated values for the intensities $(I_g)_s$ and $(I_g)_p=(R_g)_p^2$, where R_g is the value of R for glass ($n_g=1.52$). The intensity $(I_g)_p$ falls to zero at Brewster's angle which is $\tan^{-1}1.52=56°\,40'$.

The solid line in Fig. 1(c) was calculated for the case of glass coated with a film of an isotropic substance. The value of n_1 for the film was $n_1=1.233$ from Eq. (7), and D had the constant value $D=\lambda(2a+1)/2$. Therefore this curve does not represent the case of a single film reflecting light at a series of angles, but instead it represents a series of films having thicknesses which satisfy Eq. (2) for a constant value of D. The required thickness t increases with increasing values of i.

When glass is coated with a film there are two rays B_s and B_p reflected at the B boundary, and two rays C_s and C_p reflected at the C boundary. In the case of the data of Fig. 1(c)

the values of B_s, B_p, C_s and C_p were calculated by substituting in Eqs. (9) and (10) the values of the angles of incidence and refraction at the B and C boundaries. These were obtained from the equations $n_1/n_0=\sin i/\sin r_1$, and $n_g/n_1=\sin r_1/\sin r_g$, where r_g is the angle of refraction in the glass.

A film for which $D=\lambda(2a+1)/2$ reflects light with an intensity I_- given by Eq. (6). Values of $(I_-)_s$ and $(I_-)_p$ can be calculated by means of Eq. (6) for different values of i by substituting in this equation the values of B and C derived from Eq. (9) and Eq. (10). In the particular case illustrated in Fig. 1(c) the relationship $n_1^2=n_0n_g$ results in the following simplification

$$\left(\frac{B-C}{1-BC}\right)_s=-\left(\frac{B-C}{1-BC}\right)_p=\frac{\cos(i-r_g)-1}{\cos(i+r_g)+1}. \quad (11)$$

The solid line of Fig. 1(c) gives the values of

$$(I_-)_s=(I_-)_p=[(\cos(i-r_g)-1)/(\cos(i+r_g)+1)]^2. \quad (12)$$

For the case where D is constant and has the value $D=a\lambda$, and $n_1^2=n_0n_g$, the equations for the amplitude $(B+C)/(1+BC)$ of the reflected light can be reduced to the form

$$[(B+C)/(1+BC)]_s=-\sin(i-r_g)/\sin(i+r_g), \quad (13)$$

$$[(B+C)/(1+BC)]_p=-\tan(i-r_g)/\tan(i+r_g). \quad (14)$$

Equations (13) and (14) are the Fresnel equations for the amplitudes $(R_g)_s$ and $(R_g)_p$ reflected by clean glass. We therefore have the result that at any angle i the maximum light reflected by a film having a refractive index given by $n_1^2=n_0n_g$ is equal to the light reflected by clean glass. In the case of perpendicular light the intensities were found to be equal for any value of n_1 (from Eq. (8)).

The formulae of Eqs. (1) to (14) are valid only for the case of a ray which obeys the ordinary laws of reflection and refraction. The equations for B and C for the case of the extraordinary ray of a uniaxial crystal have been given in a previous paper.[6]

Skeleton Films of Cadmium Arachidate

The technique of building films by depositing successive monolayers of barium stearate has been previously described.[5, 6] It was found in the early work that the refractive index of a film which had been built in this way could be greatly decreased by soaking the film in benzene. Before the film was soaked it consisted of a mixture of barium stearate and stearic acid. The benzene dissolved the stearic acid, and left the barium stearate as a skeleton with air filling the spaces previously occupied by stearic acid.

A large percentage of fatty acid can be removed from a film without causing the film to shrink in thickness. In an experiment described in an earlier paper the removal of 36.3 percent of the substance of the film was accomplished with a shrinkage of only 0.8 percent in thickness.

If a film has initially a refractive index $n_1=1.50$, and if 50 percent of the material is removed without causing the film to shrink in thickness, the refractive index of the skeleton is 1.232. This value was calculated by means of the law of Clausius and Mosotti:

$$(n^2-1)/(n^2+2)=kd, \quad (15)$$

where d is the optical density of the film and k is a constant. The value $n_1=1.232$ is equal to the value given by Eq. (7) which is needed to extinguish perpendicular light reflected by ordinary soda-lime glass ($n=1.52$). Skeleton films of this type can be easily built.

Mr. S. Bernstein has measured the spacing of the layers of a skeleton film of lead arachidate by the methods of x-ray diffraction. A skeletonized film and an unskeletonized film were built by the writer, each having 300 layers. A test film taken from the same bath lost 43 percent of its material by being skeletonized in benzene and shrank one or two percent in its optically measured thickness. Mr. Bernstein found that the skeletonized film and the unskeletonized film gave the same x-ray grating space to within 0.1 percent. The photographic plate taken with the skeletonized film as the diffracting crystal was indistinguishable, on inspection, from the plate taken with the unskeletonized film with regard to relative intensities of the various orders and the sharpness of the x-ray lines.

In general practice the percentage of material removed from a film by the action of a solvent is approximately determined by the amount of fatty acid which is present in the monolayers of

which the film is built. When a fatty acid spreads in a monolayer on water containing a dissolved metallic salt, the fraction θ of the acid which is converted to soap is determined by the salt concentration in the water, the nature of the dissolved salt, and the hydrogen ion concentration as measured by pH.[9] If the bath contains barium chloride in a concentration $10^{-4}M$, θ is 0.5 for barium stearate when the pH of the bath is 7.0. In the case of cadmium chloride in a concentration $10^{-4}M$, $\theta=1$ at pH 7.0, and in order to have $\theta=0.5$ the bath must be made slightly acid, the pH being lowered to 5.7.

Recent experiments have demonstrated that built-up films of cadmium arachidate (Cd-Ar), made by spreading arachidic acid on a bath containing cadmium chloride, form skeleton films which have several advantages over the skeleton films made from barium stearate (Ba-St). In the case of Ba-St it is difficult to establish a constant value for $(1-\theta)$, the fraction of stearic acid in the film. This difficulty arises from the fact that if minute traces of foreign salts, such as the salts of copper, aluminum or lead, are present in a barium bath at pH 7.0, the surface film tends to combine selectively with these salts.[10] This results in lowering the value of $(1-\theta)$ far below the value which the film has on a barium bath when these salts are absent. The effect is so marked that the value of $(1-\theta)$ for a film of Ba-St is often used as a test for the presence of traces of impurities in the barium bath. When a bath is used containing a cadmium salt at pH 5.7, the foreign substances have little tendency to combine selectively with the surface film. This is due to the decrease in pH, since the fraction θ of soap formed by a given concentration of a given substance tends to decrease with decreasing pH.

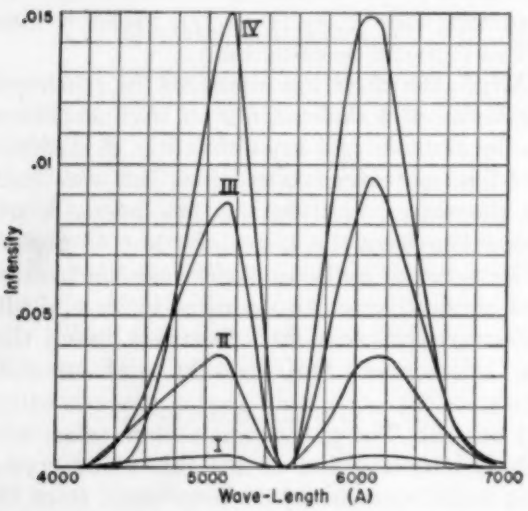

FIG. 2. Intensity of reflected light as a function of wavelength when film is illuminated by white light. Plotted for first four orders of interference minima. Curves calculated for the case of films having optical thicknesses $0.25\lambda(2a+1)$, where λ is 5550A and $a=0,1,2,3$.

Skeleton films of Cd-Ar have the further advantage that the optical quality of the films is exceptionally good. The optical quality depends on the size of the air spaces. In a perfect skeleton film these spaces are of molecular size and therefore scatter no light. If partial collapse occurs, crevices of larger size are formed which scatter more or less light and cause the film to have a fogged appearance.

The bath which is commonly used to build films of Cd-Ar is $10^{-4}M$ cadmium chloride, $10^{-3}M$ sodium acetate, $3\times10^{-5}M$ potassium cyanide, $1.2\times10^{-4}M$ hydrochloric acid. Distilled water is used which has a specific resistance 0.7 to 1.0×10^{6} ohm·cm. The sodium acetate is used as a buffer, and the potassium cyanide to remove traces of copper ions which are sometimes present in the distilled water. Oleic acid is used as piston oil. The films are built by the ordinary method. It has been found very desirable to apply the piston oil pressure immediately after the last drop of the spreading benzene solution of arachidic acid has vanished. If several seconds are allowed to elapse before the pressure is applied, the films built from the bath commonly have one or more bad streaks which are caused by imperfections in the monolayer on the water surface.

Skeleton films of Cd-Ar are made by soaking built-up films of Cd-Ar in ethyl alcohol or in acetone. One of the interesting features of skeleton films is the effect which different solvents have on films made of different substances. The most satisfactory solvent in the case of Ba-St is a mixture of 1 percent of 95 percent ethyl alcohol in benzene. This solvent acts many times more rapidly than pure benzene.

[9] I. Langmuir and V. J. Schaefer, J. Am. Chem. Soc. **58**, 284 (1936).

[10] I. Langmuir and V. J. Schaefer, J. Am. Chem. Soc. **59** 2400 (1937).

In fact, benzene is so slow in accomplishing the complete removal of stearic acid from Ba-St that the films which were supposed in the early work[6] to be completely skeletonized were found later to contain some stearic acid. In the case of calcium stearate pure benzene is as rapid as the alcohol-benzene mixture. Copper stearate forms wretched skeletons, the film collapsing to a large extent in the solvent. Lead arachidate is skeletonized very rapidly in pure benzene, to form skeletons of excellent quality. On the contrary, if Cd-Ar is soaked in benzene, carbon tetrachloride or carbon disulphide, it is nearly always cracked into a myriad of fine cracks which scatter a great deal of light. Cd-Ar films soaked in alcohol or acetone are perfectly clear.

A study of the optical properties of skeleton films can be made very simply by building a step-series of Cd-Ar monolayers on a glass slide. The layers are deposited on *both* sides of the glass. Ordinary microscope slides ($n_g = 1.51$ to 1.52) are suitable for this purpose. The slides should be prepared by rubbing them with molten ferric stearate while the glass is hot (about 110°C) until every visible trace of the stearate has disappeared. Commercial lead stearate gives almost as good results. Cd-Ar monolayers attach themselves readily to a slide prepared in this way, the first layer being deposited as the slide is lowered into the water (*A* layer).

The step-series is built in about eight two-layer or four-layer steps with thicknesses ranging on either side of the thickness corresponding to $n_1 t = 0.25\lambda$ for visible light (Fig. 1(b)). For sodium light this thickness is built by 44 to 46 layers of skeletonized Cd-Ar when $\theta = 0.5$. Before the series is skeletonized it is barely visible on a microscope slide, since the refractive index of the film ($n_1 = 1.54$ for Cd-Ar) is close to that of the glass. After it has been soaked in alcohol for ten sec. to two min. the steps appear as brightly colored bands. When the slide is first immersed in the alcohol the initial removal of stearic acid and corresponding lowering of n_1 is quite rapid, and with further time it proceeds more slowly. The slide should be raised fairly slowly from the alcohol to allow time for the surface to shed the alcohol which it does sometimes rapidly and at other times reluctantly. A hand windlass, of the type employed for building films, is convenient for this purpose.

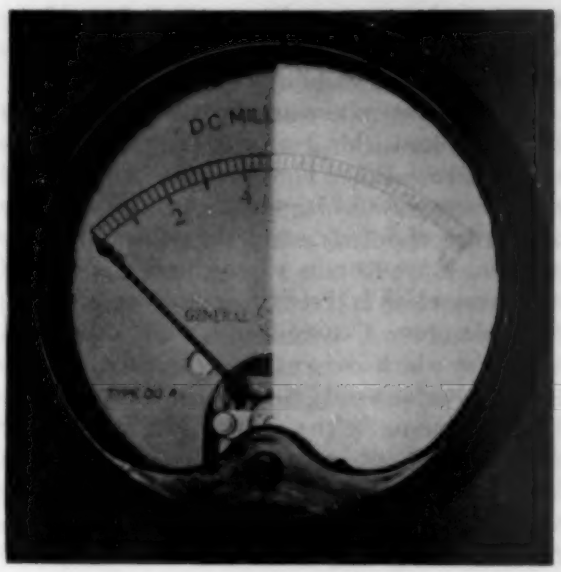

FIG. 3. Glass instrument cover illuminated by a flood light. The left side, in the photograph, was coated with a nonreflecting film.

When a slide, coated with a film, is removed from the solvent after a few seconds, the refractive index of the film in air is usually 1.35 to 1.30. At $n_1 = 1.35$ the steps seen by perpendicular white light form a series of colors which range continuously from yellow brown, to deep blue, to pale blue, as the steps increase in thickness. As n_1 is decreased toward the extinction value $n_1 = n_g^{\frac{1}{2}}$, which is accomplished by soaking the slide for a longer time, the colors all become more vivid and the series changes to red brown, purple, deep blue and pale blue. That is, a red hue becomes very noticeable which was lacking at the higher refractive index. The progressive change as n_1 is decreased may be aptly described by saying that the colors show far more "fire." No step reflects a clear red when the thicknesses are in the range of the first minimum, but when $n_1 = n_g^{\frac{1}{2}}$ the step having a thickness which extinguishes green light reflects a vivid magenta color.

The increase in the red hue serves as a very useful indicator of the approach of the refractive index to the extinction value. Dr. Langmuir has pointed out that the reason that the eye does not notice a red color in the reflected light until n_1 approaches $n_g^{\frac{1}{2}}$ is because the red color is due to

the extinction of green from white light, and the wave-length corresponding to green lies at the maximum of the visibility curve for the eye.

At the first minimum the colors pass from brown to blue within a range of thickness which is quite narrow. When films are built with optical thicknesses $n_1 t = 0.75\lambda$, which correspond to the 2nd order of interference, the minima for the different wave-lengths extend over a range of thickness which is three times as great as for the first minimum. Consequently there is no film-thickness which reduces the reflection of white light to a value nearly so low as in the case of the first minimum. At the minima of the 3rd order and of higher orders the reflection of white light becomes increasingly greater, and approaches the value $I_g = I_B + I_C$, where I_B and I_C are the intensities of white light reflected at boundaries B and C, calculated by ordinary methods.

The reflection at the successive minima, *as seen by the eye*, can be calculated by multiplying the intensity given by Fig. 1(b) by the visibility corresponding to the different wave-lengths, as given by a visibility curve. Fig. 2 shows the result of these calculations for the minima of the first, second, third and fourth orders. The data were calculated for the case of skeleton films ($n_1 = 1.233$) having optical thicknesses $n_1 t = 5550(2a+1)/4$ A where $a = 0, 1, 2$. The curves show that the first minimum is by far the most effective for diminishing reflection when white light is used. Also the first minimum is the only one for which the transmitted light appears colorless to the eye. The light transmitted by films corresponding to other minima is tinged by the color which is complementary to the color of the reflected light.

TABLE I. *Thickness and optical density of two types of film having refractive indices n_a and n_b. These are calculated for the case $n_a = 1.50$. Thicknesses t_a and t_b refer to films which reflect minimum intensity of sodium light. Optical densities d_a and d_b are calculated by means of Eq. (15).*

(1)	(2)	(3)	(4)	(5)
γ	n_b	t_a/t_b ($i=0°$)	t_a/t_b ($i=80°$)	d_b/d_a
1.0	1.50	1.0	1.0	1.0000
0.9	1.45	0.9667	0.9404	0.9136
0.8	1.40	0.9333	0.8793	0.8242
0.7	1.35	0.9000	0.8159	0.7317
0.6	1.30	0.8667	0.7500	0.6358
0.5	1.25	0.8333	0.6804	0.5369
0.4	1.20	0.8000	0.6058	0.4349

The photograph in Fig. 3 shows the result of eliminating reflection from a glass instrument cover. One-half of the cover of a milliammeter was coated with a Cd-Ar skeleton film and the other half was left as clean glass. The coated half appears on the left in Fig. 3, the film being on the back and on the front of the glass. Mr. J. T. M. Malpica illuminated the instrument with a bright light in such a way that a strong glare was reflected by the clean glass, and photographed the meter in this position. The photograph shows that whereas the scale of the instrument was barely visible through the clean glass, the scale at the left was seen as plainly as though the glass were not there. People who have seen this instrument for the first time have been deceived by the illusion that there was no glass over the left side. The glass on the left actually reflected a deep purple color, but the intensity of the reflected light was so low that the color was not noticed when the attention of the observer was caught by the instrument-scale behind the glass.

The sharp boundary line between the coated and the uncoated glass, seen in the photograph, is a useful feature of films built from monolayers. This boundary is made by the line of intersection of the glass with the water surface when the film is dipped repeatedly to the same depth in the bath. A stripe can be built in the same way by dipping the glass between two fixed limits. In this case the end of the glass below the stripe receives one layer when the glass first enters the water and one layer when it leaves it, but a thickness of two layers on glass cannot be discerned by the eye.

The glass of which the instrument cover was made had a refractive index about 1.52. The procedure which was found most satisfactory in building skeleton films having $n_1 = (1.52)^{\frac{1}{2}}$ was carried out in the following way. A film having 44 or 46 monolayers of Cd-Ar was built from the bath which has been described. This film was soaked for 2 min. in ethyl alcohol at room temperature, which reduced n_1 to a value which was usually less than 1.30. It was then soaked in acetone at 35°C to 40°C for 1-min. or 2-min. intervals of time, and after each interval the glass was withdrawn and the intensity with which it reflected sodium light was observed. As n_1 gradually approached the extinction value the

film became nearly black when seen by sodium light, and at the extinction value it was completely black and reflected no image of the sodium lamp. When the process was carried out in this way the alcohol removed the greater part of the arachidic acid, and then the warm acetone continued the skeletonization by attacking the soap itself. The rate at which acetone dissolved Cd-Ar was found to increase rapidly with temperature and at 45°C to 50°C it dissolved the soap so rapidly that the film lost a thickness of several layers in about 5 min. and was completely dissolved after a longer period of time. At temperatures below 40°C, however, the rate at which acetone dissolved Cd-Ar throughout the body of a partially skeletonized film, i.e., the rate at which it continued to skeletonize the film, was sufficiently rapid compared with the rate at which it dissolved the surface so that the desired degree of skeletonization was accomplished before the film had lost a thickness of more than about 2 to 4 layers.

The method described in the preceding paragraph has usually given films of better quality than where fatty acid alone was dissolved. The method employed films which were built of monolayers for which the soap-fraction θ was a little greater than 0.5, rather than monolayers for which θ was 0.5 or less. From previous experience with films of other substances it seems probable that the films built with the higher value of θ had greater mechanical strength with which to withstand the strains of the processes of skeletonization. The value of θ can be varied over any desired range by adjusting the pH of the bath by means of HCl or NaOH.

In order to determine the correct number of monolayers for a light-extinguishing film of uniform thickness when the film is built from a given bath, it is usually desirable to test the films coming from the bath by building and skeletonizing a step-series. Films built by the processes described in the preceding paragraphs commonly suffer a loss of thickness of two to four layers, and after this number has been determined by a test run other films can be built so as to have exactly the correct thickness when skeletonized. The test is accomplished most conveniently by determining from a skeletonized two-layer step-series the number of layers having the desired thickness.

It has been shown that the thickness which a film must have in order to extinguish monochromatic light increases with increasing angles of incidence. When a film is to be built which will diminish the light as much as possible over a range of angles i_1 to i_2 this thickness can also be determined from a step-series. The film will have an effective thickness D which is greater than $0.25\lambda(2a+1)$ at $i=i_1$ and less than this value at $i=i_2$, where $i_1<i_2$.

The refractive index of a film can be measured by several methods, which will be described.

(a) When the film is a built-up film, so that a step-series can be duplicated on several different samples of glass, the most satisfactory method of measuring n_1 is to determine the glass for which the minimum of the step-series reduces the light to zero intensity. The refractive index of the film is then given by Eq. (7). The writer has used for this purpose a series of glasses ranging from lead glass, $n_1=1.7854$, to silica glass, $n_1=1.459$, which covers a range for the film from $n_1=1.336$ to $n_1=1.208$. When the refractive index of the step-series is given by $n_1^2>n_g$, the intensity of the minimum of the series increases as i is increased from $i=0$, and therefore the contrast shown by successive steps is diminished. On the contrary, in the case where $n_1^2<n_g$ the contrast increases and passes through a maximum as the angle increases.

(b) If one wishes to measure a series of values of n_1 on the same plate of glass, this may be done by measuring the intensity of the light reflected by the film. Measurements of this type have been made by Mr. Malpica, using a Hewlett cell as the light-sensitive element. The values of n_1 can then be determined by means of calculations of the type illustrated in Fig. 1(a). In many cases it is nearly as satisfactory to measure the transmission of light by the glass, and this measurement can be accomplished with a simpler optical set-up than the measurement of reflection. In the case of transmitted light due allowance must be made for the absorption of light by the glass. When the glass is a microscope slide the absorption can be measured by stacking together a pile of similar slides with a very thin layer of transparent oil between them, and measuring the

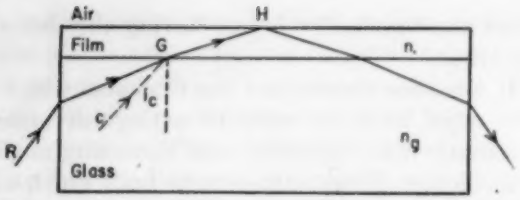

FIG. 4. Method of demonstrating the total reflection of light from the air-film boundary of a film built on glass.

decrease in transmission as the number of slides is increased. The oil should have a refractive index close to that of the glass. The effect of small differences of refractive index is small, however, for if $n_g=1.52$ for the glass and $n_1=1.49$ for the oil, the intensity reflected by a layer of oil between two glass plates is only $2(0.03/3.01)^2=2\times10^{-4}$. A batch of microscope slides, measured in this way, were found to have an absorption 0.007 per slide.

(c) A more sensitive method of measuring progressive changes of n_1 is carried out by building a step-series on a polished chromium plated slide. When films having a thickness corresponding to the first minimum for the R_s ray are built on chromium and are seen at angles of incidence 75° to 80°, a difference in thickness corresponding to 1 Cd-Ar layer (27A) is very plainly visible. If sodium light is used to illuminate a two-layer step-series on chromium, the step corresponding to the intensity minimum is seen as a black band which contrasts sharply with the brighter intensities reflected by the neighboring steps on either side.

It was shown in the section which dealt with the significance of the term "optical thickness" that as the refractive index decreases, the minimum for a given wave-length shifts to steps of higher thickness. At angles $i=75°$ to 80° the shift is nearly twice as great as for perpendicular light. This is shown by the data in columns 3 and 4, Table I.

Table I gives the values of t_a/t_b calculated for an "ideal" skeleton. An "ideal" skeleton is one which has the same thickness as the solid film from which it was made. The values were calculated by means of the equation $n_a t_a \cos r_a = n_b t_b \cos r_b$ which results from Eq. (2). Here r_a and r_b are the angles of refraction in the film corresponding to n_a and n_b. The calculations were made for the case $n_a=1.50$. The values in column 3 were calculated for $i=0°$ and in column 4 for $i=80°$. Column 1 gives values of γ where $\gamma=(n_b-1)/(n_a-1)$. Column 5 gives values of the relative density d_b/d_a calculated by means of Eq. (15). These values show that d_b/d_a is approximately equal to γ.

In order to determine the refractive index of a skeleton the value of t_a (in terms of Cd-Ar monolayers) is measured at $i=80°$ before the film is soaked. The values of n_b for the skeleton can then be determined from measurements of t_b at $i=80°$, and from the data for t_a/t_b in column 3.

The process can be carried out in another way when the skeleton is not built in a step-series. In this case the color of the skeleton film, can be matched to the color of a step-series of solid film built on a different slide. We then have $n_a \cos r_a/n_b \cos r_b = t_a'/t_b'$ where t_a' and t_b' refer to the solid film and are the thicknesses of the steps a and b of the solid film which match the skeleton before and after the latter is skeletonized. It is seen that $t_a/t_b=t_b'/t_a'$.

(d) A method for measuring n_1 has been previously described[6] which was carried out by making optical measurements of a series of eight steps having 119, 129, –189 layers of skeletonized Ba-St. This method depended for its validity on the condition that n_1 should be the same for all the steps in the series. If the steps should have a continuous variation of n_1 with thickness, this variation would result in a considerable error in the values of n_1 obtained by this method.

It has been found[8] that there are certain types of film for which the value of θ is not uniform over the area of the film, but increases continuously from one end of the slide to the other. This is due to the fact that the value of θ for each monolayer deposited as the slide descends into the water (A-layer) increases with the length of time which the slide spends under water before the next ascending layer (B-layer) is deposited. Therefore θ has a greater value at the lower end of the slide than at the upper end. In the case of a step-series built in the usual way with the thinner steps at the top of the slide and the thicker steps at the bottom, the variation in n_1 is accompanied by the variation in thickness.

The phenomenon of the increase of θ with time under water has been found to be especially characteristic of films of lead stearate, and

to occur to a less marked degree with lead arachidate. In the case of lead stearate, films built from a bath which was $10^{-4}M$ $PbCl_2$, pH = 5.0, consisted of Y layers at the top of the slide and X layers at the bottom. The results of skeletonization in benzene showed that θ was 0.75 at the top of the slide and 1.0 at the bottom. In the case of films of other substances which were built in Y layers the following method was used for testing this phenomenon. The test films were built on a chromium-plated slide with a thickness of about 40 layers over the entire dipping area. On each ascending trip, as a B layer was deposited, the slide was raised in about 1 sec. until one-half of the dipping area was out of water. It was held stationary in this position for 15 to 30 sec. and was then raised rapidly the remaining distance. The A layers were deposited in the usual manner by lowering the slide rapidly to the full depth of the dipping area. The film was skeletonized, and if θ for the A layers had increased during a time 15 to 30 sec. under water, the result was seen as a line of contrast between the colors reflected by the upper and lower halves. Tests were made with lead arachidate using the bath described above. They showed differences of refractive index amounting to two to five percent between the values of n_1 for the two halves.

(e) The method of measuring n_1 by means of Brewster's angle i_B has also been previously described.[6] This is a very useful method in the case of isotropic substances. Built-up films of the soaps of fatty acids are uniaxial crystals and retain their property of birefringence after being skeletonized. In the case of a birefringent substance the value of i_B is a function of the two refractive indices n_1 and n_3 of the ordinary and extraordinary rays. Therefore a measurement of i_B does not lead to a determination of the value of either n_1 or n_3 unless further data are available, such as the data giving the birefringence $(n_3 - n_1)$ of the substance. However, measurements of i_B have frequently proved useful in the present experiments as a rough indication of the progressive decrease of n_1 where a film is soaked for successive intervals of time. Since the film remains birefringent, i_B decreases with n_1.

Skeleton films absorb oil very readily. Oil fills the pores of the skeleton, and if the refractive index of the oil is the same as that of Cd-Ar the oil restores the refractive index of the film to the value which the film had before it was skeletonized. Oil is used to determine whether a skeleton is an ideal skeleton or has a partially collapsed structure. A drop of mineral oil is allowed to flow across the film. The oil does not wet the surface of the film permanently but withdraws from the path which it has traveled, leaving the pores of the film over which it has traveled filled with oil. If the skeleton has the thickness t of the solid film from which it was made, the oil restores the color exactly to the color of the original film; if the skeleton has shrunk in thickness the color is different.

Total Reflection

The phenomena of interference, as exhibited by thin films, have no effect whatever on the phenomena of total reflection which occur when light is reflected from a surface at angles greater than the critical angle. It follows from Eqs. (5) and (6) that if either B or C is unity, $I_+ = I_- = 1$. Lord Rayleigh[11] pointed out this interesting fact in the following way. "When a thin transparent film is backed by a perfect reflector, no colours should be visible, all the light being ultimately reflected whatever the wave-length may be. The experiment may be tried with a thin layer of gelatin on a polished silver plate."

[11] "Wave Theory of Light." Published in *Scientific Papers*, Lord Rayleigh (Cambridge University Press, 1902), Vol. III, p. 67.

Table II. *Spacings of laminae. The optical thicknesses are given in column 4 and column 5. The amplitudes B, C_1 and C_2 of the rays reflected at the air-P, PQ and Q-glass boundaries, respectively, were calculated by means of Eqs. (3) and (4). Column 9 gives the expression for the resultant of the three rays (neglecting the effect of multiple reflections).*

(1)	(2) n_P	(3) n_Q	(4) $(n_1 l/\lambda)_P$	(5) $(n_1 l/\lambda)_Q$	(6) B	(7) C_1	(8) C_2	(9) Resultant Amplitude
(a)	1.52	1.236	0.25	0.5	−0.206	0.103	−0.103	$B+C_1-C_2$
(b)	1.52	1.87	0.25	0.25	−0.206	−0.103	0.103	$B-C_1+C_2$

The experiment may be done very convincingly by building a film n_1 on a block of glass n_g and illuminating the film by means of light R traveling in the direction shown in Fig. 4. It is found that the glass then reflects light as though the film were not there whether n_1 is greater or less than n_g. Let i_C be the critical angle for glass at a glass-air boundary. It follows from the laws of reflection and refraction that a ray C which is incident on the film at an angle i_C at the glass-film boundary is refracted in the film and arrives at the film-air boundary at an angle which is the critical angle for that boundary. Therefore all rays, such as R, which arrive at G at an angle greater than i_C are totally reflected at H. A film illuminated in this way can be said to be "backed" by a perfect reflector for every wavelength, the air serving as the "backing" material. Fig. 4 illustrates the case for glass $n_g=1.50$, $n_1=1.45$.

It should be mentioned in this connection that since built-up films of Ba-St and Cd-Ar are uniaxial crystals, the birefringence can be studied in an interesting way by the method of illumination illustrated in Fig. 4. If the films are built in a series of about 8 steps having 40, 80, . . . 320 layers on glass $n_g=1.52$, and the glass is held between parallel or crossed Polaroid screens, the colors which are seen due to birefringence are very striking. Quantitative measurements of the path difference between the R_s and the R_p rays can be made as a function of film thickness, angle, and n_g. An interesting demonstration of the range of phase changes which occur at total reflection can be made by "backing" one-half of the film with a strip of paper wet with water while the remainder is backed by air. The series of colors of the steps seen between Polaroid screens is shifted, the steps backed by water having colors which correspond to a smaller phase difference between the two rays than the steps backed by air.

Laminated Films

Several types of crystals occur in nature which are composed of alternating laminae of substances of different refractive index, the laminae having spacings which are comparable with a quarter-wave-length of light. These crystals have interesting optical properties which have been studied by Lord Rayleigh, R. W. Wood,[12] and others. In the present experiments laminated films were built with combinations of skeleton and solid films, and with evaporated films of zinc sulphide and built-up Ba-St films.

Table II illustrates the spacings which laminae of two different substances of refractive index n_P and n_Q must have in order that a film composed of one lamina of each substance shall extinguish the light reflected from glass ($n_g=1.52$). The data were calculated for the case where one lamina of Q was built on the glass, and one lamina of P on top of Q.

Laminated films built in this way have total optical thicknesses greater than 0.25λ. Therefore when they are used with white light they reflect more light than a film which corresponds to curve I, Fig. 2.

Etching of Glass by Chemical Treatment

Various types of lead glass and barium glass having refractive indices 1.61 to 1.72 have been etched with nitric acid to produce films which showed interference colors. The films that were formed by the etching process were found to have a refractive index approximately 1.46. This is the refractive index of fused quartz. The film is hard and can be rubbed vigorously with a cloth or with a mild abrasive such as Shamva without being scratched or showing a decrease of thickness. It is completely dissolved by boiling NaOH. The porosity of the film is very slight. When oil is placed on part of the film and is then rubbed off with a towel, no visible trace is left of the effect of the oil on the film. This shows that the film takes up no oil, or takes up so small an amount that the refractive index is not altered by an amount which causes the interference colors seen with white light to be visibly changed.

Mr. Malpica has made the following measurements of the reflection of light by two samples of glass, No. 1 and No. 2, which were etched so as to have films of optical thickness 0.25λ:

	No. 1 $n_g=1.72$	No. 2 $n_g=1.61$
Etched glass	2.4 percent	2.83 percent
Unetched glass	11.2 percent	9.66 percent

[12] R. W. Wood, *Physical Optics* (Macmillan Co., 1914), second edition, p. 161.

It was usually found necessary to prepare a glass surface for the etching treatment by polishing the glass with a fine grade of polishing rouge or by immersing it in boiling N/5 NaOH. This preparation accelerated the rate at which the glass was etched when it was put into acid. One sample of lead glass which had not received this preliminary treatment was not visibly attacked by nitric acid after many hours in the acid, but after being boiled in NaOH to remove the surface skin it was etched quite rapidly.

Measurements were made of the rate at which glasses No. 1 and No. 2 were etched in 1 percent nitric acid. Glass No. 1 was a sample of lead glass, of the type used to make x-ray screens. Dr. L. Navias measured the refractive index of this glass and found $n_g = 1.695$ which corresponds to 60 percent PbO_2. This sample was etched in 1 percent HNO_3 at 100°C. Four pieces of the glass were boiled in NaOH until all stains had been removed, and were then plunged immediately into the boiling acid. The pieces were withdrawn one at a time, after measured intervals of time, and plunged into hot distilled water to rinse off the acid. After being removed from the water they were rubbed with molten paraffin to prepare the surface to receive built-up layers of Ba-St. The thickness of the film which resulted from the etching was measured in terms of layers of Ba-St by counting the number of layers which were needed to bring the film to the thickness corresponding to the first minimum for perpendicular sodium light, $N_I = 40$, or to the second minimum, $N_{II} = 122$. The data in Table III were obtained in two series of measurements, *A* and *B*. The same glass was used for both series, the silica film which produced the colors being completely removed by boiling NaOH after each series of measurements. The thicknesses in the table are given in terms of number of Ba-St layers ($n_1 t = 36$A per layer). When the data in Table III are plotted on double-log paper they lie quite closely on a straight line. The slope of the line shows that the thickness increases with the 0.37 power of the time.

TABLE III. *Thickness of film produced on lead glass, $n_g = 1.72$, by etching in boiling HNO_3 for lengths of time t. Thickness is given in terms of number N of layers of* Ba-St. *($n_1 t = 36A$ per layer).*

t	Thickness N_A	N_B
15 sec.	30	32
1 min.	47	51
3 "	70	72
8 "	109	
9 "		113

Glass No. 2 was received from Dr. C. E. K. Mees. It was a sample of glass obtained from Bausch and Lomb Optical Company, of a type described in their most recent catalog as "DBC-3", $n_D = 1.61088$. This sample was etched far more readily by 1 percent HNO_3 than sample No. 1. Therefore the etching was carried out in acid at 40°C since the rate of etching decreased rapidly with decreasing temperature. The rate was found to be linear with time, the thickness increasing at a rate equal to 26 Ba-St layers per min. in the acid.

A step-gauge was made by etching this glass in steps. The glass was polished with rouge and was then held in a vertical position and lowered to successive depths of 0.5 cm, 1.0 cm, etc., for one minute at each depth. The result was a step-series showing bright colors which were matched by the colors of a Ba-St series having 20, 46, 72, 98, 124 layers.

The step-gauge made with etched glass is well suited to measurements made with the gauge under water, such as are made in studying adsorption of substances from solution. The colors are more vivid when seen under water than when seen in air, since n_1 for the film has more nearly the value given by Eq. (7) when $n_0 = 1.33$ for water than when $n_0 = 1.0$ for air. On the contrary the colors of the usual type of step-gauge, which is made of Ba-St steps built on polished chromium, are so faint under water as to be almost invisible when seen by perpendicular light.

Films of Evaporated Substances

Dr. C. W. Hewlett has reported the following experimental results:

"Thin films were made by evaporating in vacuum various substances such as calcium fluoride, sodium fluoride, and lithium fluoride. The films were evaporated on glass microscope slides. After the glass was cleaned by the ordinary processes, and heated in a blue Bunsen

flame, it was subjected to a glow discharge for a few minutes before evaporation began.

"The material to be evaporated was melted down to a clear bead on a platinum or tungsten filament, and a small amount was allowed to evaporate before the glass plate was moved into position to receive the deposit. Special magnetic rotating devices were provided for moving the plate, and also for rotating it during the evaporation so as to deposit a film on each side of the plate. The thickness of the evaporated film was controlled by observing the reflected image of the filament in the surface of the deposit, and discontinuing the evaporation when the correct color was reached.

"Films of calcium fluoride, CaF_2, were found to have the lowest refractive index of the films which were made in this way. When the CaF_2 was evaporated in vacuum the refractive index of the film was 1.22. The refractive index was determined from a measurement of Brewster's angle for the film. Glass of refractive index 1.52 transmitted 92 percent of white light when the glass was not coated, and 99 percent when both surfaces were coated with CaF_2. These films had very poor mechanical properties, being easily scratched by light pressure from a handkerchief. Various heat and chemical treatments were ineffectual in hardening them. The films were not removed by being immersed in hot water.

"Sodium fluoride films were harder, but were not quite so good optically, and were soluble in water. The refractive index of the NaF films was 1.29, and glass coated on both sides with films having an optical thickness of a quarter-wave-length transmitted 98 percent of white light. It required considerable pressure and rubbing with a soft cloth to scratch them. A mixture of four parts CaF_2 and one part NaF, by molecular weight, produced a film of intermediate hardness, refractive index 1.27, and transmission 98.5 percent.

"Lithium fluoride produced films which were quite satisfactory mechanically, they would stand vigorous rubbing with a soft cloth without being scratched. Glass covered on both sides with quarter-wave-length films transmitted 98 percent. Unfortunately these films were readily soluble in cold water.

"The refractive index of each of these three substances could be controlled within certain limits by adjustment of the gas pressure during evaporation, the greater the pressure the lower the refractive index. However, if the pressure was as high as 5μ there resulted a perceptible decrease in the hardness of the film, and if the pressure was as high as 10μ there was non-uniformity in the thickness of the evaporated layer, owing apparently to the presence of convection currents."

Effect of Quartz Filters on the Distribution of Energy in Laue Patterns

GERALD W. FOX AND DEAN W. STEBBINS*
Department of Physics, Iowa State College, Ames, Iowa
(Received November 2, 1938)

Laue pictures were taken of *AT*- and *Y*-cut quartz crystals with radiation filtered by another crystal of the same cut and orientation. Either one, or both, of the crystals could be oscillated in different harmonics at different temperatures. Oscillation of the first crystal (nearest the x-ray tube) produced no effect on the pattern of the second crystal. Oscillation of the second crystal alone gave an increase of intensity of its pattern comparable to that observed when unfiltered radiation was incident. Oscillation of both crystals gave a greater increase than oscillation of only the second one. These results are explained by a reduction of primary extinction and an increased range of wave-length reflected from the interior during oscillation. The effect of temperature was too small to be evident in this investigation.

INTRODUCTION

FOX and Carr,[1] Nishikawa, Sakisaka, and Sumoto,[2] and Klauer[3] have shown that the Laue spots of a quartz crystal are more intense when it is oscillating piezoelectrically than when it is not. Fox and Carr employed *Y*-cut plates oscillating in the fundamental. Nishikawa *et al.* used *X*-, *Y*-, and *R*-cut plates oscillating in the first and third harmonics. Klauer used *X*-cut plates oscillating in the first, third, and fifth harmonics and varied the angle of incidence through 72°.

A change in intensity of the central beam during oscillation of the crystal was reported by Fox and Fraser.[4] However, Jauncey and Deming[5] were unable to repeat the observations by using an ionization chamber. Jauncey and Jaques[6] ascribed the increased blackening of the central spot to photographic reversal and halation.

The energy diffracted by a crystal into a given Laue spot has a definite wave-length determined by the Bragg equation. Obviously, there must be a band of wave-lengths going into each spot. One might ask whether all the energy of that particular wave-length band is diffracted by a given crystal. The following investigation was designed to try to answer that question and to try to observe any change in the intensity of the central beam during oscillation.

EXPERIMENTAL PROCEDURE

AT- and *Y*-cut plates were used. The *Y*-cut plates were some that had been used in an earlier problem. The *AT* plates were prepared by cutting a thin slab from the face of a crystal segment which had previously been ground to a true *AT* cut. The slab was then cut into a square and ground to a thickness of ±0.002 mm with No. 120 carborundum powder. This square was then cut into four smaller squares of equal size, each being seven-eighths of an inch on a side. Two of these had the same frequency within the limits of a General Radio Type 22L wave meter, and were used throughout the investigation.

A schematic diagram of the crystal holder is shown in Fig. 1. The baffle plate, *B*, was of $\frac{1}{8}''$ lead with brass plates soldered to each side to insure accurate machining. It was one inch square and the sides were parallel within 0.0001 inch. The thickness was enough so that all the energy diffracted by the first crystal was absorbed in the plate and only the central beam went through to the second crystal. The hole through the plate was the same size as those in the collimator (No. 60 drill) and concentric with them. Electrical leads to the baffle plate and to each of the end plates made it possible to oscillate either one or both of the crystals.

A cold chamber in which solid carbon dioxide and acetone were used to provide a low

* Now at State College of Washington, Pullman, Washington.
[1] G. W. Fox and P. H. Carr, Phys. Rev. **37**, 1622 (1931).
[2] S. Nishikawa, Y. Sakisaka, and I. Sumoto, Sci. Papers Inst. Phys. and Chem. Res., Tokyo **25**, 20 (1934).
[3] F. Klauer, Physik. Zeits. **36**, 208 (1935).
[4] G. W. Fox and W. A. Fraser, Phys. Rev. **47**, 899 (1935).
[5] G. E. M. Jauncey and J. J. Deming, Phys. Rev. **48**, 462 (1935).
[6] G. E. M. Jauncey and A. T. Jaques, Phys. Rev. **50**, 672 (1936).

temperature accommodated the crystal assembly.

Radiation from an x-ray tube with a tungsten target and operating at eight milliamperes and fifty-five kilovolts was used.

The following pictures were taken with *AT* plates at room and cold temperatures: (1) Neither oscillating; (2) *A* oscillating at first harmonic; (3) *C* oscillating at first harmonic; (4) Both oscillating at first harmonic; (5) *A* oscillating at third harmonic; (6) *C* oscillating at third harmonic; (7) Both oscillating at third harmonic. Pictures of the *Y* plates were taken at room temperatures and with conditions as in the first four above.

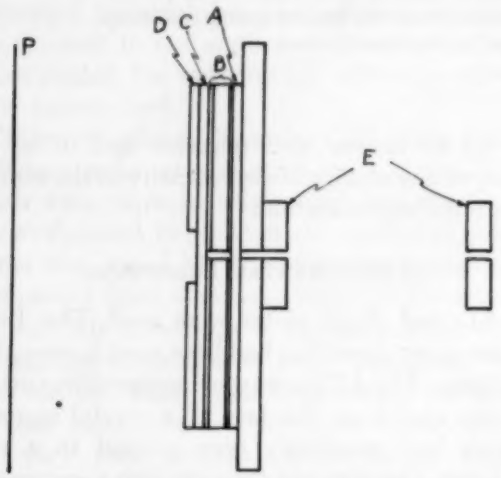

FIG. 1. Schematic diagram of double crystal holder. *A* and *C*, quartz crystals; *B*, baffle plate; *D*, brass plate for electrode; *E* and *E*, collimating holes; *P*, photographic film.

RESULTS

The pictures were studied visually and with a microphotometer and the following results were indicated:

1. A given crystal does not diffract all the energy of a given $\Delta\lambda$ since a good pattern was obtained on picture 1.

2. The intensity of the central beam is not appreciably altered since there was no noticeable difference between pictures 1 and 2.

3. Oscillation of a crystal increases the intensity of the diffraction images when the incident radiation has been filtered by an identical crystal. In this case picture 3 was more intense than 1.

4. Oscillating both crystals at once gives an intensity greater than that observed on picture 3. This seems to be an anomalous result for it would seem that if this observation were true, then the intensity of 2 should be greater than 1. An explanation is offered in the next section.

5. The effect of temperature, in the range from room temperature to that of solid carbon dioxide and acetone, on the intensity of the diffraction pattern is too small to be observed photographically.

6. The effect of oscillating a crystal of the dimensions of those used in the third harmonic is the same as that observed when the crystal oscillates in the first harmonic.

7. The type of cut makes some difference on the amount of increase of intensity. The increase with the *Y* plates was greater than that of the *AT* plates.

DISCUSSION

According to the theory of x-ray diffraction maxima, for a given wave-length there is an angle of a few seconds over which complete reflection occurs from the lattice planes of a perfect crystal. Quartz has a high degree of perfection and we should expect the above condition to be fulfilled for the interior planes. However, at the surface of a prepared crystalline plate, stresses have been set up by grinding and polishing so that small crystallites of slightly different orientation from that of the interior planes cover the surfaces. Therefore, we can never deal with a truly perfect crystal section.

The Laue pattern is formed by energy which has been diffracted by these crystallites. This energy is so near the wave-length of that suffering extinction in the interior and the crystallites are of so nearly the same orientation as the interior that the energy goes approximately to the same spot on the photographic plate. And yet the wave-lengths are different enough from the critical one ($\lambda = (2d/n) \sin\theta$) that the energy does not suffer extinction. Since each of the crystallites is large enough to diffract only a small percentage of its critical wave-length, and since the crystallites all have a slightly different orientation, it is hard to realize the necessary condition to remove all the energy of a given $\Delta\lambda$ from an x-ray beam. While the

central portion of the crystal will extract 100 percent of the energy over small $\Delta\lambda$'s, the $\Delta\lambda$'s are so small that the total energy is hardly measurable.

Now if a second crystal of the same orientation is placed in the transmitted central beam, there will be present sufficient energy of the wave-lengths diffracted by the crystallites to give a good diffraction pattern. The wave-lengths suffering extinction in the first crystal are not present but they would likewise suffer extinction in the second crystal.

Figure 2 shows suggested $I-\lambda$ curves for (A) the incident beam, (B) the central beam from the first crystal, and (C) the central beam from the second crystal.

If we assume that the amplitude of an oscillating crystal is 1000A and that the motion is sinusoidal and transverse, the angle between the x-ray beam and the interior crystalline planes may vary by as much as 100 seconds. Since the angle of complete reflection is of the order of ten seconds, it is evident that during oscillation the

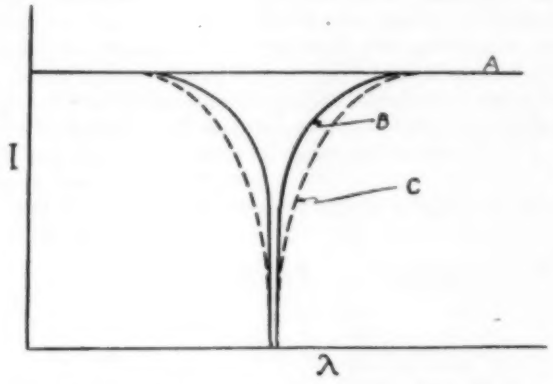

FIG. 2. Intensity, wave-length curves for the radiation in immediate vicinity of a Laue spot. A, incident radiation; B, central beam from one crystal; C, central beam from two crystals.

primary extinction has been greatly reduced. Also, with the different angles between the x-ray beam and the planes, wave-lengths adjacent to the critical one for the nonoscillating crystal will be reflected from the interior of the crystal, and the region between double spots will be blackened also.

During oscillation of the first crystal, then, its central beam will contain some energy of the critical wave-lengths and probably less of the adjacent wave-lengths. One might expect the $I-\lambda$ curve of the transmitted beam in the neighborhood of one of the critical wave-lengths to be represented by Fig. 3. It is seen that there is still present sufficient energy of the necessary wave-lengths to form a good diffraction pattern from the second crystal. While there is some energy of the critical wave-lengths present, it suffers extinction in the second crystal. Thus no

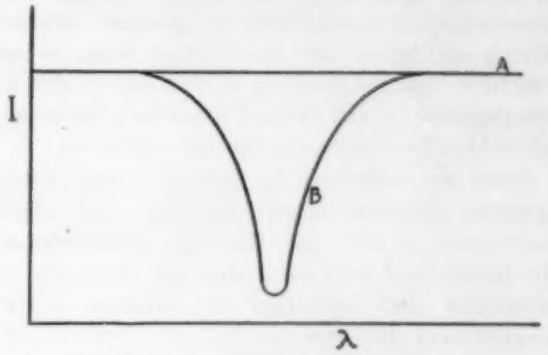

FIG. 3. Intensity, wave-length curves for radiation in immediate vicinity of a Laue spot. A, incident radiation; B, central beam from an oscillating crystal.

noticeable change of intensity of the pattern is observed with oscillation of the first crystal.

Consider the case when only the second crystal was oscillating. If one assumes the increase was due to a reduction of primary extinction, then one must admit that the central beam from the first crystal contained a considerable amount of energy of the critical wave-lengths. However, this would not agree with the explanation of the results already given. We propose, instead, that the increase was caused by the reflection of wave-lengths adjacent to the critical one. These wave-lengths would be transmitted by the first crystal, except for a small percentage diffracted by the surface crystallites, and reflection of them from the interior would be possible because of the warped planes. We conclude that the increase of intensity of the Laue spots during oscillation is due to (1) a reduction of primary extinction and (2) increased reflection of wave-lengths adjacent to the critical ones.

This explanation does not agree with that of Jauncey and Bruce[7] who attribute the increase of

[7] G. E. M. Jauncey and W. A. Bruce, Phys. Rev. 54, 163 (1938).

intensity to a reduction of secondary extinction. However, we feel that it is better to treat the interior of a quartz crystal as being perfect enough to provide for primary extinction.

In the "anomalous" result, the intensity with both crystals oscillating was greater than that with only the second one oscillating. This indicates that more energy, which normally suffers extinction in the second crystal, was transmitted by the first crystal during oscillation. The only wave-lengths transmitted in greater amount during oscillation are the critical ones, so we conclude that the increase in this case is due to the presence of the critical wave-lengths transmitted by the first crystal during oscillation.

Since no difference of intensity was noted between pictures from the first and third harmonics, we conclude that the amplitudes of the oscillations were such that the reduction of extinction and reflection of adjacent wave-lengths were the same.

An explanation of the greater increase of intensity during oscillation of the *Y* plates over the increase during oscillation of the *AT* plates would lead into the actual type of motion taking place within an oscillating crystal and this is not accurately known. The suggestion can be offered that the particular type of motion in the case of the *AT* plates was not the best to greatly reduce the extinction or that the planes were not of the right type to extract sufficient energy to make a great difference.

It was expected that the increase of intensity and the increase of piezoelectric activity with the lower temperature would produce something noticeable on a photographic plate. It might be possible that the primary extinction had been reduced to zero at normal temperatures so that increased oscillation at lower temperatures could produce no greater effect. If this were so, the only factor altering the intensity would be the increase of intensity of diffraction maxima with lower temperatures and this is known to be small.

The authors wish to acknowledge the helpful discussions of Professor J. V. Atanasoff of this department.

LETTERS TO THE EDITOR

Prompt publication of brief reports of important discoveries in physics may be secured by addressing them to this department. Closing dates for this department are, for the first issue of the month, the eighteenth of the preceding month, for the second issue, the third of the month. Because of the late closing dates for the section no proof can be shown to authors. The Board of Editors does not hold itself responsible for the opinions expressed by the correspondents.

Communications should not in general exceed 600 words in length.

Variation of Light Output with Current Density and Classification of Willemite Phosphors

F. Seitz,[1] in a recent paper on the properties of zinc sulphide, concludes, on the basis of its measured decay characteristic

$$[L(0)/L(t)]^{\frac{1}{2}}=\alpha t+1 \qquad (1)$$

and its absorption properties and photoconductivity that its phosphorescence is due to the ionization and recombination with freed electrons of interstitial metal (Zn or Cu) atoms distributed through the lattice. He leaves open the question whether the luminescence of willemite (zinc orthosilicate) is of similar character or is due to the excitation of substituted foreign atoms as in the case of thallium-activated alkali halides, which show exponential decay characteristics. A study of the variation of the (phosphorescent) light output with the current density of an electron beam bombarding a willemite surface supports the view that its luminescence is similar in character to that of ZnS.

Let the specific light output be L, the concentration of centers in the willemite be M and that of excited (or ionized) centers at equilibrium N_0. Furthermore, let p be the probability that any one unexcited center be excited in unit time by an electron stream of current density ρ (p is thus proportional to ρ).

For monomolecular reactions (alkali halides) we have the decay characteristic

$$\text{const.}\cdot L=-dN/dt=aN; \qquad N=N(0)e^{-at} \qquad (2)$$

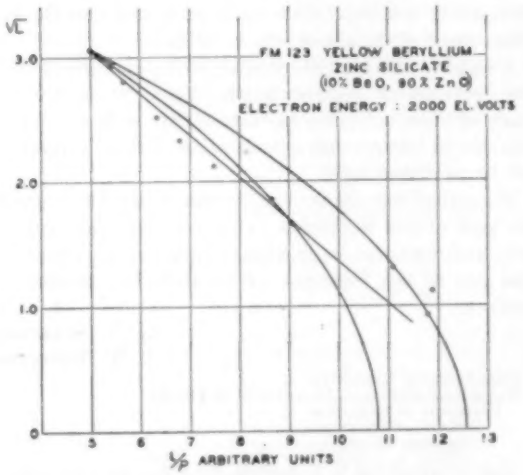

FIG. 1. Test of the relationship between the specific light output of yellow beryllium-zinc silicate and the electron current density.

and under equilibrium conditions we must have

$$p(M-N_0)dt=aN_0dt,$$

from which we conclude

$$N_0=Mp/(p+a)$$

and hence

$$1/L=a_1+a_2/\rho, \qquad (3)$$

where a_1 and a_2 are constants.

For bimolecular reactions, on the other hand, the decay characteristic is

$$\text{Const.}\cdot L=-dN/dt=bN^2; \qquad N=N(0)/[1+N(0)bt] \qquad (4)$$

and, for equilibrium conditions, we have

$$p(M-N_0)dt=bN_0^2dt,$$

which leads to

$$bN_0^2/p+N_0-M=0$$

and

$$L^{\frac{1}{2}}=b_1-b_2L/\rho, \qquad (5)$$

where b_1 and b_2 again are constants.

Both the variations (3) and (5) show an initial linear increase of the light output with the current density (slope $1/a_2$ and b_1/b_2, respectively) and ultimate saturation ($L_\infty=1/a_1$ and b_1^2, respectively). Plotting $L^{\frac{1}{2}}$ against L/ρ provides a particularly sensitive test of the two relations, if we write (3), with new constants, in the form:

$$L^{\frac{1}{2}}=(c_1-c_2L/\rho)^{\frac{1}{2}}. \qquad (6)$$

Figure 1 shows data obtained for a sample of willemite (yellow beryllium-zinc silicate) by S. T. Martin plotted in this manner. A straight line drawn through these (favoring the points corresponding to the higher intensities and thus measured with greater accuracy) represents the relation (5), while the two parabolic arcs represent relation (6) fitted to two pairs of observed points. It is seen that the bimolecular relation (5) fits the points definitely better than the monomolecular relation (6). The same was found to hold for measurements on fused willemite, also carried out by S. T. Martin. The evidence here presented thus favors the view that willemite falls into the same class as the ZnS phosphors.

E. G. RAMBERG
G. A. MORTON

Electronic Research Laboratory,
RCA Manufacturing Company,
Camden, New Jersey,
January 25, 1939.

[1] F. Seitz, J. Chem. Phys. **6**, 454–461 (1938).

The Inner, Initial Permeability of Iron and Nickel from 98 to 410 Megacycles

The *inner*, initial permeability of iron is known[1] to decrease from the comparatively constant value at the longer wave-lengths (above approximately 3 m) to unity for heat waves. Our investigations have been continued along two lines. First, as reported here, we have sought to close the gap in these values which exists between the wave-lengths 120 and 390 cm. Second, we have sought to increase the accuracy of the measurements, as will be reported shortly in detail by J. L. Glathart.

For the frequency range from 98 to 410 megacycles per second, we have modified the method used by Hoag and Jones (H-J), by moving the oscillator, as suggested by King,[2] instead of the double shorting bridge, thus eliminating the need for matching the oscillator impedance with the characteristic line impedance. It was also possible to use type 56 and 955 tubes instead of a magnetron, and a thermocouple galvanometer instead of a crystal detector. The sample of iron used (commercial mild Bessemer) was comparable with that of H-J (S.A.E. No. 1120 screw stock). Data were also obtained for a somewhat impure sample of nickel (0.13 percent C, 0.31 percent Mn, 0.04 percent Cu, 0.13 percent Fe).

λ_i cm =	305	266	184	128	73
Iron, μ_i =	65	60	50	41	35
Nickel, μ_i =	19	14	10	7	

The curve of permeability as a function of wave-length for iron forms a smooth extension of that of H-J, rising to the constant, long wave-length value. This curve is overlapped, at its lower end (below 120 cm) by that of Potapenko and Sänger. The latter is slightly above our curve and also that of H-J, but not more so than expected from the inaccuracy of the work and the difference in the iron samples.

The values of the *inner*, initial permeability of iron and nickel given in the accompanying table are, to our knowledge, the first to be reported in the range from 120 to 305 cm.

J. Barton Hoag
N. Gottleib

Ryerson Physical Laboratory,
University of Chicago,
Chicago, Illinois,
January 27, 1939.

[1] W. Arkadiew, Ann. d. Physik **81**, 649 (1926); Phys. Rev. **43**, 671 (1933). J. B. Hoag and H. Jones, Phys. Rev. **42**, 571 (1932). J. B. Hoag, Proc. Inst. Rad. Eng. **21**, 29 (1933). G. Potapenko and R. Sänger, Naturwiss. **21**, 818 (1933); Zeits. f. Physik, **104**, 779 (1937).
[2] R. King, Proc. Inst. Rad. Eng. **21**, 1142 (1933).

Nuclear Isomerism and Chemical Separation of Isomers in Tellurium

The growth of an electron-emitting 8-day iodine from a radioactive tellurium of 1.2 days half-life (produced by the deuteron bombardment of tellurium) has been reported by Livingood and Seaborg.[1] Their experiments indicated that this iodine activity was formed also by the decay of a tellurium of shorter life. We have made a more careful examination of this shorter lived parent of the 8-day iodine. Tellurium activated with slow neutrons was used in these experiments in order to avoid the formation of any radioactive iodine by direct transmutation. Successive extractions of iodine from such neutron-activated samples have been made, and it has thus been definitely established that the 8-day iodine is growing from a parent of about 25 minutes half-life as well as from the 1.2-day parent.

This demonstration that the 8-day iodine grows from both periods proves that the 1.2-day tellurium is isomeric with the activity of 25 minutes half-life. Both activities are formed directly by the neutron or deuteron bombardment of tellurium. We have also proved that these isomers are genetically related by separating chemically the 25-minute tellurium from the 1.2-day tellurium long after the directly formed 25-minute activity was dead.

A method of separation of genetically related nuclear isomers depending upon the appearance of the daughter activity in a form chemically separable from the parent isomer has been worked out by Segrè, Halford and Seaborg[2] and applied by them and DeVault and Libby[3] to the separation of the bromine isomers. For the separation in the present case telluric acid was synthesized from a sample of tellurium which had been irradiated with deuterons to produce a strong 1.2-day activity. Inactive tellurous acid was added as carrier; a few hours later this tellurous acid was precipitated as tellurium element, thus separating it from the telluric acid. (Sulfur dioxide in 3 *N* hydrochloric acid quickly reduces to tellurium the tellurous but not the telluric acid.) This precipitate contained the 25-minute activity with no observable 1.2-day period. It was possible to make such extractions at intervals until the 1.2-day activity had completely decayed.

We may conclude that the 1.2-day period corresponds to the upper state of this radioactive tellurium nucleus. The lower state is formed by a transition from this upper state, and decays with a 25-minute half-life by beta-particle emission to radioactive iodine. In turn this iodine decays with a half-life of 8 days to xenon.

By using a very strong sample of the 25-minute tellurium activity *obtained by extraction from its parent isomer* we were able to observe by successive extractions of iodine the growth of the radioactive iodine from the short period obtained in this way. This experiment provides the most direct proof of the above scheme of decay.

A number of other tellurium activities are formed during the deuteron or neutron bombardment of tellurium. A study of these activities has shown that some of them are also due to isomers and a description of these experiments will be published later.

We extend our thanks to Professor E. O. Lawrence and the staff of the Radiation Laboratory for their generous help and cooperation in these experiments. Thanks are also due to the Research Corporation for its continued support.

G. T. Seaborg
J. W. Kennedy

Department of Chemistry,
Radiation Laboratory, Department of Physics,
University of California,
Berkeley, California,
January 31, 1938.

[1] J. J. Livingood and G. T. Seaborg, Phys. Rev. **54**, 775 (1938).
[2] E. Segrè, R. S. Halford and G. T. Seaborg, Phys. Rev. **55**, 321 (1939).
[3] D. C. DeVault and W. F. Libby, Phys. Rev. **55**, 322 (1939).

Note on the Biological Effects of Densely Ionizing Radiation

Experiments with densely ionizing radiation offer an interesting possibility of testing some consequences of the so-called target-hypothesis of the biological action of radiation. As has been pointed out by Kingdon and Tanis[1] high concentration of ionization may be obtained by using either very great intensities of radiation or else radiations with very dense spatial distribution of ionization along the track of a primary or secondary particle. After describing their most interesting experiments with very high radiation intensities, the authors give some theoretical considerations on the possible influence of spatial density of ionization on the biological effect and are led to the conclusion that no appreciable influence is to be expected in such reactions which require only one ionization to occur within a certain target volume (e.g., the production of gene mutations[2]). This conclusion seems to us to be open to doubt because it would hold only if the radiation doses in question were such that the majority of all atoms present would be ionized with a probability equalling unity. Actually the dosages are of the order of 1000 r, producing 2×10^{15} ion pairs per cc of water and ionizing every 10^{5}th atom. In order to estimate the possible influence of spatial ionization density it seems, therefore, sufficient to make a determination of the probability for one ionization to occur within a certain volume (target volume) when the same total number of ion pairs is produced by different types of radiations. The size of the target volume for gene mutations varies according to the experimental technique used for their detection between 10^{8} and 10^{9} atoms,[3] but is always smaller than the average volume of 10^{8} atoms within which an ionization occurs at a dose of 1000 r. It is therefore obvious that not every target volume is "supplied" with one ionization by a dose of 1000 r and that the probability of a given number of ionizations occurring within as many target volumes as possible is greatest when they are distributed homogeneously in space and not crowded along a track. To illustrate this it may be mentioned that the length of all tracks of secondary particles (Compton electrons and recoil protons, respectively) which are produced by the same dose of 1000 r within 1 cc of water is about 100 times longer for gamma-rays than for fast neutrons. A differential biological action of gamma-rays and neutrons is therefore to be expected irrespective of the number of ionizations per target volume required to bring about the biological change. It has, in fact, been observed not only in reactions requiring two or more ionizations per target volume (Zirkle and co-workers[4]) but also for one-hit reactions such as the production of gene mutations[5]) (Fig. 1).

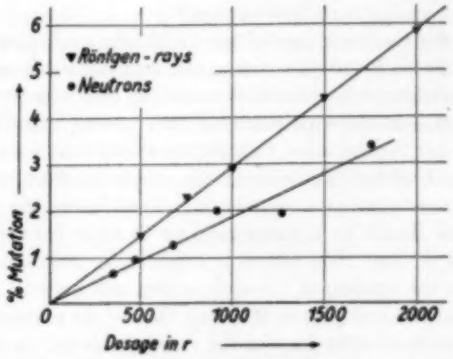

FIG. 1. Differential biological action of Röntgen rays and neutrons as a function of dosage.

K. G. ZIMMER
N. W. TIMOFÉEFF-RESSOVSKY

Genetics Department,
Kaiser Wilhelm Institute,
Berlin-Buch, Germany,
January 7, 1939.

[1] K. H. Kingdon and H. E. Tanis, Jr., Phys. Rev. **53**, 128 (1938); K. H. Kingdon, P. A. Zahl, C. P. Haskins and H. E. Tanis, Radiology **31**, 52 (1938).
[2] N. W. Timoféeff-Ressovsky, K. G. Zimmer and M. Delbrück, Göttingen Nachrichten N. F. **1**, 189 (1935).
[3] N. W. Timoféeff-Ressovsky and M. Delbrück, Zeits. indukt. Abstammungs- u. Vererbgsl. **71**, 322 (1936).
[4] R. E. Zirkle and P. C. Aebersold, Proc. Nat. Acad. Sci. **22**, 134 (1936); R. E. Zirkle, Occasional Publications A. A. A. S. No. 4, 220 (1937); R. E. Zirkle, P. C. Aebersold and E. R. Dempster, Am. J. Cancer **29**, 556 (1937); R. E. Zirkle and I. Lampe, Am. J. Röntgenol. **39**, 613 (1938).
[5] N. W. Timoféeff-Ressovsky and K. G. Zimmer, Naturwiss. **26**, 362 (1938); K. G. Zimmer, Strahlentherapie **63**, 517 (1938); K. G. Zimmer and N. W. Timoféeff-Ressovsky, Strahlentherapie **63**, 528 (1938).

Theory of Electrodisintegration of Beryllium

A disintegration or ionization of a nucleus by fast electrons can occur provided the energy of the electrons exceeds the binding energy of one of the constituents of the nucleus. The lowest threshold values occur for the beryllium nucleus and the deuteron. According to recent data[1] the threshold value for beryllium should be 1.65 Mev. The process for the electrodisintegration is the following one:

$$Be^{9}+e_{V}=Be^{8}+n^{1}+e_{V'},$$

where V and V' indicate the voltage of the electrons before and after disintegration. The Be^{8} nucleus disintegrates almost instantly into two slow alpha-particles.

For the calculation of the cross section it was assumed (based on the known theoretical work on the structure of light nuclei) that in the Be^{9} nucleus a neutron is bound in a p state. The process taking place when an electron collides with a Be^{9} nucleus can be described as follows. The electron collision causes the formation of an intermediate Be^{9} nucleus with a neutron bound in an s state of the continuous spectrum leading to a disintegration and a spherically symmetrical distribution of the ejected neutrons.

The cross section was calculated both by using Møller's method and the semi-classical method. The order of the magnitude of the cross section for the electrodisintegration turns out to be:

$$\sigma_{el}\sim\alpha\cdot\sigma_{photo};\qquad \alpha=1/137.$$

For a voltage slightly above the threshold: σ is approximately 10^{-31} cm², in agreement with the experimental data reported below by Collins, Waldman and Polye.

EUGENE GUTH

Department of Physics,
University of Notre Dame,
Notre Dame, Indiana,
February 1, 1939.

[1] S. K. Allison, E. R. Graves, L. S. Skaggs and N. M. Smith, Phys. Rev. **55**, 107 (1939).

Electrodisintegration of Beryllium

We have succeeded in disintegrating beryllium with electrons having energies in excess of the photoelectric threshold. It is assumed (cf. preceding letter), as is the case with the photodisintegration of beryllium, that the products of disintegration are Be^8 and a neutron. The effect was detected by means of the activity which these neutrons produced in silver or rhodium. The activity was observed with a G-M counter system.

A sheet of beryllium 0.04 cm in thickness (in the vacuum system) was surrounded with a silver or rhodium foil and the whole encased in paraffin. When bombarded with 10 μa of 1.72-Mev electrons from an electrostatic generator for one minute the silver or rhodium gave about 90 net counts in the first minute. Both silver and rhodium decayed with the appropriate periods, 22 sec. and 44 sec., respectively. Assuming that, with the geometry used, 900 neutrons per second produce one count per minute from a silver detector (determined by using a known γ-ray source of radon and a cross section for photodisintegration of 3×10^{-25} cm^2) the cross section for the electrodisintegration process at this voltage is about 2×10^{-31} cm^2 in good agreement with the theoretical value predicted by Guth (cf. preceding letter). The threshold for this effect was established at about 1.65 Mev.

The possibility that the silver and rhodium activity was produced by photoneutrons resulting from stray x-rays, or x-rays produced in the beryllium, was eliminated; (1) by introducing sheets of graphite in front of the beryllium which reduced the activity essentially to zero; (2) by increasing the thickness of the beryllium target. Since the electrodisintegration should not increase for thicknesses of beryllium greater than 0.04 cm, while the photodisintegration is proportional to the thickness, it was possible to show that the activity produced in the thin target was essentially all due to electrons.

We wish to acknowledge our indebtedness to Dr. E. Guth who suggested this problem and who has provided many helpful suggestions.

GEORGE B. COLLINS
BERNARD WALDMAN
WILLIAM R. POLYE

Department of Physics,
University of Notre Dame,
Notre Dame, Indiana,
February 1, 1939.

The Advantages of Scaling Circuits in Recording Random Counts

There are two distinct functions performed by a scaling circuit when used in electrical counting systems for nuclear investigations. The first function is that of reducing the input rate to the mechanical recorder. The second is that of changing the random distribution of pulses into one in which the time intervals between pulses are more nearly equal, before feeding these pulses to the mechanical recorder. The great importance of this second function for the reduction of the counting losses *in the mechanical recorder* does not yet seem to be generally recognized, although the matter has already been treated by others.[1]

The counting losses in a counting system, such as a Geiger-Müller system, arise from two causes; the finite resolving time of the components of the system and the random distribution of counts encountered with radioactive sources. The counting losses are determined by a function which is extremely sensitive to the distribution of counts and much less sensitive to the resolving times. The losses are rather surprisingly large in nuclear work mainly because one is dealing with random distributions of counts. For this reason, a method for the reduction of counting losses which depends on removing the random element in the distribution will be much more effective than a method which depends on reducing the resolving time of the mechanical recorder. It is this property which makes the scaling circuit method so powerful and elegant. A scale-of-n circuit changes a random distribution more and more nearly into a periodic one as the scaling ratio, n, increases. The marked periodicity of the counts is easily noted experimentally. If the scaling ratio is great enough, the recorder can be used at counting rates almost equal to its maximum counting rate for equally spaced pulses without the occurrence of appreciable counting losses. Experiment shows that a vacuum tube scale-of-eight is sufficient for counting rates up to about 20,000 counts a minute or more if the recorder is a Cenco counter.[2] Also it is found that the maximum counting rate which may be recorded with inappreciable counting losses in the mechanical recorder (say, one percent) increases by a factor of three hundred or more when changing from a scale-of-one to a scale-of-eight.[2] This is in general agreement with the theory of Alaoglu and Smith.[1]

A recent proposal[3] for the reduction of counting losses, in which the method of attack is that of decreasing the resolving time of the mechanical recorder in a scale-of-one circuit, is thus seen to be incapable of yielding an appreciable increase in the counting rate which may be recorded with negligible counting losses. Such high speed mechanical recorders would, of course, be very useful *in connection with* a scaling circuit, but cannot *replace* such circuits.

Some numerical results for a typical case, obtained by means of the theory of Alaoglu and Smith,[1] will give a quantitative idea of the magnitude of the scaling effect. This theory has been accurately verified experimentally for the case of a scale-of-one[2] and additional results in general agreement with the theory obtained by comparing a scale-of-eight against a scale-of-sixteen.[2]

Let the resolving time of the G–M tube and quenching circuit be $\sigma=5\times10^{-4}$ sec. Let us also consider two mechanical recorders, a fast one with resolving time $\tau_1=10^{-3}$ sec. and a slower one with resolving time $\tau_2=10^{-2}$ sec. These values are typical ones. Calculation shows that a vacuum tube *scale-of-two* circuit using the slower recorder will be just as accurate as a scale-of-one circuit using the faster recorder (faster by a factor ten) up to input rates to the system of over 1000 counts a minute. At 2000 counts a minute the reading of the scale-of-two will only be about two and one-half percent less than that of the scale-of-one. For a scale-of-eight feeding the slower recorder, there will be inappreciable losses *in the recorder* up to 30,000 counts a

minute. The corresponding figures for scales-of-one are 60 and 1200 counts a minute for the slow and the fast recorders, respectively.

The writers wish to take this opportunity to correct a misprint in reference (2) below. In that reference, Eq. (10) reads $1/n_{1\,\max}$. This should be corrected to read $1/(n_{1\,\max}\times e)$.

HAROLD LIFSCHUTZ
O. S. DUFFENDACK

University of Michigan,
Ann Arbor, Michigan,
February 2, 1939.

[1] L. Alaoglu and N. M. Smith, Phys. Rev. **53**, 832 (1938).
[2] H. Lifschutz and O. S. Duffendack, Phys. Rev. **54**, 714 (1938).
[3] H. V. Neher, Rev. Sci. Inst. **10**, 29 (1939).

On the Equilibrium of Massive Spheres

It is usually stated[1] that general relativity sets an upper limit to the mass and radius of a sphere of constant proper energy density ρ. This result is obtained by considering only those solutions of Einstein's field equations which give a finite central proper pressure p; the minimum mass and radius for which p first becomes infinite at the center are taken as the limiting values. In his original paper[1] Schwarzschild points out the existence of other solutions with infinite central p, but dismisses them as physically inadmissible because of this singularity without a further discussion of their properties. However, an examination of these solutions, which are described below, shows that they lead to arbitrarily large masses and radii.

On the other hand a cold neutron gas model[2] leads to an upper limit on the size of a static sphere. It is of interest to try to account for the difference in behavior of these two models. If for a material consisting of particles in motion (and which may exert forces on each other) the energy-momentum tensors for the particles, and for the force fields (apart from gravitation) associated with them, are additive and have non-negative traces, then for such a material $T=\rho-3p\geqq 0$ must always hold. The $\rho=$const. model for sufficiently high pressures has $T<0$. This not altogether consistent model corresponds to the case of perfectly incompressible particles packed tightly together and treated essentially nonrelativistically in that the contribution of the forces to ρ is not taken into account. A negative T near the center of the sphere, such as makes possible an arbitrarily large mass for the $\rho=$const. model, may be regarded as analogous to a negative (repulsive) mass which keeps the sphere from collapsing.

Both the original Schwarzschild solutions, and the new singular solutions leading to arbitrarily large spheres, may be obtained by a method considerably simpler than the one used by Schwarzschild. Einstein's equations for constant ρ and for the line-element

$$ds^2=-e^{\lambda(r)}dr^2-r^2d\theta^2-r^2\sin^2\theta d\phi^2+e^{\nu(r)}dt^2$$

reduce to:[2]

$$e^{\nu(r)}=\frac{(1-2u_b/r_b)p^3}{[p(r)+\rho]^3} \tag{1}$$

$$dU/dx=3x^2 \tag{2}$$

and

$$\frac{dP}{dx}=-\frac{P+3}{2x(x-U)}[Px^3+U], \tag{3}$$

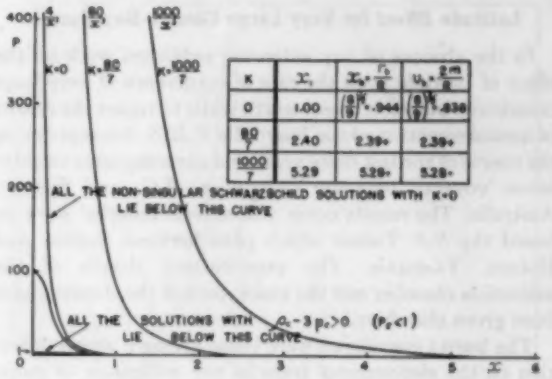

K	x_1	$x_b=\frac{r_b}{R}$	$U_b=\frac{2m}{R}$
0	1.00	$(\frac{8}{9})^{\frac{1}{2}}$=.944	$(\frac{8}{9})^{\frac{1}{2}}$=.838
80/7	2.40	2.39+	2.39+
1000/7	5.29	5.29+	5.29+

FIG. 1.

where x, U, P, are dimensionless quantities defined by $x=r/R$, $U=2u/R$, $P=8\pi R^2p$; $u=\frac{1}{2}r(1-e^{-\lambda})$, R is a characteristic length determined in terms of the given constant ρ by $R^2=3/8\pi\rho$; and relativistic units, making $c=1$, $G=1$, are used throughout. The radius r_b of the sphere is determined by that value x_b of x where P first vanishes, and the gravitational mass of the sphere is given by $m=u_b$, the value of u at $x=x_b$. The integral of (2) above is $U=x^3-K$, where $K\geqq 0$ in order that $e^{-\lambda}=[1-r^2/R^2+KR/r]$ should nowhere change sign. The usual procedure[1] corresponds to making $K=0$, and then Eq. (3) may be at once explicitly integrated, and gives the well known Schwarzschild interior solution:

$$P=\frac{3(P_c+1)(1-x^2)^{\frac{1}{2}}-(P_c+3)}{(P_c+3)-(P_c+1)(1-x^2)^{\frac{1}{2}}},$$

where P_c is the value of P at $x=0$. If $P_c\to\infty$, which is commonly taken as the limiting solution, then as $x\to 0$, $P\sim 4/x^2$, and the corresponding radius and mass are fixed by $x_b=(8/9)^{\frac{1}{2}}$, and $U_b=(8/9)^{\frac{1}{2}}$. This solution makes $e^{\nu}\to 0$ and $e^{\lambda}\to 1$ as $r\to 0$.

The new singular solutions are obtained by making $K>0$. Eq. (3) now can not be explicitly integrated in terms of known functions, but it may be shown that solutions exist which near the origin behave like $P\sim 7K/x^3$. Numerical integration of (3) for several values of K shows that x_b is very closely given by the largest positive root x_1 of $x-U=x-x^3+K=0$. Thus $x_b\sim x_1$, $U_b=x_b^3-K\sim x_1^3-K=x_1$. For very large K, $x_1\sim K^{\frac{1}{3}}$, so that $x_b\sim K^{\frac{1}{3}}$, $U_b\sim K^{\frac{1}{3}}$, and it is seen that no upper limit on the size of the sphere exists, if the singular solutions for the pressure are not excluded. For these solutions both $e^{\lambda}\to 0$ and $e^{\nu}\to 0$ as $r\to 0$. Fig. 1 gives a general idea of the various solutions, including the Schwarzschild limiting solution and the last one for which $\rho_c-3p_c\geqq 0$ ($P_c\leqq 1$) holds.

G. M. VOLKOFF

Department of Physics,
University of California,
Berkeley, California,
January 28, 1939.

[1] K. Schwarzschild, Berl. Ber. (1916), p. 424; A. S. Eddington, *The Mathematical Theory of Relativity* (Cambridge, 1924), p. 168; R. C. Tolman, *Relativity, Thermodynamics and Cosmology* (Oxford, 1934), pp. 246-247, and others.
[2] J. R. Oppenheimer and G. M. Volkoff, this issue, Phys. Rev. **55**, 374 (1939). Eqs. (1), (2) and (3) are Eqs. (7), (9) and (10) of that article rewritten for constant ρ.

Latitude Effect for Very Large Cosmic-Ray Bursts

In the absence of any extensive published work on the effect of latitude upon the rate of occurrence of very large cosmic-ray bursts, it seems worth while to report the results of measurements made on board the *R.M.S. Aorangi* during the course of the last three years and covering some twenty-seven voyages between Vancouver, B.C. and Sydney, Australia. The results cover also several months' work on board the *S.S. Talune* which plies between Sydney and Hobart, Tasmania. The experimental details of the ionization chamber and the exact route of the *Aorangi* have been given elsewhere.[1]

The bursts considered were those giving a sharp deflection on the electrometer trace of one millimeter or more. With the low electrometer sensitivity used, this minimum corresponds to 28×10^6 ion pairs formed within the chamber. For a specific ionization in standard air of 60 ions per centimeter path, the minimum size burst corresponds approximately to the passage of 280 particles through the chamber.[2] Table I includes all bursts observed which are of the above minimum size and over. These are grouped within the latitude zones in which they occur. The error for the burst rate is computed by dividing the rate by the square root of the number of bursts counted.

No attempt was made to apply a barometer correction to the observed rate of occurrence of bursts. Readings made at constant geomagnetic latitude (i.e., during the stay in port at Vancouver and more extensively during the part of the trip from Auckland to Sydney where the ship follows almost a parallel of geomagnetic latitude) show no definite correlation between the number of bursts per hour and the barometric height. This was also the conclusion of Doan[3] from data taken with the same type meter. Even if some small barometric dependence exists, the effect would probably be negligible in the average of three years' readings.

Figure 1 shows the data plotted with the results for the northern and southern hemispheres grouped together and with the burst rate given in terms of percent of the maximum value. The latitude change is seen to be about thirty percent with a statistical uncertainty of plus or minus six percent to which, of course, any possible systematic errors must be added. This is a much greater effect than that of six percent found by Neher and Pickering[4] for showers. The two results are not necessarily inconsistent, however, when one considers that the showers observed through 1.6 cm of lead are probably due principally to electrons while the large bursts under the 12 cm of lead used here are probably due to mesotrons.

TABLE I. *Burst data for various geomagnetic latitude zones.*

Geomagnetic latitude zone	55N−35N	35N−15N	15N−15S	15S−35S	35S−52S
Number of bursts	365	178	181	138	915
Hours	3416	1937	2342	1690	8122
Bursts per hour	0.107 ±0.006	0.092 ±0.007	0.077 ±0.006	0.093 ±0.007	0.113 ±0.004

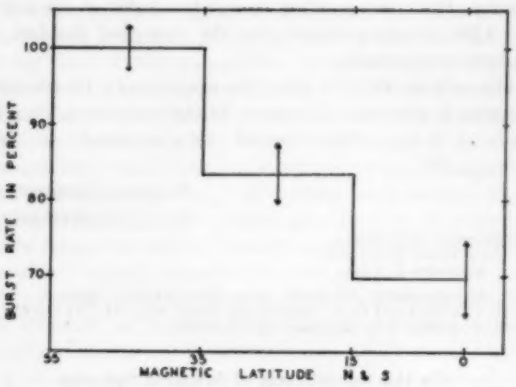

FIG. 1. Relative burst rate as a function of magnetic latitude.

Although one should not place too great reliance upon the absolute values obtained from data with such large statistical uncertainties, we believe that the above results show: (1) That the latitude effect for large bursts is greater than that given by other observers for small showers and (2) that the latitude effect for large bursts is probably greater than the latitude effect for the total cosmic-ray intensity under similar conditions.[1]

We wish to express to Professor A. H. Compton our thanks for generously placing at our disposal the meter records used above and for his continued interest in this problem.

WILLIAM P. JESSE
PIARA S. GILL

Ryerson Laboratory,
University of Chicago,
Chicago, Illinois,
January 31, 1939.

[1] A. H. Compton and R. N. Turner, Phys. Rev. **52**, 799 (1937).
[2] R. D. Bennett, G. S. Brown and H. A. Rahmel, Phys. Rev. **47**, 437 (1935).
[3] R. L. Doan, Phys. Rev. **49**, 107 (1936).
[4] H. V. Neher and W. H. Pickering, Phys. Rev. **53**, 111 (1938).

Radioactive Antimony from I+n and Sn+D

By the bombardment of 20 grams of sodium iodide with the fast neutrons from 725 microampere-hours of eight-Mev deuterons on lithium, we have produced a chemically identified antimony isotope with the single half-life of 60 days; this decay has been followed for 140 days. Since there is but one stable form of iodine the reaction must be $I^{127}(n,\alpha)Sb^{124}$. (As far as we are aware, this is the farthest up the periodic table that this type of reaction has been established, except for neutron bombardments of the very heaviest elements that are naturally unstable with respect to alpha-particle emission.) Electron-emitting antimony isotopes with half-lives 2.5 days[1, 2] and 60 days,[2] formed by slow neutron and deuteron bombardment of antimony, are already known, but it had not previously been established which belonged to Sb^{122} and which to Sb^{124}, if indeed they were not isomers. (The stable isotopes of antimony are Sb^{121} and Sb^{123}.) The present experiment shows conclusively that the 60-day period is associated with Sb^{124} and makes it practically certain that the 2.5-day period belongs to Sb^{122}.

A third antimony isotope with 16 to 18 minutes half-life, emitting positrons, is known to be due to Sb^{120}, since it is formed by fast neutrons[2-5] or gamma-rays[6] on antimony, as well as by deuterons[2] on tin, and is not formed by neutrons or deuterons on antimony.

We have been following for two years the complex activities found in the antimony precipitated from several samples of tin which had been bombarded with five-Mev deuterons. The longest half-life appears to be about two years; on this basis the shorter periods are 45 days (approximately), 2.5 days, 3 hours, and 17 minutes. (These figures supersede our earlier estimates that were quoted by Livingston and Bethe.[7] The periods of 13 hours and 112 days previously reported[8] as due to antimony from Sn+D are now known to be due to impurities.)

Of these five activities only two can be immediately identified: the 17-minute period is due to $Sn^{119}(d,n)Sn^{120}$, as previously reported,[2] while the 2.5-day period must be due to $Sn^{122}(d,2n)Sb^{122}$ or to $Sn^{120}(d,\gamma)Sb^{122}$.

We wish to thank the Research Corporation for its continued support.

J. J. LIVINGOOD*
G. T. SEABORG

Radiation Laboratory, Department of Physics (J.J.L.),
Department of Chemistry (G.T.S.),
University of California,
Berkeley, California,
January 30, 1939.

* Now at Harvard University.

[1] E. Amaldi, O. d'Agostino, E. Fermi, B. Pontecorvo, F. Rasetti and E. Segrè, Proc. Roy. Soc. **A149**, 522 (1935).
[2] J. J. Livingood and G. T. Seaborg, Phys. Rev. **52**, 135 (1937).
[3] F. A. Heyn, Nature **139**, 832 (1937).
[4] W. Y. Chang, M. Goldhaber and R. Sagane, Nature **139**, 962 (1937).
[5] M. L. Pool, J. M. Cork and R. L. Thornton, Phys. Rev. **52**, 239 (1937).
[6] W. Bothe and W. Gentner, Naturwiss. **25**, 126 (1937).
[7] M. S. Livingston and H. A. Bethe, Rev. Mod. Phys. **9**, 336 (1937).
[8] J. J. Livingood and G. T. Seaborg, Phys. Rev. **50**, 435 (1936).

Gamma-Rays from B+D

In a recent issue of *The Physical Review* Gaerttner, Fowler and Lauritsen[1] presented the results of a measurement on the gamma-ray energy spectrum emitted from boron bombarded with deuterons. We have made some independent observations on the same spectrum, and our results are essentially in agreement with the values they have given. We think it is worth while to add our data to that already published, for the sake of confirmation.

Amorphous boron (Eimer and Amend) was bombarded with deuterons of 700-kev maximum energy, by means of the high voltage accelerating tube.[2] A beam of the resulting gamma-rays, limited by a channel in a lead block, was allowed to strike a slab of carbon (graphite) 1.5 mm thick, in the center of a cloud chamber.[3] The negative electrons which originated in the carbon and whose initial directions were within 15 degrees of the direction of the gamma-ray beam were counted and plotted in an energy diagram,

TABLE I.

H. & C.	1.4	2.4	4.2	6.0	8.6
G., F. & L.	1.5	2.2	4.4	6.9	9.1
C., D., F. & L.	—	2.7	4.5	5.9	7.0
	—	2.6	4.2	5.9	7.5

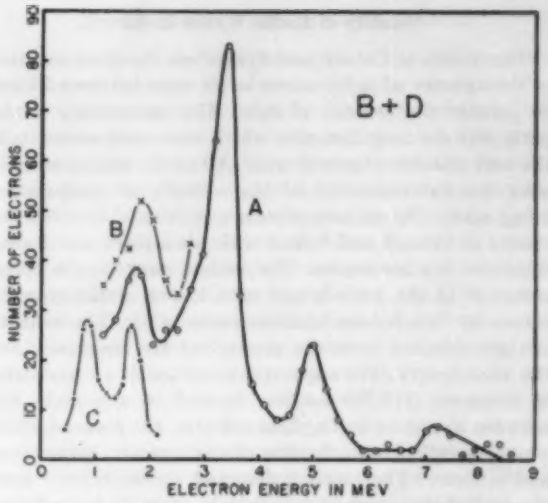

FIG. 1. Negative electrons ejected from 1.5-mm carbon by the gamma-rays from B+D. Curves A and B, 1600 gauss magnetic field; curve C, 530 gauss.

shown in Fig. 1, curve A. A remeasurement of the lower end of the spectrum, from the same photographs, is shown as curve B. Curve C represents the results of a separate experiment, in which a lower magnetic field was used, for the purpose of extending the measurements to lower electron energy and of increasing the resolving power at the low energies.

The energies of the gamma-ray lines indicated by our measurements are given in Table I, together with the values given by Gaerttner, Fowler and Lauritsen, and the values taken from the earlier work of Crane, Delsasso, Fowler and Lauritsen.[4] In the last-mentioned work only the electron energies were given, so we have added 0.25 Mev to these to obtain the gamma-ray energies. It is seen that four prominent lines have appeared in all measurements. In addition, it now seems that there is a line at about 1.5 Mev.

We find relative intensitives of 1, 1, 6, 2 and 1 for the 1.4, 2.4, 4.2, 6.0 and 8.6-Mev lines, respectively. The relative intensities of the 4.2, 6.0 and 8.6-Mev lines are roughly in agreement with previous data, but the 1.4 and 2.4-Mev lines are much weaker, relative to the other three. This is not alarming, because the gamma-rays probably arise from several different reactions involving the two boron isotopes, and the relative probabilities of the various reactions depend upon the energy spectrum of the deuteron beam. The relative intensities of the gamma-ray lines will have to be investigated with monochromatic beams of deuterons of several different energies.

J. HALPERN
H. R. CRANE

University of Michigan,
Ann Arbor, Michigan,
January 30, 1939.

[1] E. R. Gaerttner, W. A. Fowler and C. C. Lauritsen, Phys. Rev. **55** 27 (1939).
[2] H. R. Crane, Phys. Rev. **52**, 11 (1937).
[3] H. R. Crane, Rev. Sci. Inst. **8**, 440 (1937).
[4] H. R. Crane, L. A. Delsasso, W. A. Fowler and C. C. Lauritsen, Phys. Rev. **46**, 1109 (1934).

Velocity of Radio Waves in Air

The results of Colwell and Friend[1] on the determination of the velocity of radio waves in air were between 50 and 80 percent the velocity of light. The uncertainty of the path over the long distances which were used seems to be the only possible source of error. All earlier measurements[2] were the determination of the velocity of propagation along wires. The authors therefore attempted to check the results of Colwell and Friend with ultra-short waves over distances of a few meters. The method used was the determination of the wave-length of a known radiofrequency source by interference measurements in air. The velocity is then obtained from the product of the frequency and the wave-length. The apparatus consisted of a transmitter of frequency 113.749 mc/sec. located on a straight line between a receiver and a plane reflector, the plane of which was perpendicular to the line of the receiver, transmitter and reflector. The receiver detected waves directly from the transmitter and also indirectly after being reflected from the movable reflector. By moving the reflector along the line of the apparatus, the length of path of the indirect wave could be varied. The distance between positions of the reflector which give maximum responses in the receiver is equal to half a wave-length. The distance between positions of the reflector which give minimum responses in the receiver is also half a wave-length. A typical set of measurements is shown below.

Figure 1 is shown simply to point out the accuracy that might be expected in these measurements. Actually the positions of maxima and minima were obtained more accurately by taking more readings about these points.

The frequency was known to be accurate to 0.03 percent. It was obtained from a crystal-controlled oscillator of frequency 28.437 mc/sec. which was doubled twice. To insure operation of the crystal frequency it was checked by the heterodyne method with a General Radio Type 684-A oscillator which has a calibration accurate to within one percent. The final output of the transmitter was monitored by means of a cathode-ray oscilloscope to insure an output exactly four times the crystal frequency and not some stray oscillation originating in the circuits after the crystal. This was accomplished by applying the crystal frequency to one set of deflecting plates and the output frequency to the other set of deflecting plates. A Lissajous figure characteristic of a frequency ratio of 1 : 4 was then a definite assurance of the proper frequency output. The inaccuracy in the wave-length measurements was due almost in full to the movement of the cumbersome reflector as it was impossible in the present apparatus to keep the plane of the reflector perpendicular to the axis of the antennas of the transmitter and receiver as the reflector was moved. A thermocouple ammeter was used in the transmitter antenna to monitor the power output which was about two watts. This was done to be sure the movement of the reflector did not introduce a variable mutual impedance in the transmitter antenna and hence vary the output of the transmitter as the reflector was moved. If the closest position of the reflector to the transmitter was greater than two wave-lengths the output remained constant.

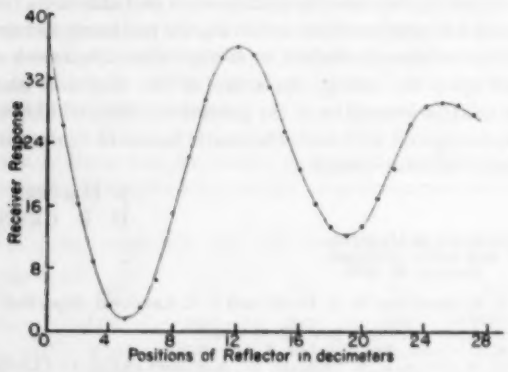

FIG. 1.

The results of these measurements for the velocity of radio waves in air were $(2.98 \pm 0.07) \times 10^{10}$ cm/sec.

A. L. VITTER
L. C. BRIEGER

Department of Physics,
University of Notre Dame,
Notre Dame, Indiana,
January 20, 1939.

[1] R. C. Colwell, A. W. Friend, N. I. Hall and L. R. Hill, Phys. Rev. **50**, 4, 381 (1936); R. C. Colwell and A. W. Friend, Phys. Rev. **51**, 11, 990 (1937).
[2] M. J. Mercier, J. Physique **5**, 6, 168 (1924); MacLean, Phil. Mag. **48**, 115 (1899).

Droplet Fission of Uranium and Thorium Nuclei

The Fifth Washington Conference on Theoretical Physics, sponsored jointly by George Washington University and the Carnegie Institution of Washington, began January 26, 1939, with a discussion by Professor Bohr and Professor Fermi of the remarkable chemical identification by Hahn and Strassmann in Berlin of radioactive barium in uranium which had been bombarded by neutrons. Professors Bohr and Rosenfeld had brought from Copenhagen the interpretation by Frisch and Meitner that the nuclear "surface-tension" fails to hold together the "droplet" of mass 239, with a resulting division of the nucleus into two roughly equal parts. Frisch and Meitner had also suggested the experimental test of this hypothesis by a search for the expected recoil-particles of energies well above 100,000,000 electron-volts which should result from such a process. The whole matter was quite unexpected news to all present.

We immediately undertook to look for these extremely energetic particles, and at the conclusion of the Conference on January 28 were privileged to demonstrate them to Professors Bohr and Fermi. It was subsequently learned that the particles had been observed independently by Fowler and Dodson at Johns Hopkins the same day, by Dunning and co-workers at Columbia on January 25, and by Frisch in Copenhagen two weeks earlier.

For observations of the high energy particles, an ionization-chamber, about five mm deep, was placed about three cm below the neutron-source and was so arranged that interchangeable copper disks about three cm in diameter could be placed on the collector, which was connected to a linear pulse-amplifier. The upper faces of these disks were then coated with the materials to be tested.

TABLE I.

Neutron-reaction	Maximum neutron-energy	Uranium		Thorium	
		No Cd	With Cd	No Cd	With Cd
	Mev				
Li+D	13.5	100	70	100	100
D+D	2.5	100	70	100	100
C+D	0.5	100	10	0	0

With the amplifier feeding a cathode-ray oscillograph the usual alpha-particle pulses were observed when a layer of uranium oxide was placed on the disk. On exposure to neutron-radiation from (Li+D) at 1000 kv two additional groups of pulses were observed. The first group corresponded to the "neutron-recoils" from the air in the chamber, as previously measured with the same amplifier gain and without the uranium. These neutron-recoils gave pulses about four times the size of the alpha-particle pulses. The second additional group was 20 to 40 times larger than the largest "recoil"-pulse, thus corresponding to energies of 75 to 150 Mev released in the chamber, or 150 to 300 Mev total energy for each individual process. With paraffin surrounding source and chamber the yield was roughly 30 counts per min. per μA of 1000-kv deuterons, which is a neutron-intensity corresponding to about 10,000 millicuries of radon-beryllium. The yield from thorium was of the same order of magnitude.

No effect was observed from bismuth, lead, thallium, mercury, gold, platinum, tungsten, tin or silver with as much as 1/1000 the intensity of that from uranium and thorium.

No effect was observed with either uranium or thorium produced by the gamma-rays from 3 μA of 1000-kv protons on lithium or on fluorine.

To determine roughly the energy-range of the neutrons involved in the fission-process, observations were made with the neutrons from several reactions, both with and without cadmium surrounding the ionization-chamber to filter out the thermal neutrons produced in the surrounding paraffin. Bearing in mind that the ratio of the counts with cadmium and without cadmium depends to a large extent on the amount of paraffin surrounding the source and chamber, the results of these tests may be deduced from Table I in which the relative number of "fissions" is given, with the total yield for uranium and thorium with high energy neutrons, being approximately equal, taken as 100 on an arbitrary scale.

From these comparisons it appears that the uranium fissions are produced by different processes for fast and slow neutrons, the fast-neutron process requiring more than 0.5 Mev but less than 2.5 Mev for effective operation. For thorium, on the other hand, only the fast-neutron process is effective, but somewhat surprisingly it also appears to require between 0.5 and 2.5 Mev.

R. B. ROBERTS
R. C. MEYER
L. R. HAFSTAD

Department of Terrestrial Magnetism,
Carnegie Institution of Washington,
Washington, D. C.,
February 4, 1939.

Heavily Ionizing Particles from Uranium

After reading in local papers of Hahn's discovery of the splitting of uranium into heavy elements, we wired Professor Gamow for further details. He answered that Tuve had observed the heavily ionizing particles in a differential linear amplifier chamber. We have confirmed this by using a thin ionization chamber, one of whose plates was covered with U, or U_3O_8. With a certain gain, the U natural alphas gave two-mm kicks on an oscilloscope, Po alphas passing parallel to the plates gave eight-mm pulses, and the Hahn-Tuve particles gave deflections of four cm. The energy released in a path length of less than 0.5 mm was about 10 Mev, so the particles must carry several charges, and therefore be "heavy." Check runs on Pb, Cu, Zn, W and Th showed no such bursts. After confirming the existence of these particles, we investigated the type of reaction responsible. A thin Cd covering around the chamber reduced the counting rate to less than five percent. This is unexpected in view of the fact that about half of the "transuranic" activity is due to resonance neutrons which could penetrate Cd. This result shows that Hahn's effect is due largely to thermal neutrons. By the use of a modulated beam of neutrons, we have looked for a time delay in the emission of heavy particles, after the neutron irradiation. The time delay is less than 3×10^{-4} sec. Our thanks are due Professor E. O. Lawrence for his interest in this experiment, and the Research Corporation for financial support.

G. K. GREEN*
LUIS W. ALVAREZ

Radiation Laboratory,
Department of Physics,
University of California,
Berkeley, California,
January 31, 1939.

* National Research Fellow.

Intensely Ionizing Particles Produced by Neutron Bombardment of Uranium and Thorium

We have bombarded uranium nitrate and also thorium oxide with deuteron-deuteron neutrons in a three-millimeter brass ionization chamber and found particles producing an intense ionization. We attribute the results to extremely high energy particles of roughly half the mass of the bombarded nucleus, and believe that they confirm the recent work of Hahn and Strassmann[1] and of Frisch and Meitner[2] on uranium, and also establish a similar effect with thorium.

The substance was bombarded in the form of a layer (about 0.5 gram) stuck with collodion on a paper disk three centimeters in diameter and placed in contact with a mesh-covered opening into the ionization chamber. The gain of the oscilloscope was set so that the kicks resulting from the natural alpha-radiation were about one centimeter high. During neutron bombardment kicks of height greater than five centimeters (peak outside the field of vision) were observed. These were counted visually. Counts were made at various deuteron beam intensities with the chamber directly under the neutron source and also about a meter away, with paraffin and without paraffin

TABLE I. *Number of counts per minute of heavily ionising particles from the bombardment of uranium and thorium with deuteron-deuteron neutrons for deuteron currents of 0.5 and 1.0 ma at 260 kv.*

	No paraffin		Paraffin	
	$i=1.0$ ma	0.5 ma	$i=1.0$ ma	0.5 ma
U	35	—	69	38
Th	21	11	20	—

around the chamber. Also background counts were made with no uranium or thorium and ran consistently zero over five-minute periods.

Results are given in Table I. The numbers represent counts per minute and are the means of five to ten observations for each case. The paraffin effects in the table were obtained with paraffin around chamber but not between chamber and neutron source. Placing paraffin between source and chamber reduced the counts for uranium to 34 per minute.

The ionization due to nitrogen and oxygen ions produced by neutrons was approximately the same as that due to the natural uranium alpha-particles. Our linear amplifier did not possess a calibrated gain variable over sufficiently wide limits to enable us to determine accurately the ionization produced by the heavy particles. However, on removing one stage of amplification, we were still able to observe the kicks due to heavy particles, and therefore we believe the ionization due to the heavy particles is at least one hundred times that produced by the alphas or recoil ions.

Thus the effect is obtained with 2.4-Mev neutrons for both thorium and uranium. Paraffin doubles the yield for uranium but has no effect on that for thorium. The reality of the effect is confirmed by its proportionality to the intensity of the deuteron beam.

The apparatus used in this research was constructed with the aid of a grant from the Research Corporation.

R. D. FOWLER
R. W. DODSON

Chemical Laboratory,
Johns Hopkins University,
Baltimore, Maryland,
February 3, 1939.

[1] Hahn and Strassmann, Naturwiss. January, 1939.
[2] Frisch and Meitner, Private Communication from Dr. M. A. Tuve. We are informed by Dr. Tuve that Frisch and Meitner have also observed this effect with thorium on or about January 16, 1939.

Cleavage of the Uranium Nucleus

We have been studying what seemed to be L x-rays from the seventy-two-hour "transuranic" element. These have now been shown by critical absorption measurements to be iodine K x-rays. The seventy-two-hour period is definitely due to tellurium as shown by chemical test, and its daughter substance of two-and-a-half-hour half-life is separated quantitatively as iodine. This seems to be an unambiguous and independent proof of Hahn's hypothesis of the cleavage of the uranium nucleus.

PHILIP ABELSON

University of California,
Berkeley, California,
February 3, 1939.

Resonance in Uranium and Thorium Disintegrations and the Phenomenon of Nuclear Fission

The study of the nuclear transmutations by neutron bombardment in uranium and thorium, initiated by Fermi and his collaborators, and followed up by Meitner, Hahn and Strassmann, and by Curie and Savitch, has brought to light a number of most interesting phenomena. Above all, as pointed out by Meitner and Frisch,[1] the recent discovery of Hahn and Strassmann of the appearance of a radioactive barium isotope as the product of such transmutations offers evidence of a new type of nuclear reaction in which the nucleus divides into two nuclei of smaller charges and masses with release of an energy of more than a hundred million electron volts. The direct proof of the occurrence of this so-called nuclear fission was given by Frisch[2] for thorium as well as for uranium by the observation of the very intense ionization produced in a gas by the high speed nuclear fragments.

In a recent note[3] commenting on the ingenious suggestions put forward for the explanation of the fission phenomenon by Meitner and Frisch, the writer has stressed that the course of the new type of reactions, just as that of ordinary nuclear reactions, may be assumed to take place in two well-separated stages. The first of these is the formation of a compound nucleus, in which the energy is stored in a way resembling that of the heat motion of a liquid or solid body; the second consists either in the release of this energy in the form of radiation or in its conversion into a form suited to produce the disintegration of the compound nucleus. In the case of ordinary reactions, resulting in the emission of a proton, neutron or α-particle from this nucleus, we have to do with a concentration of a considerable part of the excitation energy on some particle at the nuclear surface, sufficient for its escape, which resembles the evaporation of a molecule from a liquid drop. In the case of the fission phenomena, the energy has to be largely converted into some special type of motion of the whole nucleus causing a deformation of the nuclear surface sufficiently large to lead to a rupture of the nucleus comparable to the division of a liquid drop into two droplets. From considerations of statistical mechanics analogous to those applied to the evaporation-like nuclear disintegrations, it follows indeed that the probability of occurrence of fission becomes comparable to that of ordinary nuclear reactions when, with increasing nuclear charge, the deformation energy concerned has decreased to values of the same order of magnitude as that demanded for the escape of a single particle.

Here I should like to show how such considerations would seem to offer a simple interpretation of the peculiar variation with neutron velocity of the cross sections of the different transmutation processes of uranium and thorium observed by Meitner, Hahn and Strassmann.[4] In the light of the new discoveries, the great variety of processes obtained, which could not be disentangled on the ordinary ideas of nuclear disintegrations, would seem, according to Meitner and Frisch, to be reduced to only two types of transmutations. Of these the one consists in an ordinary radiative capture of the incident neutron, resulting in the

formation of the normal state of the compound nucleus, which is subsequently transmuted by β-ray emission into a stable nucleus. The other consists in the fission of the excited compound nucleus, which may take place in a large number of different ways, in which a wide range of mass and charge numbers of the fragments may occur. This last point, which makes it impossible without a closer study of the statistical distribution of the fragments to trace a product of given chemical properties and radioactive period back to its origin from some particular isotope of the original element, is, as we shall see, of especial importance for the understanding of certain striking peculiarities in the case of uranium.

For the capture processes, which lead to the radioactive uranium and thorium isotopes of periods 24 and 33 minutes, respectively, Meitner, Hahn and Strassmann found evidence of resonance phenomena for neutrons of comparatively small velocities. In uranium, where the phenomenon was more completely investigated, they found for neutron energies of about 25 volts a capture cross section at least 30 times larger than that for thermal neutrons. Since in this resonance region the cross section amounts to about 10^{-21} cm^2, it is, as they pointed out, obviously necessary from simple arguments of dispersion theory to ascribe the phenomenon to the abundant uranium isotope of mass number 238. From the fact that neither for uranium nor thorium is the resonance capture accompanied by any large increase of the cross section for the fission processes, we may further conclude that the probability of radiation by the compound nucleus in the excited states concerned is considerably larger than the fission probability, and that the normal states of these nuclei, apart from their β-ray radioactivity, are essentially stable.

As regards all other transmutation processes, which are now to be ascribed to fission, marked differences between uranium and thorium were found in the investigations of Meitner, Hahn and Strassmann as well as in the direct experiments of Frisch. With fast neutrons, fission cross sections of the same order of magnitude were found for uranium and thorium, but with neutrons of thermal velocities a large increase of the fission cross section was observed for uranium and not for thorium. The results for fast neutrons are simply explained on the basis of the general picture of nuclear processes outlined above, according to which we should expect the fission probability to increase much more rapidly with excitation than the radiation probability, and to become considerably larger than the latter for the high excitations of the compound nucleus concerned. The peculiar effect in uranium for slow neutrons could obviously, however, not be reconciled with the above considerations if it were to be attributed to the formation of the compound nucleus of mass number 239; but since, as already indicated, the periods of the most frequent radioactive fragments should be independent of the isotope undergoing fission, we have the possibility of attributing the effect concerned to a fission of the excited nucleus of mass 236 formed by the impact of the neutrons on the rare isotope of mass 235.

From the fact that the binding energy of a neutron in a nucleus of even charge number should be appreciably larger if the mass number is even than if it is odd, we should actually expect for a given neutron velocity a higher excitation energy for the compound nucleus 236 than for 239, and accordingly a much denser distribution of resonance levels and a much larger probability of fission in the former than in the latter case. Even for excitations produced by impacts of slow neutrons, we may therefore expect that the probability of fission of the nucleus 236 will be larger than that of radiative capture; and due to the corresponding broadening of the levels, the level distribution of 236 in this region might even be continuous. In any case, provided the fission probability is high enough, we shall expect for small neutron energies cross sections inversely proportional to the velocity, allowing us to account both for the observed yields of the process concerned for thermal neutrons and for the absence of any appreciable effect for neutrons of somewhat higher velocities. For fast neutrons the cross sections can, of course, never exceed nuclear dimensions, and because of the scarcity of the isotope concerned the fission yields will be much smaller than those obtained from neutron impacts on the abundant isotope.

It would thus seem that all the known experimental facts receive a simple explanation without any assumption of peculiarities of special levels. Such assumptions as have hitherto been thought necessary to account for these phenomena would in fact seem difficult to reconcile with general ideas of nuclear excitation. In a forthcoming paper in collaboration with Professor John A. Wheeler, a closer discussion will be given of the fission mechanism and of the stability of heavy nuclei in their normal and excited states.

N. BOHR

Institute for Advanced Study,
Princeton, New Jersey,
February 7, 1939.

[1] L. Meitner and R. Frisch, Nature (in press) where references to the previous literature are given.

[2] R. Frisch, Nature (in press). The manuscript of this note as well as that of Professor Meitner and Dr. Frisch have kindly been communicated to me by the authors. As I have learned from other friendly communications, further most interesting evidence regarding the fission phenomenon has in the meantime been obtained in several laboratories in America and Europe.

[3] N. Bohr, Nature (in press).

[4] L. Meitner, O. Hahn and F. Strassmann, Zeits. f. Physik 106, 249 (1937); 109, 538 (1938).

Proceedings of the American Physical Society

Minutes of the Los Angeles, California Meeting, December 19, 1938

THE 224th regular meeting of the American Physical Society was held in Los Angeles, California, on Monday, December 19, 1938, at the University of California at Los Angeles. Morning and afternoon sessions were held for presentation of the contributed papers abstracted below. Samuel J. Barnett served as presiding officer. About seventy-five persons attended.

At noon a luncheon was tendered to attending members of the American Physical Society by the University and upon this occasion Professor M. L. E. Oliphant of Birmingham University spoke informally upon the reactions of English physicists to recent political events. Professor William V. Houston spoke briefly of the scientific achievements and personal influence of Arnold Sommerfeld and the Secretary was requested to convey the felicitations of those present to Professor Sommerfeld in view of the recent attainment of his seventieth birthday.

The regular scientific program consisted of nineteen contributed papers. The abstracts of these papers are given in the following pages. The author index will be found at the end.

PAUL KIRKPATRICK,
Local Secretary for the Pacific Coast

Abstracts

1. Distribution of Eigentones at Low Frequencies. RICHARD H. BOLT, *University of California at Los Angeles (Introduced by Joseph Kaplan).*—Rayleigh presented an asymptotic formula for the number of characteristic frequencies or eigentones, N, per unit volume, up to a given frequency, ν, and the derivative form which gives the number of eigentones in the range ν to $\nu+d\nu$. This dN form was applied successfully to quantum radiation laws.[1] It is shown that these simple formulae do not apply accurately to sound waves, especially in small rooms and at low frequencies. The discrepancy is attributable to the small number of eigentones involved, compared to the number usually concerned in the case of electromagnetic radiation. More accurate expressions are derived, for a rectangular room, from a consideration of the density of characteristic points in frequency space. The new formulae are:

$$N=\frac{4\pi V}{3c^3}\nu^3\left[\frac{2V\nu+cR\nu}{2V\nu+(c/2)R\nu}\right]^3$$

and, after expansion and simplification:

$$dN=\frac{4\pi V}{c^3}\left[\nu^2+\frac{cR}{2V}\nu\right]d\nu,$$

where $R=(L_xL_y)^2+(L_yL_z)^2+(L_xL_z)^2$; L_x, L_y, L_z are the dimensions of the rectangular room, V is its volume, and c is the velocity of sound. These new equations fit the "exact," stepped curves very nicely, even for the first few eigentones. This development has certain practical applications in acoustics. A new expression is given for the average sound energy, in a room, as a function of frequency. Preliminary experimental confirmation has been obtained.

[1] Richtmyer, *Introduction to Modern Physics*, p. 221–6; p. 237.

2. Conservation of Momentum in Electrical Conductivity. W. V. HOUSTON, *California Institute of Technology.*—For a number of years the theory of electrical conductivity has been marred by a conservation theorem of Peierls. This theorem established the invariance of a function of the electron wave numbers and the lattice vibrations of the crystal, and seemed to indicate for metals at low temperatures a much larger conductivity than is observed. An alternative explanation of the observations was based on the existence of "umklapp" processes by which the conserved quantity could change by an integer. The effective intervention of such processes required, however, a rather special distribution of energy levels as a function of the electron wave numbers. It can be shown that if the Hamiltonian function is properly selected to guarantee the conservation of momentum the theorem of Peierls is merely a part of the conservation of momentum. Its rather peculiar form is associated with the fact that the assumption of periodicity in the crystal lattice restricts its momentum to a series of discrete values. The "umklapp" processes can then be regarded as occurring in the lattice, rather than with the electrons, and representing the transfer of momentum to the lattice.

3. The Quadratic Zeeman Effect. F. A. JENKINS AND E. SEGRÈ, *University of California.*—This effect is a violet shift of the Zeeman components of a line proportional to the square of the magnetic field. It is predicted by the theory of diamagnetism, but has not heretofore been satisfactorily observed. Theoretically the displacement is proportional to n^4, and hence should be detected in the lines of series running to high n. We have studied the Zeeman effect of the higher members of the principal

series of Na and K, using a column of absorbing vapor 30 cm long in the new 60-in. cyclotron magnet of the Crocker Radiation Laboratory. With a field of 27,000 gauss, the quadratic effect becomes detectable at about $n=10$, and follows the simple theory accurately to $n=20$. Beyond this there is an additional violet shift, smaller in K than in Na, which is attributed to the perturbation of the ^2P states by the ^2F, ^2H $\cdots$ states, since these come close to the ^2P states in this region. The measured perturbations agree quantitatively with the calculations of Schiff and Snyder (see following abstract) as far as $n=26$. Here the lines begin to broaden rapidly toward the red, until they merge into a continuum at $n=35$. The various features of this broadening agree with the conclusion of Schiff and Snyder that it is caused by the interaction of states of different n.

4. On the Theory of the Quadratic Zeeman Effect. H. SNYDER AND L. I. SCHIFF, *University of California.*—The quadratic Zeeman effect observed by Jenkins and Segrè (see preceding abstract) in absorption to large orbits in strong magnetic fields is caused by the diamagnetic term in the Hamiltonian, proportional to the square of the vector potential. For the alkalis, the problem involves essentially only one electron, and its spin can be ignored. m_l and parity are always exactly defined, while n and l are not. The observed spectrum can be divided up with increasing n into three regions, according as the lines are broadened asymmetrically (region I), broadened further, but nearly symmetrically (region II), and broadened so much as to overlap into a continuum (region III). It is shown that region I corresponds to n being a good quantum number and l a fairly good one; region II to n being a fairly good quantum number and l not good at all; and region III to both n and l breaking down completely as quantum numbers. Good quantitative agreement with the experiments is obtained as long as inter-n perturbations can be neglected. When this can no longer be done (large n), the theory becomes prohibitively complicated, although some qualitative indications can still be obtained from it.

5. The Fine Structure of Hα and Dα. SIMON PASTERNACK, *California Institute of Technology.*—Kemble and Present[1] pointed out that the discrepancy between the experimental and theoretical values for the doublet separations of Hα and Dα could be accounted for by a large deviation from the Coulomb law at small distances from the nucleus, which leads to a displacement of the S levels. Later experimental work[2] indicated a departure from the theoretical positions of both components (2) and (3) relative to (1). More recently Williams[3] obtained for Dα the separations 0.319 cm^{-1} between components (1) and (2), and 0.135 cm^{-1} between components (3) and (2), these values being, respectively, smaller and greater than the theoretically predicted values. Both of these deviations can be explained on the basis of a displacement of the $2\,^2S$ level of deuterium. Such a displacement would seem to imply a repulsive interaction between the electron and proton at small distances. A first order perturbation treatment indicates that an extremely large interaction would be required to account for the displacement.

Observations by Chu on He II are not in contradiction with an S level displacement. Also, a very small discrepancy found by Edlén[4] in the wave-length of the Li III line $1s\,^2S-2p\,^2P$ can be accounted for by an S level displacement, using the first order perturbation treatment together with an interaction indicated by the Dα perturbation.

[1] Kemble and Present, Phys. Rev. **44**, 1031 (1932).
[2] Houston, Phys. Rev. **51**, 446 (1937).
[3] Williams, Phys. Rev. **54**, 558 (1938).
[4] Edlén, *Wellenlängen und Termsysteme an den Atomspektren der Elemente Li, Be, B, C, N, O* (Uppsala, 1934), p. 29.

6. A Continuously Sensitive Diffusion Cloud Chamber. ALEXANDER LANGSDORF, JR.,* *University of California.*—Photographs of ion-tracks have been obtained with the thermally activated diffusion cloud chamber previously described,[1] in which vapor diffuses vertically downward through a gas from a heated top plate to a refrigerated floor plate. The diffuse rain of condensation previously reported has been nearly eliminated by heating liquid in a glass flask by radiation from above the flask, to produce vapor free of aggregates. The ion-sensitive region is about three inches deep in a chamber six inches deep. The maximum steady ion-load the present chamber can carry and still show tracks has been determined approximately, and is not much greater than the normal background ionization without shielding. An analysis of the operation of the chamber has been made. Some precautions necessary for successful operation, and some limitations upon the use of this type of apparatus are now rather well known.

* National Research Fellow.
[1] A. Langsdorf, Jr., Phys. Rev. **49**, 422(A) (1936); **51**, 1026(A) (1937).

7. Faint L-series Lines from K Auger Transitions in Silver. CECIL J. BURBANK, *Stanford University.*—By using a single-crystal vacuum spectrograph weak lines having wave-lengths of 4.030A, 4.016A and 3.805A have been obtained from a thin silver target bombarded with 80-kv electrons. These lines are located among the L lines of silver but L critical potentials do not suffice to produce them; in no case have they been observed except with electron energies exceeding the K excitation energy. This fact, and the observed wave-lengths, are in agreement with the supposition that the condition prerequisite for such an emission is a double L ionization resulting from Auger processes succeeding direct K ionization by a cathode electron. The low observed intensities are also consonant with this explanation. The wave-lengths given above have been assigned, respectively, to the transitions $L^2_{\rm III}-L_{\rm III}M_{\rm V}$, $L^2_{\rm II}-L_{\rm II}M_{\rm IV}$, $L^2_{\rm III}-L_{\rm III}N_{\rm V}$. These lines are much farther removed from related diagram lines than are previously observed satellites. Their observation is rendered difficult by the intense background of high voltage continuous spectrum which appears in high orders of reflection.

8. On the Equilibrium of Massive Neutron Cores. G. M. VOLKOFF, *University of California.*—Equilibrium of spherically symmetric distributions of matter obeying the

equation of state appropriate to a cold degenerate Fermi gas has been studied by using the gravitational theory of general relativity. It has been found that with this equation of state a single quasi-Newtonian spherically symmetric stable equilibrium configuration exists for distributions with total mass between O and M_1, two equilibrium configurations, one of which is stable and the other unstable, exist for masses greater than M_1 and less than M_2, and no equilibrium configurations exist for masses greater than M_2, where M_1 and M_2 are inversely proportional to the square of the mass of the elementary particles composing the Fermi gas. For a cold neutron gas $M_1 \sim \frac{1}{4} M_\odot$ and $M_2 \sim \frac{1}{4} M_\odot$ ($M_\odot$ = sun's mass). No physically plausible modifications of the equation of state seem essentially to alter this conclusion, or to change radically the order of magnitude of M_2. Nonstatic solutions for the cases $M > M_2$ are being investigated at present.

9. Positive Point-to-Plane Corona Onset Studies. ARTHUR F. KIP, *University of California.*—Positive point-to-plane corona studies[1] have been continued with special emphasis on pre-onset and Geiger counter regions. Oscillographic and photographic studies show two kinds of current pulses occurring below onset voltages. Both types of pulses can be observed by inductive effects on a plate placed near the gap and by the ion currents produced. At lowest voltages for counting action, pulses lasting for about 0.003 second are recorded on the oscillograph and are accompanied by a glow around the point as described by Trichel[2] for steady corona. These correspond to the regular corona process continuing for several thousand bursts after which space charge modification of the field causes extreme likelihood of extinction. At voltages approaching corona onset, *streamers* are observed which extend far out into the gap and which can propagate only into a space charge free gap. The steady corona process is normally initiated by one of these streamers. Streamers occurring just prior to spark breakdown of the gap are associated with the pre-onset streamers. In this case the higher voltage near breakdown gives the high field necessary for streamer propagation despite space charge modification of the field.

[1] Kip, Phys. Rev. **54**, 139 (1938).
[2] G. W. Trichel, Phys. Rev. **54**, 242 (1938).

10. On the Paths of Ions in the Cyclotron. L. I. SCHIFF, *University of California.*—Thomas[1] has recently shown that a variation of the magnetic field of a cyclotron with polar angle, together with a radial increase in the field, can produce a focusing effect on the beam while maintaining resonance. For polar angle variations of period 2π or π, the orbits are unstable, while for period $\pi/2$ they are stable. The calculations are here extended to polar angle variations of period $2\pi/3$, and it is shown that the orbits are stable. Compared with the $\pi/2$ period, smaller variations both with polar angle and with radius are required to produce focusing with resonance; the combination of longer period and smaller variation would make such a field easier to construct. The stability of orbits in the electric field due to "triants" operated by three-phase power is also investigated. It is found that these orbits are stable.

[1] L. H. Thomas, Phys. Rev. **54**, 580, 588 (1938).

11. Multiple Scattering of Cosmic-Ray Particles in 1 cm of Platinum. JOSEPH A. VARGUS, JR., *California Institute of Technology.*—451 photographs of cosmic-ray tracks, including many previously used for energy loss measurements, have been measured. The scattering angles and energies observed are compared with the theoretical calculations of Williams. 361 particles (>500 Mev) showed a mean angle of scattering and a distribution in rough accord with theory. It is necessary to use the energy-distribution of Anderson and Neddermeyer[1] for these tracks, whose energies could not be measured; no single curve for any one assumed mean energy can be made to fit the data. Blackett and Wilson[2] have already reported a distribution in the low energy range in accord with theory, and the distribution is now extended to higher energies. 90 particles of measurable energy (<500 Mev) showed a mean angle of scattering roughly in agreement with theory. In disagreement with Blackett and Wilson, however, the distribution of scattering angles in the low energy range indicates an excess of particles scattered at small and at large angles. The departure, though marked, could possibly lie within the limits of error. The discrepancy is similar to that found by Fowler[3] for scattering of electrons (5–17 Mev).

[1] *International Conference on Physics*, vol. 1 (1934), p. 173.
[2] Proc. Roy. Soc. **A165**, 209 (1938).
[3] Phys. Rev. **51**, 773 (1938).

12. The Measurement of γ-Ray Energies. D. C. KALBFELL, *University of California.*—A magnetic electron spectrograph has been constructed to measure the energies of γ-rays from artificially radioactive materials. A photographic plate is used as detector. The γ-rays give rise to electrons either by internal conversion in the radioactive atom itself, or by the photoelectric effect in a thin strip of lead or gold. A number of cases of internal conversion in artificial radioelements are now known and some of these have already been photographed. Ga^{67} was the first substance tried. Lines due to conversion in both the K and L electron shells were observed and indicated a γ-ray of 80 kv. An isotope of element 43 (half-life 6 hours) gave lines from a 129-kv γ-ray. A mixture of long-lived (half-lives greater than 30 days) isotopes of element 43 showed lines from two γ-rays of energies 87 kv and 184 kv. These electron groups have not been previously reported and it is not yet known with what periods they are associated. These last two γ-rays were also measured by using the photoelectrons knocked out of a gold foil by the unconverted fraction of the γ-rays. The energy measured in this way checked up with that determined from internal conversion. The annihilation radiation from Cu^{64} and N^{13} has also been measured by use of the photoelectrons from lead.

13. Abundance of Interstellar Atoms and Ions. R. M. LANGER, *California Institute of Technology.*—The recent[1] estimate of the strength of nebular hydrogen emission lines provides data needed for the calculation of the abundance of various ionic species known to exist in interstellar space. The computation is based on a previous investigation by the present writer of the intensity and spectral distribution of starlight in our galactic neighborhood. The degree of ionization of the gaseous matter is determined with the help of the dubious but usual assumption of equilibrium between the photoionization due to starlight and the recombination between ions and electrons. Relative abundances in qualitative agreement with observation had already been obtained and from the work of Struve and Elvey the electron concentration could be obtained by calculating the degree of ionization of the hydrogen. The results are in accordance with general

Ionic Species	e	H^+	H	Na
Number per cm³	1	1	10^{-3}	2×10^{-9}
Density in g/cm³	10^{-27}	2×10^{-24}	1.6×10^{-24}	10^{-31}

Ionic Species	Na^+	Ca	Ca^+	Ca^{++}
Number per cm³	3×10^{-9}	2×10^{-14}	10^{-9}	3×10^{-7}
Density in g/cm³	10^{-29}	1.3×10^{-36}	6×10^{-32}	2×10^{-29}

notions excepting that the low abundance of neutral Ca makes it difficult to understand the presence of the arc lines of Ca in interstellar spectra.

[1] O. Struve and C. T. Elvey, Astrophys. J. **88**, 364 (1938).

14. Nocturnal *E*-Layer Ionization. N. E. BRADBURY, *Stanford University.*—The existence of weak nocturnal *E*-layer ionization is difficult to explain on the basis of a purely solar ultraviolet light hypothesis since radically different values of the recombination coefficient are required during the day and night. Accordingly it is suggested that the nocturnal *E*-layer arises in the same process suggested by Dauvillier which produces the general nonpolar aurora. Pertinent experimental data are meager, but it may be noted that: (1) The nocturnal variation of the *E* layer at Huancayo is similar to the variation in intensity of the light of the night sky reported by Rayleigh and others with a maximum near midnight. (2) While no systematic studies of the variation of night-sky light with latitude exist, the measurements of Rayleigh show a slight decrease with latitude. This agrees with the apparently relatively weaker nocturnal *E* layer at Huancayo than in England. (3) The maximum in occurrence frequency and light intensity of polar aurora at 100 km agrees closely with the height of the *E* layer. Absence of correlation between *E* ionization and night-sky light would support the theory of Chapman that the energy source for the night-sky light is due to the recombination of dissociated oxygen atoms.

15. The Fine Structure of Hydrogen Isotopes. C. F. ROBINSON, *California Institute of Technology.*—The fine structure of deuterium has been studied by using a high frequency oscillator for electrodeless excitation, and conventional cooling. One plate has been subjected to Fourier analysis according to the method developed by Houston. Results are in essential agreement with those of Houston in showing a displacement of the second and third components toward the strongest. In a determination of e/m based on the spectra of hydrogen and deuterium, it is necessary to know by what amounts the strong components of Hα and Dα are displaced, and it is now fairly generally agreed that the positions and intensities of the components of these lines are not in agreement with theory. The method of Fourier analysis is capable of giving the positions and separations of all the lines in the multiplet, and the results show that the strong component of Dα is displaced by a negligible amount from the position of the maximum. With Hα the displacement is still small because of the use of an interferometer separation such as to space the components uniformly along the pattern. A preliminary evaluation gave $e/m=1.7592\pm.0005\times10^7$.

16. The Calculation of Internal Conversion Coefficients. S. M. DANCOFF AND P. MORRISON, *University of California.*—We generalize the calculation of internal conversion coefficients to γ-rays of arbitrary multipole order and type in the range $Z<40$ to help understand the spectra and the isomerism of artificially radioactive nuclei. The selection rules show that for nuclear transitions involving a change in angular momentum $J\to J'$, where $|J-J'|=L$, we may expect the radiation to be predominantly electric 2^L-pole+magnetic 2^{L+1}-pole, or electric 2^{L+1}-pole+magnetic 2^L-pole, depending on the parity change. We represent the potentials of a 2^L-pole in the Hansen-Heitler-gauge, in which $\operatorname{div} A=\varphi=0$. The singularities involved in this gauge introduce supplementary terms in the calculation of the matrix elements. We list formulae for certain limiting cases: If $\begin{Bmatrix}\alpha_k{}^l\\ \beta_k{}^l\end{Bmatrix}$ is the internal conversion coefficient for two K electrons for $\begin{Bmatrix}\text{electric}\\ \text{magnetic}\end{Bmatrix}$ 2^l-pole radiation, we find *neglecting binding:* $(n=Ze^2/h\nu<<1)$

$$\alpha_k{}^l=\frac{2Z^3\alpha^4}{x^3}\left(\frac{x+2}{x}\right)^{l-\frac{1}{2}}\left[\frac{(l+1)x^2+4l}{l+1}\right],$$

$$\beta_k{}^l=\frac{2Z^3\alpha^4}{x^3}\left(\frac{x+2}{x}\right)^{l+\frac{1}{2}},$$

with $x=h\nu/mc^2$. When binding must be taken into account, closed formulae can be obtained only in the nonrelativistic limit. In particular, the asymptotic form for large l is:

$$\alpha_k{}^l=Z^3\alpha^4\,\frac{l}{l+1}\left(\frac{2}{e}\right)^{l+s/2}\left[1-2n\sqrt{l}\,\frac{(1+n^2+(1/2l)-n\mu/2)^l}{(2+l\mu^2)^{\frac{1}{2}}}\right],$$

where $\mu=n+(n^2+2/l)^{\frac{1}{2}}$.

17. The Fine Structure of the Line λ4686 of Ionized Helium. DJEN-YUEN CHU, *California Institute of Technology.*—The fine structure of the line λ4686 of ionized helium, emitted at a pressure of about 0.3 mm from a hollow cathode cooled by liquid air, was measured with a

Fabry-Perot interferometer at four different separations. The formula for the interferometer pattern expressed in Fourier series was applied in the analysis. Because of the overlapping, not all of the eight components predicted by theory could be resolved, but four of them were definitely observed, and the remaining weaker ones were inferred from the pattern to be present. The relative intensities and the positions of the eight components were found to be in general agreement with the theory. The wave-lengths of three strong components were 4685.7017±0.0004 I.A., 4685.8012±0.0005 I.A. and 4685.5298±0.0015 I.A. respectively, referred to the helium line 5015.6750 I.A. as standard. The separation between the two strongest components was 0.4529±0.0029 cm^{-1}, while the theoretical value calculated on the assumption that the fine structure constant $\alpha=1/137.0$ was 0.4556 cm^{-1}. The Rydberg constant for helium was calculated to be 109,722.430±0.010, neglecting any uncertainty in the index of refraction of air.

18. The Identification of X-Rays Emitted during the Decay of Radioactive Elements. PHILIP ABELSON, *University of California.*—It is now well known from absorption measurements that intense x-rays are emitted from many of the artificial radioactive isotopes; some are caused by electron capture and others by internal conversion of gamma-rays. By means of a suitably designed bent crystal spectrograph[1] the following x-rays have been identified. The x-rays associated with the disintegration of Ga^{67} were found to be those characteristic of zinc in confirmation of the absorption measurements of Alvarez.[2] The x-rays emitted in the decay of Cu^{64} were shown to be characteristic of Ni. X-rays characteristic of bromine were identified with the decay of the 4.5-hour period of Br^{80}.

[1] Bozorth and Haworth, Phys. Rev. 53, 538 (1938).
[2] Alvarez, Phys. Rev. 54, 486 (1938).

19. Photoconductivity of Crocoite Crystals. JAMES J. BRADY AND WILLIAM H. MOORE, *Oregon State College.*—Crocoite crystals were placed between two brass electrodes, one of which was connected to the grid of an FP-54 amplifier. The other electrode was connected to a battery. With an applied potential of 50 volts, the dark currents were in the order of magnitude of 10^{-11} ampere. When light from a carbon arc illuminated the crystal, the current increased 10^{-11} ampere. The current increased with time of illumination until it reached a maximum value after several minutes. When the light was turned off, the current immediately dropped to a small value, and then gradually reduced to zero after several minutes. Spectral distribution curves were obtained for different applied voltages. The spectral maximum was not shifted by a change of voltage. Some of the crystals showed a current, when illuminated, even though the external voltage was zero. Those which did not show this actinoelectric effect could be made to do so by first causing a current to flow through them by applying an external e.m.f. This activation process depended both on the applied potential and the length of time the current flowed through the crystal. Immediately after activation, the actinoelectric currents decreased with the time of illumination, but finally reached a constant value

AUTHOR INDEX TO ABSTRACTS OF LOS ANGELES MEETING

Abelson, Philip—No. 18
Bolt, Richard H.—No. 1
Bradbury, N. E.—No. 14
Brady, J. J. and W. H. Moore—No. 19
Burbank, Cecil J.—No. 7
Chu, Djen-Yuen—No. 17
Dancoff, S. M. and P. Morrison—No. 16
Houston, W. V.—No. 2
Jenkins, F. A. and E. Segrè—No. 3
Kalbfell, D. C.—No. 12
Kip, Arthur F.—No. 9
Langer, R. M.—No. 13
Langsdorf, Alexander, Jr.—No. 6
Moore, W. H.—see Brady, J. J.
Morrison, P.—see Dancoff, S. M.
Pasternack, Simon—No. 5
Robinson, C. F.—No. 15
Schiff, L. I.—No. 10
—— see Snyder, H.
Segrè, E.—see Jenkins, F. A.
Snyder, H. and L. I. Schiff—No. 4
Vargus, Joseph A.—No. 11
Volkoff, G. M.—No. 8